Design and prototyping of a test facility to investigate the transport properties of dilute phase gas-particle flows applicable to coal-fired power plants

Prepared by:

Colin F. du Sart

DSRCOL001

Department of Mechanical Engineering

University of Cape Town

Supervisor:

Pieter G. Rousseau

June 2017

Submitted to the Department of Mechanical Engineering at the University of Cape Town in partial fulfilment of the academic requirements for a Masters of Science degree in Mechanical Engineering

Key Words: Pneumatic Conveying; Pulverised Coal; Pulverised Fuel; Pulverised Fuel Ash; Fly Ash; Multi-Phase Flows; Dilute Phase Gas-Particle Flows; Slip Velocity; Saltation; Choking; Cyclone Design; Calibration Uncertainty; Regression Uncertainty

Dedicated to Colin Francois du Sart (SNR)

08 May 1952 – 06 March 2016

Plagiarism Declaration

I know the meaning of plagiarism and declare that all the work in the document, save for that which is properly acknowledged, is my own. This thesis/dissertation has been submitted to the Turnitin module (or equivalent similarity and originality checking software) and I confirm that my supervisor has seen my report and any concerns revealed by such have been resolved with my supervisor.

Signed by candidate Signature Removed

C F DU SART

Acknowledgements

I would like to acknowledge the assistance, guidance and support received from my supervisor, Prof. Pieter G. Rousseau, which enabled me to complete this project.

I would also like to acknowledge the comments, suggestions, criticism and praise received from my peers whom I discussed or consulted in during the duration of this project.

I would like to thank CFW Fans and their staff members, particularly Mr. Ausef Raad, Mr. Eddie Raad, Mr. Morné van Schoor, Mr. Achmad Davids and Mr. Victor Jonah, who assisted and provided me with equipment, tools and the space to complete this project.

I would also like to thank the Eskom Power Plant Engineering Institute's Centre for Energy Efficiency, the National Research Foundation and the Ada & Bertie Levenstein Trust for funding this project.

Finally, I would like to thank my partner, my immediate family and my uncle, Mr. Thomas du Sart, who provided me with much needed support throughout the duration of this project.

Abstract

Understanding the properties of dilute phase gas-particle transport and the applicability of the different empirical correlations found in literature for these properties are crucial in the study of Pulverised Fuel conveying applicable to South African coal-fired power plants. Having access to a test facility in which empirical data can be generated under controlled operating conditions would enhance this understanding and will allow more informed application of these correlations. The aim of this thesis was to develop a concept design and prototype of a pneumatic conveying test facility that can be used to evaluate these empirical correlations and property relationships.

A comprehensive literature review was conducted of the empirical correlations available and a study was conducted to determine the scaling required to achieve similarity. A theoretical process model was also developed together with a methodology to determine the operating envelope of the blower. The model and methodology were subsequently used in the design of a prototype test facility that would demonstrate the critical particle feed and extraction processes, and to derive suitable specifications for the blower. The prototype, including a complete data acquisition and control system, was developed, constructed and commissioned in cooperation with a commercial engineering company. The facility allows for the control, online measurement and recording of the gas and particle mass flow rates.

Practical tests were then conducted with Fly Ash, as a substitute for Pulverised Coal, to demonstrate the particle feed and extraction processes and to evaluate the accuracy of control of the gas and particle mass flow rates. Tests were conducted for loadings (particle to gas mass flow ratios) between 0.988 and 6.860 at gas mass flow rates between 0.051 and 0.115kg/s and particle mass flow rates between 0.077 and 0.600kg/s. A methodology to determine the particle mass flow rate and its associated uncertainty from the Loss In Weight and Gain In Weight systems was developed from basic principles and demonstrated. The relative uncertainties calculated for the measured particle mass flow rates are less than ±1% for all tests. The maximum relative uncertainties calculated for the measured gas mass flow rates and loadings are ±6%.

The conceptual overall system layout for the final test facility, including the instrumentation design, was then refined based on the experience gained and recommendations are made for consideration in the detail design. The conceptual design allows for the control of the gas and particle mass flow rates as well as the gas temperature and pressure level. The final test facility will be suitable to conduct pressure drop tests, saltation and choking tests, as well as mass balances and visual observations. The process model and methodologies developed here may now be applied in the detail design and operation of such a final test facility.

Table of Contents

List of Figures

List of Tables

Nomenclature

The following descriptions and units given apply unless otherwise stated:

General Symbols		
A	Projected area	m^2
A_{pipe}	Pipe cross section area	m^2
A_r	Archimedes number	
A_r^*	Modified Archimedes number	
A_s	Surface area	m^2
c	Speed of sound	m/s
C_d	Orifice discharge coefficient	
C_D	Drag coefficient	
$C_{D\infty}$	Drag coefficient in an infinitely dilute mixture	
C_M	Mass concentration of solids	
C_V	Volume concentration of solids	
dP	Differential pressure	Pa

dT	Change in temperature	K or °C
D_p	Particle diameter	m
D_p^*	Fine and course particle boundary diameter	m
D_{pipe}	Pipe diameter	m
D_V	Volume weighted diameter	m
e	Euler's number	
F	Force	N
Fr	Froude number	
Fr_p	Particle Froude number	
Fr_{salt}	Froude number at saltation	
Fr_{t0}	Froude number at the single particle terminal velocity	
g	Acceleration due to gravity	m/s^2
I	Current	A
k_{filter}	Filter loss factor	$Pa \cdot s/m^3$
k_{HX}	Heat exchanger loss factor	$Pa \cdot s^2/m^2$
L	Length	m
M_p	Mass of particles	kg
M_r	Relative Mach number	
$\dot{m}_g$	Local gas mass flow rate	kg/s
$\dot{m}_p$	Local particle mass flow rate	kg/s
$\dot{M}_g$	System gas mass flow rate	kg/s
$\dot{M}_p$	System particle mass flow rate	kg/s
$\dot{M}_{pc}$	System particle mass flow rate at choking	kg/s
N	Number of particles	
P	Pressure	Pa
R_g	Gas constant for air	J/kgK

Re	Pipe Reynolds number	
Re_p	Particle Reynolds number	
Re_p^*	Pseudoparticle Reynolds number	
Re_r	Relative particle Reynolds number	
Re_{salt}^*	Modified Reynolds number at saltation	
Re_{t0}	Reynolds number at the single particle terminal velocity	
St	Stokes number	
t	Time	s
T	Temperature	K or °C
u	Uncertainty	%
u_g	Gas velocity	m/s
u_{gc}	Gas velocity at choking	m/s
u_p	Particle velocity	m/s
u_r	Relative (slip) velocity	m/s
u_t	Terminal velocity	
u_{t0}	Single particle terminal velocity	m/s
U_g	Superficial gas velocity	m/s
U_{gc}	Superficial gas velocity at choking	m/s
U_p	Superficial particle velocity	m/s
U_{pc}	Superficial particle velocity at choking	m/s
U_{salt}	Superficial gas velocity at saltation	m/s
V	Volume	m^3
V_g	Volume of gas	m^3
V_p	Volume of particles	m^3
$\dot{V}$	Volume flow rate	m^3/s
$\dot{V}_g$	Volume flow rate of gas	m^3/s

$\dot{V}_p$	Volume flow rate of particles	m^3/s
x_i	Mass fraction of particle with u_{t0i}	
z	Local loading	
Z	System loading	
Greek Symbols		
α_g	Gas volume fraction (voidage)	
α_{gc}	Voidage at choking	
α_p	Particle volume fraction	
β	Ratio of orifice bore to pipe diameter	
γ	Specific heat ratio/ isentropic coefficient	
ε	Pipe roughness	m
ε_g	Gas expansibility factor	
ε_r	Pipe relative roughness	
η	Cyclone efficiency	%
η_{blower}	Blower isentropic efficiency	%
$\lambda_D = 4\lambda$	Friction factor	
λ_{Dg}	Gas-wall friction factor	
λ_{Dp}	Solids friction factor	
λ_{Dpc}	Solids friction factor at choking	
μ_g	Gas dynamic viscosity	kg/ms
ρ_g	Gas density	kg/m^3
ρ_{H2O}	Density of water	kg/m^3
ρ_m	Mixture density	kg/m^3
ρ_p	Particle density	kg/m^3
$\overline{\rho_g}$	Gas bulk density	kg/m^3
$\overline{\rho_p}$	Particle bulk density	kg/m^3

τ	Pressure ratio	
τ_v	Momentum response time	s
Ψ	Shape Factor	
ψ	Inertia Parameter	
∇	Gradient	

The Nomenclature for Section 3.8 and Section 3.9 differ slightly to that given above. The following descriptions and units apply:

General Symbols		
A	Cross section area	m^2
$\bar{A}$	Average cross section area	m^2
F	Force	N
g	Acceleration due to gravity	m/s^2
m	Mass of elements	kg
$\dot{m}$	Rate of mass transfer	kg/s
N / n	Number of elements	
p	Pressure	Pa
P	Average perimeter	m
R_h	Average hydraulic radius	m
t	Time	s
u	Continuous phase velocity	m/s
U	Mixture velocity	m/s
v	Dispersed phase velocity	m/s
V	Volume	m^3
x	Length	m
Greek Symbols		
α_c	Continuous phase volume fraction	

α_d	Dispersed phase volume fraction	
β_V	Drag coefficient	
λ_c	Continuous phase friction factor	
λ_d	Dispersed phase friction factor	
ρ_c	Continuous phase density	kg/m^3
ρ_d	Dispersed phase density	kg/m^3
ρ_m	Mixture density	kg/m^3
$\overline{\rho_c}$	Continuous phase bulk density	kg/m^3
$\overline{\rho_d}$	Dispersed phase bulk density	kg/m^3
τ_w	Wall shear stress	Pa

The following abbreviations appear in this text:

AF	Air fuel
CAD	Computer aided design
CD	Compact disc
CV	Control volume
DAC	Data acquisition and control
EOM	Equation of motion
EPPEI	Eskom Power Plant Engineering Institute
FBD	Free body diagram
FDM	Finite difference method
FS	Full scale
GIW	Gain-In-Weight
GUI	Graphical user interface
LCA	Load cell amplifier
LIW	Loss-In-Weight

NI	National Instruments
PC	Pulverised coal
PF	Pulverised fuel
PFA	Pulverised fuel ash
PFD	Primary flow diagram
P&ID	Piping and instrumentation diagram
PID	Proportional-integral-derivative
PLC	Primary logic controller
PSD	Particle size distribution
RSS	Root sum squares
RTD	Resistance temperature device
SSR	Solid state relay
VSD	Variable speed drive

1 Introduction

1.1 Background and Motivation

Coal-fired power plants account for over 90% of the electricity produced in South Africa (Eskom Power Plant Engineering Institute (EPPEI), 2014). Research and development contributing to the continued improvement of these plants are therefore important, as these plants have a major impact on the quality of life in South Africa. Environmental legislation also requires that these plants implement pollution reduction technologies (EPPEI, 2014). ESKOM is therefore installing and retrofitting future and current coal-fired power plants with low-NOx burners, which as the name suggests, facilitate the reduction of NOx emissions by 40 to 50% (Van der Merwe, 2014). Figure 1-1 shows the position of these burners within a typical coal-fired power plant.

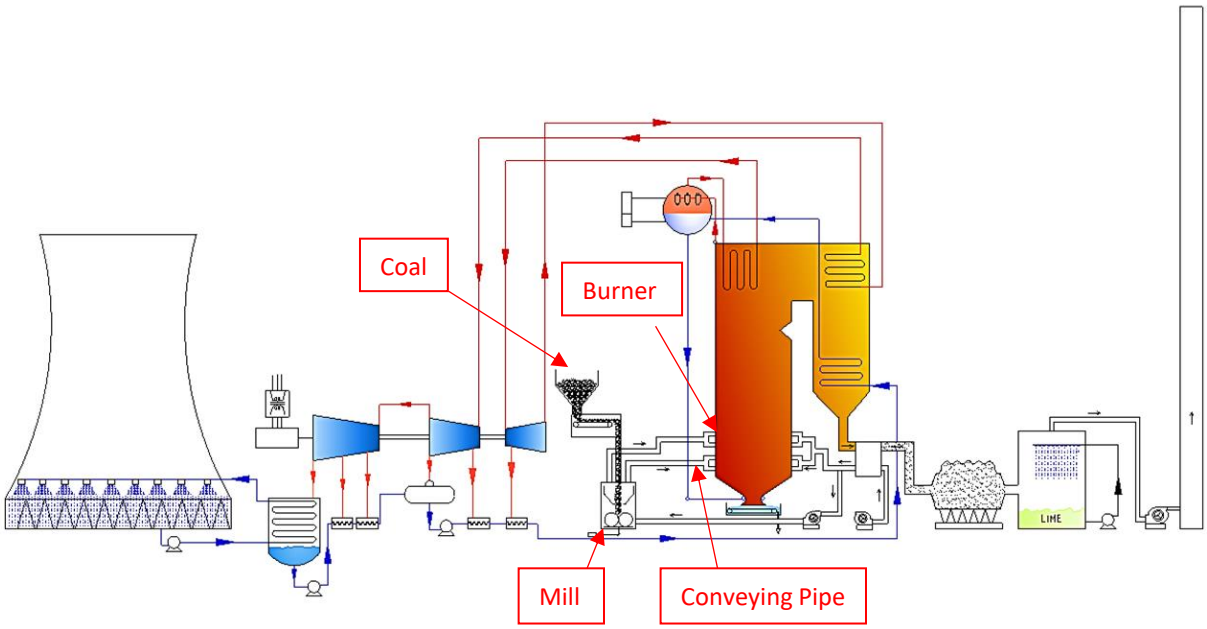

Figure 1-1 – Schematic of a typical coal-fired power plant, taken from EPPEI (2014)

Pulverised Coal (PC) is fed from mills to these burners via pneumatic conveying pipelines. This mixture of PC and air is known as Pulverised Fuel (PF). To ensure the stable operation and ignition at these burners, it is vital that the distribution of PF fed to the burners is homogenous and that the air fuel (AF) ratio lies within the range of 1.5 to 2.5 (Van der Merwe, 2014). According to Van der Merwe (2014), this can only be achieved through dilute phase conveying.

Dilute phase conveying is a flow regime associated with gas-particle flows, where the concentration of solids is relatively low and the gas-particle mixture is mostly homogenous. In contrast, there exists a dense phase flow regime, where the concentration of solids is relatively high and the gas-particle mixture is not always homogenous. Image (a) in Figure 1-2 illustrates dilute flow in horizontal conveying, images (c), (d)

and (e) illustrate dense flow, while image (b) illustrates the transition. Similarly, Figure 1-3 illustrates dilute and dense flow in vertical conveying.

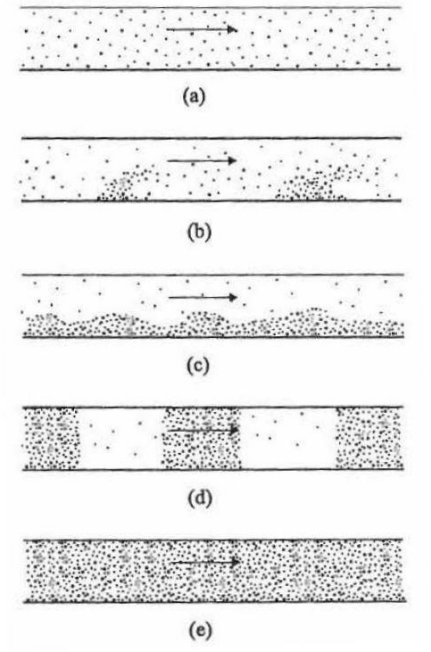

(a) Dilute suspension flow; (b) Dune formation; (c) Stratified flow; (d) Plug flow; (e) Moving bed flow

Figure 1-2 – Flow regimes in horizontal conveying, taken from Fan & Zhu (1998)

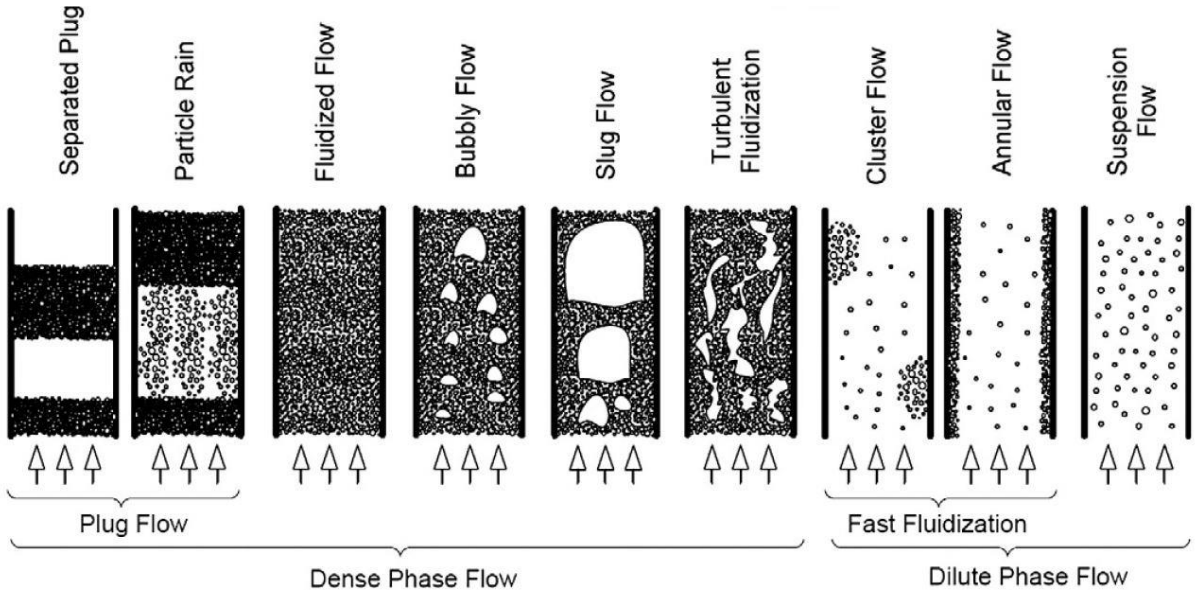

Figure 1-3 – Flow regimes in vertical conveying, taken from Rabinovich & Kalman (2011)

In practice, dilute phase conveying is not always achieved in Eskom coal-fired power plants, and the less desirable dense phase flow occurs. This leads to maldistribution of PF to individual burners and also PC settling in the conveying pipelines (Van der Merwe, 2014), as shown in Figure 1-4. This can be attributed to a number of factors, including but not limited to the conveying air pressure or density, the conveying

velocity and/or the geometry of the pipes in which the conveying takes place. Therefore, as a first step to ensure that the required distribution of PF is obtained, a better understanding of the flow properties associated with the pneumatic conveying of PC (hereafter referred to as PF conveying) is required.

Figure 1-4 – A clogged pipe due to PC settling at a power station, taken from Van der Merwe (2014)

1.2 Problem Description

There are several criteria in literature which define whether a flow is dilute or dense. Rhodes (2008) describes dilute flow as having gas velocities greater than 20m/s, solids volume concentrations less than 1% and pressure drops per unit length less than 0.5kPa/m. Rhodes (2008) also characterises dense flow as having a solids volume concentration above 30%, whereas Fan & Zhu (1998) quote values greater than 40 or 50%. Furthermore, Fan & Zhu (1998) quote three different studies stipulating that dense flow occurs for solids to gas mass flow ratios greater than 15, 20 or 80. These values provide minimum insight into the flow properties required for dilute phase conveying. However, various different correlations exist in literature which can be used to determine the minimum transport velocities which facilitate dilute phase pneumatic conveying.

For horizontal conveying, Fan & Zhu (1998) define the saltation velocity to be equivalent to the minimum transport velocity which prevents particle settling. This is not to be confused with the pick-up velocity, which is equivalent to the minimum transport velocity required to re-entrain already settled particles (Fan & Zhu, 1998). The former is lower by a factor of 2 to 2.5 (Zenz, 1964) and is generally considered the more important velocity in literature for dilute pneumatic conveying design. This is likely due to the fact that (i) conveying velocities above the saltation velocity should ensure that no settling occurs and therefore prevent the onset of dense phase conveying, and (ii) conveying velocities near the saltation velocity mitigates large pressure drops, which are associated with unnecessarily high conveying velocities.

For vertical conveying, choking is synonymous to saltation i.e. particles dropping out of suspension. According to Van der Merwe (2014), the choking velocity is 2 to 3 times lower than the saltation velocity. Rabinovich & Kalman (2011) define the choking velocity as the transition between the dilute and dense phase flow regimes. Other definitions for choking are given in literature. These definitions are usually more intricate and relate to specific experiments performed. It is noted that this is also the case for saltation.

Correlations for calculating the saltation or choking velocity are often based on different variables, were developed using a variety of theoretical and empirical methods, and are also subjective with regard to the definition of the saltation or choking velocity employed in developing the correlation. As a result, these different correlations don't always agree well when compared in literature. It should be noted that many of these comparisons were made using experimental data from previous studies, where test conditions varied significantly. The value of the results of such studies is therefore limited.

It is therefore unclear which, or if any, correlation is suitable for PF conveying under specific operating conditions, for instance those typically encountered in South African coal-fired power plants. However, having access to a test facility in which empirical data can be generated under various controlled operating conditions would enhance the understanding of the transport properties and of the applicability of the different correlations. This will allow a more informed application of these correlations in the study of PF conveying.

1.3 Project Objectives

The objectives of this project are to:

- Conduct a thorough literature review of the different correlations in literature applicable to dilute phase gas-particle transport phenomena such as saltation and choking.
- Develop a theoretical process model applicable to the design of a dilute phase gas-particle transport test facility and a methodology to determine the operating envelope of the blower.
- Develop a concept layout design for a gas-particle transport test facility.
- Develop, construct and operate a physical prototype test facility of reduced complexity but consisting of the most important components of the proposed final test facility.
- Develop a data acquisition and control (DAC) system containing the key elements required for the proposed final test facility.
- Develop and demonstrate the data analysis methodologies required to determine the values of the measured gas and particle mass flow rates and its associated uncertainties.
- Based on the results of tests conducted in the prototype test facility, refine the overall system layout and instrumentation design for the final test facility.

1.4 Project Scope

The scope of this project is to develop a system layout, instrumentation design and applicable data analysis techniques for a test facility which will provide the means to empirically investigate the transport properties of dilute phase particle flows applicable to coal-fired power plants. This system layout and instrumentation design is to be based on theoretical models and knowledge gained during the development and operation of a physical prototype facility of reduced complexity. The purpose of this project is not to do the detail design of the final test facility or to conduct detail tests to investigate the transport properties of PF conveying.

2 Literature Review

A review of published literature which provides the basis for this project is presented here. Gas-particle flow fundamentals are presented first followed by a review of slip, saltation, choking, pressure drop and particle acceleration length correlations.

2.1 Gas-Particle Flow Fundamentals

Gas-particle flows are multi-phase flows which consist of particles flowing within a gas. Intrinsic flow properties pertaining to gas-particle flows are discussed below.

2.1.1 Voidage

Consider the gas-particle mixture in volume δV, as shown in image (a) of Figure 2-1. The volume fraction of the particle phase is defined as (Crowe, et al., 1998)

$$\alpha_p = \lim_{\delta V \to \delta V^0} \frac{\delta V_p}{\delta V}$$

Equation 2-1

and the volume fraction of the gas phase, known as the void fraction or voidage as

$$\alpha_g = \lim_{\delta V \to \delta V^0} \frac{\delta V_g}{\delta V}$$

Equation 2-2

δV^0 is the limiting volume that ensures a stationary average and the sum of the volume fractions is unity, namely

$$\alpha_p + \alpha_g = 1$$

Equation 2-3

In pneumatic conveying literature, δV is often represented by a pipe element of length δL such as that shown in image (b) of Figure 2-1.

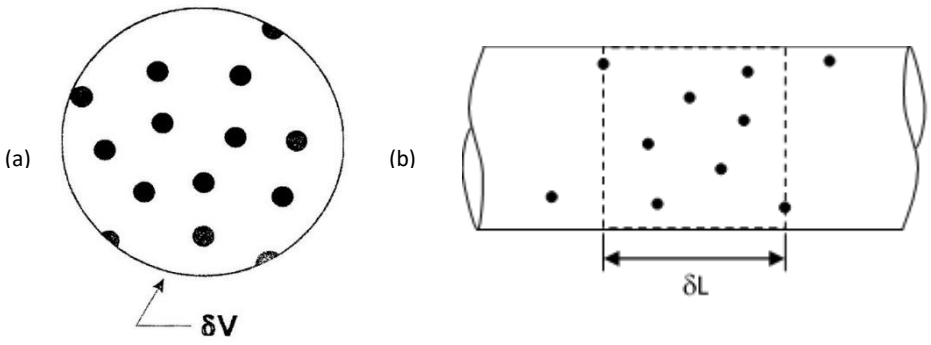

Figure 2-1 – (a) Gas-particle volume, taken from Crowe, et al. (1998); (b) Pipe element

2.1.2 Loading

Loading (essentially the inverse of the AF ratio) is the ratio of the particle to gas phase mass flow rates (Crowe, et al., 1998). System loading Z refers to the mass flow ratio put through a system and local loading z refers to the mass flow ratio within a limiting volume such as the pipe element given in Figure 2-1.

According to Crowe, et al. (1998) the system loading can be taken to be indicative of the local loading i.e.

$$z = \frac{\dot{m}_p}{\dot{m}_g} = Z = \frac{\dot{M}_p}{\dot{M}_g}$$

Equation 2-4

where $\dot{M}$ and $\dot{m}$ are the system and local mass flow rates, and the subscripts p and g refer to the particle and gas phases respectively.

2.1.3 Superficial Velocity

The mass flow rate of the gas phase within a pipe with cross section area A_{pipe} in m^2 can be given by (Crowe, et al., 1998)

$$\dot{m}_g = \rho_g(1 - \alpha_p)u_g A_{pipe} = \rho_g \alpha_g u_g A_{pipe}$$

Equation 2-5

where ρ_g is the density of the gas in kg/m^3 and u_g is the actual gas velocity in m/s. Here, $U_g = \alpha_g u_g$ is the superficial gas velocity in m/s, which is the flow velocity of the gas phase if it is assumed it is the only phase present. U_g can also be calculated if the mass flow rate of gas through a system is known i.e.

$$U_g = \alpha_g u_g = \frac{\dot{M}_g}{\rho_g A_{pipe}}$$

Equation 2-6

Similarly, the superficial particle velocity can be defined as

$$U_p = \alpha_p u_p = \frac{\dot{M}_p}{\rho_p A_{pipe}}$$

Equation 2-7

where ρ_p is the particle density in kg/m^3 and u_p is the mean actual particle velocity in m/s.

2.1.4 Bulk Density

The volume fraction and density of any one of the phases can be grouped to give the bulk density of the respective phase (Crowe, et al., 1998) i.e. $\bar{\rho} = \alpha\rho$. Therefore

$$\overline{\rho_g} = \alpha_g \rho_g$$

Equation 2-8

and

$$\overline{\rho_p} = \alpha_p \rho_p = \left(1 - \alpha_g\right)\rho_p$$

Equation 2-9

Subsequently, the mixture density can be defined as

$$\rho_m = \overline{\rho_g} + \overline{\rho_p}$$

Equation 2-10

The bulk density of a material changes depending on how it is handled. Therefore, the bulk density measured during independent experiments or in material datasheets should not be used for flow calculations, as it may differ considerably to the bulk density within the conveying pipe.

2.2 Slip Velocity

In gas-particle flows, the particle phase lags behind the gas phase. This lag (or relative velocity) is known as the slip velocity, given by

$$u_r = u_g - u_p$$

Equation 2-11

Many correlations have been proposed in literature to calculate the slip velocity. The Hinkle correlation for calculating the particle velocity in horizontal flow is presented first. A method developed by Yang and his colleagues to calculate the slip velocities in both horizontal and vertical flow is presented after.

2.2.1 Hinkle's Correlation

The Hinkle correlation (Hinkle, 1953) is cited often in literature and was developed by taking high-speed photographs of particles flowing in a gas stream. However, the correlation presented is not always consistent with the correlation presented in the original publication. It is speculated that this is due to either modification of the formula, incorrect conversion from imperial to SI units or misinterpretation. The following form is given by Hinkle (1953)

$$u_r = 1.41 u_g D_p^{0.3} \left(\frac{\rho_p}{\rho_{H2O}}\right)^{0.5}$$

Equation 2-12

where D_p is the mean particle diameter in ft, u is in ft/s and ρ is in lb/ft^3.

2.2.2 Yang's Correlation

In vertical flow, the assumption that the slip velocity of a single particle is equal to the terminal velocity (the highest attainable velocity in free fall) of the particle is often made i.e.

$$u_r = u_{t0}$$

Equation 2-13

where u_{t0} is the single particle terminal velocity in m/s and can be calculated using the equations given in Section 3.7.

However, it is commonly mentioned in literature that the slip velocity increases with increasing fluid velocity. Yang (1973) observed that there were large discrepancies when comparing previously published experimental results and results obtained using the above assumption, especially at high fluid velocities and for large particle sizes and densities. Yang (1973) subsequently developed a correlation for vertical flow using the above assumption, but by modifying the terminal velocity equation to account for voidage and frictional effects. The correlation is implicit, and requires the voidage and slip velocity to be solved simultaneously.

The voidage in a pipe element of diameter D_{pipe} (in meter) is given by Equation 2-14 (Yang, 1973)

$$\alpha_g = 1 - \frac{4\dot{M}_p}{(\rho_p - \rho_g)\pi D_{pipe}^2 u_p}$$

Equation 2-14

and the slip velocity is given by Equation 2-15 (Yang, 1973)

$$u_r = u_{t0}\sqrt{\left(1 + \frac{\lambda_{Dp} u_p^2}{2D_{pipe}}\right)\alpha_g^{4.7}}$$

Equation 2-15

Where λ_{Dp} is the Darcy-Weisbach equivalent solid (or particle-wall) friction factor and can be calculated using the equations given in Section 3.6. The above correlation was further developed for horizontal conveying, where the slip velocity is given by Equation 2-16 (Yang, et al., 1973)

$$u_r = u_{t0}\sqrt{\frac{\lambda_{Dp}u_p^2}{2D_{pipe}}\alpha_g^{4.7}}$$

Equation 2-16

with u_{t0} still referring to the single particle terminal velocity in vertical flow. Equation 2-15 and Equation 2-16 are known as Yang's modified terminal velocity equations. Yang (1973) and Yang, et al. (1973) claim these correlations are good to $\pm$ 20% and $\pm$ 10% respectively if experimental values for λ_{Dp} are used. If Yang's (1974) solid friction factor correlations are used instead (see Section 3.6) then the method requires the simultaneous solution of three equations and is accurate to ±30% and ±20% for vertical and horizontal conveying respectively.

2.3 Saltation

On a plot of pressure drop per unit length vs. superficial gas velocity, saltation occurs approximately at the minimum pressure point for coarse particles, and at slightly higher velocities for fine particles (Fan & Zhu, 1998). The terms coarse and fine are used loosely here, however, Cabrejos & Klinzing (1994) define coarse particles as those greater than 100µm in diameter. The flow regime diagram (or Zenz plot as sometimes called in literature) is given in Figure 2-2 shows pressure drop per unit length vs. gas velocity curves for increasing particle mass flow rates.

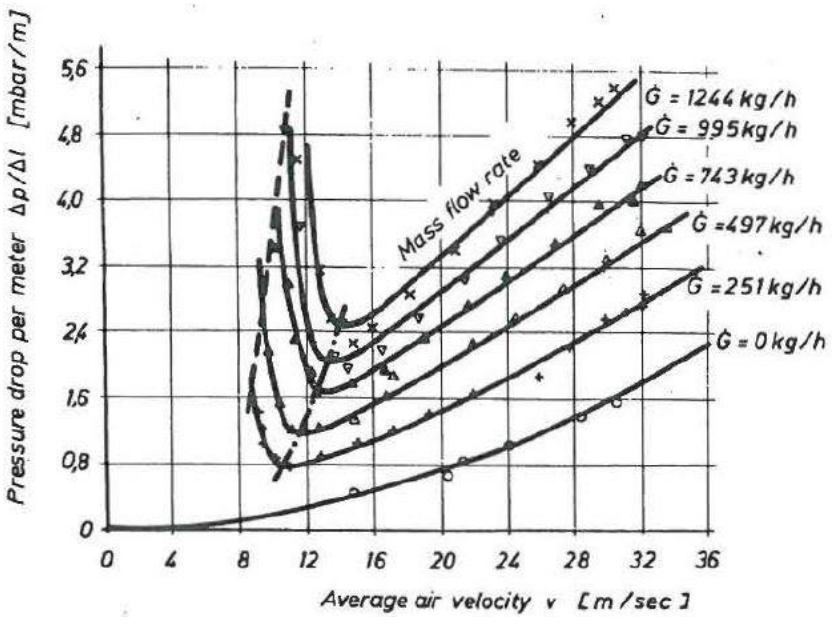

Figure 2-2 - General flow regime diagram, taken from Fan & Zhu (1998)

As can be seen in Figure 2-2, the pressure drop per unit length increases with decreasing superficial gas velocity below the pressure minimum. This is due to increased solids deposition (Cabrejos & Klinzing, 1994). The increase in pressure drop per unit length with increasing gas velocity above the pressure minimum can be attributed to an increase in the friction force opposing mixture motion (Fan & Zhu, 1998).

Furthermore, the curve passing through the minimum pressure points is known as the pressure minimum curve (Rizk, 1982) and marks the dilute (right side) and dense flow (left side) transition (Fan & Zhu, 1998).

A number of published correlations exist for calculating the saltation velocity i.e. the superficial gas velocity at saltation U_{salt}, four of which are presented below.

2.3.1 Rizk's Correlation

The Rizk correlation (Rizk, 1982) is widely referenced and approximates the pressure minimum curve shown in Figure 2-2. The correlation was developed by relating experimental data with the Froude number F_r and is given as

$$z = \frac{1}{10^a} Fr^b$$

Equation 2-17

a and b are dimensionless numbers given by

$$a = 1440 D_p + 1.96$$

Equation 2-18

and

$$b = 1100 D_p + 2.5$$

Equation 2-19

where D_p is in meter and the constants are in the appropriate units to maintain the numbers' dimensionless characteristics. The dimensionless Froude number is given by

$$Fr = \frac{U_g}{\sqrt{D_{pipe} g}}$$

Equation 2-20

Taking $z = Z = \frac{\dot{M}_p}{\dot{M}_g}$ and defining the saltation point as the minimum pressure drop point, the saltation velocity can be solved for different particle mass flow rates by substituting Equation 2-20 into Equation 2-17 and rearranging to give

$$U_{salt} = \left(\frac{4 \dot{M}_p 10^a g^{b/2} D_{pipe}^{-2+b/2}}{\pi \rho_g} \right)^{1/(b+1)}$$

Equation 2-21

where g is the acceleration due to gravity in m/s^2.

Rizk (1982) claims the above correlation is good to ±15% when compared to his own and previously published data.

2.3.2 Matsumoto, et al.'s Correlation

Matsumoto, et al. (1977) empirically investigated the effect of particle size on the minimum transport velocity, which they define as the minimum superficial gas velocity required to prevent particle deposition in a pipe i.e. the saltation velocity. They observed that fine and coarse particles had different effects on the saltation velocity, resulting in materials having a characteristic minimum saltation velocity at a given particular size. In other words, the saltation velocity decreases with increasing particle size, before reaching a minimum and then increasing with continued increasing particle size. They then corroborated this observation theoretically with an earlier developed numerical model by Matsumoto & Saito (1970) and subsequently developed the following correlations.

For fine particles i.e. $D_p < D_p^*$

$$z = 5.56\times10^3 \left(\frac{D_p}{D_{pipe}}\right)^{1.43} \left(\frac{Fr_{salt}}{10}\right)^4$$

Equation 2-22

For coarse particles i.e. $D_p > D_p^*$

$$z = 0.373 \left(\frac{\rho_p}{\rho_g}\right)^{1.06} \left(\frac{Fr_{t0}}{10}\right)^{-3.7} \left(\frac{Fr_{salt}}{10}\right)^{3.61}$$

Equation 2-23

Fr_{salt} is the Froude number at saltation

$$Fr_{salt} = \frac{U_{salt}}{\sqrt{D_{pipe} g}}$$

Equation 2-24

Fr_{t0} is the Froude number at the single particle terminal velocity

$$Fr_{t0} = \frac{u_{t0}^2}{\sqrt{D_p g}}$$

Equation 2-25

and the boundary between fine and course particles is given by

$$D_p^* = 1.39 D_{pipe} \left(\frac{\rho_p}{\rho_g}\right)^{-0.74}$$

Equation 2-26

Again, taking $z = Z = \frac{\dot{M}_p}{\dot{M}_g}$, the saltation velocity can be solved for different particle mass flow rates by substituting the Froude numbers into Equation 2-22 or Equation 2-23 and rearranging. Matsumoto, et al. (1977) claim their correlation predicts values to within ±50% of their experimental data.

2.3.3 Geldart & Ling's Correlation

Geldart & Ling (1992) imposed fixed differential pressures across an experimental rig (to vary gas density), where they measured the pressure drops and particle mass flow rates across a horizontal line. Using their experimental data, they constructed curves of particle mass flux vs. superficial gas velocity such as that given in Figure 2-3. They subsequently took the saltation velocity as the maximum point. They then compared their results with previously published correlations and also presented one of their own, concluding that their and Rizk's (1982) correlation fits their experimental data within 15%.

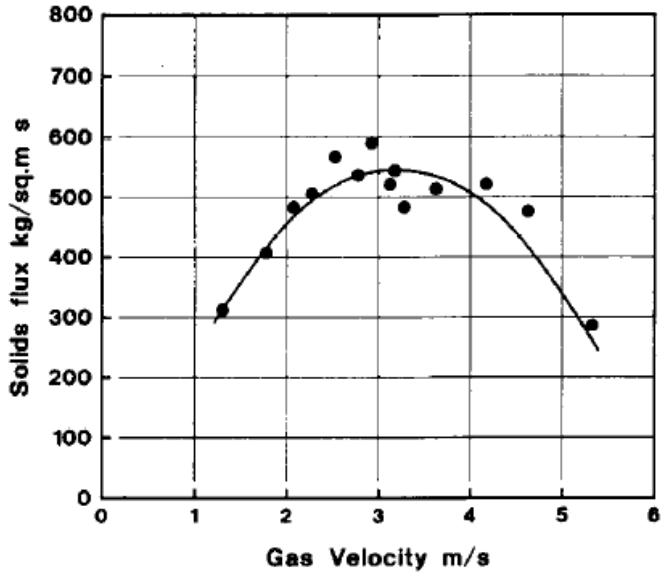

Figure 2-3 – Particle mass flux vs. Superficial gas velocity, taken from Geldart & Ling (1992)

Geldart & Ling (1992) advise that Rizk's correlation should be used in light of its simplicity when compared to their own, which is *"complicated and must be solved by an iterative method"*. A simplified version of their correlation is therefore given below, as presented by Rabinovich & Kalman (2008). The correlation is valid for SI units only.

For $\frac{\dot{M}_p}{A_{pipe}D_{pipe}} < 47\,000$

$$U_{salt} = 8.7\left(\frac{\dot{M}_p}{A_{pipe}}\right)^{0.302} D_{pipe}^{0.153}\rho_g^{-0.42}\mu_g^{0.055}$$

Equation 2-27

For $\frac{\dot{M}_p}{A_{pipe}D_{pipe}} > 47\,000$

$$U_{salt} = 1.5\left(\frac{\dot{M}_p}{A_{pipe}}\right)^{0.465} D_{pipe}^{0.465}\rho_g^{-0.42}\mu_g^{0.055}$$

Equation 2-28

Where μ_g is the dynamic viscosity of the gas in kg/ms.

2.3.4 Rabinovich & Kalman's Correlation

Rabinovich & Kalman (2008) conducted experiments in a wind tunnel to investigate the boundary saltation velocity, which they define as *"the minimum velocity at which the particles can be conveyed for an infinite length."* From their experiments, they developed a correlation to calculate the boundary saltation velocity using modified versions of the dimensionless Reynolds number and the Archimedes number. Furthermore, by modifying the Archimedes number, they then developed a correlation to calculate the *"minimum pressure velocity"* which they claim is good to ±30% when compared to previously published data. The correlation is presented below.

For $Ar^* < 2450$

$$Ar^* = Ar(1 + 30C_v^{0.35})^{2.33}$$

Equation 2-29

$$Re_{salt}^* = 14.3Ar^{*0.1}$$

Equation 2-30

For $Ar^* > 2450$

$$Ar^* = Ar\left[\left(\frac{1-e}{e}\right)^{0.1} + 30C_v^{0.35}\right]^{2.33}$$

Equation 2-31

$$Re_{salt}^* = 1.1Ar^{*\frac{3}{7}}$$

Equation 2-32

where

$$Re_{salt}^* = \frac{\rho_g U_{salt} D_p}{\mu_g\left(2.7 - 3.1e^{-\frac{Dpipe/D_{50}}{1.6}}\right)}$$

Equation 2-33

$$Ar = \frac{\rho_g(\rho_p - \rho_g)gD_p^3}{\mu_g^2}$$

Equation 2-34

and

$$C_V = \frac{\dot{V}_p}{\dot{V}_p + \dot{V}_g} = \frac{z\rho_g}{\rho_p + z\rho_g}$$

Equation 2-35

Here, C_V is the volume concentration of solids, $\dot{V}_p$ and $\dot{V}_g$ are the volume flow rates of the particle and gas phases respectively in m^3/s, and D_{50} corresponds to a 50mm diameter pipe.

In order to solve for U_{salt}, A_r and C_v need be to calculated first using Equation 2-34 and Equation 2-35 respectively. The results are then substituted into the appropriate equation for Ar^*, which is then solved and substituted into the corresponding equation for Re^*_{salt}. U_{salt} can then be calculated by equating the resultant equation with Equation 2-33 and rearranging.

2.4 Choking

Yang (2004) discusses the different definitions for choking available in literature. The *"classical choking"* classification (Yang, 2004), initially coined by Zenz (1949), refers to points E and H on the curves shown in Figure 2-4. It can be seen that the curves in Figure 2-4 are analogous to those in Figure 2-2. Again, as with the curve presented in Figure 2-2, the pressure drop per unit length increases to the left and right with increasing local loading (due to particles dropping out of suspension) and friction forces respectively.

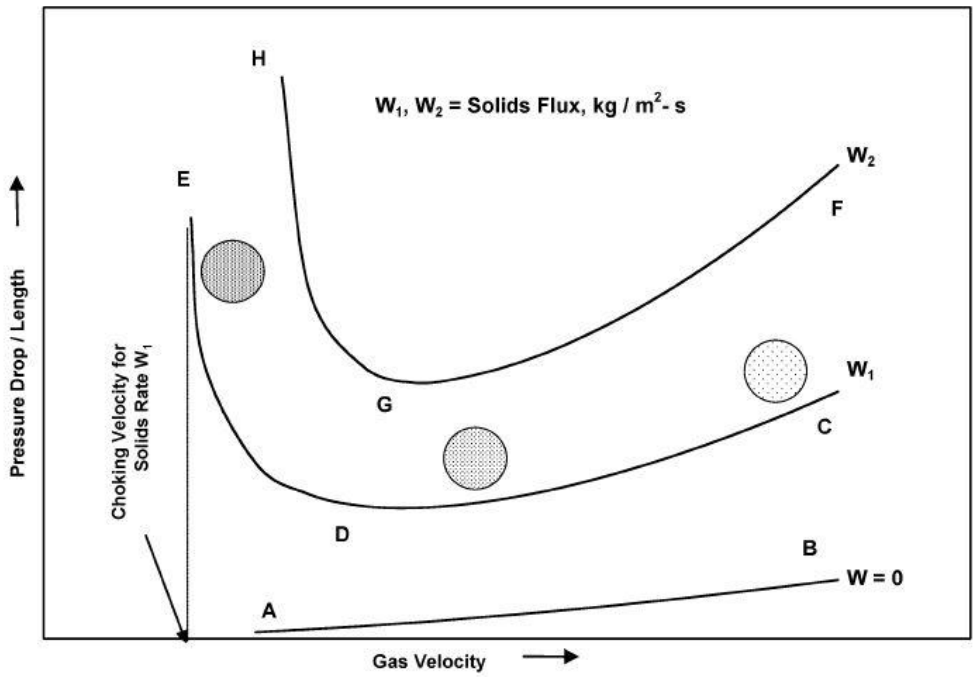

Figure 2-4 - Pressure Drop vs. Gas Velocity in Vertical Conveying, taken from Yang (2004)

As with saltation, a number of correlations exist for calculating the choking velocity i.e. the superficial gas velocity at choking U_{gc}, three of which are presented below. These correlations were recommended by Klinzing, et al. (1997) for their reliability when comparing calculated results and published experimental data. It is noted that Klinzing, et al. (1997) advise that a safety factor of 1.5 be employed when using these correlations.

2.4.1 Leung, et al.'s Correlation

From the literature reviewed, the majority of gas-particle flow correlations incorporate the use of the mean particle diameter. However, Leung, et al. (1971) developed a method to calculate the choking velocity for both uniform and non-uniform particle size distributions (PSD). Their method is based on the assumptions that $u_r = u_{t0}$ and $\alpha_g = 0.97$ at choking. Various experiments in literature were cited to motivate the use of these assumptions. From Equation 2-13

$$\frac{U_{gc}}{\alpha_{gc}} - \frac{U_{pc}}{(1-\alpha_{gc})} = u_{t0}$$

Equation 2-36

where the subscript c refers to choking. Substituting $\alpha_{gc} = 0.97$, Equation 2-36 reduces to the following

$$U_{gc} = 32.3U_{pc} + 0.97u_{t0}$$

Equation 2-37

which can be used to calculate the choking velocity for a uniform PSD for a given particle mass flow rate (See Equation 2-7).

For a non-uniform PSD, the choking velocity is higher than that of a uniform PSD, behaving similarly to a uniform PSD of a higher mean diameter (Leung, et al., 1971). Leung, et al. (1971) explain this behaviour by observing that smaller particles rise faster in vertical pneumatic conveying than larger particles, resulting in a higher fraction of large particles to be present in the pipe when compared to the particles in the feeder. Leung, et al. (1971) provide the following equations to calculate the choking velocity for non-uniform PSDs

$$U_{pc}x_{if} = (1-\alpha_{gc})x_{ipipe}\left(\frac{U_{gc}}{\alpha_{gc}} - u_{t0i}\right)$$

Equation 2-38

and

$$U_{pc} = (1-\alpha_{gc})\sum x_{ipipe}\left(\frac{U_{gc}}{\alpha_{gc}} - u_{t0i}\right)$$

Equation 2-39

where x_{if} and x_{ipipe} are the mass fractions of particles in the feeder and pipe respectively and with u_{t0i}.

The calculation to solve for U_{gc} is not straight-forward. Therefore, an example procedure similar to the one in Leung, et al. (1971) is given. Consider a particle mixture with the properties in Table 2-1.

Size Fraction	x_{if}	u_{t0} (m/s)
1	0.2	1
2	0.5	5
3	0.3	10

Table 2-1 – Example PSD

Using Equation 2-38 and Equation 2-39, the following set of equations can be formulated:

$$0.2U_{pc} = 0.03\left(\frac{U_{gc}}{0.97} - 1\right)x_{1pipe}$$

$$0.5U_{pc} = 0.03\left(\frac{U_{gc}}{0.97} - 5\right)x_{2pipe}$$

$$0.3U_{pc} = 0.03\left(\frac{U_{gc}}{0.97} - 10\right)(1 - x_{1pipe} - x_{2pipe})$$

Noting that U_{pc} is constant in the set of equations, the choking velocity can then be determined by solving for the three unknowns U_{gc}, x_{1pipe} and x_{2pipe} simultaneously for a given particle mass flow rate (See Equation 2-7). Leung, et al. (1971) claim their method correlates to within ±70% of previously published data and advise that a safety factor of 2 be employed in calculations. That is, the choking velocity is assumed to happen at double the calculated velocity.

2.4.2 Yang's Correlation

Yang (1975) maintained Leung, et al.'s (1971) assumption that $u_r = u_{t0}$ at choking. However, he replaced the $\alpha_{gc} = 0.97$ assumption with the assumption that $\lambda_{Dpc} = 0.01$. Experimental data were cited to motivate this assumption. From Equation 2-15

$$\frac{U_{gc}}{\alpha_{gc}} - u_p = u_{t0}\sqrt{\left(1 + \frac{\lambda_{Dp}u_p^2}{2D_{pipe}}\right)\alpha_g^{4.7}}$$

Equation 2-40

At choking this reduces to (Yang, 1975)

$$\frac{2gD_{pipe}(\alpha_{gc}^{-4.7} - 1)}{\left(\frac{U_{gc}}{\alpha_{gc}} - u_{t0}\right)^2} = 0.01$$

Equation 2-41

Also, from Equation 2-7 and Equation 2-36

$$\dot{M}_{pc} = U_{pc}\rho_p A_{pipe} = \left(\frac{U_{gc}}{\alpha_{gc}} - u_{t0}\right)(1-\alpha_{gc})\rho_p A_{pipe}$$

Equation 2-42

If the mass flow rate of particles to be transported is known, Equation 2-41 and Equation 2-42 can be solved iteratively to calculate the superficial gas velocity and voidage at choking. Also, for a known superficial gas velocity, the maximum mass flow rate of particles which can be transported without choking can be calculated. Yang (1975) claims his method is good to ±30% when compared to previously published data.

2.4.3 Punwani, et al.'s Correlation

Punwani, et al. (1976) reviewed previously published choking correlations and also further developed the correlation by Yang (1975) to better predict the choking velocity in high pressure systems. Using previously published data, the following empirical correlation for the particle-wall friction factor at choking was developed.

$$\lambda_{Dpc} = 0.074\rho_g^{0.77}$$

Equation 2-43

This modifies Equation 2-41 to

$$\frac{2gD_{pipe}(\alpha_{gc}^{-4.7} - 1)}{\left(u_{gc} - u_{t0}\right)^2} = 0.074\rho_g^{0.77}$$

Equation 2-44

Here, ρ_g is in lb/ft^3 and the constant 0.074 is in the appropriate units to maintain the dimensionless characteristic of λ_{Dpc}. Equation 2-42 and Equation 2-44 can then be used to calculate U_{gc} and α_{gc}, or $\dot{M}_{pc}$.

It is noted that for non-uniform PSDs, Punwani, et al. (1976) recommend solving Equation 2-38 and Equation 2-39 simultaneously with Equation 2-41 if Yang's (1975) method is followed, or together with Equation 2-44 if their own method is followed.

2.5 Other Correlations in Literature

The correlations presented in the preceding text are not exhaustive. For a list of additional slip velocity correlations, the reader is referred to the research of Wei, et al. (2011) who experimentally evaluated published slip velocity correlations. Chong & Leung (1986) and Punwani, et al. (1976) compared published choking velocity correlations with published data. The reader is referred to these papers for a list of

additional choking velocity correlations. For a list of additional saltation velocity correlations, the reader is referred to the research of Rabinovich & Kalman (2008). Klinzing, et al. (1997) also provide a list of choking and saltation velocity correlations. Other correlations important to the design of pneumatic conveying systems pertain to the particle acceleration length and pressure drop.

2.5.1 Pressure Drop

For straight pipe sections, Modi, et al. (1978) compared published pressure drop correlations with published data and found Yang's theory (1977) to be within ±35%. The theory is presented Section 3.10 and also includes methods to calculate particle velocities, friction factors and acceleration lengths in both vertical and horizontal flow. For bends, Schuchart's (1969) correlation, presented in Appendix A, can be used.

2.5.2 Particle Acceleration Length

The pressure drop in the particle acceleration region, where particles introduced in the flow accelerate to a steady state velocity, can differ significantly from the pressure drop once steady state is reached (Klinzing, et al., 1997). Rose & Duckworth (1969) developed a correlation to calculate the particle acceleration length L_a after performing an extensive dimensionless analysis, and conducting experiments at different angles of inclination. The correlation is given by

$$\frac{L_a}{D_{pipe}} = 6\left[\left(\frac{\dot{M}_p}{\rho_g g^{1/2} D_{pipe}^{5/2}}\right)\left(\frac{D_{pipe}}{D_p}\right)^{1/2}\left(\frac{\rho_p}{\rho_g}\right)\right]^{1/3}$$

Equation 2-45

Two additional correlations, presented by Klinzing, et al. (1997), are given by

$$\frac{L_a}{D_{pipe}} = 0.527\left(\frac{D_{pipe}}{D_p}\right)^{-1.26}(1+z)\left(\frac{\rho_g D_{pipe} U_g}{\mu_g}\right)$$

Equation 2-46

and

$$L_a = e^{3.32}\left(\frac{D_p}{D_{pipe}}\right)^{0.953} z^{-0.0912}\left(\frac{\rho_g}{\rho_p}\right)^{-0.924}$$

Equation 2-47

For the above correlations, the units of the coefficients were not given in the literature reviewed. It is also unclear if they were formulated for horizontal or vertical conveying.

Plan of Development

Following this literature review, the theories used to complete this project are presented. The test facility concept designs, DAC system and a design phase uncertainty analysis is then presented together with the approach taken to arrive at a revised final facility system layout and instrumentation design. Design calculations performed (or theoretical models developed) are then presented. A short chapter regarding the construction of the prototype facility is then presented, before presenting the analysis and results of tests conducted. A revised system layout and instrumentation design is then presented with recommendations for a proposed final test facility. Finally, a summary of the work completed and conclusions are made.

3 Theory

There are various flow regimes associated with gas-particle flows. Figure 1-2 and Figure 1-3 in Section 1.1 illustrate these flow regimes, as defined in Fan & Zhu (1998) and Rabinovich & Kalman (2011) respectively. These flow regimes have traditionally been categorised into the two main groups mentioned in Section 1.1, namely, dilute and dense flow (Rabinovich & Kalman, 2011). In dilute flow, particle motion is controlled by gas-particle interactions, whereas particle-particle interactions are dominant in dense flow (Crowe, et al., 1998). These classifications are important when analysing gas-particle flows mathematically, as a number of assumptions can be made for dilute flow which cannot be made for dense flow. The following chapter presents the theory behind the models developed for this project, which includes the justification of assumptions made.

3.1 Gas-Particle Interactions

Coupling is the exchange of properties between the continuous and dispersed phases in two-phase flow through phase interaction (Crowe, et al., 1998). In PF conveying, the gas and particle phases are considered as the continuous and dispersed phases respectively. Mass, momentum, and energy couplings exist, and can be one-way or two-way couplings. One-way coupling is when the flow of one phase affects the other phase with no reverse effect, whereas two-way coupling implies a mutual effect (Crowe, et al., 1998). Figure 3-1 illustrates the effects of one and two-way coupling between the temperatures T and velocities u of the continuous and dispersed phases in two-phase flow.

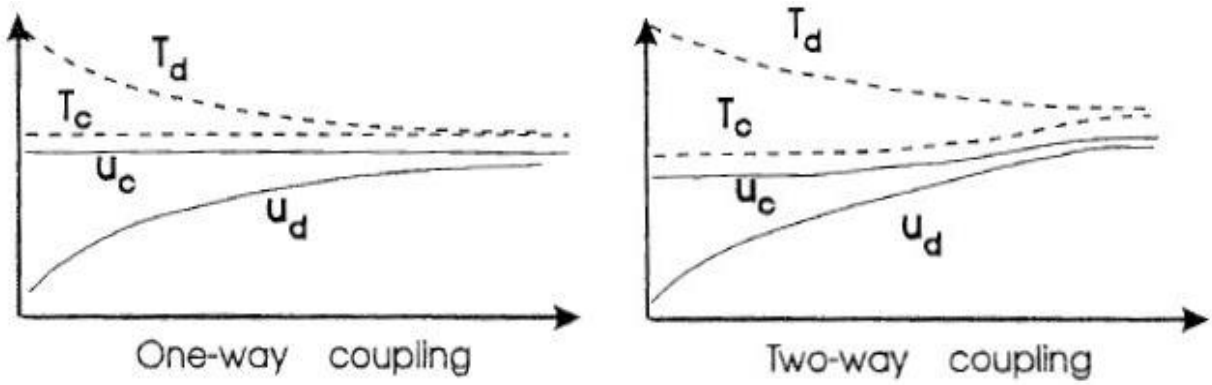

Here subscripts c and d indicate the continuous and dispersed phase respectively

Figure 3-1 – Coupling Effects, taken from Crowe, et al. (1998)

If particle loading and the mass exchange between phases are low then mass coupling can be neglected (Crowe, et al., 1998). This is the case during PF conveying provided that the moisture content of the PC is negligible. Also, if there are no phase changes due to latent heat and mass coupling effects are negligible, then energy coupling effects can also be neglected (Crowe, et al., 1998). Therefore, the energy couplings during PF conveying can be considered negligible, provided the conveying temperatures are lower than the devolitisation temperature of the coal being conveyed.

Momentum is transferred through mass transfer as well as via drag and lift forces (Crowe, et al., 1998). Literature regarding drag relevant to PF conveying is presented in the following section. The effects of lift forces are considered negligible and the complexities associated with it are not covered in this project.

3.2 Drag Force

For a particle in a uniform pressure field, where there is no change in the relative velocity between phases, the steady state drag force acting on the particle is (Crowe, et al., 1998)

$$F_d = \frac{1}{2}\rho_g C_{D\infty} A|u_g - u_p|(u_g - u_p)$$

Equation 3-1

where A is the projected area in the direction of the relative velocity in m^2. $C_{D\infty}$ is the drag coefficient for a single particle, or an infinitely dilute mixture as defined by Klinzing, et al. (1997), in a quiescent environment.

$C_{D\infty}$ depends on the particle shape and orientation, the relative particle Reynolds number, Mach number effects, as well as turbulence and particle rotation (Crowe, et al., 1998).

3.2.1 Reynolds Number Effects

The relative particle Reynolds number is defined as

$$Re_r = \frac{\rho_g D_p (u_g - u_p)}{\mu_g}$$

Equation 3-2

Where D_p is the mean particle diameter in meter and μ_g is the dynamic viscosity of the gas in kg/ms.

According to Klinzing, et al. (1997), the variation of $C_{D\infty}$ with Re_r is as follows:

1. For creeping flow ($Re_r < 2$), Stokes' law applies

$$C_{D\infty} \cong 24 Re_r^{-1}$$

Equation 3-3

2. For intermediate flow ($0.5 < Re_r < 500$), Allen's equation applies

$$C_{D\infty} \cong 18.5 Re_r^{-0.6}$$

Equation 3-4

3. For fully developed flow ($500 < Re_r < 2{\times}10^5$), Newton's law applies

$$C_{D\infty} \cong 0.44$$

Equation 3-5

4. For turbulent flow ($Re_r \geq 2\times10^5$)

$$C_{D\infty} \cong 0.1, \text{ increasing slowly with } Re_r$$

Equation 3-6

The standard drag curve, which represents the relationship between $C_{D\infty}$ and Re_r is illustrated in Figure 3-2 with shape factor ψ effects for non-spherical particles. According to preliminary calculations and results from Van der Merwe (2014), Re_r lies within the Stokes and Intermediate flow ranges for PF conveying.

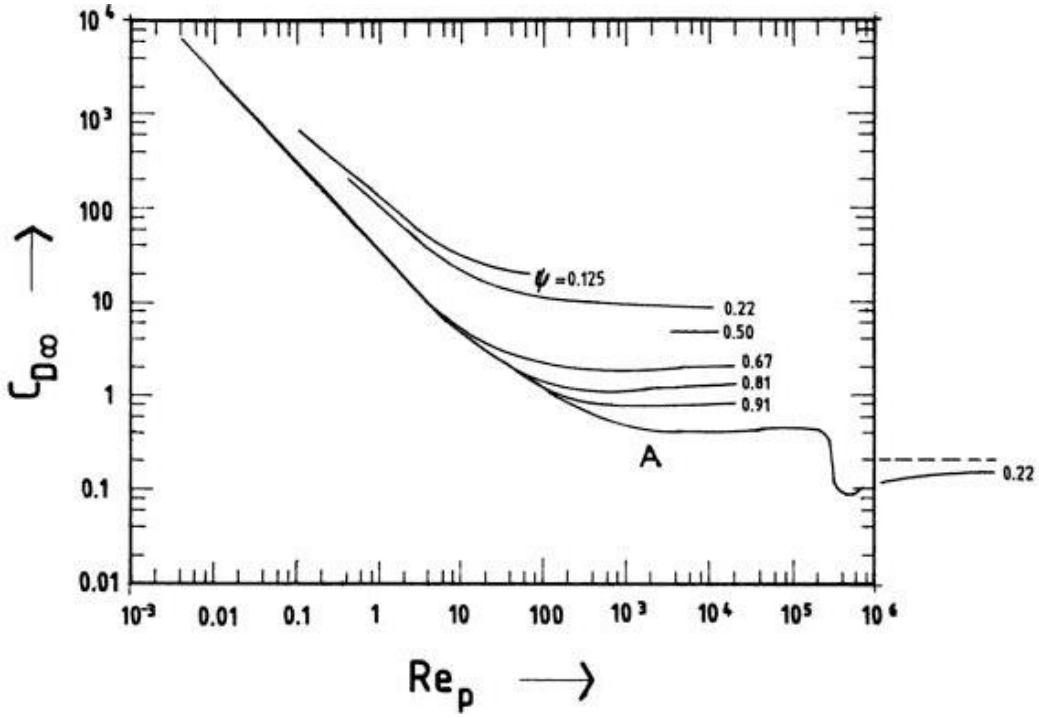

Here Re_p is the relative particle Reynolds number

Figure 3-2 - Drag coefficient vs. Relative Reynolds number, taken from Klinzing, et al. (1997)

3.2.2 Shape Effects

Various shape factors ψ are available and applied differently in literature. One such factor is presented in Section 3.7.

3.2.3 Mach Number Effects

The relative Mach number is defined as

$$M_r = \frac{u_g - u_p}{c}$$

Equation 3-7

where c is the speed of sound in the gas phase in m/s.

According to Crowe, et al. (1998), Mach number effects become significant when M_r reaches 0.6. This requires a relative velocity around 230 m/s at PF conveying temperature conditions, which is much greater than the velocities associated with PF conveying. Therefore, Mach number effects during PF conveying can be considered negligible and the flow can be considered incompressible during analysis.

3.2.4 Effects of Turbulence

Crowe et al. (1998) present correlations which can be used to account for the effects of turbulence, but warns against their use as a result of various discrepancies. Crowe, et al. (1998) further reiterate that more detailed experiments need to be conducted to better understand the effects of turbulence. The use of the standard drag curve, neglecting turbulence effects, is therefore suggested.

3.2.5 Effects of Rotation

Crowe, et al. (1998) discuss previous studies on the effects of particle rotation. The general findings indicate that rotation doesn't affect $C_{D\infty}$ for smooth particles and for relative Reynolds numbers of the order of unity.

3.2.6 Voidage Effects

For a mobile particle in a mixture of voidage α_g, Wen & Yu (1966) proposed that $C_{D\infty}$ be corrected by a factor of $\alpha_g^{-4.7}$ to give

$$C_D = C_{D\infty}\alpha_g^{-4.7}$$

Equation 3-8

Equation 3-8 correctly predicts that the drag force increases with increased loading. Also, because it was developed empirically, it is useful for the analysis of dilute gas-particle flows where particle-particle interactions are neglected, as it takes into account any particle-particle collisions that do occur.

3.3 Pressure Gradient and Buoyancy Forces

There exists a local pressure gradient during pneumatic conveying which produces a net pressure force in the direction of the pressure gradient (Crowe, et al., 1998). Crowe, et al. (1998) show that the net pressure force acting on a particle includes the buoyancy force. Crowe, et al. (1998) further argue that pressure gradient forces and therefore the buoyancy force can be neglected in gas-particle flows, as the ratio of the gas and particle densities is of the order 10^{-3}.

3.4 Virtual Mass and Basset Forces

The virtual mass effect and the Basset force are forces that arise due to the acceleration of the relative velocity between phases (Crowe, et al., 1998). These forces are mentioned here because of their

importance in two phase flow. However, they will not be discussed further, as they can be neglected for gas-particle flows where the ratio of gas and particle densities is of the order 10^{-3} (Crowe, et al., 1998).

3.5 Body Forces

Gravity and buoyancy acting between phases are applicable body forces to PF conveying. However, it is worth noting that other body forces may become important depending on the application, e.g. Coulomb forces become important when an electrostatic precipitator is used for gas-particle separation (Crowe, et al., 1998).

3.6 Friction Forces

Friction occurs as a result of gas-wall and particle-wall interactions during PF conveying. These interactions are complex and therefore empirical correlations for gas and solids friction factors are generally used with Equation 3-9 and Equation 3-10 in mathematical models. For gas-wall interactions

$$F_{fg} = \frac{1}{2}\,\rho_g \lambda_g A_s u_g^2$$

Equation 3-9

and for particle-wall interactions (note the bulk density is used)

$$F_{fp} = \frac{1}{2}\,\overline{\rho_p} \lambda_p A_s u_p^2$$

Equation 3-10

where λ represents the respective phase friction factors and A_s is the surface (or wall) contact area in m^2.

For turbulent flow in tubes (i.e. $Re > 10\,000$), the Darcy-Weisbach gas friction factor λ_{Dg} can be calculated using the implicit Colebrook equation (Cengel, 2006). Note $\lambda_D = 4\lambda$.

$$\frac{1}{\sqrt{\lambda_{Dg}}} = -2\log\left(\frac{\varepsilon/D_{pipe}}{3.7} + \frac{2.51}{Re\sqrt{\lambda_{Dg}}}\right)$$

Equation 3-11

Here, $\varepsilon_r = \varepsilon/D_{pipe}$ is the relative pipe roughness and the pipe Reynolds number is defined as

$$Re = \frac{\rho_g D_{pipe} U_g}{\mu_g}$$

Equation 3-12

Yang (1974) proposed correlations for estimating the solid friction factor λ_{pD} in both horizontal and vertical conveying. For horizontal conveying

$$\lambda_{Dph} = 0.117\frac{(1-\alpha_g)}{\alpha_g^3}\left[(1-\alpha_g)\frac{Re_{t0}}{Re_r}\frac{u_g}{\sqrt{gD_{pipe}}}\right]^{-1.15}$$

Equation 3-13

and for vertical conveying

$$\lambda_{Dpv} = 0.0206\frac{(1-\alpha_g)}{\alpha_g^3}\left[(1-\alpha_g)\frac{Re_{t0}}{Re_r}\right]^{-0.869}$$

Equation 3-14

where Re_{to} is the Reynolds number at the single particle terminal velocity (see Section 3.7) and g is the acceleration due to gravity. The correlation for vertical conveying was later updated in Yang (1978), and is given for dilute phase transport as

$$\lambda_{Dpv} = 0.0126\frac{(1-\alpha_g)}{\alpha_g^3}\left[(1-\alpha_g)\frac{Re_{t0}}{Re_r}\right]^{-0.979}$$

Equation 3-15

It is worth noting that Dhodapkar & Zaltash (1989) observed the solids friction factor to be significantly higher in vertical conveying than horizontal conveying.

3.7 Terminal Velocity

The terminal velocity of a single particle u_{t0} in m/s can be determined by equating drag and buoyancy forces with gravity to give (Klinzing, et al., 1997)

$$u_{t0} = \left(\frac{4}{3}\frac{D_p}{C_{D\infty}}\frac{\rho_p - \rho_g}{\rho_g}g\right)^{\frac{1}{2}}$$

Equation 3-16

The Reynolds number at the single particle terminal velocity is defined as

$$Re_{t0} = \frac{\rho_g D_p u_{t0}}{\mu_g}$$

Equation 3-17

Substituting the values for $C_{D\infty}$ given in Equation 3-3 to Equation 3-6 into Equation 3-16, and using Re_{t0} in place of Re_r, the corresponding terminal velocities for spherical particles are obtained:

1. For $Re_{t0} < 2$

$$u_{t0} = \frac{D_p^2(\rho_p - \rho_g)g}{18\mu_g}$$

Equation 3-18

2. For $0.5 < Re_{t0} < 500$

$$u_{t0} = \left(\frac{8}{111}\frac{D_p^{1.6}(\rho_p - \rho_g)g}{\mu_g^{0.6}\rho_g^{0.4}}\right)^{\frac{5}{7}}$$

Equation 3-19

3. For $500 < Re_{t0} < 2{\times}10^5$

$$u_{t0} = \left(\frac{100}{33}\frac{D_p(\rho_p - \rho_g)g}{\rho_g}\right)^{0.5}$$

Equation 3-20

4. For $Re_{t0} \geq 2{\times}10^5$

$$u_{t0} = \left(\frac{40}{3}\frac{D_p(\rho_p - \rho_g)g}{\rho_g}\right)^{0.5}$$

Equation 3-21

The above equations are valid for spherical particles. For non-spherical particles, the following correlation can be used to calculate the terminal velocity (Klinzing, et al., 1997)

$$\frac{u_{t\Psi}}{u_{t1}} = 0.843\log\left(\frac{\Psi}{0.065}\right)$$

Equation 3-22

where $u_{t\Psi}$ is the terminal velocity of a particle with sphericity (or shape factor) of Ψ and u_{t1} is the terminal velocity of a spherical particle of the same volume.

Here, the shape factor is given by

$$\Psi = \frac{surface\ area\ of\ sphere\ with\ same\ volume\ as\ particle}{surface\ area\ of\ particle} = \frac{\pi D_V^2}{A_s}$$

Equation 3-23

where D_V is the equivalent volume diameter of a particle.

3.8 Continuous Phase Equations

In the analysis of the continuous phase it would be ideal to solve the mass, momentum and energy conservation equations, taking into account the boundary conditions imposed by every single particle in the flow field (Crowe, et al., 1998). However, this would require the grid size to be at least as small as the smallest particle in the field, and would therefore require vast computational power (Crowe, et al., 1998). Averaging procedures are therefore used abundantly in the development of numerical models. Noting that mass and energy couplings can be considered negligible during PF conveying, as mentioned in

Section 3.1, this section presents the volume averaged momentum conservation equation for a quasi-one-dimensional flow as given in Crowe, et al. (1998). Literature on volume averaging and the full derivation of the momentum conservation equation can be found in Crowe, et al. (1998).

3.8.1 Momentum Conservation

For the quasi-one-dimensional control volume (CV) presented in Figure 3-3 and the assumptions listed thereafter, Crowe, et al. (1998) presents the continuous phase momentum conservation equations for multi-phase flows given in Equation 3-24 and Equation 3-25. As these equations are valid for multi-phase and not just gas-particle flows, the subscript c is used instead of g.

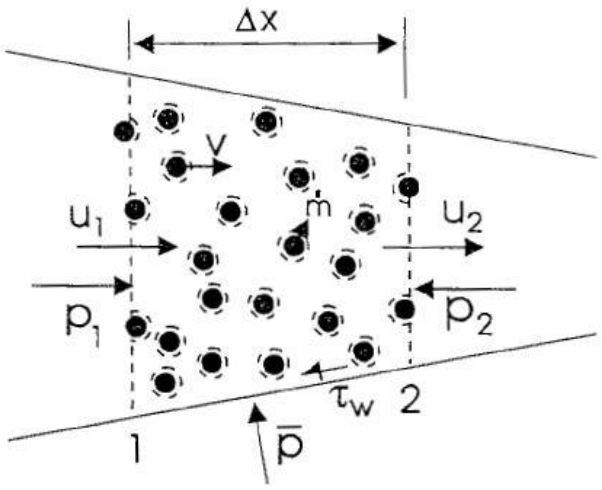

Figure 3-3 – Quasi-one dimensional flow in a duct, taken from Crowe, et al. (1998)

The following assumption are made:

1. All particles/ droplets are spherical and are of the same size.
2. The particle/ droplet velocity is the average velocity over the CV.
3. Mass transfer between the continuous phase and all particles/ droplets is at the same rate.
4. The forces acting on the continuous phase are drag and boundary pressure forces, wall shear stress, and gravity.
5. Mach number, turbulence, and rotation effects on particle/ droplet drag are neglected.
6. Virtual mass and Basset force effects on particle/ droplet motion are neglected.

The momentum equation in difference form is

$$V\Delta_t(\overline{\rho_c}u) + \Delta(\overline{\rho_c}u^2A) = -\alpha_c\bar{A}\Delta p - N\dot{m}v + \beta_V V(v-u) - \tau_w P\Delta x + \overline{\rho_c}\vec{g}V$$

Equation 3-24

and in differential form

$$\frac{\partial}{\partial t}(\overline{\rho_c}u) + \frac{1}{A}\frac{\partial}{\partial x}(\overline{\rho_c}u^2 A) = -\alpha_c\frac{\partial p}{\partial x} - n\dot{m}v + \beta_V(v-u) - \frac{1}{R_h}\tau_w + \overline{\rho_c}\vec{g}$$

Equation 3-25

Where:

V is the volume of the CV in m^3.

Δ_t is the difference operator defined as $\Delta_t(\,) = \Delta(\,)/\,\Delta t$.

u is the continuous phase velocity in m/s.

A is the cross section area of the CV in m^2.

$\bar{A}$ is the average cross section area of the CV in m^2.

Δp is the pressure difference across the CV in Pa.

v is the dispersed phase velocity in m/s.

τ_w is the wall shear stress in Pa.

P is the average perimeter of the CV in m.

Δx is the length of the CV in m.

R_h is the average hydraulic radius of the CV in m.

$\vec{g}$ is the acceleration due to gravity in the flow direction, which will be zero for horizontal flow and negative for upward flow.

$\overline{\rho_c}$ is the bulk density of the continuous phase and is equal to the product of the continuous phase volume fraction α_c and density ρ_c respectively.

$\beta_V V(v-u)$ and $\beta_V(v-u)$ are the respective momentum source terms due to drag interaction with the dispersed phase. These terms account for the number of particles within the CV.

$N\dot{m}v$ and $n\dot{m}v$ are the respective momentum source terms due to mass transfer between phases. The negative sign indicates evaporation of the dispersed phase. These terms are assumed to be negligible for PF conveying.

3.9 Dispersed Phase Equations

The dispersed phase is generally analysed using the Lagrangian, or the Eulerian approach (Crowe, et al., 1998). This section provides some insight into these approaches and discusses their respective advantages and disadvantages. A summary of the equations presented in this and the preceding section is also given.

3.9.1 Lagrangian Approach

The Lagrangian approach involves the tracking or calculation of the velocity, mass and temperature over time (Crowe, et al., 1998) for each and every particle. Crowe, et al. (1998) present two methods which follow the Lagrangian approach, namely, the trajectory method and the discrete element approach. The approaches are not too different and are therefore not presented here separately. In essence, the trajectory method is a simplified discrete element approach applicable for dilute flow only. The principle on which both approaches are based is therefore presented.

The particle equation of motion (EOM) is solved for each particle, or a "parcel of particles" (Crowe, et al., 1998), at time steps using a preferred integration scheme. The rotation, temperature and mass of each particle/ parcel are subsequently calculated at each time step using their respective time based equations. Noting that mass and energy couplings and rotation effects on particle drag can be considered negligible during PF conveying as mentioned in Sections 3.1 and 3.2.5 respectively, only the particle EOM is presented here. The particle/ parcel EOM is simply

$$\frac{\delta \vec{v}}{\delta t} = \frac{\sum \vec{F}}{m}$$

Equation 3-26

where $\sum \vec{F}$ is the sum of the fluid, friction and body forces, and m is the mass of the particle or parcel of particles.

The fluid forces considered, size of parcel, and the integration scheme is chosen depending on the level of accuracy desired (Crowe, et al., 1998). Furthermore, the initial conditions used in the integration scheme are problem dependant (Crowe, et al., 1998). Figure 3-4 shows an example of distributed parcels in a 2-D discretised spray field.

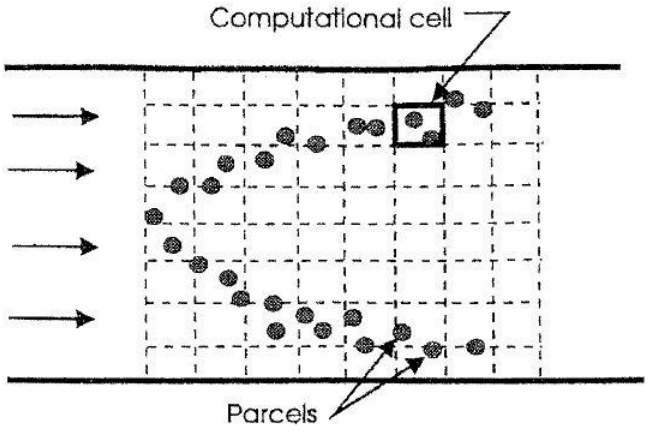

Figure 3-4 – Parcels in a spray field, taken from Crowe, et al. (1998)

3.9.2 Eulerian Approach

The Eulerian approach treats the dispersed phase as a fluid which behaves like a continuum (Crowe, et al., 1998). Averaging procedures are therefore used in deriving equations suitable for numerical modelling. The approach is synonymous to the approach followed in the derivation of the momentum conservation for the continuous phase, which also followed the Eulerian approach. In literature, the approach is commonly called the *two-fluid*, or the *Eulerian-Eulerian* approach.

Crowe, et al. (1998) presents the two-fluid dispersed phase momentum conservation equation for multi-phase flows given in Equation 3-27 and Equation 3-28. As these equations are valid for multi-phase and not just gas-particle flows, the subscript d is used instead of p. The quasi-one-dimensional CV is given in Figure 3-5 and the assumptions are listed thereafter.

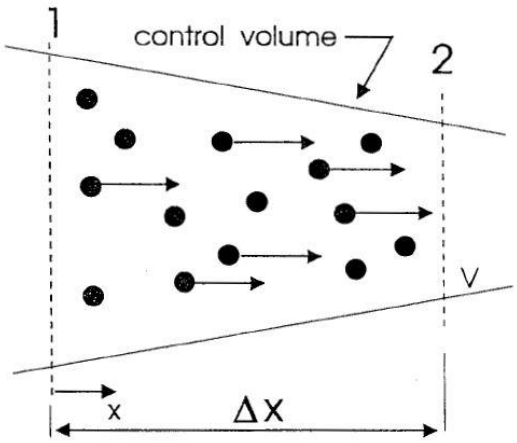

Figure 3-5 – Particles in a quasi-one-dimensional duct, taken from Crowe, et al. (1998)

The following assumptions are made:

1. All particles/ droplets are spherical and are of the same size.
2. The particle/ droplet velocity is the average velocity over the CV.
3. Mass transfer between the continuous phase and all particles/ droplets is at the same rate.
4. The forces acting on the dispersed phase are drag and pressure gradient forces, friction, and gravity.
5. Mach number, turbulence, and rotation effects on particle/ droplet drag are neglected.
6. Virtual mass and Basset force effects on particle/ droplet motion are neglected.

The momentum equation in difference form is

$$V\Delta_t(\overline{\rho_d}v) + \Delta(\overline{\rho_d}v^2A) = -\alpha_d\bar{A}\Delta p + N\dot{m}v + \beta_V V(u-v) - \frac{1}{2}\lambda_d\overline{\rho_d}v|v|P\Delta x + \overline{\rho_d}\vec{g}V$$

Equation 3-27

and in differential form

$$\frac{\partial}{\partial t}(\overline{\rho_d}v) + \frac{1}{A}\frac{\partial}{\partial x}(\overline{\rho_d}v^2A) = -\alpha_d\frac{\partial p}{\partial x} + n\dot{m}v + \beta_V(u-v) - \frac{1}{2R_h}\lambda_d\overline{\rho_d}v|v| + \overline{\rho_d}\vec{g}$$

Equation 3-28

Here, λ_d is the dispersed phase friction factor which can be determined using the correlations presented in Section 3.6.

$\overline{\rho_d}$ is the bulk density of the dispersed phase and is equal to the product of the dispersed phase volume fraction α_d and density ρ_d respectively.

$N\dot{m}v$ and $n\dot{m}v$ are the respective momentum source terms due to mass transfer between phases. Here, the sign is positive and indicates evaporation of the dispersed phase. These terms are zero for PF conveying.

3.9.3 Mixture Equations

Mixture equations can be obtained by adding the continuous and two-fluid dispersed equations, and defining a mixture velocity (Crowe, et al., 1998). The mixture velocity is defined as

$$\rho_m U = \overline{\rho_d}v + \overline{\rho_c}u$$

Equation 3-29

The momentum conservation equation in difference form is then given by

$$V\Delta_t(\rho_m U) + \Delta[A(\overline{\rho_d}v^2 + \overline{\rho_c}u^2)] = -\bar{A}\Delta p - \frac{1}{2}\lambda_d\overline{\rho_d}v|v|P\Delta x - \frac{1}{2}\lambda_c\rho_c u|u|P\Delta x + \rho_m\vec{g}V$$

Equation 3-30

and in differential form

$$\frac{\partial}{\partial t}(\rho_m U) + \frac{1}{A}\frac{\partial}{\partial x}[A(\overline{\rho_d}v^2 + \overline{\rho_c}u^2)] = -\frac{\partial p}{\partial x} - \frac{1}{2R_h}\lambda_d\overline{\rho_d}v|v| - \frac{1}{2R_h}\lambda_c\rho_c u|u| + \rho_m\vec{g}$$

Equation 3-31

Note that the continuous phase wall shear stress term has been replaced by the equivalent friction term, where λ_c is the continuous phase friction factor.

3.9.4 Comparison

The Lagrangian approach is applicable for both dilute and dense flows, and is easy to implement for dilute flows using the trajectory method according to Crowe, et al. (1998). Advantages of the Lagrangian approach are that it correctly models the parabolic nature of dilute flows (Crowe, et al., 1998) and an effective phase viscosity and thermal conductivity need not be selected (Crowe, et al., 1998), as they can be calculated at each time step. Furthermore, if each and every particle is accounted for, *"the discrete*

element approach provides a direct numerical simulation" (Crowe, et al., 1998). However, this would require vast computational power and is therefore not always feasible.

The advantages of the two-fluid approach are that it is not limited by the number of particles in a system (Crowe, et al., 1998) and it can be combined with the continuous phase equations to form mixture equations. It also has the added benefit of being compatible with empirical friction factor correlations, whereas the Lagrange approach requires complex modelling of particle-wall interactions. These models are available in literature, however, they were considered too complex for the scope of this project.

3.10 Yang's Unified Design Theory

The following section contains a proposed design method for pneumatic conveying systems as presented by Yang (1977). The theory consists of semi-empirical correlations which were developed over a series of papers by Yang and his colleagues.

3.10.1 Volume Analysis

Assuming spherical particles and using the effective mass of the particles, the number of particles in a differential section of pipe length δL is given as

$$\delta N = \frac{\delta M_p}{(\rho_p - \rho_g)\left(\frac{\pi D_p^3}{6}\right)}$$

Equation 3-32

or

$$\delta N = \frac{6\dot{M}_p \delta L}{(\rho_p - \rho_g)\pi D_p^3 u_p}$$

Equation 3-33

where δM_p is the effective mass of the particles in δL. The voidage in section δL is then given by

$$\alpha_g = 1 - \frac{4\dot{M}_p}{(\rho_p - \rho_g)\pi D_{pipe}^2 u_p}$$

Equation 3-34

3.10.2 Force Balance

From Newton's Second Law, the acceleration of the particles is equal to the sum of the forces acting on the particles, divided by the mass of the particles

$$\delta M_p \frac{\delta u_p}{\delta t} = \delta F_d - \delta F_g - \delta F_f$$

Equation 3-35

where the gravitational force term may be neglected for horizontal conveying. The drag force on δN particles in δL is

$$\delta F_d = \frac{3}{4}\left(C_{D\infty}\alpha_g^{-4.7}\right)\frac{\rho_g\left(u_g - u_p\right)^2}{\left(\rho_p - \rho_g\right)D_p}\delta M_p$$

Equation 3-36

The gravitational force on δN particles in δL is

$$\delta F_g = \delta M_p g$$

Equation 3-37

and the friction force on δN particles in δL is

$$\delta F_f = \frac{\lambda_{Dp}u_p^2}{2D_{pipe}}\delta M_p$$

Equation 3-38

3.10.3 Particle Velocities

Equation 3-36 to Equation 3-38 can be substituted into Equation 3-35 to give the vertical particle velocity at steady state

$$u_p = u_g - u_{t0}\sqrt{\left(1 + \frac{\lambda_{Dp}u_p^2}{2D_{pipe}}\right)\alpha_g^{4.7}}$$

Equation 3-39

and the horizontal particle velocity at steady state

$$u_p = u_g - u_{t0}\sqrt{\frac{\lambda_{Dp}u_p^2}{2D_{pipe}}\alpha_g^{4.7}}$$

Equation 3-40

3.10.4 Friction Factors

The solid friction factor in vertical conveying can be estimated using empirical correlations. For vertical conveying

$$\lambda_{Dpv} = 0.0206\frac{\left(1-\alpha_g\right)}{\alpha_g^3}\left[\left(1-\alpha_g\right)\frac{Re_{t0}}{Re_r}\right]^{-0.869}$$

Equation 3-41

and for horizontal conveying

$$\lambda_{Dph} = 0.117\frac{(1-\alpha_g)}{\alpha_g^3}\left[(1-\alpha_g)\frac{Re_{t0}}{Re_r}\frac{u_g}{\sqrt{gD_{pipe}}}\right]^{-1.15}$$

Equation 3-42

For vertical flow, Equation 3-34, Equation 3-39 and Equation 3-41 are solved simultaneously for the voidage, particle velocity and the solid friction factor at steady state. For horizontal flow, Equation 3-34, Equation 3-40 and Equation 3-42 are solved.

3.10.5 Acceleration Length

Noting that $\frac{\delta u_p}{\delta t} = \frac{u_p \delta u_p}{\delta L}$, Equation 3-36 to Equation 3-38 can be substituted into Equation 3-35 to estimate the particle acceleration length for vertical conveying

$$\Delta L_a = \int_{u_{p0}}^{u_p} \frac{u_p \delta u_p}{\frac{3}{4}C_{D\infty}\alpha_g^{-4.7}\frac{\rho_g(u_g-u_p)^2}{(\rho_p-\rho_g)D_p} - \left(g + \frac{\lambda_{Dp}u_p^2}{2D_{pipe}}\right)}$$

Equation 3-43

Here u_p is the steady state velocity and u_{p0} is calculated using Equation 3-34 at a voidage of 0.45. For horizontal conveying the gravitational term is dropped. Yang (1977) claims Equation 3-43 accurately predicts the acceleration length to $\pm$ 30%.

3.10.6 Pressure Drop

The total pressure drop in the conveying lines is given as

$$\Delta P_t = \Delta P_a + \Delta P_g + \Delta P_f$$

Equation 3-44

Here, ΔP_a is the pressure drop in the particle acceleration phase and can be calculated using Equation 3-45 for vertical conveying. For horizontal conveying the gravitational term is dropped.

$$\Delta P_a = \int_0^{L_a} \overline{\rho_p} g \delta L + \int_0^{L_a} \frac{\lambda_{Dg}\rho_g u_g^2}{2D_{pipe}}\delta L + \int_0^{L_a} \frac{\lambda_{Dp}\overline{\rho_p}u_p^2}{2D_{pipe}}\delta L + [(\overline{\rho_p}u_p^2)\ at\ L_a]$$

Equation 3-45

ΔP_g is the static head term beyond the acceleration region for a conveying length L, and is zero for horizontal conveying. For vertical conveying

$$\Delta P_g = \overline{\rho_p} L g$$

Equation 3-46

ΔP_f is the friction term beyond the acceleration region. For the gas and particle phases respectively

$$\Delta P_{fg} = \frac{\lambda_{Dg}\rho_g u_g^2 L}{2D_{pipe}}$$

Equation 3-47

and

$$\Delta P_{fp} = \frac{\lambda_{Dp}\overline{\rho_p} u_p^2 L}{2D_{pipe}}$$

Equation 3-48

3.10.7 Literature Comparison

Dhodapkar & Zaltash (1989) present the same equation as Yang for calculating the particle acceleration length. However, they advise that the lower limit of integration should be zero, which is justified by the particles having zero velocity in the flow direction at the entrance region.

Klinzing, et al. (1997) also present the same equation for calculating the particle acceleration length. Furthermore, they mention that the length can then be used to calculate the pressure drop within the region using steady state values. However, they advise that the method probably over-predicts the actual pressure drop due to the use of steady state values.

It is further noted that careful analysis of Equation 3-45 and Equation 3-31, i.e. Yang's (1977) pressure drop equation and the mixture momentum conservation equation, show that they are in fact the same.

Additionally, a particle EOM for vertical flow is derived in Appendix C and is given by

$$\frac{\delta u_p}{\delta t} = \frac{3}{4} C_{D\infty} \alpha_g^{-4.7} \frac{\rho_g (u_g - u_p)^2}{\rho_p D_p} - g\left(1 - \frac{\rho_g}{\rho_p}\right) - \frac{\lambda_{Dp} u_p^2}{2D_{pipe}}$$

Equation 3-49

where

$$\alpha_g = 1 - \frac{\rho_g U_g Z}{\rho_p u_p}$$

Equation 3-50

or

$$\alpha_g = 1 - \frac{4\dot{M}_p}{\rho_p \pi D_{pipe}^2 u_p}$$

Equation 3-51

For horizontal flow, the gravitational term is equal to zero.

The EOM is almost identical to that given by Equation 3-35 to Equation 3-38. The difference being the inclusion of buoyancy in the gravitational term and the use of the actual mass of the particles (and not the effective mass) in the derivation of α_g.

4 Test Facility Concept Design

This chapter presents the approach taken to arrive at a conceptual overall system layout for the final test facility, the dimensionless numbers used to scale the test rig and the prototype concept design. Additionally, the data acquisition and control (DAC) system, as well as a design phase uncertainty analysis performed on the instrumentation are presented.

4.1 Project Approach

This following section describes the approach taken to arrive at a conceptual overall system layout for the final test facility, together with a concept instrumentation design.

As a first step additional literature was reviewed regarding the different components normally found in pneumatic conveying systems such as particle feeders, cyclones etc., as well as a review of previous test facilities built by others. A list of references that were consulted during the study is given in Appendix Q.

An investigation was then conducted to determine the dimensionless numbers to be used when scaling the test rig from real world plant operating conditions. Data from Van der Merwe (2014) was analysed to determine typical power-plant flow conditions and the required test rig flow properties to obtain similarity were determined.

This was followed by the initial concept design phase. This included the iterative development of a functional analysis, a system layout or high-level piping and instrumentation diagram (P&ID), and a functional allocation for both open and closed loop options. The output of this phase included an initial system layout of a selected closed loop concept.

Additional literature was then reviewed where necessary and individual component models and process models for the complete system were created. The outputs of these models and practical aspects were then considered to refine the initial system layout, develop a physical concept layout, specify component sizes and identify potential equipment and instrumentation.

The next step would be to design, construct and commission a physical prototype facility of reduced complexity to demonstrate the operation of the most important components of the proposed final test facility. A decision was taken to design the prototype facility for pulverised fuel ash (PFA) (or fly ash) as a replacement material for PF. The reason for this is that a proper PF test facility would have to be designed according to stringent regulations in order to render it explosion-proof, which was deemed to be too expensive and overly complex for the scope of this project. The prototype test facility is therefore a less complex, non-explosion-proof plant, which can be used to demonstrate the functionality of the most important components such as the particle feed and extraction systems, together with the gas and particle mass flow control and measurement concepts. Where possible, components were sized to be

compatible with the final test facility design as well as to be explosion-proof, in order to be reusable and thereby reduce the cost of the final test facility.

The models developed for the final test facility were then adapted for the prototype facility and refined. The outputs of these models were used to determine component sizes and identify equipment and instruments for the prototype facility. When comparing these component sizes, equipment and instruments with those for the final facility, it was found that most of the items were compatible with both facilities. However, before procurement, a design phase uncertainty analysis was performed to estimate the quality of the data that would be acquired. The results of the analysis were deemed acceptable and the items then procured.

The DAC system was then developed and partially tested using existing laboratory apparatus. In parallel with this, the detailed design and construction of the prototype facility was completed in cooperation with a commercial engineering company.

The next phase of the project was to commission the facility. Calibration and testing procedures were drawn up and then executed, after which it was found that several modifications needed to be made to both the physical facility and the DAC system. These modifications were necessary to (i) improve the quality of the construction of the physical facility, (ii) correct design flaws and (iii) to improve the performance of the DAC system. After the modifications were completed, certain instruments were re-calibrated and after the commissioning was deemed successful, several tests were conducted at predetermined test conditions. The data gathered were then analysed and used to characterise the performance of the system.

Finally, the design of the final test facility and its associated instrumentation layout were revised and recommendations were made for future work.

4.2 Test Facility Scaling

This section presents the methodology and results obtained in the analysis of plant data and the determination of scaling parameters for power plant similarity tests. The inputs, methodology, and key findings of the analysis performed are presented. A copy of the detail analysis is given in Appendix L.

4.2.1 Inputs

Initially, data obtained from Van der Merwe (2014) were averaged and the values used as inputs for the analysis. Coal-fired power plants operate at low and high load conditions and therefore the minimum and maximum mass flow rate values are used in the analysis.

The particle size distribution of PC is evaluated using a Rosin-Rammler distribution (Van der Merwe, 2014). An example of an ideal particle size distribution (the middle line) as per ESKOM power plant specifications

is given in Figure 4-1. As per the Rosin-Rammler, a distribution which crosses the top line is considered too fine, and a distribution which crosses the bottom line is considered too coarse. At the extreme points it can be seen that 65% to 75% of the particles by mass should be less than or equal to 75µm, and 99% to 99.8% less than or equal to 300µm. The minimum D_p was therefore taken to be 37µm, which is the minimum measurable size using a Tyler Standard sieve (Fan & Zhu, 1998) and the maximum D_p was taken to be equal to 300µm. A particle density ρ_p of 1550kg/m3 was used for PC (Van der Merwe, 2014).

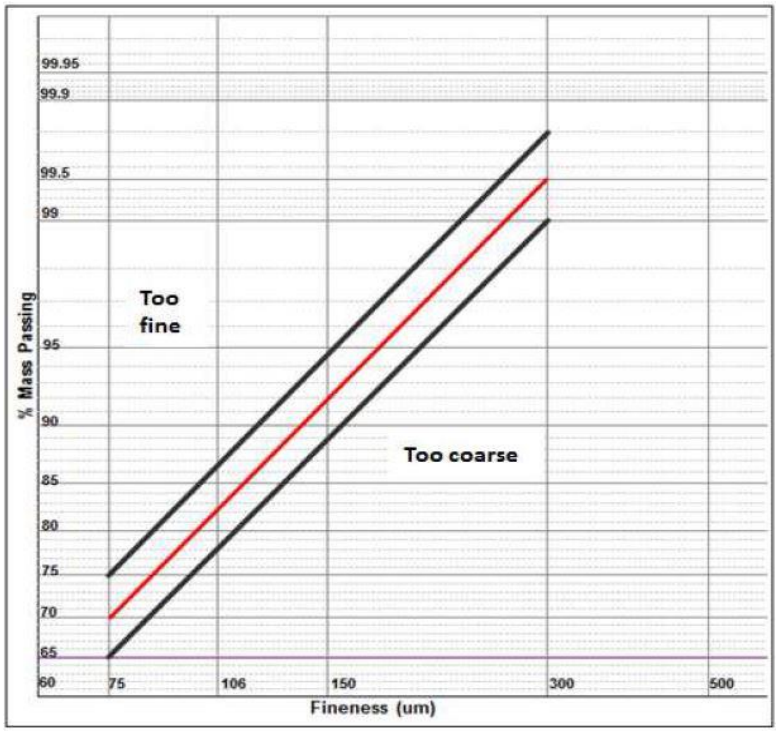

Figure 4-1 – Rosin-Rammler of ideal PC PSD, taken from Van der Merwe (2014)

Table 4-1 lists the inputs used to perform the analysis

Property	**Symbol**	**Minimum**	**Maximum**	**Unit**
Air pressure	P_g	85		kPa
Air temperature	T_g	90		°C
Particle density	ρ_p	1550		kg/m^3
Pipe Diameter	D_{pipe}	450		mm
Particle Diameter	D_p	37	300	µm
Air Mass Flow Rate	$\dot{M}_g$	3.12	3.93	kg/s
Particle Mass Flow Rate	$\dot{M}_p$	1.28	2.50	kg/s

Table 4-1 – Plant flow properties analysis inputs

4.2.2 Methodology

The analysis assumes the flow is incompressible and fully developed.

To determine a range of flow properties, the subsequent calculations were performed for the minimum D_p at low load conditions, and for the maximum D_p at high load conditions. Going forward these will be referred to as the lower limit and the upper limit values.

The gas density ρ_g was calculated using the ideal gas law

$$\rho_g = \frac{P_g}{R_g T_g}$$

Equation 4-1

where $R_g = 287.058 \frac{J}{kgK}$ is the specific gas constant for air.

The gas dynamic viscosity μ_g was calculated using Sutherland's formula, given by Equation 4-2 (Sutherland, 1893).

$$\mu_g = \mu_{ref} \left(\frac{T_g}{T_{ref}}\right)^{\frac{3}{2}} \left(\frac{T_{ref} + S}{T_g + S}\right)$$

Equation 4-2

where $\mu_{ref} = 1.716 \times 10^{-5} \frac{kg}{ms}$ is the gas dynamic viscosity at a reference temperature $T_{ref} = 273.15K$ and $S = 110.4K$ is Sutherland's constant

The loading $z = Z$ was calculated using Equation 2-4.

The superficial gas and particle velocities $U_g \; and \; U_p$ were calculated using Equation 2-6 and Equation 2-7 respectively.

The particle terminal velocity u_{t0} was calculated using Equation 3-18 or Equation 3-19, depending on the Reynolds number at the single particle terminal velocity Re_{t0}, which was calculated using Equation 3-17.

The slip velocity for horizontal flow u_{rh} was calculated using the Hinkle correlation (Equation 2-12).

The slip velocity for vertical flow u_{rv} was then calculated, assuming that it is equal to the single particle terminal velocity u_{t0}.

Equation 4-3 and Equation 4-4, derived in Appendix C, were then used to calculate the volume fractions $\alpha_p \; and \; \alpha_g$ for both horizontal and vertical flow.

$$\alpha_p = \frac{\rho_g U_g Z}{\rho_p u_p}$$

Equation 4-3

$$\alpha_g = 1 - \frac{\rho_g U_g Z}{\rho_p u_p}$$

Equation 4-4

The saltation and choking velocities $U_{salt}\ and\ U_{gc}$ were then calculated using the Rizk correlation (Equation 2-21) and Yang's choking theory (Equation 2-41 and Equation 2-42) respectively.

The pipe Reynolds number Re was calculated using Equation 3-12.

An investigation (See Appendix L) was then conducted to determine the dimensionless numbers to use for test rig scaling. It was found that the particle Reynolds number Re_p, the particle Froude number Fr_p, and the inertia parameter ψ were the most important numbers to consider when scaling to achieve similarity with South African coal-fired power plants. Re_p, Fr_p and ψ are given by Equation 4-5 to Equation 4-7.

$$Re_p = \frac{\rho_g D_p U_g}{\mu_g}$$

Equation 4-5

$$Fr_p = \frac{U_g}{\sqrt{g D_p}}$$

Equation 4-6

$$\psi = \frac{\rho_p D_p U_g}{\mu_g}$$

Equation 4-7

A matrix of test rig flow properties required to satisfy similarity of corresponding power plant properties was then generated and is given in Appendix O. Initially, $Re_p, Fr_p\ and\ \psi$ were evaluated, given a U_g of 24, 26, 28 and 30m/s and for representative particle diameters of 37, 150 and 300µm. The required test rig operating pressures, gas velocities and particle diameters, given operating temperatures and particle densities, were then calculated simultaneously such that they collectively satisfy the values of the dimensionless numbers calculated.

4.2.3 Results

Table 4-2 and Table 4-3 lists key results of the analysis.

Property	Symbol	Unit	Lower Limit	Upper Limit
Pipe Reynolds Number	Re		4.143 x 10^5	5.219 x 10^5
Saltation Velocity	U_{salt}	m/s	12.045	15.786
Choking Velocity	U_{gc}	m/s	2.801	4.203
Superficial Gas Velocity	U_g	m/s	24.059	30.305

Table 4-2 – Flow properties of a typical PF pipeline in a South African coal-fired power plant flow

INPUTS		OUTPUTS		
$\boldsymbol{D_p\ (\mu m)}$	$\boldsymbol{U_g\ (m/s)}$	$\boldsymbol{Re_p}$	$\boldsymbol{Fr_p}$	$\boldsymbol{\psi}$
37	24	33.984	1260	64600
37	26	36.816	1365	69990
37	28	39.648	1470	75370
37	30	42.48	1575	80750
150	24	137.773	625.756	261900
150	26	149.254	677.903	283700
150	28	160.736	730.049	305500
150	30	172.217	782.195	327400
300	24	275.547	442.477	523800
300	26	298.509	479.786	567400
300	28	321.471	516.223	611100
300	30	344.433	553.096	654700

Table 4-3 – Dimensionless flow properties of a typical South African coal-fired power plant

4.2.4 Discussion

From Table 4-2, it can be deduced that the gas phase is in the turbulent flow regime. It is therefore appropriate to use the Colebrook equation (Equation 3-11) to evaluate the gas friction factor in these pipelines.

Furthermore, Table 4-2 provides the typical superficial gas velocities found in a PF pipeline in South African coal-fired power plants. Ideally, similarity tests should be conducted within these velocity ranges. An

example of a similarity test would include measuring the pressure drop per unit length at the scaled flow properties given in Table 4-3. Additionally, when testing saltation and choking correlations, it would be beneficial to cover a range of velocities where saltation and choking are expected to occur in power plant pipelines.

Note that aside from the particle diameter, Re_p, Fr_p and ψ do not include geometrical properties such as pipe diameters and lengths. Therefore, a pipe with a nominal bore (NB) of 100mm was initially chosen for the conveying pipelines, as it was deemed big enough to allow for flow visualization, and small enough so that the volume of gas and particles to be conveyed are manageable.

4.3 Initial Concept Design

Open and closed loop concepts were developed after considering the basic requirements of a pneumatic test facility needed to test saltation and choking correlations. At the time of development, these requirements included the need for:

- An air mover.
- A particle feeding system.
- A particle separation or gas cleaning system.
- A horizontal test section.
- A vertical test section.
- A method to control the gas density at test sections.
- A method to measure and control the particle flow rate.
- A method to measure and control the gas flow rate.

Open Loop Concept

Figure 4-2 shows the open loop concept. The concept features an induced draft blower (with speed control) to facilitate negative conveying pressures, as would be the case in typical South African coal-fired power plants, where the absolute conveying pressure is estimated to be 85kPa (Van der Merwe, 2014). A globe valve is situated after the intake, which can be used to lower the conveying pressure and therefore the gas density. Particle feeding is facilitated via a screw feeder (with speed control) and a gravimetric feed junction. The particles are then conveyed through horizontal and vertical test sections. A temperature and absolute pressure reading is taken at the beginning of each of these test sections, before taking a delta pressure measurement across each test section. These test sections also include sight glasses for visual inspection of the flow. Particle separation is then achieved via a cyclone separator, which transfers the particles to a weigh hopper (or silo), which is used to perform a particle mass flow rate calculation. A filter is attached to the gas outlet of the cyclone to separate any fine particles from the gas.

The gas then passes through an orifice plate. The pressure drop across the plate is used to perform a gas mass flow rate calculation. The intake and exhausts are used to minimise the total pressure drop across the system.

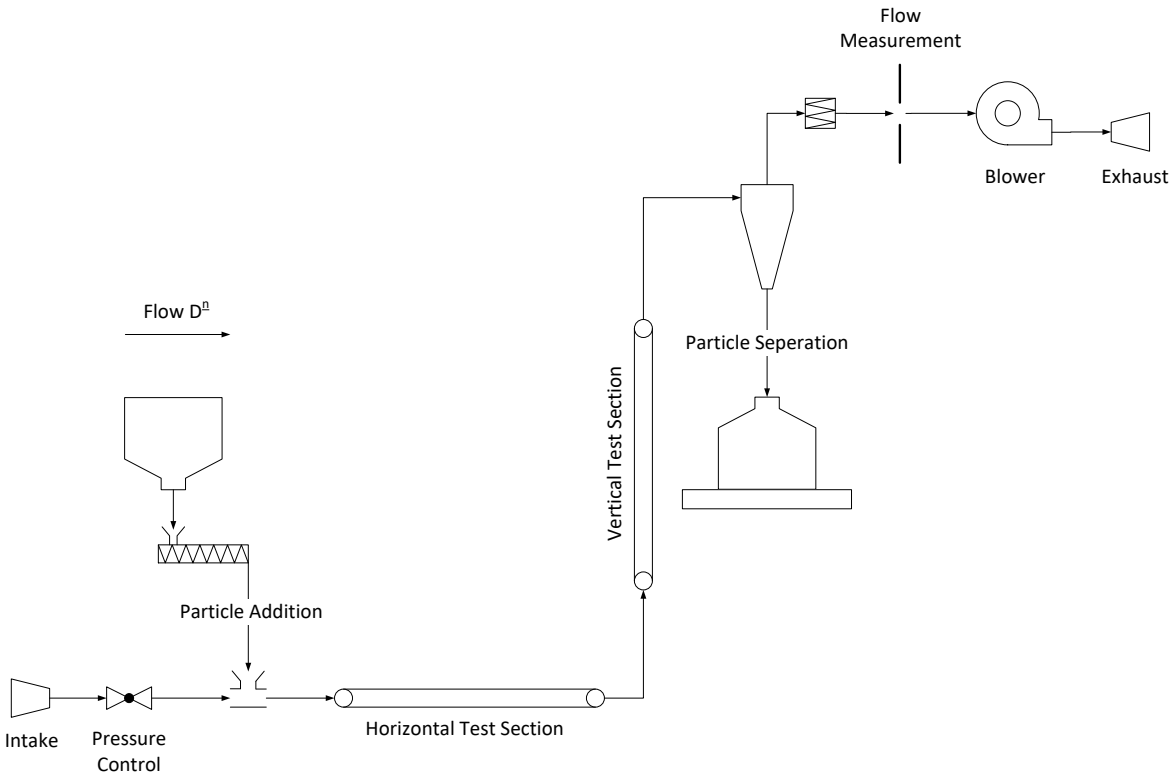

Figure 4-2 – Open loop concept

Closed Loop Concept

Figure 4-3 shows the closed loop concept. The concept shares many similarities with the open loop. However, the globe valve is removed and replaced with a pressure regulating system, which can not only reduce the conveying pressure within the loop, but also increase it. There is also the addition of a temperature control system. The feeding system then features a rotary feeder in place of a gravimetric feed junction. The use of a rotary feeder is common in positive conveying systems as it restricts the flow of gas up into the feeding hopper. The orifice plate has also been moved from the blower inlet, to the blower outlet.

In summary, both concepts meet the basic requirements listed above and share many similarities. The closed loop however allows for greater control of the gas density through both pressure and temperature regulation. If the physical layout of the concepts were the same and for a given set of flow properties, it is also probable that the pressure drop would be less across the closed loop, as there are no losses due to an intake and exhaust.

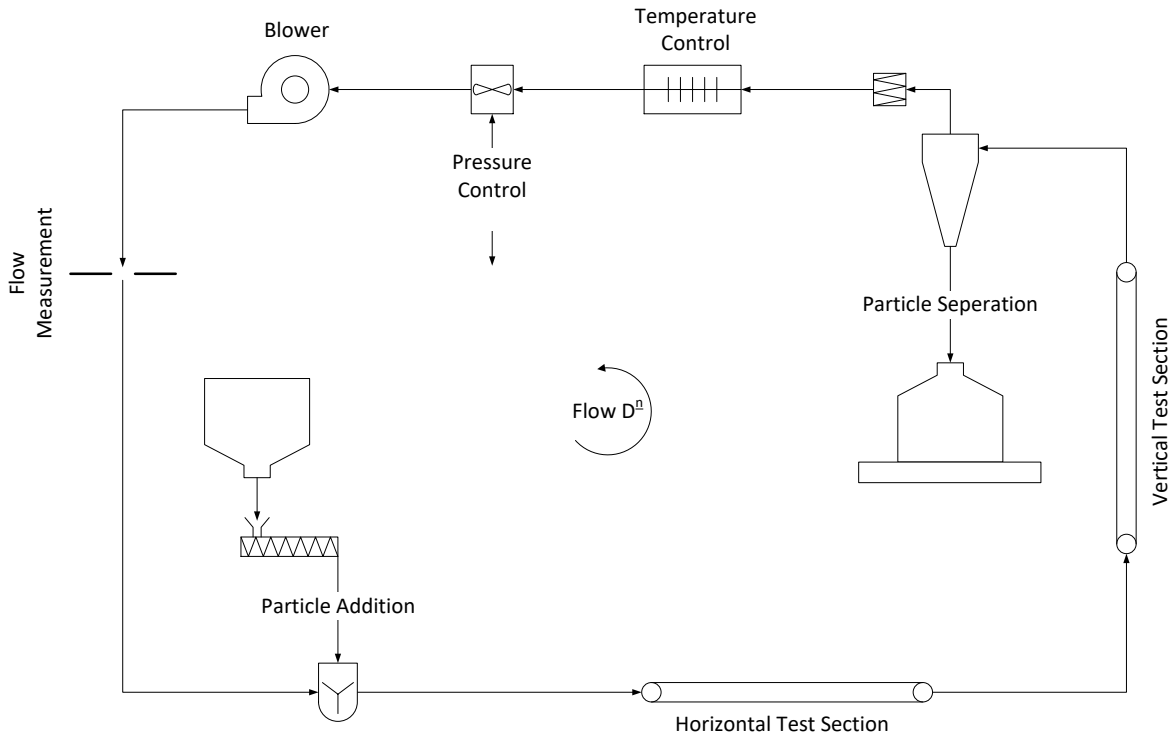

Figure 4-3 – Closed loop concept

Concept Design

The closed loop concept, although more intricate, was viewed as more advantageous. The closed loop concept was therefore further developed. A P&ID of the concept, developed before construction and testing of the prototype rig, is given in Figure 4-4. High level CAD models of the physical layout positioned within the designated laboratory space is shown in Figure 4-5 and Figure 4-6 respectively.

The concept features a blower, with speed control via a variable speed drive (VSD). The flow measurement section consists of two orifice plates in parallel, one for low gas flow rates (ratio of orifice bore to pipe bore (β) value of 0.55) and one for medium to high gas flow rates (β = 0.75). Valves are used to select the appropriate orifice to use during testing. These valves are placed at the end of the flow measurement lines to limit flow disturbances through the orifice. Full-bore ball valves are used to minimise the pressure drop and for easy operation.

The feeding system consists of a hopper suspended on load cells and a screw feeder (also called an auger), with speed control facilitated by a VSD. A pressure equalising line pressurises the top hopper to prevent gas flow up into the hopper, as two separate feed junctions are used in place of a rotary feeder.

As the gas velocity at saltation is significantly less than choking, Feed junction A is used for choking tests, where the horizontal conveying line diameter (with a nominal bore (NB) of 50mm) is significantly less than the test diameter (100NB) to increase the gas velocity and prevent particle settling. Feed junction B is

used for saltation and power plant similarity tests. Here, the diameter of the horizontal acceleration line (90NB) is slightly smaller than the test diameter, to prevent saltation from occurring before the horizontal test section. Similarly, the diameter of the vertical acceleration line (90NB) is also smaller, to prevent choking from occurring before the vertical test section. The line to use during testing is determined by the position of the shutter on the screw feeder and the isolation valves before the feeding section.

The receiving system features a hopper suspended on load cells just above the feeding hopper. This allows a mass balance to be performed on the feeding and receiving side. A knife gate valve separates the receiving and feeding hopper. Cyclones are designed to operate at a particular gas flow rate and therefore, three cyclones are used in parallel to cover the range of operating flow rates. For choking tests, a single cyclone, fed by the 50NB line is used. For saltation and similarity tests, one cyclone is fed by the 90NB line and is used to cover low gas flow rates. An additional cyclone is then used in parallel with this cyclone to cover high gas flow rates. Isolation valves are used to determine the line(s) to use during testing. These valves are placed at the cyclone outlets to minimise their exposure to dust.

A cooling system consisting of a heat exchanger and cooling tower is employed to regulate the temperature within the loop. Although the system is only used for cooling, it is noted that there is a temperature rise through the blower, which is dependent on the pressure rise through the blower. The temperature within the loop will therefore increase during operation, mitigating the need for a heater. Isolation valves within the loop can also be partially closed to increase the pressure rise and therefore increase the temperature more quickly before testing. A cartridge filter is built into the inlet of the heat exchanger to remove any fine particles not removed by the cyclone.

A fan, with speed and direction control facilitated by a VSD, is then used to regulate the pressure within the loop by feeding or extracting air from the system. Finally, pressure and temperature measurements are taken before the flow measurement and test sections. Differential pressure measurements are also taken across the orifice plates and test sections.

Note that the blower, orifice plates, hopper, cyclone, pipe sizes and the required instrument operating ranges were determined from theoretical models, which are presented in Chapter 5.

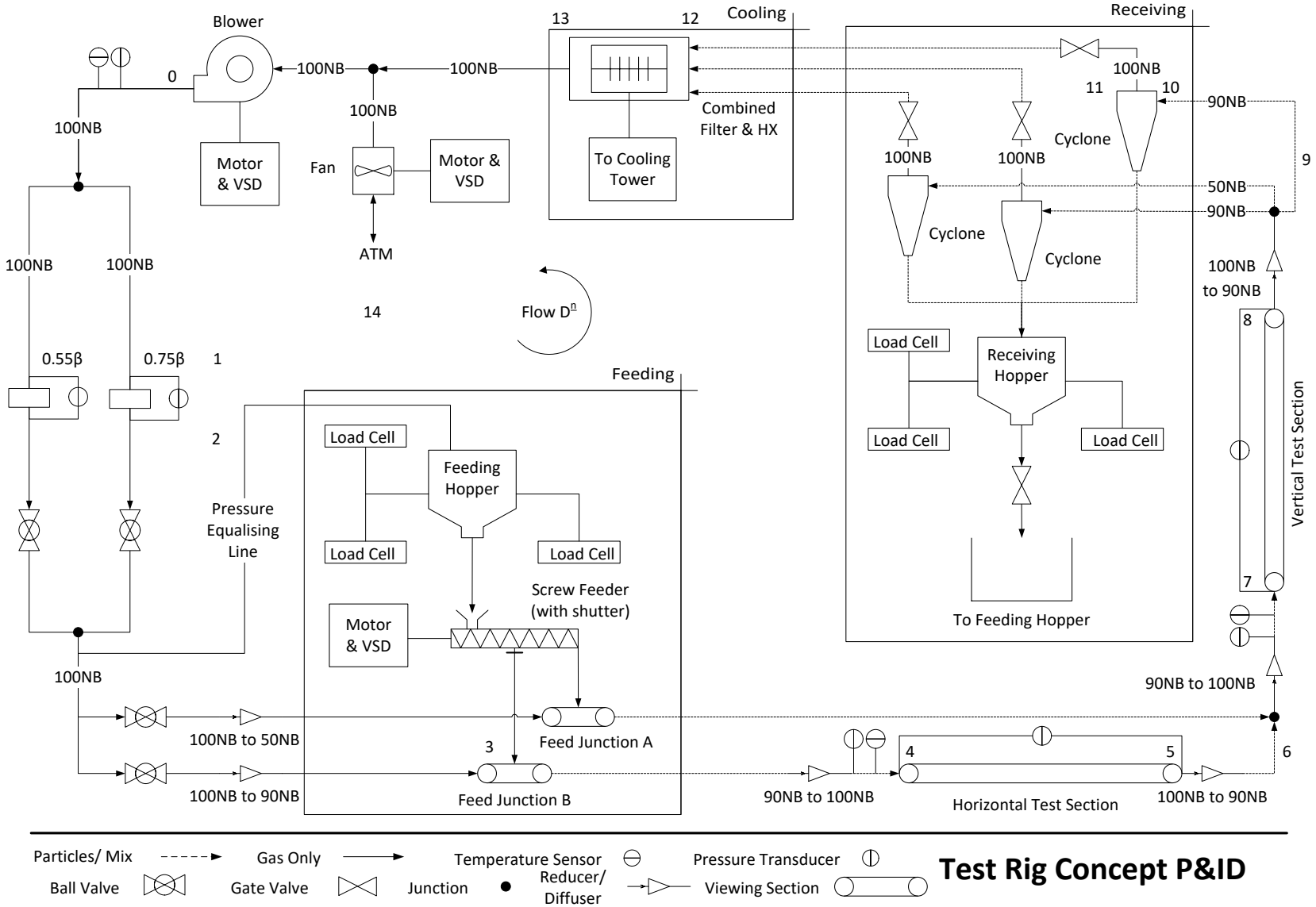

Figure 4-4 – Concept P&ID

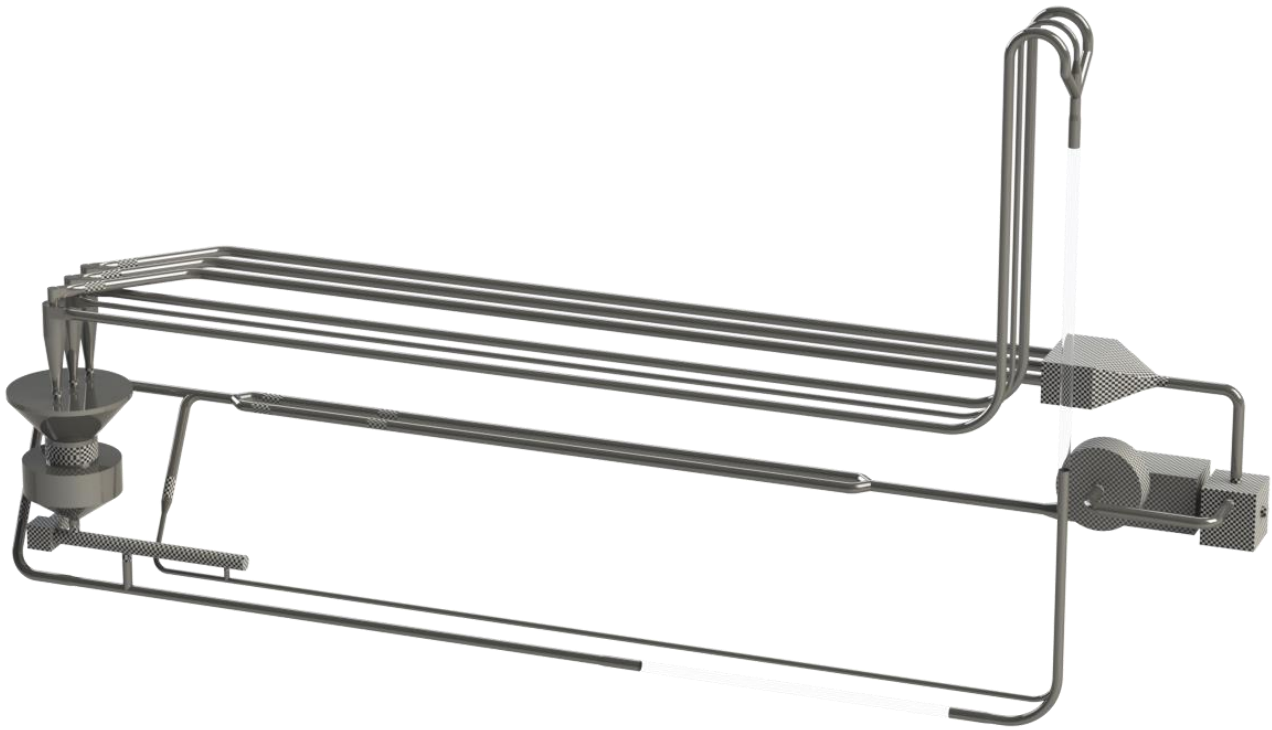

Figure 4-5 – Physical layout of concept

Figure 4-6 – Physical layout of concept within the designated laboratory space

4.4 Prototype Design

A prototype facility, containing the important components but of reduced complexity, was developed to limit the risk in the construction of the final facility by demonstrating the process beforehand. As part of this process, particular attention was given to the design of the feeding system, which was viewed as a high-risk system. An experimental rig was constructed to test the initially proposed feeding method, which featured a screw feeder coupled to a single feed junction. The rig is illustrated in Figure 4-7, where the hopper and support frame were specially constructed and an existing screw feeder was used.

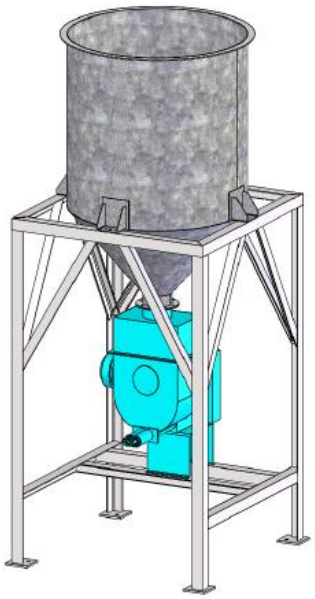

Figure 4-7 – Screw feeder testing

The rig was used to observe the flow of material from the hopper, through the screw feeder and into a bucket. It was observed that the design resulted in ratholing (see Figure 4-8) within the hopper and inconsistent material flow at the screw feed outlet. This may be attributed to an insufficient cone angle (Klinzing, et al., 1997), resulting in funnel flow and eventual ratholing instead of the desired uniform mass flow. Figure 4-9 illustrates the difference between a mass and funnel flow hopper.

Figure 4-8 – Ratholing through hopper

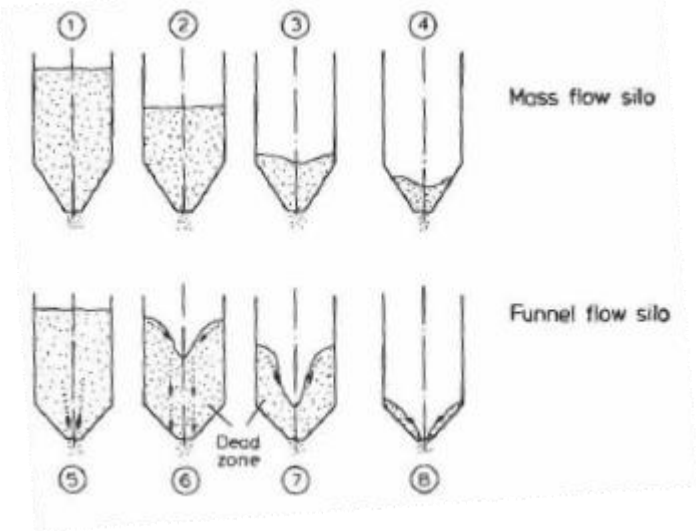

Figure 4-9 – Hopper flow types, taken from Klinzing, et al. (1997)

Further experiments using the rig were therefore suspended and the design of the feeding system was changed to feature a re-designed hopper geometry and a blow through rotary valve in place of a feed junction. The system is illustrated in Figure 4-10 and is comprised of a combination of standard explosion-proof components offered by the supplier.

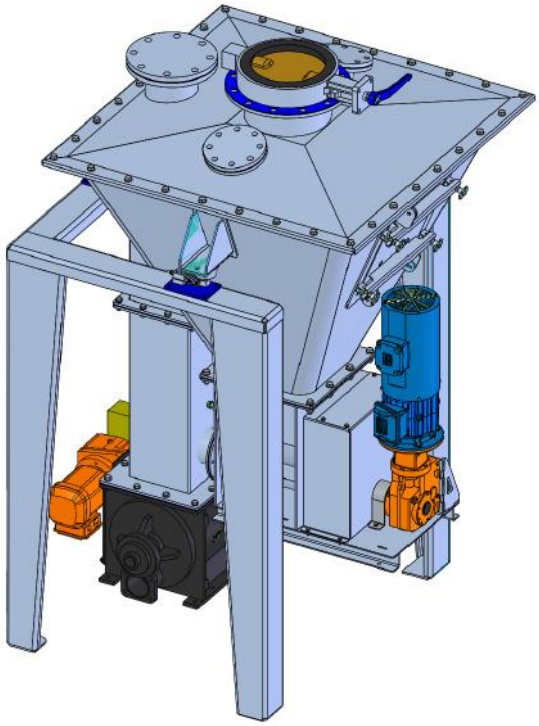

Figure 4-10 – Feeding system

With the updated design, the feed rate is controlled by the auger and by operating the rotary feeder at increased speeds, small batches are introduced into the pipeline at relatively quick rates. In theory, this provides a near constant feed rate and the supplier was mandated to conduct a test of the flow of the material through the system before procurement. The physical tests proved that the proposed design was

acceptable to achieve a smooth and controllable flow rate of material. A picture of the flow through the hopper is given in Figure 4-11.

Figure 4-11 – Top view of flow through hopper

A P&ID for the prototype facility was then developed and is given in Figure 4-12. The prototype facility features an open loop design consisting of the important components and subsystems needed for the final facility. These include the feeding system, the receiving system (albeit with a single cyclone) and a similar piping network including instrumentation and a suitably sized blower.

As the prototype facility is not intended to be used for scientific testing, the horizontal and vertical test sections were removed. However, a sight glass is situated in the vertical conveying section for visual inspection of the process. The facility also features flexible connections between the cyclone and top hopper, between the hoppers and at the feeding point. These flexible connections are used to isolate the hoppers so that proper mass readings can be taken. Finally, two knife gate valves are used to isolate the flow of material between the hoppers instead of one. This is important, as any pressure fluctuations within the system would exert a fluctuating net pressure force equal and opposite in direction on each hopper if only one valve was used. Consequently, this would affect the mass readings on the hoppers.

CAD models of the prototype facility are given in Figure 4-13 to Figure 4-15 and photos of the prototype facility are given in Appendix U. The overall dimensions of the prototype facility in length x height x width are 8.3 x 4.9 x 2.4 meters.

Note that the blower, orifice plates, hopper, cyclone, pipe sizes and the required instrument operating ranges were again determined from the theoretical models presented in Chapter 5.

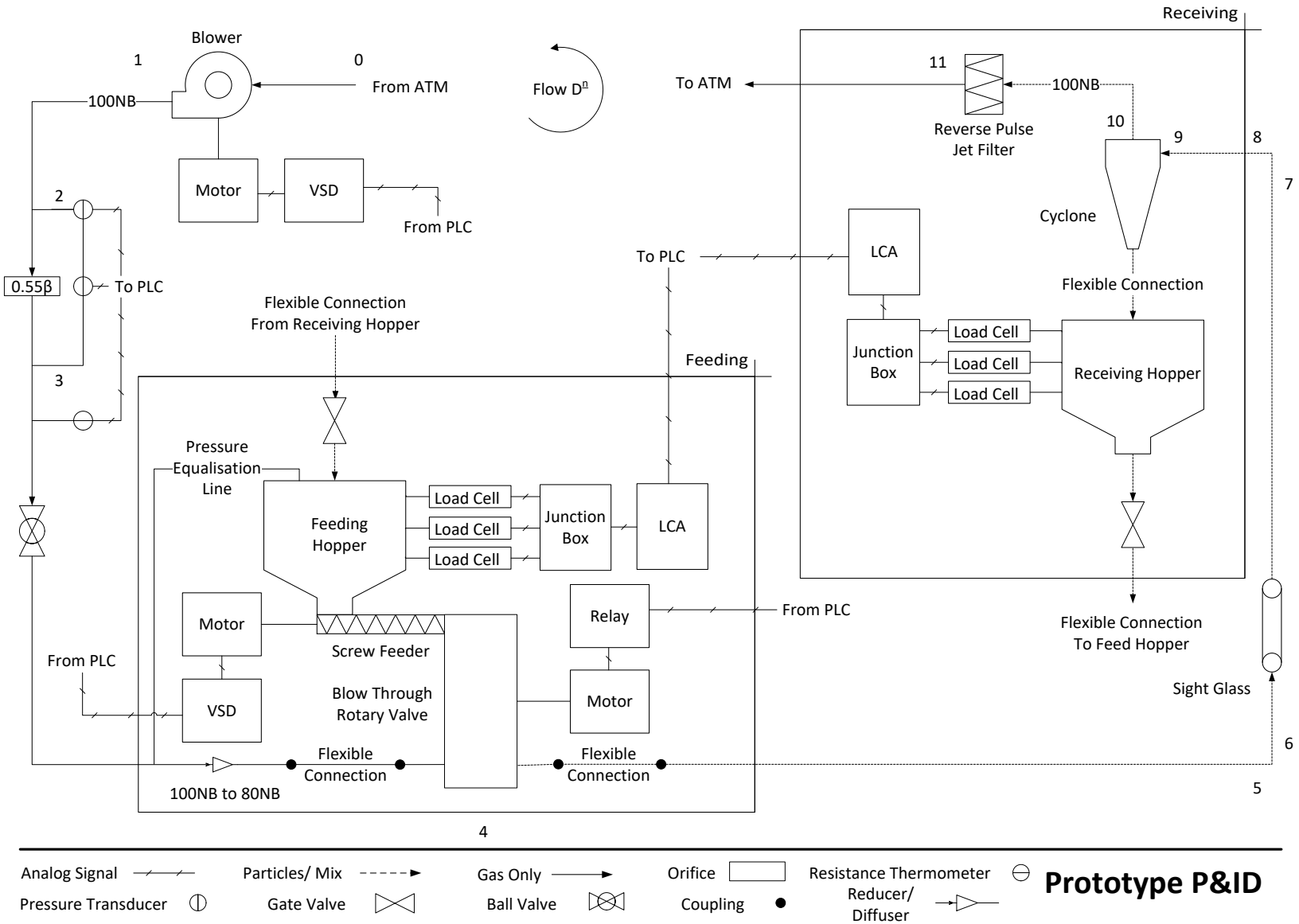

Figure 4-12 – Prototype P&ID

Figure 4-13 – Front view of prototype facility

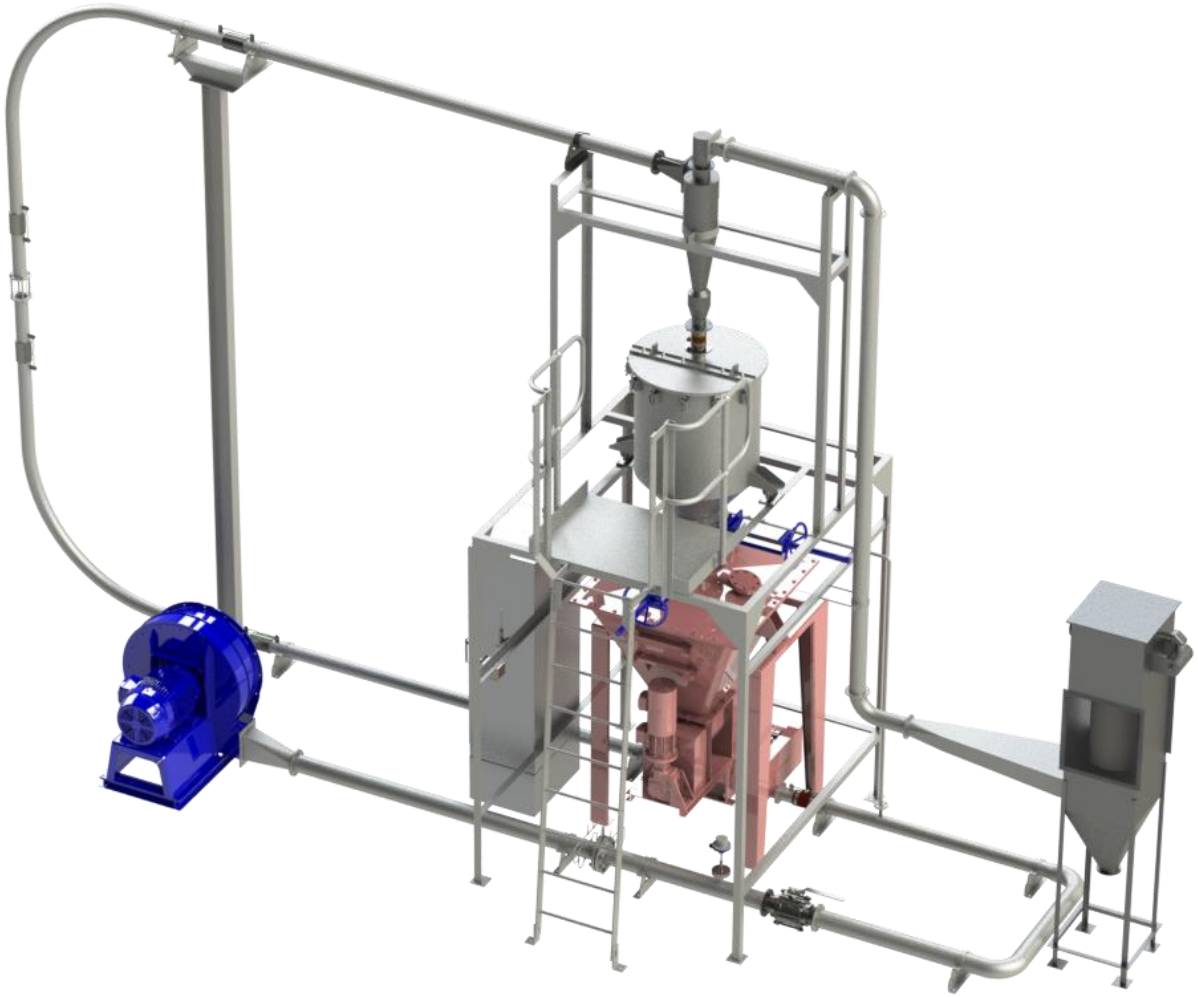

Figure 4-14 – Trimetric view of prototype facility

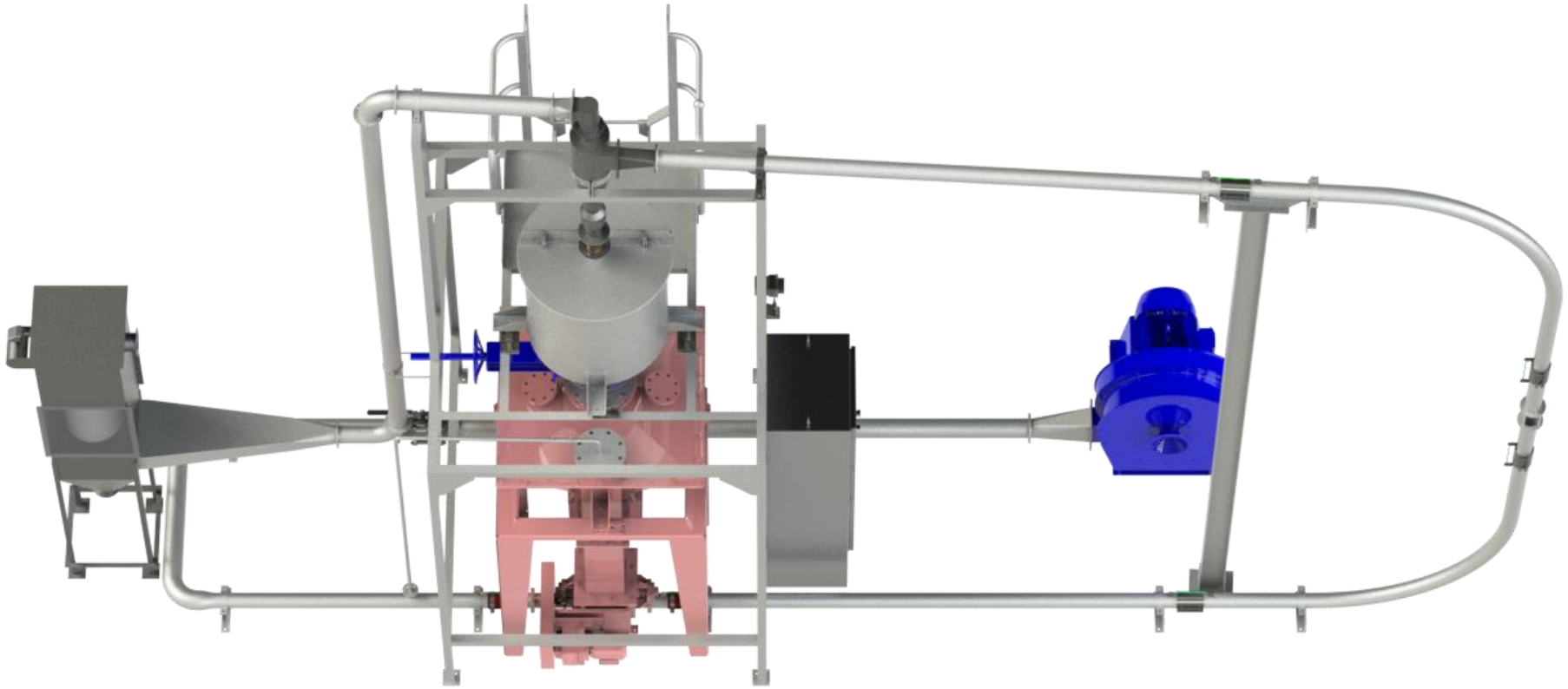

Figure 4-15 – Elevated back view of prototype facility

4.5 DAC System

The DAC system employed on the prototype facility was developed in its entirety by the candidate. This included the selection and specification of all instrumentation as well as programming of the control loops and the data collection and analysis software. The basis of the DAC system is a modular programmable logic controller (PLC) assembled using National Instruments (NI) components. Signals are input to the PLC hardware from various sensors, namely a resistance temperature device (RTD), a pressure transducer, a differential pressure transducer and two independent load cell packages. Using the software component of the PLC (developed using LabVIEW), these signals are then deciphered to obtain the line temperature and pressure, the differential pressure drop across the orifice plate and the mass of each hopper. These primary properties are then used to calculate dependent properties such as the gas and particle mass flow rates during operation of the test rig, which are controlled by the PLC via output signals to the VSD of the blower and screw feed. The software component of the PLC also features a graphical user interface (GUI) which allows the operator to view operating parameters and adjust set points in real-time. The process is illustrated in Figure 4-16.

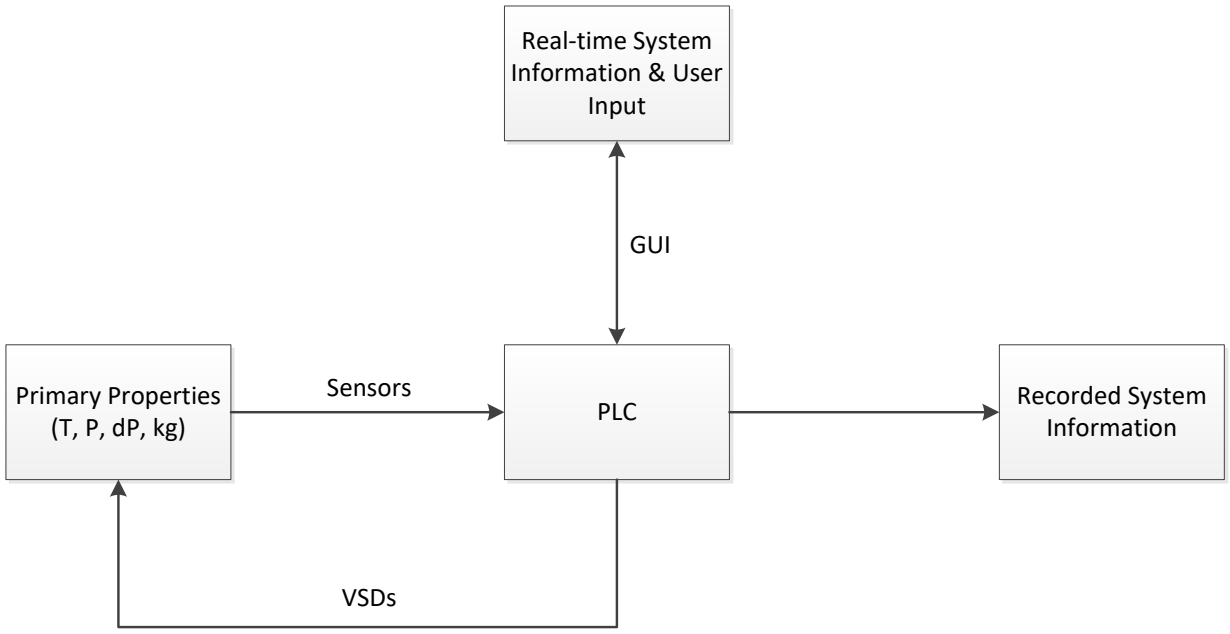

Figure 4-16 – High level flow chart of DAC process

4.5.1 System Map

A map of key instrumentation used in the DAC system, as well as their descriptions is given in Figure 4-17 and Table 4-4 respectively. Detailed electrical drawings are given in Appendix T. The first pages of the equipment datasheets are also given in Appendix S and the full datasheets are given in the compact disc (CD) accompanying this thesis.

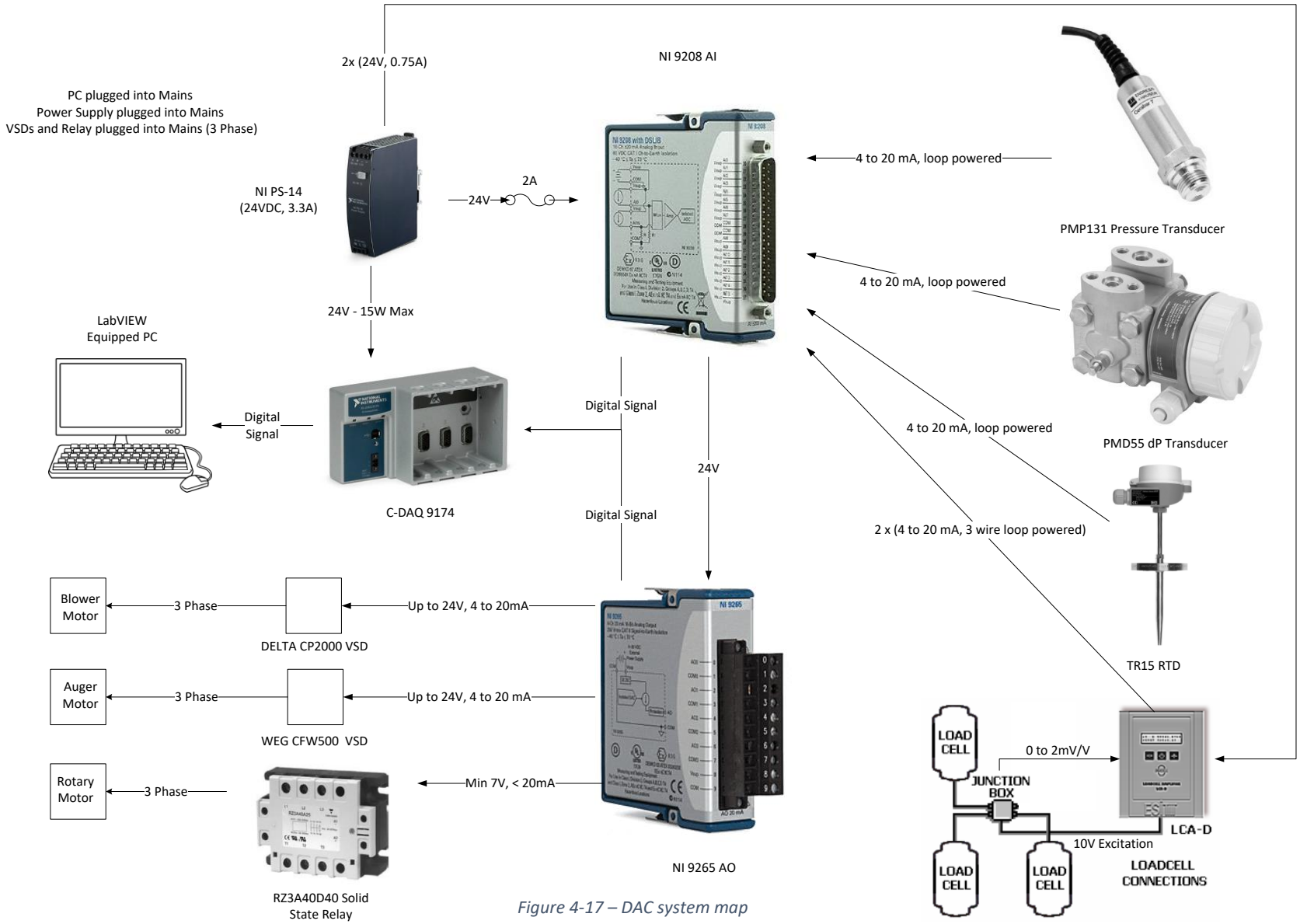

Figure 4-17 – DAC system map

Component	Description
Personal Computer	A USB enabled desktop or laptop running Windows 7 or later, with LabVIEW and Scilab installed. The software component of the PLC runs on the computer.
C-DAQ 9174	A ruggedized chassis which can house up to four NI C Series analog or digital modules. This chassis provides communication between the computer and the analog input and output modules.
NI PS-14	An 80W (24V, 3.3A) industrial power supply for stable and efficient powering of the control system instrumentation.
NI 9208 AI	A 16-channel analog input module. The module is used to measure 4 to 20mA signals from the sensors.
NI 9265 AO	A 4-channel analog output module. The module is used to output 4 to 20mA signals to the VSD's and solid state relay.
PMP131	An absolute pressure transducer used to measure the static pressure at the orifice upstream tapping. The transducer outputs a linear signal of 4 to 20mA relative to its measuring range (0 to 160kPa).
PMD55	An explosion-proof differential pressure transducer used to measure the pressure across the orifice upstream and downstream tappings. The transducer outputs a linear signal of 4 to 20mA relative to an adjustable measuring range (default is -5 to 0kPa; maximum is -10 to 0kPa).
TR15	An explosion-proof RTD with a thermowell and head transmitter, which outputs a linear signal of 4 to 20mA relative to its measuring range (0 to 80 °C).
Load Cell Packages	Two packages each consisting of 3 explosion-proof load cells (3 x 200kg and 3 x 500kg respectively), a load cell junction box and a load cell amplifier (LCA). Each individual load cell outputs a linear 0 to 2mV/V signal relative to the load applied to it, in each package these signals are then summed and averaged by a junction box and output to a LCA. The LCAs each output a linear signal of 4 to 20mA relative to an adjustable measuring range (default is 0 to 300kg).
Delta VFD-300CP4EB-21	A 30kW VSD. This VSD accepts a linear 4 to 20mA signal for control of the blower motor speed (0 to 65Hz)
WEG CFW500 VSD	A 0.75kW VSD. This VSD accepts a linear 4 to 20mA signal for control of the auger motor speed (0 to 100Hz)
RZ3A40D40 Solid State Relay (SSR)	Relays power to the rotary feed motor when 7V is applied across its control terminals.

Table 4-4 – DAC system components

4.5.2 Real-time calculations

The PLC is capable of recording samples and processing data at a maximum rate of 20Hz i.e. 20 times per second. Calculations performed by the PLC are presented in this section.

Signal Conversion

Calculations are performed to determine the physical values of the temperature T, absolute pressure P, differential pressure dP and mass $Mass$ from measured analog signals I_{out}. These calculations are based on the instrument defined relationships given in Equation 4-8 to Equation 4-11.

$$T = 5I_{out} - 20^{\circ}C$$

Equation 4-8

$$P = 10I_{out} - 40kPa$$

Equation 4-9

$$dP = \frac{span}{16} I_{out} + URV - \frac{20}{16} span$$

Equation 4-10

$$Mass\ in\ kg = \frac{LCA_{MAX}}{16} I_{out} - \frac{1}{4} LCA_{MAX}$$

Equation 4-11

Where:

I_{out} is in mA

T is in $^{\circ}C$

P and dP are in kPa

$span$ is the PMD55 set measuring range in kPa.

URV and is the PMD55 set upper range measuring value in kPa.

URL is the PMD55 upper range measuring limit in kPa.

LRV is the PMD55 set lower range measuring value in kPa.

Gas Mass Flow Rate

The mass flow rate of the gas $\dot{M}_g$ is calculated using Equation 4-12.

$$\dot{M}_g = \frac{C_d}{\sqrt{1-\beta^4}} \varepsilon_g \frac{\pi}{4} D_{vc}^2 \sqrt{2dP\rho_1}$$

Equation 4-12

Where:

$\dot{M}_g$ is in kg/s

C_d is the orifice discharge coefficient

$\beta = \frac{D_{vc}}{D_{pipe}}$ is the ratio of the orifice bore diameter to the inside diameter of the pipe

ε_g is the gas expansibility factor

dP is the pressure drop across the orifice in Pa

ρ_1 is the density at the orifice upstream face in kg/m^3

C_d is calculated using Equation 4-13, from ISO 5167-2:2003 (International Organization for Standardization (ISO), 2003)

$$C_d = 0.5961 + 0.0261\beta^2 - 0.216\beta^8 + 0.000521\left(\frac{10^6\beta}{Re}\right)^{0.7} + (0.0188 + 0.0063A)\beta^{3.5}\left(\frac{10^6}{Re}\right)^{0.3} + \left(0.043 + 0.080e_1^{-10L_1} - 0.123e^{-7L_1}\right)(1 - 0.11A)\frac{\beta}{1-\beta^4} - 0.031\left(M_2' - 0.8{M_2'}^{1.1}\right)\beta^{1.3}$$

Equation 4-13

Where $M_2' = \frac{0.94}{1-\beta}$, $A = \left(\frac{19000\beta}{Re}\right)^{0.8}$ and $L_1 = 1$ for orifice plates with D_{pipe} and $\frac{D_{pipe}}{2}$ tappings.

ε_g is calculated using Equation 4-14, from ISO 5167-2:2003 (ISO, 2003)

$$\varepsilon_g = 1 - (0.351 + 0.256\beta^4 + 0.93\beta^8)\left[1 - \frac{P_2}{P_1}\right]^{1/\gamma}$$

Equation 4-14

Where P_2 is the pressure downstream of the orifice plate and $\gamma = 1.4$ is the specific heat ratio for air, assumed to be constant.

ρ_1 is calculated using the ideal gas law (Equation 4-1).

Note that C_d is dependant on Re, which is inherently dependant on $\dot{M}_g$. An iterative calculation is therefore necessary to calculate $\dot{M}_g$. Furthermore, the dynamic viscosity of the gas μ_g is needed to calculate Re. Sutherland's formula (Equation 4-2) is used to calculate μ_g. A numerical scheme, given in ISO 5167-1:2003 (International Organization for Standardization (ISO), 2003), is used to calculate $C_d, Re\ and\ \dot{M}_g$ simultaneously using an embedded Scilab script within LabVIEW. A copy of the script is given in Appendix F.

Particle Mass Flow rate

The particle mass flow rate $\dot{M}_p$ in kg/s is calculated using Equation 4-15

$$\dot{M}_p = \frac{Mass_1 - Mass_0}{\Delta t}$$

Equation 4-15

Where $Mass_1$ and $Mass_0$ are the respective mass readings in kg at the current and previous sample points and Δt is the period between sample points in seconds.

Data Averaging

The PLC calculates physical values instantaneously at each sample point and therefore averaging is necessary to provide meaningful, or less erratic, values to the user during operation. Therefore, for each variable calculated instantaneously, a running average of the last n values is also calculated based on a user defined averaging period.

4.5.3 Graphical User Interface

The Graphical User Interface (GUI) provides real-time feedback of flow properties to the operator via text and graphic indicators. The GUI also accepts user input for control of the system. Figure 4-18 shows the main window of the GUI. Controls and time indicators are given on the left-hand side of the window, some of which are accessed via tabbed sections. Various graphs and text indicators are available in the center and right-hand sections of the window, again via tabbed sections. Note that a valid username (or password) is required to operate the system and a “Record” button needs to be pressed to record processed data. However, raw data is always recorded. The “PID Tune” graph tabs are only available in the developer mode GUI.

A second window can be accessed by dragging the bottom pane (dark grey area) upwards. This window provides additional graphs for the primary properties, including graphs for the raw signals received (if the user scrolls to the right within this window). Figure 4-19 shows this window while running the GUI using simulated sine wave signals and not during actual operation of the test facility. Notice the ability to see both real-time sample points and a moving average.

Finally, Figure 4-20 shows a final window, which can be accessed by dragging the top pane downwards. This window provides a map of key system properties as well as on/ off indicators for the blower, auger and rotary feed motors.

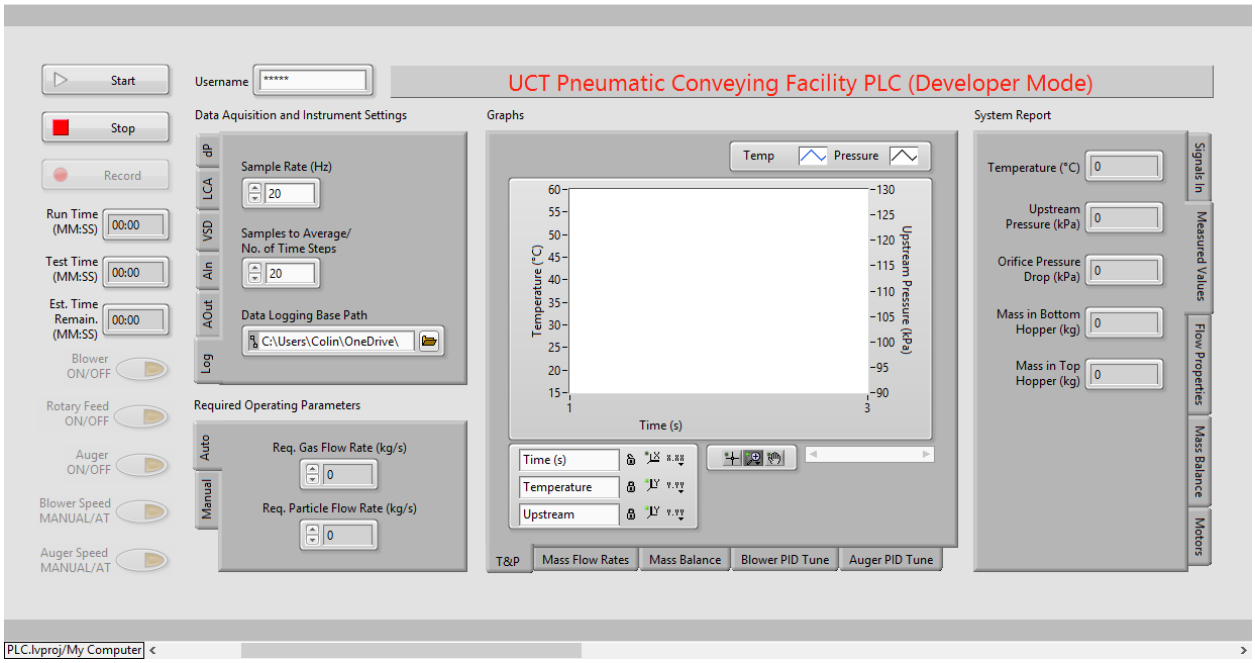

Figure 4-18 – GUI main window

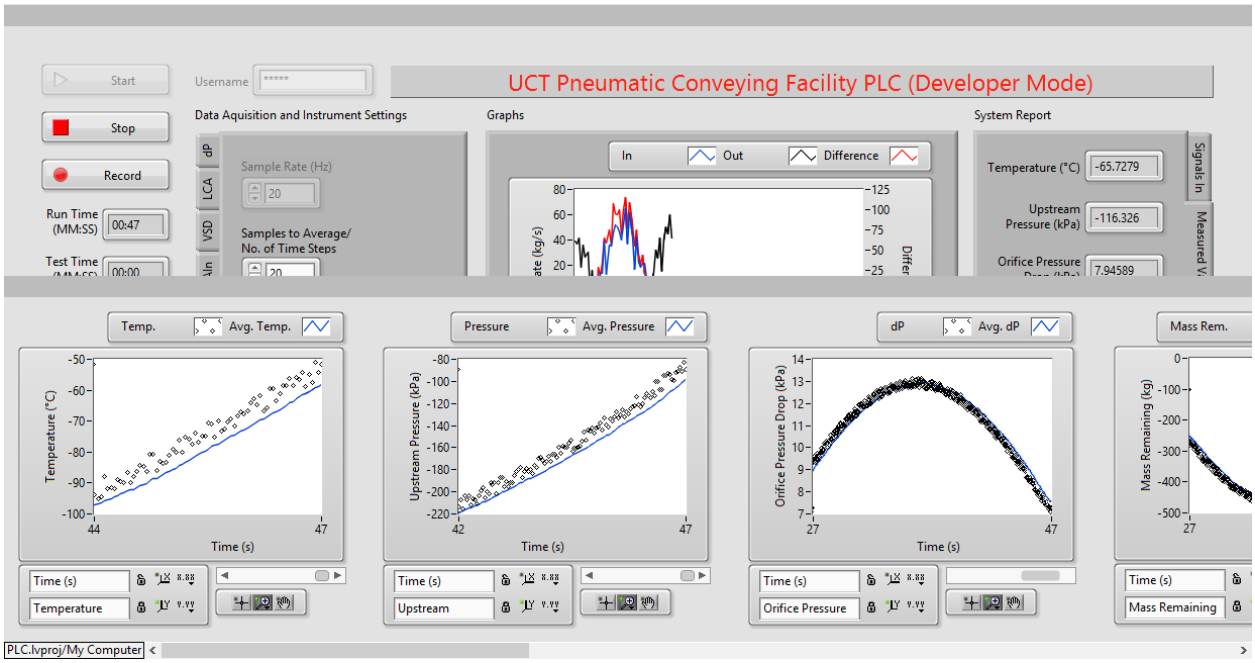

Figure 4-19 – GUI bottom window

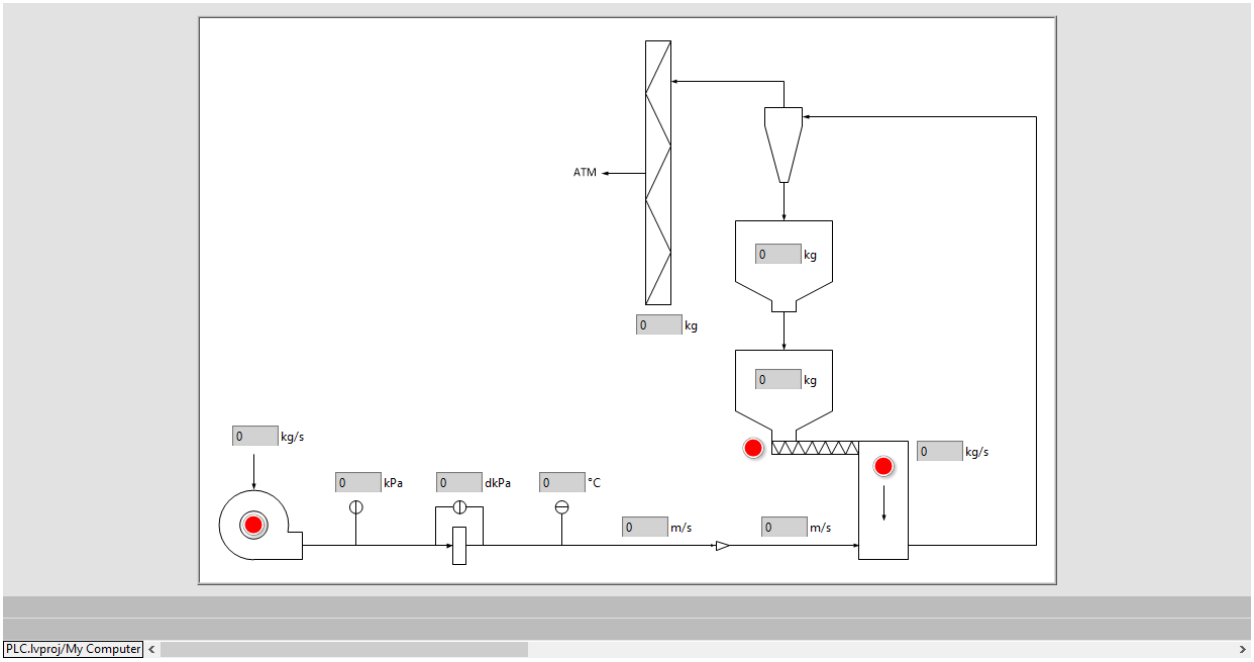

Figure 4-20 – GUI top window

4.6 Design Phase Uncertainty Analysis

The inputs, methodology and results of a design phase uncertainty analysis performed are given below. A copy of the analysis is given in Appendix K.

4.6.1 Inputs

Table 4-5 provides a list of instrument elemental uncertainties used in the analysis. A 95% probability level is assumed, as suggested by Figliola & Beasley (2011) when more details are not provided by the supplier. Other inputs used are given within the analysis methodology.

Description	**Value**
TR15	
RTD Accuracy	$0.1 + 0.0017T_g\ [^\circ C]$
Transmitter Accuracy	$0.2^\circ C$
PMP131	
Linearity including hysteresis and reproducibility	$0.5\ \%FS$
PMD55	
Current output resolution	$1\mu A$

Linearity including hysteresis and reproducibility	$0.1\%\ of\ set\ span\ if\ TD^{*} \leq 4$ $(0.012TD + 0.052)\%\ of\ set\ span\ if\ TD > 4$
Load Cells	
Resolution	$\frac{Rated\ capacity\ of\ load\ cell\ in\ kg}{3000}\ [kg]$
Combined error	$0.020\ \%FS$
Offset on output sensitivity	$0.02mV/V$
LCA	
Current output resolution	$16bits\ or\ 244\mu A^{\dagger}$
Weighing accuracy	0.01%
NI 9208 AI	
Current output resolution	$24\ bits\ or\ 42\mu A$
Accuracy of reading	0.76%
Accuracy of range	$0.04\%\ of\ 22mA$
Noise	$200nA$

Table 4-5 – Instrument elemental uncertainties

4.6.2 Methodology

The root sum squares (RSS) method was used to combine elemental uncertainties u_i as follows:

$$t_P u_{total} = \pm\sqrt{(t_P u_1)^2 + (t_P u_2)^2 + (t_P u_3)^2 + \cdots + (t_P u_n)^2} \quad (P\%)$$

Equation 4-16

Where n is the number of elemental uncertainties involved and t_p is the "students t-distribution". $t_p = 1$ implies a 68% probability, whereas $t_p = 2$ implies a 95% probability, therefore

$$u\ (68\%) = \frac{1}{2} u\ (95\%)$$

Equation 4-17

[*] See methodology for explanation of TD.

[†] See Appendix E for conversion from bits to current.

Uncertainties were calculated at a probability of 68% so that they can easily be combined with statistical uncertainties.

GAS MASS FLOW RATE

Section 5.4 presents a process model which estimates the transport properties within the prototype facility for various input conditions. Two sets of results (or scenarios) obtained from the model were considered for the gas flow rate uncertainty analysis, representing a low and a high gas mass flow rate respectively. The scenarios are given in Table 4-6.

Variable	Symbol	Units	Scenario 1	Scenario 2
Gas temperature	T_g	˚C	28	49
Absolute pressure at the orifice inlet	P_1	kPa	103.534	119.338
Pressure drop across the orifice	dP	kPa	0.429	2.035
Gas density at the orifice inlet	ρ_1	kg/m^3	1.198	1.290
Gas expansibility factor	ε_g		0.999	0.995
Discharge coefficient	C_d		0.613	0.610
Gas mass flow rate	$\dot{M}_g$	kg/s	0.051	0.115

Table 4-6 – Gas flow rate scenarios

Initially, the uncertainty of the temperature measuring instrument $u_{.T_g}$ was calculated as the RSS of the TR15 and NI 9208 AI uncertainties, which in turn were calculated as the RSS of their respective elemental uncertainties. To use the RSS method the relationship given in Equation 4-8 was used to convert between units of temperature and current.

Similarly, the uncertainty of the absolute pressure measuring instrument $u_{.P1}$ was then calculated as the RSS of the PMP131 and NI 9208 AI uncertainties. The relationship given in Equation 4-9 was used to convert between units of pressure and current.

The uncertainty of the differential pressure measuring instrument u_{dP} was then calculated as the RSS of the PMD55 and NI 9208 AI uncertainties. Here, the turn down ratio $TD = \frac{URL}{|LRV|}$ of the instrument affects the uncertainty of the PMD55, as per Table 4-5. The relationship given in Equation 4-10 was used to convert between units of differential pressure and current.

The uncertainty on the gas density at the orifice inlet u_{ρ_1} was then calculated through error propagation on the ideal gas law (Equation 4-1), where the general formula for uncertainty propagation on a multi-variable function $y = f(x_1, x_2, x_3, \dots x_n)$ is given in Equation 4-18 (Figliola & Beasley, 2011).

$$t_P u_y = \sqrt{\sum_{i=1}^{n} \left[\left(\frac{\partial y}{\partial x_i} \right) t_p u_{x_i} \right]^2} \quad (P\%)$$

Equation 4-18

The orifice plate and it's installation design conforms to specifications given in ISO 5167-1 (ISO, 2003) and ISO5167-2 (ISO, 2003). The uncertainty on the gas mass flow rate was therefore calculated using Equation 4-19, from ISO 5167-1 (ISO, 2003)

$$u_{\dot{M}_g} = \dot{M}_g \sqrt{\left(\frac{u_{C_d}}{C_d}\right)^2 + \left(\frac{u_{\varepsilon_g}}{\varepsilon_g}\right)^2 + \left(\frac{2\beta^4}{1-\beta^4}\right)^2 \left(\frac{u_{D_{pipe}}}{D_{pipe}}\right)^2 + \left(\frac{2}{1-\beta^4}\right)^2 \left(\frac{u_{D_{vc}}}{D_{vc}}\right)^2 + \frac{1}{4}\left(\frac{u_{dP_1}}{dP_1}\right)^2 + \frac{1}{4}\left(\frac{u_{\rho_1}}{\rho_1}\right)^2} \quad (95\%)$$

Equation 4-19

Where the following relative uncertainties were assumed, as per the ISO standards:

1. $\frac{u_{C_d}}{C_d} = 0.5\%$
2. $\frac{u_{\varepsilon_g}}{\varepsilon_g} = 3.5 \frac{dP_1}{\gamma P_1}\%$
3. $\frac{u_{D_{pipe}}}{D_{pipe}} = 0.4\%$
4. $\frac{u_{D_{vc}}}{D_{vc}} = 0.1\%$

PARTICLE MASS FLOW RATE

It was assumed that the particle mass flow rate $\dot{M}_p$ remains constant during the duration of a test, so that the uncertainty could be calculated through propagation of the boundary mass values $Mass_{start}, Mass_{end}$. $Mass_{start} = 250kg$ is the assumed mass at which $\dot{M}_p$ reaches steady state. $Mass_{end} = 50kg$ is the assumed mass at which $\dot{M}_p$ becomes unattainable due to insufficient hopper head. Furthermore, the $\dot{M}_p$ attainable by the feeding system is dependent on the bulk density of the material being fed. The feeding system is therefore capable of feeding at a minimum of 0.070kg/s, in the case of PC particles, and at a maximum of 0.8kg/s for PFA particles. The uncertainties on these flow rates were therefore calculated.

Initially, the uncertainty of the mass measurement u_{mass} for each load cell package (or Loss-In-Weight (LIW) and Gain-In-Weight (GIW) systems) were calculated as the RSS of the respective load cells, LCA and NI 9208 AI uncertainties, which in turn were calculated as the RSS of their respective elemental uncertainties. The relationship given in Equation 4-20 was used to convert between units of mass and voltage, whereas the relationship given in Equation 4-11 was used to convert between units of mass and current.

$$mass\ in\ kg = \frac{rated\ capacity\ of\ load\ cell\ in\ kg}{V_E(0.002V)}$$

Equation 4-20

Where $V_E = 10V$ is the load cell excitation voltage.

The time taken for the test Δt in $seconds$ was then calculated using Equation 4-15 before using Equation 4-18 to calculate the uncertainty in $\dot{M}_p$.

4.6.3 Results

Key results of the gas and particle mass flow rate uncertainty analysis are given in Table 4-7 and Table 4-8 respectively. All values are given at 68% probability.

Variable	Symbol	Units	Value		% Uncertainty	
			Scenario 1	Scenario 2	Scenario 1	Scenario 2
Gas temperature	T_g	˚C	28 ± 0.228	49 ± 0.301	0.814	0.614
Absolute pressure at the orifice inlet	P_1	kPa	103.534 ± 0.686	119.338 ± 0.735	0.662	0.616
Pressure drop across the orifice	dP	Pa	429 ± 22.543	2035 ± 16.597	5.255	0.816
Gas mass flow rate	$\dot{M}_g$	kg/hr	183.6 ± 5.056	414 ± 3.673	2.754	0.887

Table 4-7 – Results of the gas mass flow rate design stage uncertainty analysis

Variable	Symbol	Units	Value		% Uncertainty	
			Minimum	Maximum	Minimum	Maximum
LIW Mass Measurement	$Mass$	kg	50 ± 4.522	250 ± 4.665	9.043	1.866
GIW Mass Measurement			50 ± 2.164	250 ± 2.449	4.328	0.980
LIW Mass Flow Rate	$\dot{M}_p$	kg/hr	252 ± 8.186	2880 ± 93.550	3.248	3.248
GIW Mass Flow Rate			252 ± 4.117	2880 ± 47.057	1.634	1.634

Table 4-8 – Results of the particle mass flow rate design stage uncertainty analysis

4.6.4 Discussion

The gas mass flow rate is calculated from the temperature, absolute pressure and differential pressure measurements. From the Table 4-7, the relative uncertainty in the differential pressure measurement is significantly higher than that for the temperature and absolute pressure measurements. The uncertainty associated with the differential pressure measurement therefore has a significant impact on the uncertainty of the gas mass flow rate, especially in the case of the low mass flow rate.

For the particle mass flow rate, the uncertainty on the mass measurement using the LIW system is significantly higher than that for the GIW system. This is expected. The rating (total load bearing capacity) of the load cells used for the LIW system is much larger than the actual weight to be measured in order to support the auger and its motor as well as the rotary valve and its motor. Since the accuracy of the load cells is a fraction of the maximum load bearing capacity, this unavoidable oversizing results in higher overall uncertainties.

5 Design Calculations

This chapter presents individual component models and process models developed iteratively to size the pipe diameters, auger feed rates, hopper volumes, cyclone geometry, orifice bore diameters, pressure transducers and blower requirements. Additionally, the required filter area was calculated using a method presented in Klinzing, et al. (1997) and is given in Appendix J.

5.1 Cyclone Sizing

A model was developed to determine the required cyclone geometry and number of cyclones necessary to achieve a gas-particle separation efficiency of at least 99% across a range of gas volume flow rates. The model also calculates the associated pressure drops. Literature on cyclones is given in Appendix B. A copy of the model is given in Appendix M.

5.1.1 Inputs

Both the efficiency and the pressure drop across a cyclone increases with increasing gas density (Koch & Licht, 1977). Low and high gas density scenarios were therefore used as inputs to the cyclone model. For both scenarios, a gas temperature of 60°C was used. For the low-density scenario, a pressure of 70kPa was used. For the high-density scenario, a pressure of 125kPa was used. The low-density scenario corresponds to values taken from the similarity matrix, given in Appendix O. The high-density scenario corresponds to the chosen maximum design temperature and pressure.

Densities given for PC in literature range from 1350 to 2000kg/m^3. However, this range considers not only South African PC, but PC found worldwide. A range of 1450 to 1700kg/m^3 was specified as appropriate to use for South African PC. The range is approximately ±10% of 1550kg/m^3, which is the density of PC used in calculations by Van der Merwe (2014). Cyclone efficiency increases with increasing particle size and density. In order to be conservative the minimum particle size and density was therefore used in the model.

At the time of development, the intended operating gas velocities of the test rig (in the test section) was specified as 3 to 30m/s to allow for a range of tests, from choking to similarity tests. These velocities were therefore used to calculate the operating design volume flow rates for the cyclone system.

Table 5-1 lists the inputs used in the model.

Property	Symbol	Value	Unit
Gas Temperature	T_g	60	°C
Min. Gas Pressure	$P_{g.min}$	70	kPa
Max. Gas Pressure	$P_{g.max}$	125	kPa
Pipe Diameter	D_{pipe}	102.26	mm
Min. Gas Velocity	$U_{g.min}$	3	m/s
Max. Gas Velocity	$U_{g.max}$	30	m/s
Min. Particle Diameter	D_p	37	µm
Min. Particle Density	ρ_p	1400	kg/m^3

Table 5-1 – Inputs to cyclone model

5.1.2 Model Explanation

The model sizes a cyclone based on the Stairmand type cyclone geometry, given in Figure 5-1, as it has relatively higher efficiencies and lower pressure drops when compared with other standard cyclone designs, according to the literature presented in Appendix B.

D is the cyclone diameter

$a = 0.5D$ is the inlet height

$b = 0.2D$ is the inlet width

$S = 0.5D$ is the exit length

$D_e = 0.5D$ is the exit diameter

$h = 1.5D$ is the cylinder height

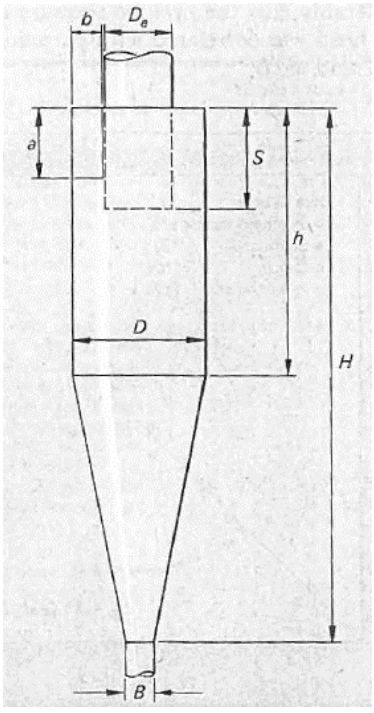

Figure 5-1 – Cyclone geometry, adapted from (Casal & Martinez-Benet, 1983)

Initially, the gas density ρ_g and dynamic viscosity μ_g are calculated using the ideal gas law (Equation 4-1) and Sutherland's formula (Equation 4-2) respectively.

Using $U_{g.min}$, Equation 5-1 to Equation 5-3 (Koch & Licht, 1977) are then solved simultaneously for the cyclone vortex exponent n and the cyclone body diameter D.

$$\eta_{D_p} = 1 - \exp\left\{-2\left[\frac{G\tau_{D_p}\dot{V}_g}{D^3}(n+1)\right]^{\frac{1}{2(n+1)}}\right\}$$

Equation 5-1

Where:

η_{Dp} is the cyclone efficiency for a particle diameter D_p

G is the dimensionless cyclone configuration factor, which is dependent on the cyclone geometry and is equal to 551.3 for a Stairmand type cyclone.

τ_{D_p} is the particle relaxation time in seconds for D_p defined by

$$\tau_{D_p} = \frac{\rho_p D_p^2}{18\mu_g}$$

Equation 5-2

and n is the vortex exponent correlation, given by

$$n = 1 - \left[1 - \frac{(12D)^{0.14}}{2.5}\right]\left[\frac{T_g + 460}{530}\right]^{0.3}$$

Equation 5-3

Equation 5-1 to Equation 5-3 are valid for imperial units only i.e. $\dot{V}_g$ is in ft^3/s; D is in ft; ρ_p is in lb/ft^3; μ_g is in lb/ft-s; and T_g is in °F.

The remaining cyclone dimensions are then calculated using the relationships given in Figure 5-1.

Using $P_{g.min}$, η_{D_p} is then plotted as a function of $\dot{V}_g$ using Equation 5-1.

$R_{salt} = \frac{v_i}{v_s}$ i.e. the cyclone inlet velocity v_i over cyclone saltation velocity v_s ratio is then plotted on the same axis as η_{D_p} using Equation 5-4 to Equation 5-6 (Kalen & Zenz, 1974).

$$v_i = \frac{\dot{V}_g}{ab}$$

Equation 5-4

$$v_s = 2.055\omega \left[\frac{\left(\frac{b}{D}\right)^{0.4}}{\left(1-\frac{b}{D}\right)^{\frac{1}{3}}} \right] D^{0.067} v_i^{\frac{2}{3}}$$

Equation 5-5

Where

$$\omega = \left[\frac{4g\mu_g(\rho_p - \rho_g)}{3\rho_g^2} \right]^{\frac{1}{3}}$$

Equation 5-6

Equation 5-5 and Equation 5-6 are valid for imperial units only.

Using $P_{g.max}$, the associated cyclone pressure drop ΔP_c is then plotted as a function of $\dot{V}_g$ using Equation 5-7 (Chuah, et al., 2003).

$$\Delta P_c = \frac{1}{2}\rho_g v_i^2 N_H$$

Equation 5-7

Where N_H is the inlet velocity head and is equal to 6.40 for a Stairmand type cyclone (Koch & Licht, 1977).

5.1.3 Results

The calculated cyclone dimensions are given below:

$D = 206mm$

$a = 103mm$

$b = 41mm$

$S = 103mm$

$D_e = 103mm$

$h = 309mm$

$H = 824mm$

$B = 77mm$

Figure 5-2 and Figure 5-3 provide plots of the cyclone efficiency and pressure drop vs. gas volumetric flow rates.

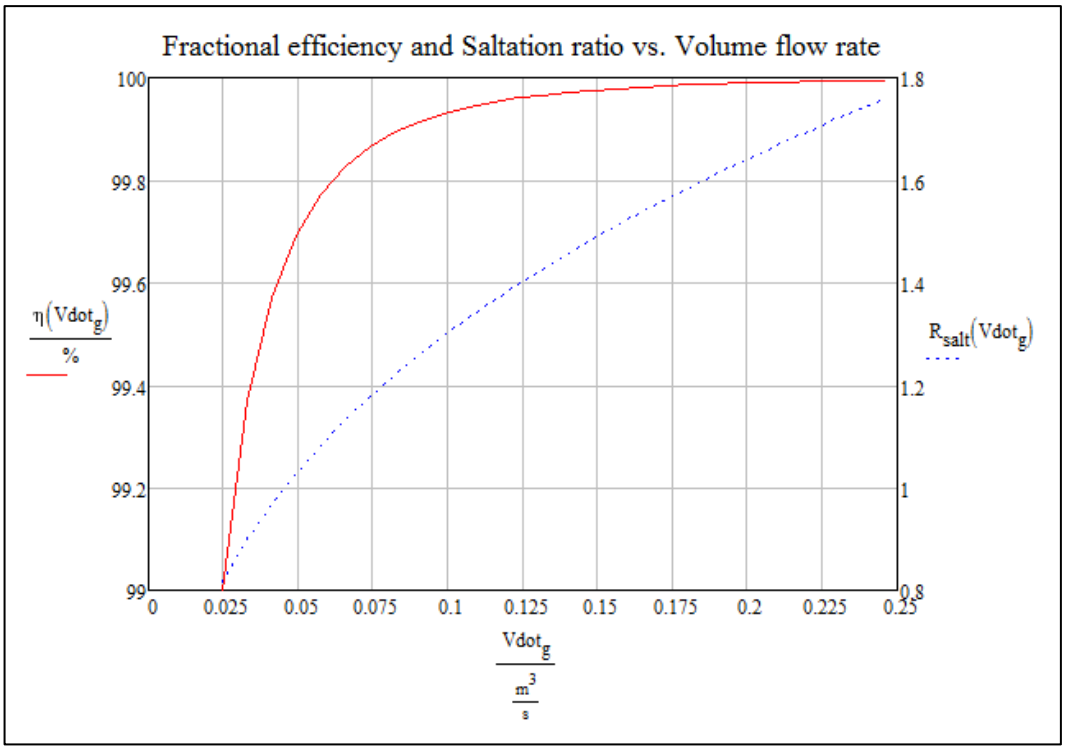

Figure 5-2 – Cyclone efficiency curve for low-density scenario

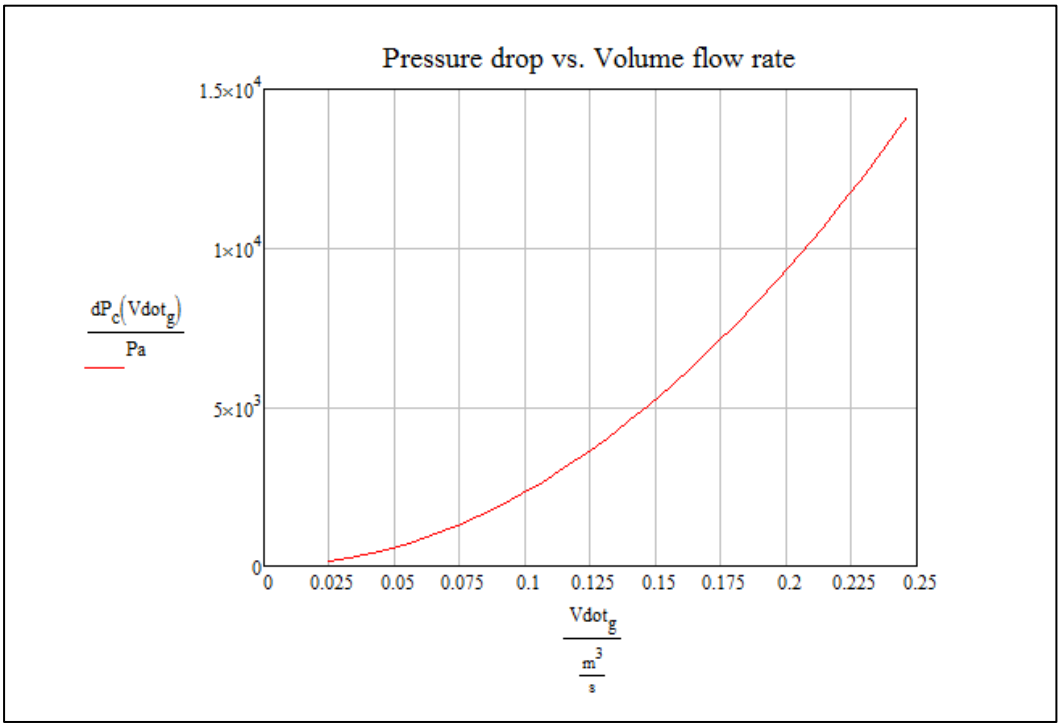

Figure 5-3 – Cyclone pressure drop curve for high-density scenario

5.1.4 Discussion

Referring to Figure 5-2, the cyclone separation efficiency is equal to or greater than 99% across the range of operating gas volume flow rates. However, the efficiency curve plotted does not account for particle re-entrainment which, according to the cyclone theory presented in Appendix B, begins to occur at R_{salt} values greater than 1.5. Therefore, the separation efficiency of the cyclone will begin to decrease at gas volume flow rates above 0.15m^3/s due to re-entrainment. One cyclone, with the dimensions given in Section 5.1.3, can therefore be used to obtain a 99% separation efficiency at gas flow rates up to 0.15m^3/s. However, for gas flow rates greater than 0.15m^3/s, two cyclones in parallel are required to prevent re-entrainment. The use of two cyclones at high gas flow rates also serves to reduce the pressure drop through the system. It is therefore recommended that one cyclone be used up to half of the maximum volume gas flow rate (0.125m^3/s) and two cyclones in parallel thereafter. Three cyclones were therefore procured to fit the physical layout of the initial concept, presented in Section 4.3. The dimensions for the actual cyclones procured are given in Appendix S.

5.2 Orifice Sizing

The pressure drop across the orifice plate contributes towards the overall system pressure drop and is also a factor in the selection of pressure transducers. From a design point of view, it is preferred to limit the overall pressure drop. However, for accurate measurement of the gas mass flow rate, a higher pressure drop across the orifice plate is preferred. At the time of development, the intended operating gas velocities of the test rig were known and not necessarily the gas mass flow rates. A model was therefore developed to plot the pressure drop vs gas velocity for orifice plates with different β values and used as a tool to select orifice plates for the prototype and proposed final test facility. A copy of the model is given in Appendix M.

5.2.1 Inputs

For fixed gas velocities in a pipeline, the mass flow rate of the gas is directly proportional to gas density. Low and high gas density scenarios were therefore used as inputs to the orifice model. For the proposed final test facility, the scenarios and rationales are the same as those given in Section 5.1.1.

For the prototype facility, a temperature and pressure of 25°C and 101.3kPa were used for the low-density scenario. For the high-density scenario, a temperature and pressure of 60°C and 125kPa were used. The low-density scenario corresponds to the chosen standard for room temperature and atmospheric pressure. The high-density scenario corresponds to the chosen maximum design temperature and pressure.

The gas velocities used for the prototype facility calculations correspond to the approximate minimum velocity needed to prevent saltation and half of the maximum volume flow rate required for the final test facility.

Table 5-2 and Table 5-3 list the inputs to model for the prototype and final test facility.

Property	**Symbol**	**Value**	**Unit**
Min. Gas Temperature	$T_{g.min}$	25	°C
Max. Gas Temperature	$T_{g.max}$	60	°C
Min. Gas Pressure	$P_{g.min}$	101.3	kPa
Max. Gas Pressure	$P_{g.max}$	125	kPa
Pipe Diameter	D_{pipe}	102.26	mm
Min. Gas Velocity	$U_{g.min}$	4	m/s
Max. Gas Velocity	$U_{g.max}$	15	m/s

Table 5-2 – Inputs to orifice model for prototype facility

Property	**Symbol**	**Value**	**Unit**
Gas Temperature	T_g	60	°C
Min. Gas Pressure	$P_{g.min}$	70	kPa
Max. Gas Pressure	$P_{g.max}$	125	kPa
Pipe Diameter	D_{pipe}	102.26	mm
Min. Gas Velocity	$U_{g.min}$	3	m/s
Max. Gas Velocity	$U_{g.max}$	30	m/s

Table 5-3 – Inputs to orifice model for final test facility

5.2.2 Model Explanation

Calculations are performed for both low and high-density scenarios.

Initially, the gas density ρ_g and dynamic viscosity μ_g are calculated using the ideal gas law (Equation 4-1) and Sutherland's formula (Equation 4-2) respectively.

The model assumes a pressure ratio $\tau = \frac{P_1}{P_2}$ of 95% and calculates the pipe Reynolds number Re using Equation 3-12.

Equation 4-12 to Equation 4-14 is then subsequently used to calculate the pressure drop dP across orifices with β values of 0.35, 0.45, 0.55, 0.65 and 0.75 over the range of gas velocities $U_{g.min}$ to $U_{g.max}$.

To account for uncertainty in the method, dP is then multiplied and divided by a factor of 0.95 for the low and high-density scenarios respectively, before being plotted on graphs of dP vs U_g.

The pressure loss after recovery $d\omega$ is also calculated using Equation 5-8, from ISO 5167-2:2003 (ISO, 2003).

$$d\omega = \frac{\sqrt{1-\beta^4(1-C_d^2)} - C_d\beta^2}{\sqrt{1-\beta^4(1-C_d^2)} + C_d\beta^2} dP$$

Equation 5-8

5.2.3 Results

For the prototype facility, the pressure drop vs. gas velocity for each orifice plate is given by Figure 5-4 and Figure 5-5. Here, Figure 5-4 is the low-density scenario and Figure 5-5 is the high-density scenario.

For the final test facility, the pressure drop vs. gas velocity for each orifice plate is given by Figure 5-6 and Figure 5-7. Here, Figure 5-6 is the low-density scenario and Figure 5-7 is the high-density scenario.

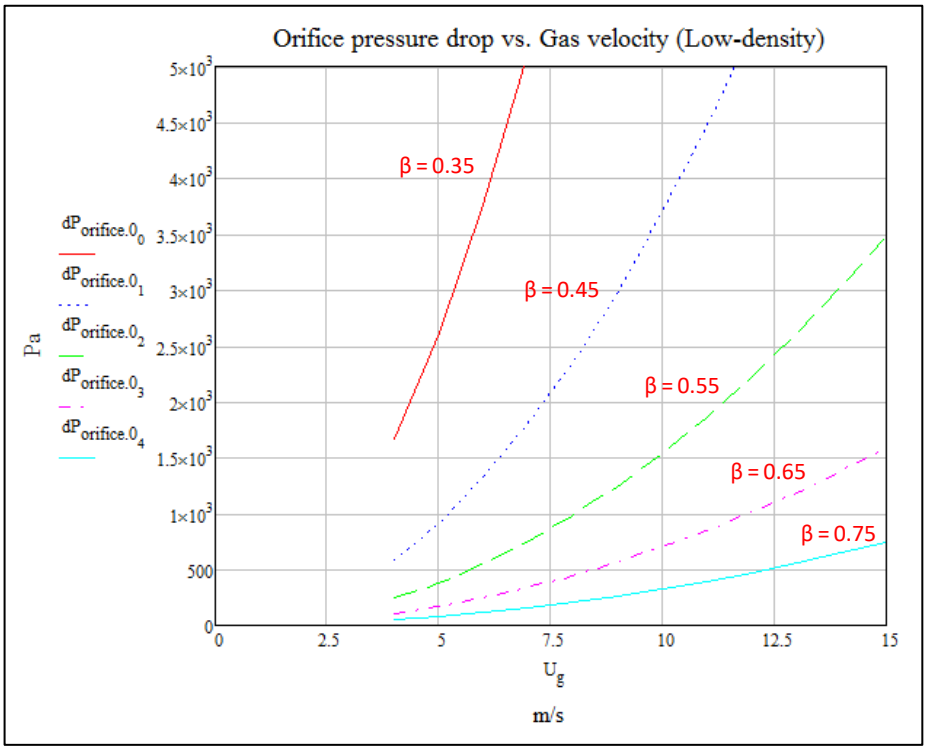

Figure 5-4 – Prototype orifice curves for low-density scenario

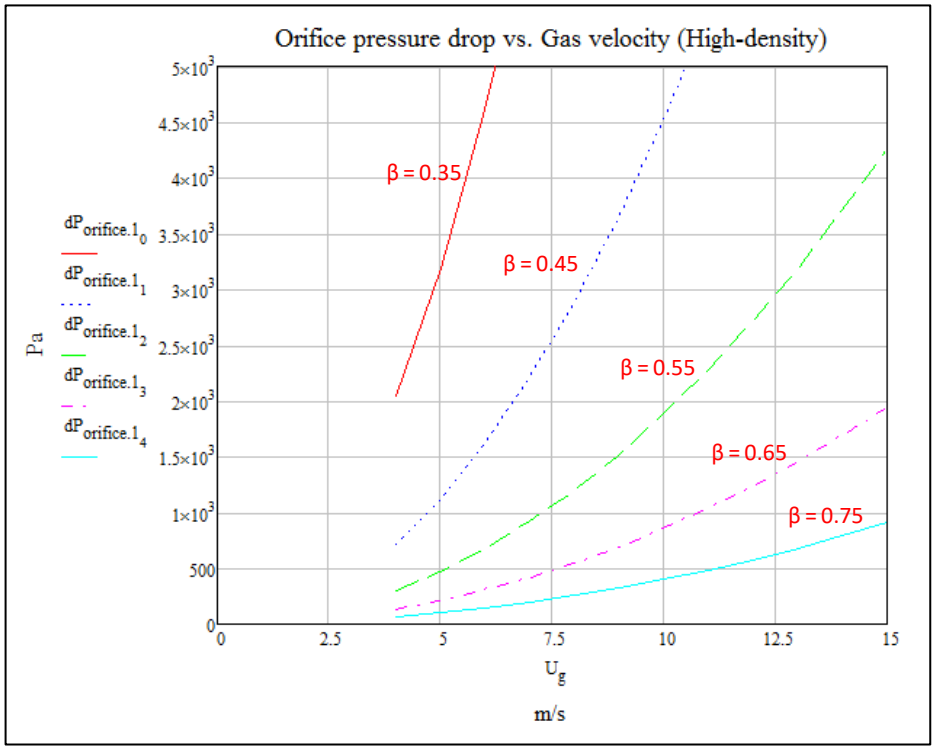

Figure 5-5 – Prototype orifice curves for high-density scenario

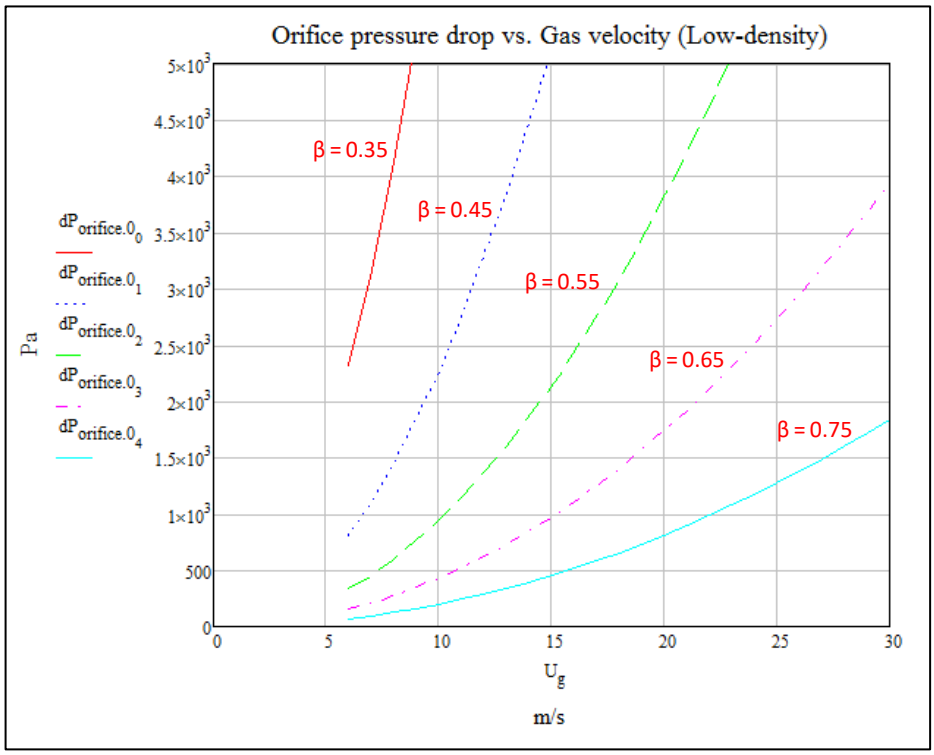

Figure 5-6 – Final facility orifice curves for low density scenario

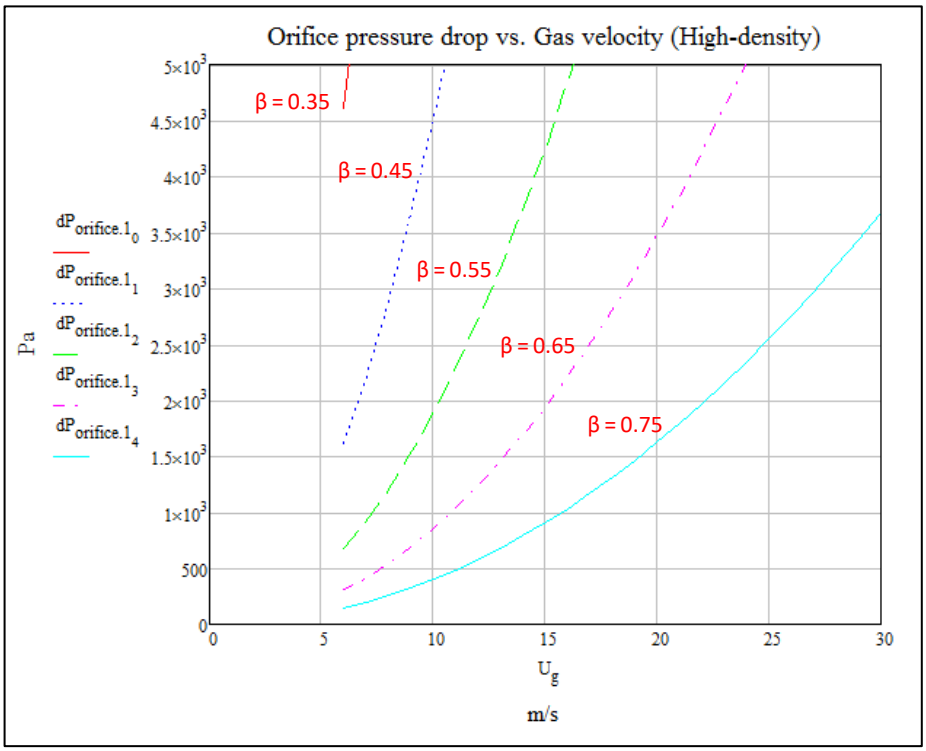

Figure 5-7 – Final facility orifice curves for high-density scenario

5.2.4 Discussion

For the prototype facility, an orifice with $\beta = 0.55$ was procured. According to Figure 5-4 and Figure 5-5, this will result in a minimum and maximum dP of 0.243 and 4.26kPa respectively and a maximum $d\omega$ of 2.76kPa.

For the final test facility, two orifice plates are recommended. One with $\beta = 0.55$ for gas velocities up to 15m/s and one with $\beta = 0.75$ thereafter. According to Figure 5-6 and Figure 5-7., this will result in a minimum and maximum dP of 0.337 and 4.26kPa respectively and a maximum $d\omega$ of 2.76kPa. It is noted here that an orifice with $\beta = 0.45$ could be used to increase the minimum pressure drop. However, using a $\beta = 0.55$ orifice is more practical, as it can be used for both the prototype and final facilities. Furthermore, for the β values selected, the range of pressure drops fall easily within the 0-10kPa measuring range of the PMD55 dP transducer presented in Section 4.5.1.

The uncertainty on the measurement of the minimum pressure drop of 0.243kPa was determined using the design phase uncertainty analysis given in Section 4.6. With the PMD55 measuring range set to default (between 0 and -5kPa), the uncertainty is approximately ±10%. With the PMD55 measuring range set between 0 and -1kPa, the uncertainty is less than ±1%. For perspective, the results given in Section 4.6.3 show that for a pressure drop of 0.429kPa, the uncertainty is approximately ±5% with the PMD55 measuring range set to default. It is therefore recommended that the default PMD55 measuring range be

used, except for tests at extremely low gas velocities, where the range can be adjusted for greater accuracy if desired.

5.3 Pipe, Feeder & Hopper Sizing

The final test facility needs to operate over a broad range of gas and particle mass flow rates. Tests conducted in the horizontal and vertical test sections also need to be isolated from upstream processes. This cannot be achieved with a constant pipe diameter. For example, if the pipe diameter were constant throughout, saltation would occur upstream of the horizontal test section during saltation tests. Also, saltation would occur in the horizontal conveying section during choking tests. A model was therefore developed as a tool, to select pipe diameters for different test rig sections and to determine the feed rate requirements for the auger and the hopper volume. The model is also used to supplement the process model presented in Section 5.4. A copy of the model is given in Appendix M.

5.3.1 Inputs

The model contains constant, iterative and varying inputs. Constant inputs include the particle and loose poured bulk densities for PC and PFA. A particle density of 2300kg/m^3 is used for PFA based on the results (given in Appendix R) of solids density tests conducted on PFA from two different power stations. A bulk density of 750kg/m^3 is used for PC (Van der Merwe, 2014) and a bulk density of 860kg/m^3 is used for PFA, as this is the value used by the supplier of the hopper and auger. Iterative inputs include the minimum and maximum particle mass flow rates, as well as pipe diameters. Varying inputs include the gas temperature and pressure, as well as a representative particle diameter.

The final facility is required to operate over a wide range of flow properties. The model was therefore run for several varying input scenarios. Table 5-4 lists the inputs for one such scenario.

Property	**Symbol**	**Value**	**Unit**
Density of PC	$\rho_{p.PC}$	1550	kg/m^3
Density of PFA	$\rho_{p.PFA}$	2300	kg/m^3
Bulk Density of PC	$\bar{\rho}_{p.PC}$	750	kg/m^3
Bulk Density of PFA	$\bar{\rho}_{p.PFA}$	860	kg/m^3
Min. Particle Mass Flow Rate	$\dot{M}_{p_0}$	0.07	kg/s
Max. Particle Mass Flow Rate	$\dot{M}_{p_1}$	0.697	kg/s
Horizontal Test Pipe Bore Diameter	$D_{pipe.100}$	102.26	mm

Vertical Test Pipe Bore Diameter	$D_{pipe.250}$	242.88	mm
Feed Pipe Bore Diameter	$D_{pipe.80}$	77.92	mm
Acceleration Pipe Bore Diameter	$D_{pipe.90}$	90.12	mm
Gas Pressure	P_g	70	kPa
Gas Temperature	T_g	60	°C
Particle Diameter	D_p	37	µm

Table 5-4 – Inputs to pipe, feeder & hopper sizing

5.3.2 Model Explanation

The reader is referred to Figure 8-1 to Figure 8-3 for the proceeding text.

The model assumes that P_g and T_g remain constant at each pipe section.

Initially, the gas density ρ_g and dynamic viscosity μ_g are calculated using the ideal gas law (Equation 4-1) and Sutherland's formula (Equation 4-2) respectively.

The superficial particle velocity U_p in each pipe line is calculated using Equation 2-7.

The particle terminal velocity u_{t0} was calculated using Equation 3-18 or Equation 3-19, depending on the Reynolds number at the single particle terminal velocity Re_{t0}, which was calculated using Equation 3-17.

The saltation and choking velocities U_{salt} *and* U_{gc} in each pipeline were calculated using the Rizk correlation (Equation 2-21) and Yang's choking theory (Equation 2-41 and Equation 2-42) respectively. No safety factors were employed.

For the horizontal test pipe, the model lists the required U_{salt} and loading at saltation $z = Z$ for saltation tests. For the remaining pipe lines, U_{salt}, U_{gc}, Z and the expected superficial gas velocity U_g during saltation tests are then listed for comparison purposes.

For the vertical test pipe, the model lists the required U_{gc} and loading at choking $z = Z$ for choking tests. For the remaining pipe lines, U_{salt}, U_{gc}, Z and the expected superficial gas velocity U_g during choking tests are then listed for comparison purposes.

The above velocities and loadings are then compared and manual iteration of the pipe bore diameters is required such that settling does not occur in pipe sections other than the test section. For example, saltation should not occur in the acceleration section or horizontal test pipe during choking tests. Bore diameters for standard ASTM A106 seamless pipes are used.

Note that the values for $\dot{M}_{p_0}$ and $\dot{M}_{p_1}$ given in Table 5-4 correspond to the minimum and maximum feed rates attainable for PC using the procured auger. The range of required particle feed rates was constantly adjusted throughout the project based on results obtained during the development of the process models given in Section 5.4. However, $\dot{M}_{p_1}$ was limited such that a hopper volume no greater than 300L was necessary for a 5-minute test.

5.3.3 Results

For the inputs given in Table 5-4, saltation tests can be conducted in a pipe with a 102.26mm bore diameter for U_g between 7.42 and 14.19m/s with Z between 1.57 and 8.47. For the preceding flow properties, Table 5-5 lists the actual U_g in the remaining pipelines, together with U_g and Z required for saltation or choking in these pipelines. A determination on whether saltation or choking occurs is made by the following check: If the actual U_g is greater than the required U_g and the actual Z is less than the required Z, then saltation or choking does not occur. Note that the actual Z values for each pipeline are between 1.57 and 8.47.

Pipe	**Actual U_g (m/s)**	**U_g Req. for Saltation/ Choking (m/s)**	**Z Req. for Saltation/ Choking**	**Does Saltation/ Choking Occur?**
Feed Pipe (77.92mm)	12.77 to 24.44	7.84 to 15.01	2.56 to 13.30	No
Horizontal Acceleration Pipe (90.12mm)	9.55 to 18.27	7.61 to 14.57	1.97 to 10.25	No
Vertical Acceleration Pipe (90.12mm)	9.55 to 18.27	1.83 to 3.90	8.22 to 38.28	No
Vertical Test Pipe (242.88mm)	1.32 to 2.52	1.32 to 2.81	1.57 to 7.32	Yes (See discussion)

Table 5-5 – Checking for settling in pipelines during saltation tests

For the inputs given in Table 5-4, choking tests can be conducted in a pipe with a 242.88mm bore diameter for U_g between 1.32 and 2.81m/s with Z between 1.57 and 7.32. For the preceding flow properties, Table 5-6 lists the corresponding U_g in the remaining pipelines, together with U_g and Z required for saltation or choking in these pipelines. The same check is then made to determine whether saltation or choking occurs. Here, the actual Z values for each pipeline are between 1.57 and 7.32.

Pipe	Actual U_g (m/s)	U_g Req. for Saltation/ Choking (m/s)	Z Req. for Saltation/ Choking	Does Saltation/ Choking Occur?
Feed Pipe (77.92mm)	12.80 to 27.30	7.84 to 15.01	2.56 to 13.30	No
Horizontal Acceleration Pipe (90.12mm)	9.57 to 20.41	7.61 to 14.57	1.97 to 10.25	No
Horizontal Test Pipe (102.26mm)	7.43 to 15.85	7.42 to 14.19	1.57 to 8.17	No (See discussion)
Vertical Acceleration Pipe (90.12mm)	9.57 to 20.41	1.83 to 3.90	8.22 to 38.28	No

Table 5-6 – Checking for settling in pipelines during choking tests

5.3.4 Discussion

For the proposed pipelines choking will occur in a vertical test pipe with a nominal bore diameter of 242.88mm. It is therefore suggested that this pipe only be used for choking tests and replaced with a 102.26mm pipe for similarity and saltation tests.

Furthermore, saltation may occur in the horizontal test pipe during choking tests. It is noted that by changing the inputs to the model, it was observed that the probability of this occurring increases with decreasing D_p. To mitigate this, a vertical test pipe with a larger bore diameter can be used during choking tests. However, increasing this bore diameter will increase the required gas mass flow rate needed to conduct choking tests and consequently, increase the pressure drop through the system.

5.4 Process Models

Four process models were developed for the proposed final test facility to simulate four different test scenarios namely: for similarity in horizontal flow, for vertical flow, for saltation and for choking. A final model was then developed for the prototype facility and is presented in this section. Should these models be employed in a follow up project to do the detail design of the final facility, it will require further refinement to include the exact geometry. The process model for the prototype facility is given in Appendix I. The process models for the proposed final test facility are given in the CD accompanying this thesis.

5.4.1 Inputs

The prototype facility is required to operate over a wide range of flow properties. The model therefore contains constant and varying inputs. Table 5-7 lists fixed model inputs, whereas Table 5-8 lists the unique inputs for a selected scenario. Rationales for the fixed inputs are as follows:

ISO 5167-1 2003 (ISO, 2003) specifies a typical pipe roughness value of ≤3mm for hot drawn seamless pipes. This was used to estimate the relative pipe roughness.

A filter loss factor of 0.1Pa·s/m^3 was assumed based on the performance curve for the filter cartridge presented in Appendix S.

ISO 5167-1 2003 (ISO, 2003) specifies required upstream and downstream lengths for orifice installations. Pipe lengths for clean gas flow were chosen to meet these requirements and to ensure that the flow was fully developed before introducing particles into the pipeline. Gas-particle mixture pipe lengths were chosen to minimise the space and blower pressure rise requirements, but to allow for sufficient particle acceleration before bends. A long bend radius was chosen to minimise the system pressure drop.

A blower isentropic efficiency of 60% was assumed.

Variable	**Symbol**	**Units**	**Value**
Particle density	ρ_p	kg/m^3	2300
Ambient temperature	$T_{g.0}$	˚C	25
Ambient pressure	$P_{g.0}$	kPa	101.3
Orifice beta value	β		0.55
Test pipe diameter (ID)	$D_{pipe.test}$	mm	77.92
Gas only pipe diameter	$D_{pipe.gas}$	mm	102.26
Test pipe relative roughness	$\varepsilon_{r.test}$		3.85×10^{-4}
Gas only pipe relative roughness	$\varepsilon_{r.gas}$		2.934×10^{-4}
Filter loss factor	k_{filter}	Pa·s/m^3	0.1
Return line length	L_{89}	m	4
Vertical acceleration length	L_{67}	m	2.5
Test section bend radius	$R_{b.test}$	m	1
Horizontal acceleration length	L_{45}	m	4

Length from orifice outlet to feed point	L_{34}	m	6
Length from blower to orifice inlet	L_{12}	m	2.5
Blower isentropic efficiency	η_{blower}	%	60

Table 5-7 – Fixed model inputs for the prototype process analysis

Variable	**Symbol**	**Units**	**Value**
Test temperature	$T_{g.test}$	˚C	43
Absolute pressure at feed point	$P_{g.test}$	kPa	114
Particle mass flow rate	$\dot{M}_p$	kg/s	0.4
Superficial gas velocity at feed point	$U_{g.test}$	m/s	14
Representative particle diameter	D_p	µm	65

Table 5-8 – Unique model inputs for prototype process analysis 25

5.4.2 Model Explanation

The reader is referred to Figure 4-12 for the proceeding text. Note that the facility has been discretized into smaller pipe sections. For the inputs given in Table 5-8, the model calculates the flow properties at each point, by stepping forward or backwards through each pipe section. Frequently used equations are listed first. The calculations performed for the discretized sections are then explained.

- The gas density ρ_g is calculated using Equation 4-1.
- The gas dynamic viscosity μ_g is calculated using Equation 4-2.
- The single particle terminal velocity for Stoke's flow $u_{t0.stokes}$ is calculated using Equation 3-18.
- The single particle terminal velocity for intermediate flow $u_{t0.int}$ is calculated using Equation 3-20.
- The Darcy-Weisbach solids-wall friction factor for vertical conveying λ_{pv} is calculated using Equation 3-41. Note that the subscript D is omitted.
- The Darcy-Weisbach solids-wall friction factor for horizontal conveying λ_{ph} is calculated using Equation 3-42.
- The Darcy-Weisbach gas friction factor λ_g is calculated using Equation 3-11.
- The infinitely dilute particle drag coefficient $C_{D\infty}$ for intermediate flow is calculated using Equation 3-4.
- Equation 3-49 is used for the particle EOM.
- Equation 3-50 is used to calculate the voidage α_g.
- The pipe Reynolds number Re_{pipe} calculated using Equation 3-12.

Check for Saltation

Initially, the Pipe, Feeder & Hopper Sizing model presented in section 5.3 is used to check if saltation occurs for the given model inputs. The inputs are then adjusted if required.

Intermediate Calculations

The model assumes that T_g is constant and equal $T_{g.test}$ throughout. Initially, the gas density ρ_g and the dynamic viscosity μ_g at the feed point are calculated. Here, the density at the feed point is calculated using $P_{g.test}$. Subsequently, the gas mass flow rate, the AF ratio and the loading $z = Z$ are calculated.

Across Filter (Points 10 to 11)

The model assumes that ρ_g across a pipe section is constant and equal to either the inlet or outlet ρ_g at that section. The density across the filter ρ_{g1011} is calculated using the pressure at the filter outlet P_{g11}. The volume flow rate through the filter is then simply calculated. The pressure drop across the filter is then calculated as follows:

$$dP_{1011} = k_{filter}\dot{V}_{g1011}$$

Equation 5-9

The pressure at the filter inlet P_{g10} is then calculated as the sum of P_{g11} and dP_{1011}.

Across Cyclone (Points 9 to 10)

The density across the cyclone ρ_{g910} is calculated using the pressure at the cyclone outlet P_{g10}. The volume flow rate through the filter is then simply calculated. Using the method presented in Section 5.1.2, the pressure drop across the cyclone dP_{910} is then calculated. As a check, the cyclone efficiency η and inlet velocity over cyclone saltation velocity ratio $\frac{v_i}{v_s}$ is also evaluated. The pressure at the cyclone inlet P_{g9} is calculated as the sum of P_{g10} and dP_{910}.

Return Line (Points 8 to 9)

The density across the return line ρ_{g89} is calculated using P_{g9}. U_{g89} is then simply calculated. Note that the model assumes that U_g across a pipe section is constant and equal to either the inlet or outlet U_g at that section. The particle velocity at the beginning of the return line u_{p8} is then assumed to be equal to $0.5U_{g89}$. Re_{89} and α_{g8} are subsequently calculated. λ_g is then calculated using a numerical scheme built into Mathcad.

The particle EOM is then solved using the finite-difference method (FDM) presented in Appendix G. The results of which include vectors of the particle displacement x, particle velocity u_p, gas velocity u_g and voidage α_g as a function of time. The solids-wall friction factor at the end of the return line λ_{p9} is then calculated. As a check, u_p and x are plotted against time, to evaluate if the pipe length is long enough for sufficient particle acceleration.

The pressure drop across the return line dP_{89} is then calculated using Equation 3-44 to Equation 3-48 and multiplied by 1.3 to account for uncertainty in the correlations used. The pressure at the beginning of the return line $P_{g.8}$ is then calculated as the sum of $P_{g.9}$ and dP_{89}.

Vertical Section (Points 6 to 7)

Initially, the pressure drop from the beginning of the vertical section up until the beginning of the return line dP_{68} is assumed, so that the pressure at the beginning of the vertical section P_{g6} can be calculated as the sum of P_{g8} and dP_{68}. The density across the vertical section ρ_{g67} is then calculated using P_{g6}. The pressure drop across the vertical section dP_{67} is then calculated using the same method presented for the return line. The pressure at the end of the vertical section P_{g7} is then calculated by subtracting dP_{67} from P_{g6}.

Top Bend (Points 7 to 8)

u_p, u_g, α_g and λ_p across the top bend is assumed constant and equal to u_p, u_g, α_g and λ_p at the end of the vertical section. The pressure drop across the top bend dP_{78} is then calculated using the bend pressure drop theory presented in Appendix A, where the gas contribution is assumed negligible. The pressure at end of the top bend P_{g8} is then calculated by subtracting dP_{78} from P_{g7}.

dP_{68} is calculated as the sum of dP_{67} and dP_{78} and the previously assumed value updated manually (and the vertical and top bend calculations repeated) until it is approximately equal to the calculated value.

Horizontal Section (Points 4 to 5)

Initially, the pressure drop from the feed point up until the beginning of the vertical section dP_{46} is assumed, so that the pressure at the feed point can P_{g4} can be calculated as the sum of P_{g6} and dP_{48}. The density across the horizontal section ρ_{g45} is then calculated using P_{g4}. The pressure drop across the horizontal section dP_{45} is then calculated using the same method presented for the return line. However, the assumption that u_p at the beginning of the section is equal to $0.5U_g$ is replaced by the assumption that α_g at the beginning of the section is equal to 0.45. The pressure at the end of the horizontal section P_{g5} is then calculated by subtracting dP_{45} from P_{g4}.

Bottom Bend (Points 5 to 6)

The bottom bend pressure drop dP_{56} is calculated using the same method presented for the top bend. dP_{46} is then calculated as the sum of dP_{45} and dP_{56} and the previously assumed value updated manually (and the horizontal and bottom bend calculations repeated) until it is approximately equal to the calculated value.

The value for $P_{g.test}$ is then updated manually (and all the above calculations repeated) until it is approximately equal to P_{g4}.

Orifice Outlet to Feed Point (Points 3 to 4)

The gas density from the orifice outlet to the feed point ρ_{g34} is calculated using P_{g4}. U_{g34} and Re_{34} are then simply calculated, before calculating λ_g using a numerical scheme built into Mathcad. The pressure drop from the orifice outlet to the feed point dP_{34} is then calculated using Equation 3-47. The pressure at the orifice outlet P_{g3} is then calculated as the sum of P_{g4} and dP_{34}.

Across Orifice (Points 2 to 3)

Initially, a pressure ratio τ is assumed so that the pressure at the orifice inlet P_{g2} and subsequently the density at orifice inlet ρ_{g2} can be calculated. Equation 4-12 to Equation 4-14 is then used to calculate the pressure drop across the orifice dP_{23} and divided by a factor of 0.95 to account for uncertainty in the method. P_{g2} is then re-calculated as the sum of P_{g3} and dP_{23} and τ updated manually (and the orifice calculations repeated) until the initially calculated value for P_{g2} is approximately equal to the final calculated value.

Blower Outlet to Orifice Inlet (Points 1 to 2)

The gas density from the blower outlet to the orifice inlet ρ_{g12} is calculated using P_{g2}**.** The pressure drop from the blower outlet to the orifice inlet dP_{12} is calculated using the same method presented for the orifice outlet to feed point. The pressure at the blower outlet P_{g1} is then calculated as the sum of P_{g2} and dP_{12}**.**

Blower Temperature Rise

The pressure drop across the system dP_{01} is then calculated by subtracting P_{g0} from P_{g1}. The temperature at the blower outlet T_g is then calculated as follows:

$$T_g = T_{g.0} + dT$$

Equation 5-10

Where, from (Anderson, 2002)

$$dT = \frac{T_{g.0}}{\eta_{blower}}\left(\frac{P_{g1}}{P_{g0}}^{\frac{\gamma-1}{\gamma}} - 1\right)$$

Equation 5-11

$T_{g.test}$ is then manually updated (and all the above calculations repeated) until it is approximately equal to T_g.

Check for Saltation and Choking

The Pipe, Feeder & Hopper Sizing model presented in Section 5.3 is used to check if saltation or choking occurs for the output flow properties. If required, the inputs are then adjusted and the entire process restarted.

Furthermore, note that the following additional assumptions are made in the model:

- There is no pressure recovery after the orifice plate.
- The pressure drop in gas only bends, pipe reducers and expanders and pipe joins are negligible.
- The sight glass is considered part of the adjoining pipes.
- The bore diameter of the blow through rotary feeder is equal to the test pipe bore diameter.
- The pressure drop due to the rotary feeder blades/ buckets is negligible.

Comparison with Final Facility Models

The process models for the final facility differ from the process model for the prototype facility in the following ways:

- There are additional inputs relating to the geometry of the final facility. For example, the number of cyclones to use during operation and the different pipe diameters.
- There is an additional calculation for the pressure drop across the heat exchanger dP_{HX}. The pressure drop is calculated using Equation 5-12.

$$dP_{HX} = k_{HX}\left(\frac{\dot{V}_g}{A_{HX}}\right)^2$$

Equation 5-12

Where $k_{HX} = 320\frac{Pa \cdot s^2}{m^2}$ is the assumed heat exchanger loss factor and $A_{HX} = 0.106m^2$ is the assumed frontal area of the heat exchanger.

- The sequence in which calculations are performed differ in each model. The flow chart given in Figure 5-8 illustrates the sequence for the prototype model. Additional flow charts are given for the final facility in Appendix H.

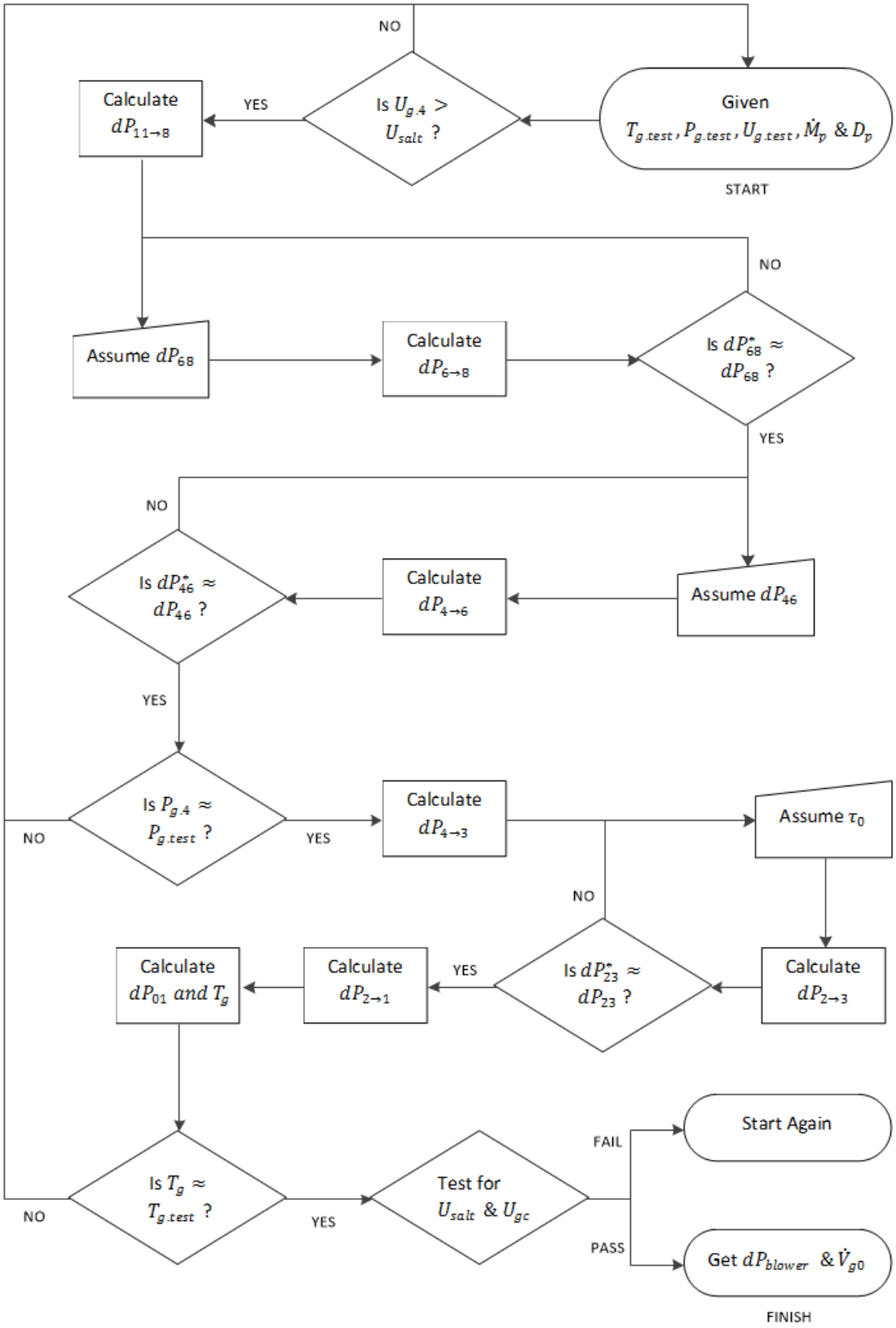

Figure 5-8 – Flowchart for prototype process model

5.4.3 Blower Operating Envelope

The process model calculates the pressure drop across the system dP_{system}, as well as the gas density $\rho_{g.in}$ and the volume flow rate $\dot{V}_{g.in}$ at the blower inlet. The blower pressure rise dP_{blower} required at standard atmospheric conditions (i.e. $\rho_{g.std}$ = 1.2kg/m^3) is also calculated using Equation 5-13, derived from the similarity laws for fans.

$$dP_{blower} = dP_{system}\left(\frac{\rho_{g.std}}{\rho_{g.in}}\right)$$

Equation 5-13

To determine the required blower operating envelope, dP_{blower} is plotted against $\dot{V}_{g.in}$ for a number of model inputs. Figure 5-9 shows the required blower operating points for the prototype facility as well as the operating curve of the blower (at maximum speed) used for the prototype facility.

Additionally, although the final facility models require refinement, Figure 5-10 shows a selection of predicted operating points for the prototype and final test facility, as well as the operating curve of the blower (at maximum speed) used for the prototype facility, at standard atmospheric conditions.

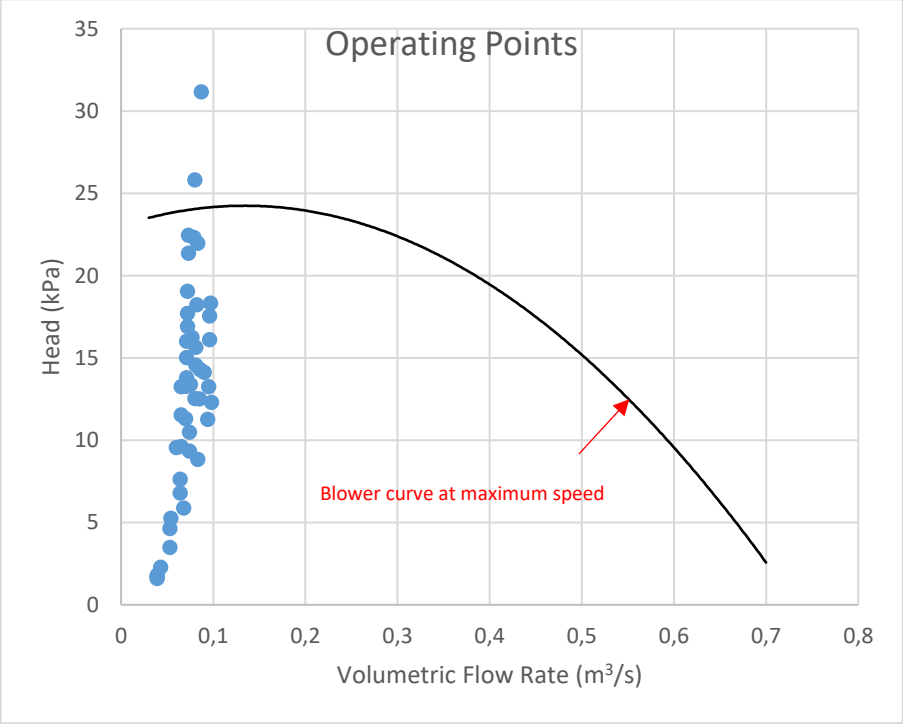

Figure 5-9 – Predicted prototype operating points

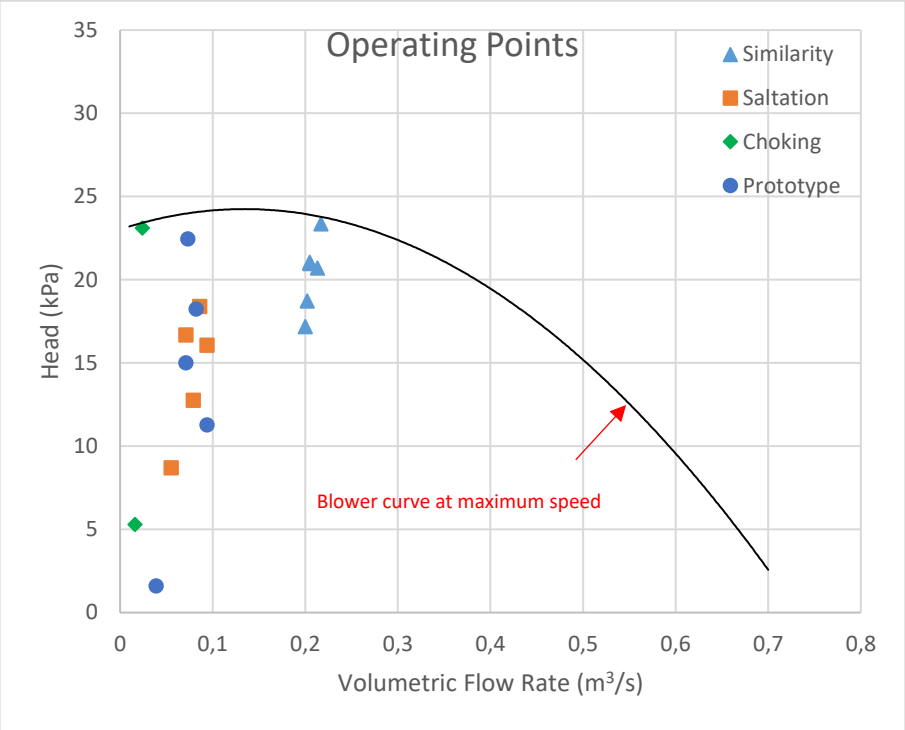

Figure 5-10 – Predicted prototype and final facility operating points

5.4.4 Process Flow Diagrams

Figure 5-11 to Figure 5-13 show selected primary flow diagrams (PFDs) for the prototype facility, generated using the results of the prototype model. The bottom right hand corner of each PFD shows the respective variable inputs used.

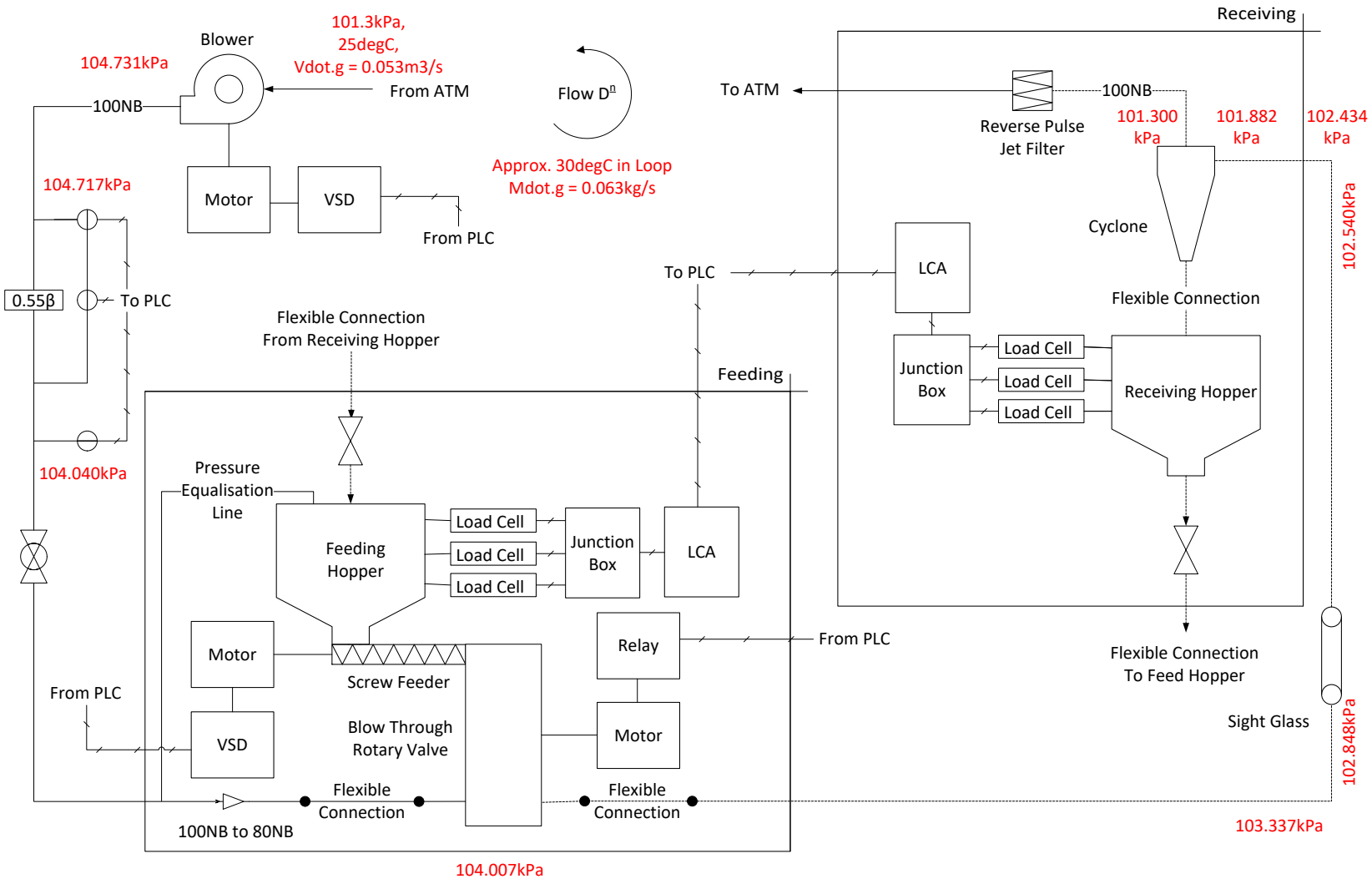

Figure 5-11 – Prototype PFD 19

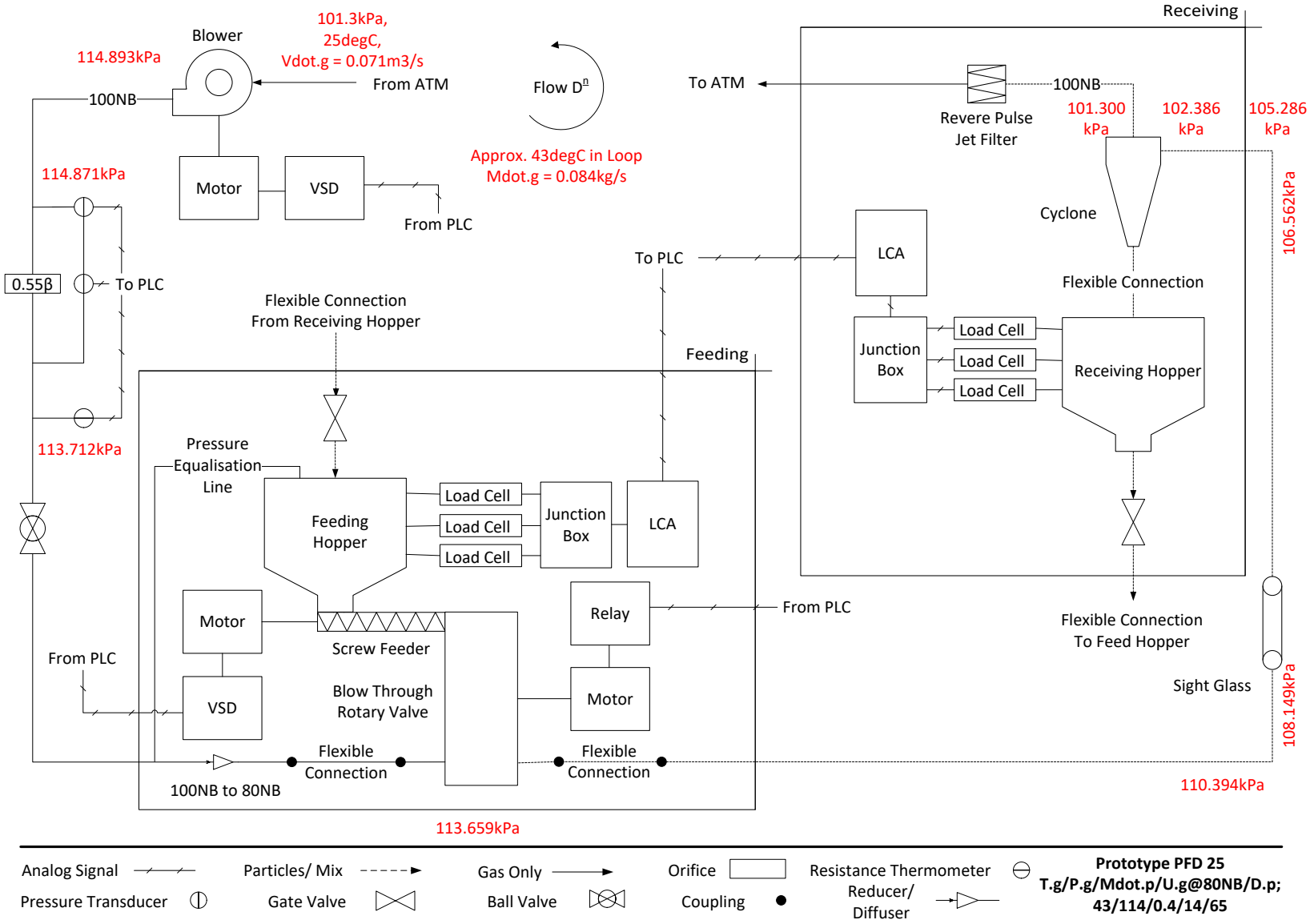

Figure 5-12 – Prototype PFD 25

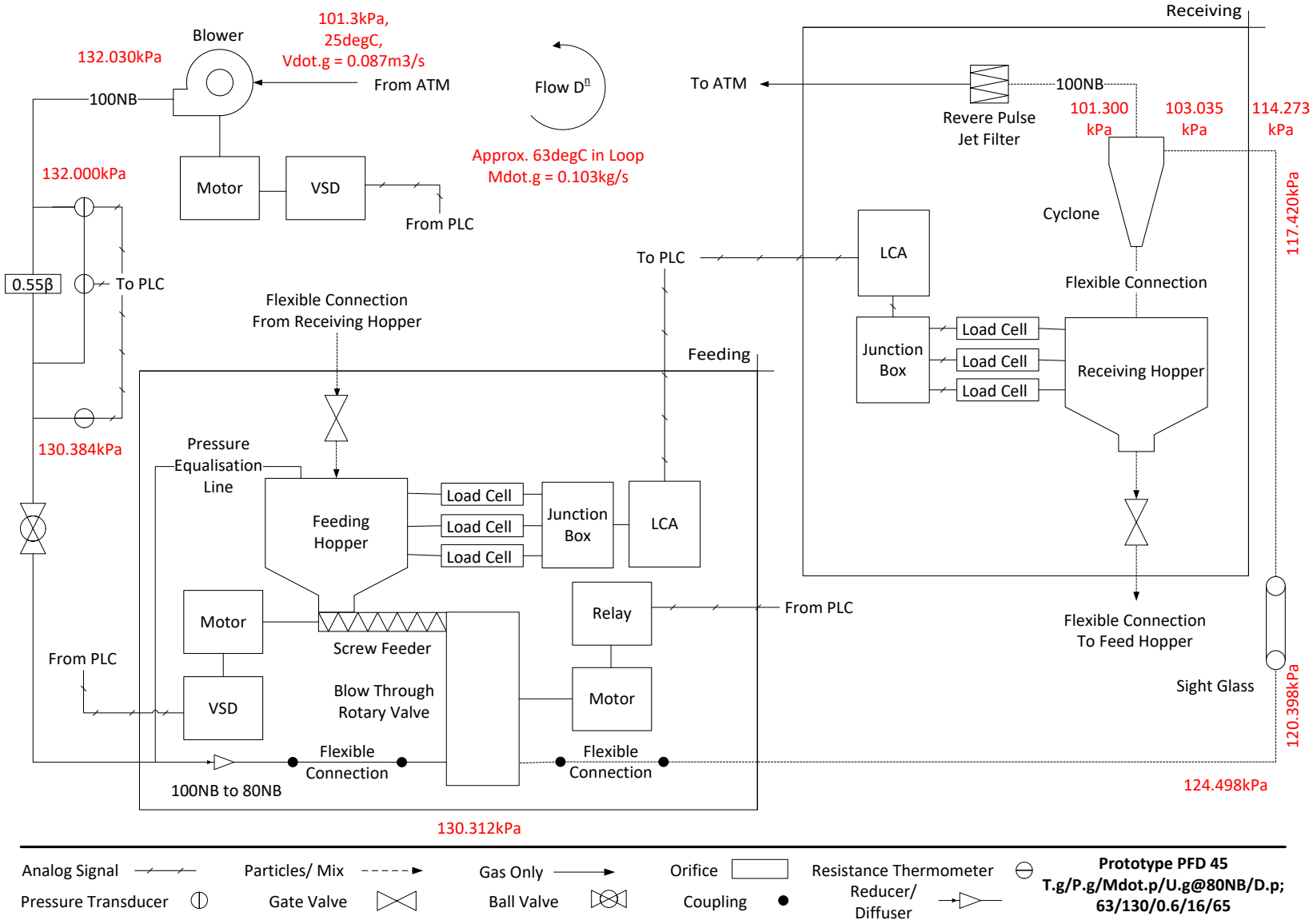

Figure 5-13 – Prototype PFD 45

5.4.5 Discussion

The process models predict the system operating points for desired input test conditions, which enable the selection of a suitable blower. It is noted that a simplified approach was taken to model the filter pressure drop, which resulted in a negligible pressure drop for all variable inputs. The pressure drop through the cyclone was also modelled using the geometry of the cyclone calculated in Section 5.1, instead of the actual final cyclone geometry. Furthermore, the cyclone diameter was incorrectly input into the model as 204mm, instead of 206mm. Due to time limitations this was not corrected since the geometry used results in a conservative estimate of the cyclone pressure drop.

The models can also be used to plot PFDs, which enables the selection of suitable instrumentation such as pressure transducers and RTDs. The PFDs also enable a visual evaluation of the process for different test conditions. For example, referring to Figure 5-11 to Figure 5-13, it can be seen that the pressure drops in the horizontal, vertical and gas bends increase with increased gas and particle mass flow rates. This is useful, in that a sensitivity analysis can be conducted to determine how each input variable affects the corresponding system pressure drop. A sensitivity analysis was not performed during this project. However, from model results obtained, it is seen that the system pressure drop increases significantly with a decreasing representative particle diameter.

The blower used for the prototype facility was readily available. According to Figure 5-9, only two points lie above the operating envelope of the blower. Furthermore, according to Figure 5-10, the blower is capable of providing the sufficient pressure and flow requirements to allow for choking, saltation and similarity tests to be conducted. It was therefore deemed unnecessary to purchase a larger blower. However, it is advised that the final test facility models be revised first before selecting a blower.

6 Prototype Construction and Commissioning

A commercial engineering company was contracted to produce the detail construction drawings, construct the prototype facility and to assemble the electrical components. Space was allowed within the electrical cabinet to allow for additional equipment that may be required for the final test facility. Photos of the facility and the electrical cabinet are given in Figure 6-1 and Figure 6-2 respectively. Additional photos are given in Appendix U.

Commissioning of the facility was entirely done by the candidate. During commissioning, the following issues were realised and need to be attended to in the design of the final test facility:

- It was found that leaks were more prominent at interfaces where a pressure clamping force was used (flanged interfaces, the top hopper lid and the bottom hopper door) as opposed to areas where couplings were used.
- It was found that the cyclone induced vibrations onto the supporting frame structure.

Figure 6-1 – Prototype Facility

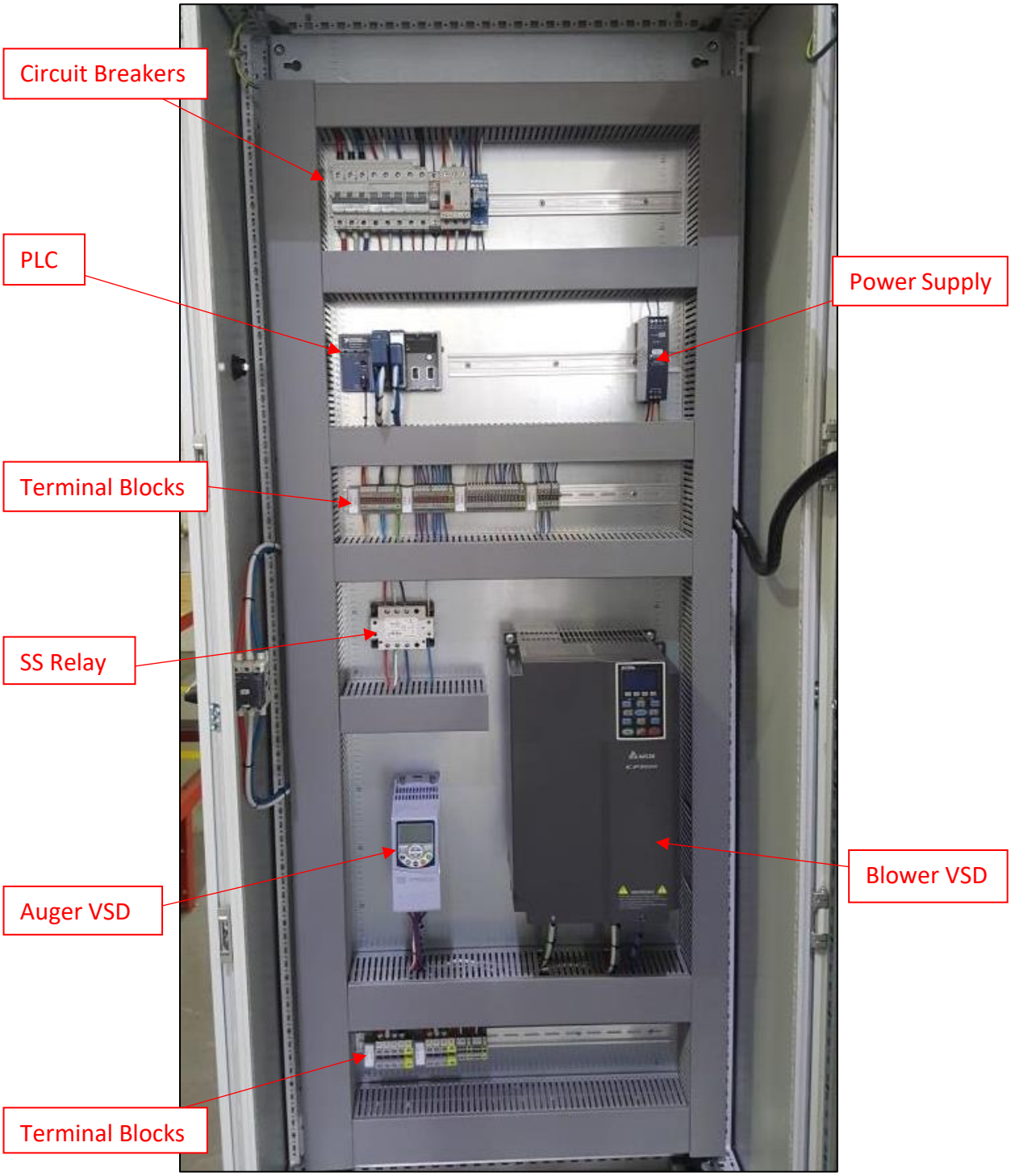

Figure 6-2 – Electrical Cabinet

7 Prototype Test Results

This chapter presents the results of load cell calibrations performed, the test procedures followed as well as the results and discussion of analyses performed on data obtained during testing.

7.1 Load Cell Calibration

The load cells or GIW and LIW systems were calibrated in situ using 15 x 20kg certified test weights. The procedures followed are listed below:

1. Place 300kg of test weights on top of the bottom hopper.
2. Remove the test weights.
3. Set the measured value on the bottom hopper LCA to 0kg.
4. Place 240kg of test weights on top of the bottom hopper.
5. Set the measured value on the bottom hopper LCA to 240kg.
6. Remove the test weights.
7. Place a single test weight (20kg) on top of the bottom hopper and subsequently record the mass reading on the PLC.
8. Repeat step 7 at denominations of 60, 120, 180, 240, 280 and 300kg.
9. Determine the straight-line calibration constants for the actual vs. measured values.
10. Repeat steps 1 to 9 for the top hopper.

Table 7-1 and Table 7-2 provide the measured vs. actual values, as well as the predicted values after calibration. Figure 7-1 and Figure 7-2 provide plots of the calibration curves fitted using linear regression.

Bottom Hopper (LIW)								
Actual load (kg)	0	20	60	120	180	240	280	300
Measured load (kg)	0.110	20.191	60.125	119.989	180.081	240.091	280.181	300.550
Estimated load after calibration (kg)	0.045	20.113	60.020	119.844	179.896	239.866	279.930	300.285

Table 7-1 – LIW calibration data and results

Top Hopper (GIW)								
Actual load (kg)	0	20	60	120	180	240	280	300
Measured load (kg)	-0.075	20.427	62.749	123.672	186.055	244.795	283.459	304.650
Estimated load after calibration (kg)	-1.151	19.065	60.796	120.868	182.380	240.300	278.424	299.319

Table 7-2 – GIW calibration data and results

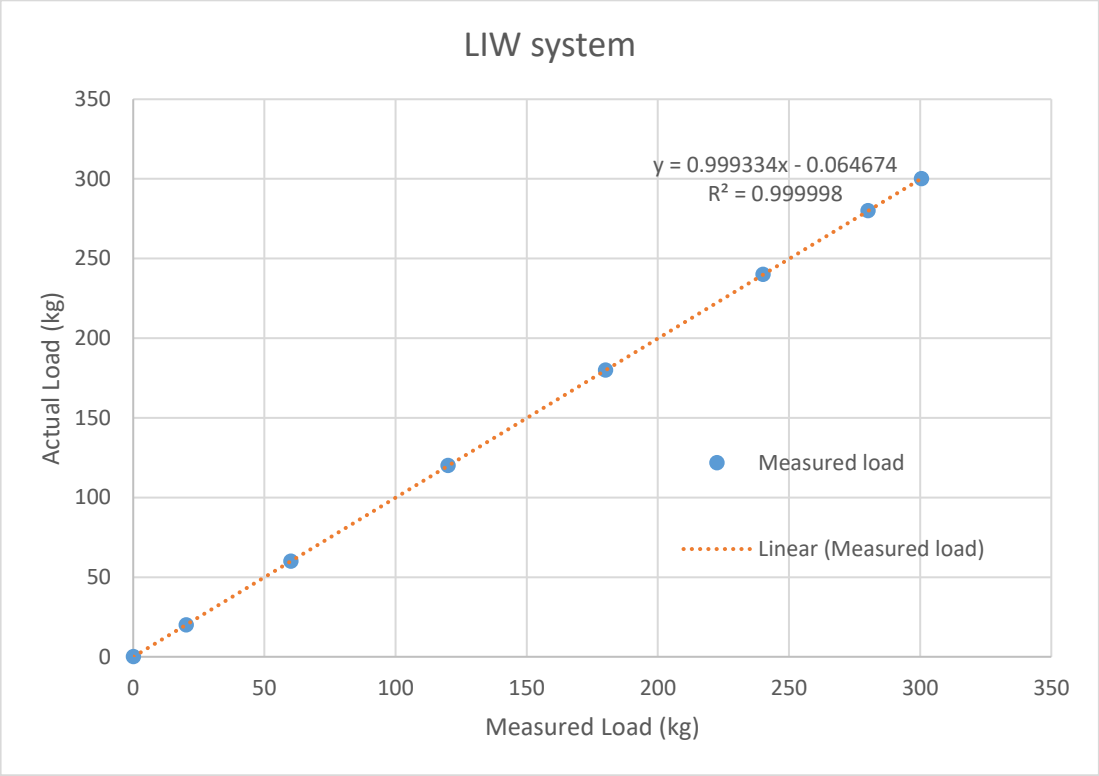

Figure 7-1 – LIW weight calibration curve

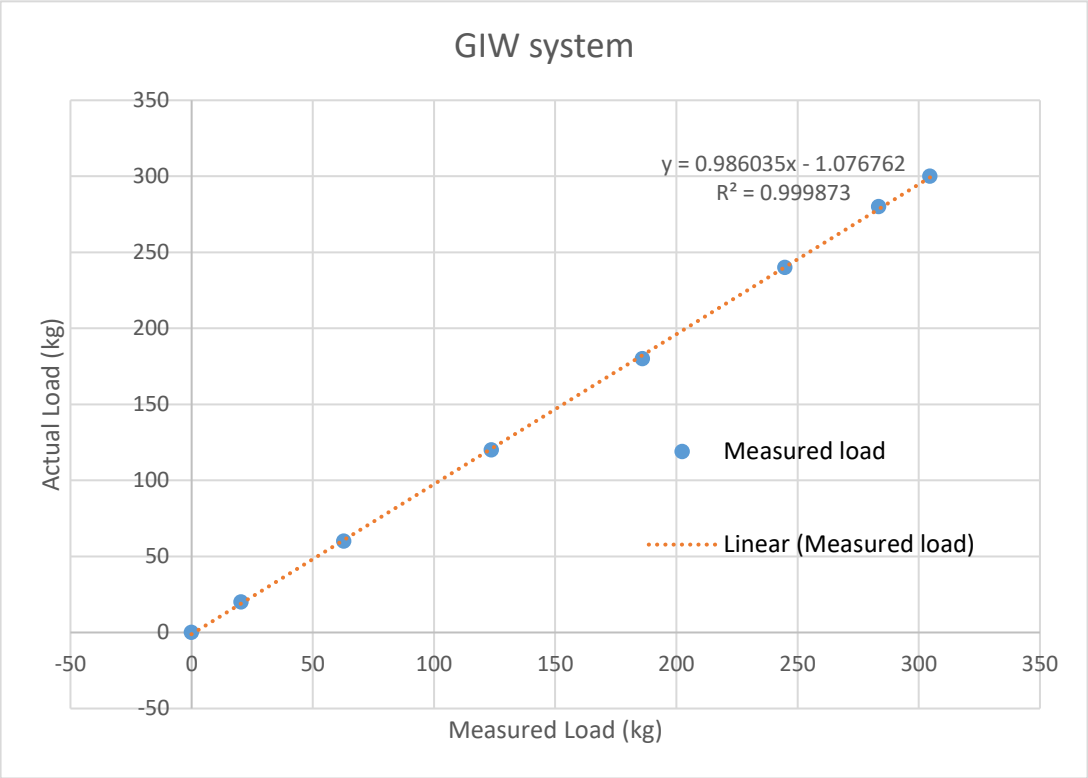

Figure 7-2 – GIW calibration curve

7.2 Test Procedures

To demonstrate and characterise the performance of the gas and particle mass flow rate control systems, as well as to estimate the efficiency of the cyclone and evaluate the feasibility of the proposed test facility in its entirety, 25 tests were conducted at the flow rates given in Table 7-3. The apparatus and test procedures are given first, followed by analyses performed on the gas and particle mass flow rates. A mass balance analysis is also presented before comparing test results with the outputs of the process model presented in Section 4.6 and discussing the results.

Apparatus

1. ±300kg FA.
2. 1 x Prototype facility.
3. 1 x LabVIEW and Scilab enabled computer.
4. 1 x 20L bucket.
5. 1 x Electronic scale.

Test Procedures

1. Ensure that ±300kg of PFA is in feed hopper.
2. Using the PLC, run the blower at 45Hz.

3. Monitor the upstream pressure. If greater than 112kPa, run the reverse pulse jet filter unit for 5 minutes.
4. Feel for leaks at the knife gate valves. If necessary, tighten the valves.
5. Stop the PLC and turn off and empty the reverse pulse jet filter unit.
6. Using the PLC, enable the blower and the “Record” button.
7. Manually record the weight of each hopper.
8. Set the blower to run at the desired gas mass flow rate. Allow the gas mass flow rate to reach steady state.
9. If necessary, partially close the ball valve such that the process temperature increases to the desired value.
10. Open the ball valve and subsequently enable the rotary feed and the auger. Set the auger to run at the desired particle flow rate.
11. Once the desired particle flow rate becomes unattainable, disable the auger and rotary feed.
12. Run the blower at 45Hz for 1 minute to clear any residual particles from the conveying pipelines.
13. Disable the blower and manually record the weight of each hopper.
14. Stop the PLC and run the reverse pulse jet unit for 5 minutes.
15. Empty the PFA within the reverse pulse jet unit into the 20L bucket.
16. Using the electronic scale, record the weight of the PFA within the 20L bucket.
17. Repeat procedures 1 to 16 for each set of test conditions given in Table 7-3.
18. Should an undesirable event occur during testing, stop the PLC and investigate.
19. Should the PLC become unresponsive at any stage, engage the emergency stop button.

Test No.	Gas Flow Rate (kg/s)	Particle Flow Rate (kg/s)	Expected Temp. (˚C)	Expected Gas Vel. (m/s)	Loading	PFD Reference	Run Time for 300kg (min)
1	0.086	0.6	53	14	6.954	30	8.3
2	0.094	0.6	57	15	6.36	44	8.3
3	0.103	0.6	63	16	5.837	45	8.3
4	0.077	0.5	43	13	6.478	32	10
5	0.085	0.5	46	14	5.915	33	10
6	0.093	0.5	54	15	5.381	46	10
7	0.077	0.4	40	13	5.179	26	12.5
8	0.084	0.4	43	14	4.770	25	12.5

9	0.091	0.4	46	15	4.417	24	12.5
10	0.099	0.4	53	16	4.057	29	12.5
11	0.076	0.3	38	13	3.929	43	16.67
12	0.082	0.3	40	14	3.639	42	16.67
13	0.089	0.3	43	15	3.368	41	16.67
14	0.096	0.3	46	16	3.132	40	16.67
15	0.076	0.2	35	13	2.642	22	25
16	0.088	0.2	39	15	2.278	21	25
17	0.102	0.2	44	17	1.970	20	25
18	0.115	0.2	49	19	1.745	28	25
19	0.063	0.16	31	11	2.536	39	31.25
20	0.075	0.16	34	13	2.127	38	31.25
21	0.088	0.16	37	15	1.827	37	31.25
22	0.107	0.16	44	17	1.502	36	31.25
23	0.051	0.08	28	9	1.564	31	62.5
24	0.063	0.08	30	11	1.276	19	62.5
25	0.081	0.08	33	14	0.994	18	62.5

Table 7-3 – Test matrix

7.3 Gas Flow Rate Analysis

The inputs, methodology and results of the gas mass flow rate analysis are given below. A copy of the detailed analysis is given in Appendix N.

7.3.1 Inputs

20 Samples were recorded per second for all tests. Figure 7-3 shows a 10 second moving average of the instantaneous (calculated at each sample) gas and particle mass flow rates. For each test, the approximate steady state period was identified as depicted.

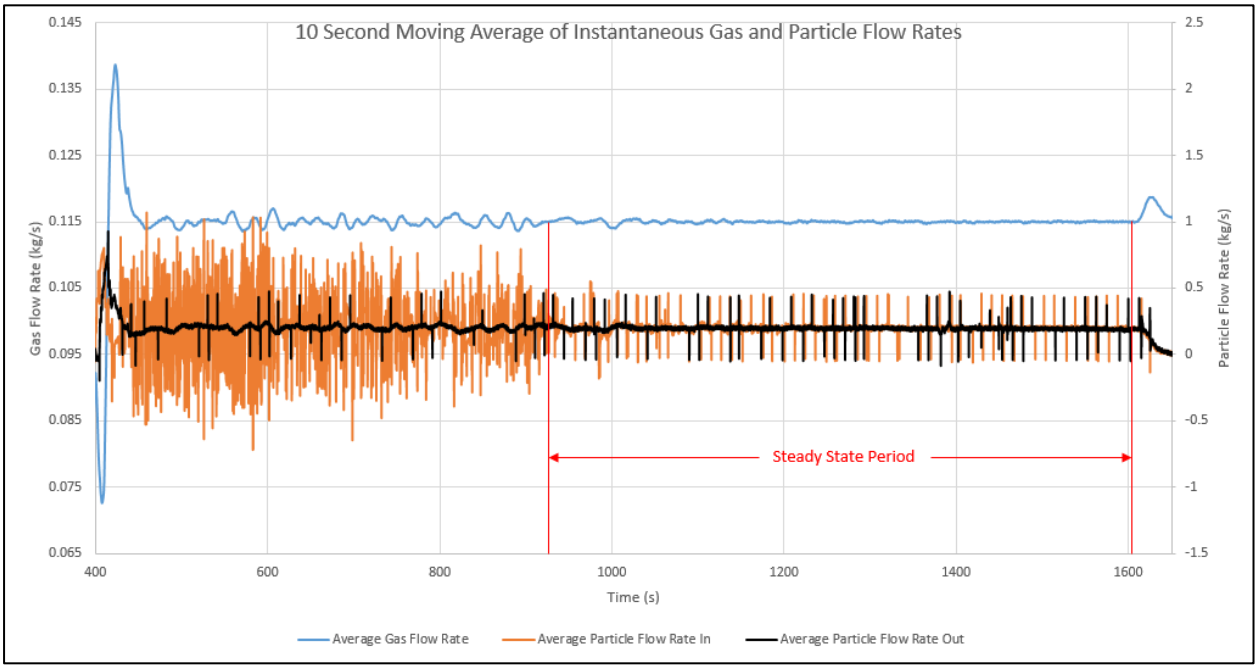

Figure 7-3 – Gas and particle mass flow rate readings

The average (or mean) and the standard deviation (or statistical uncertainty) during the steady state period were then calculated for the following variables, which were used as inputs for the analysis:

- Gas temperature T_g in ˚C.
- Absolute pressure at the orifice inlet P_1 in kPa.
- Pressure drop across the orifice dP in kPa.
- Gas expansibility factor ε_g.
- Orifice discharge coefficient C_d.

7.3.2 Methodology

For each test, the instrument uncertainties for the mean values of T_g, P_1 and dP were calculated using the methodology presented in the design phase uncertainty analysis (Section 4.6). These uncertainties were then combined with their respective statistical uncertainties using the RSS method.

The mean density at the orifice inlet ρ_1 during the steady state period was calculated using the ideal gas law (Equation 4-1) and its corresponding uncertainty using Equation 4-18.

The design based uncertainties for C_d, ε_g, D_{pipe} and D_{vc} were calculated using the methodology presented in the design phase uncertainty analysis and combined with their respective statistical uncertainties using the RSS method.

The mean gas mass flow rate $\dot{M}_g$ was then calculated using Equation 4-12 and its uncertainty using Equation 4-19.

7.3.3 Results

Figure 7-4 shows a graph of the actual gas mass flow rate achieved for each test vs. the required gas mass flow rate. Tabulated results for the gas mass flow rate as well as the measured gas temperature, orifice upstream pressure and the pressure drop across the orifice are given in Appendix P.

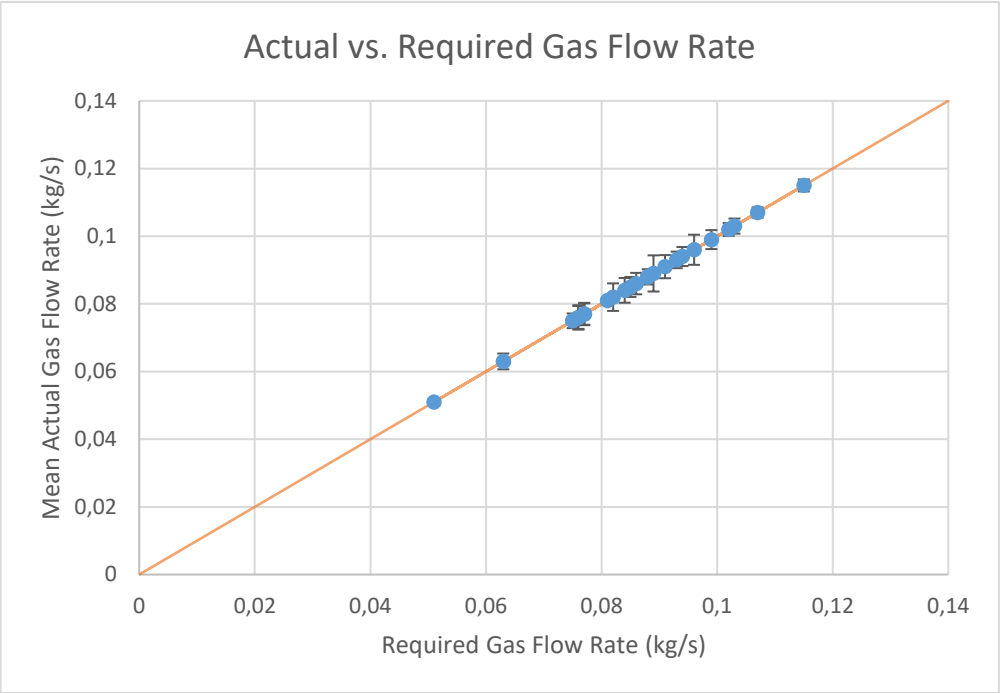

Figure 7-4 – Actual vs. required gas flow rate

7.4 Particle Flow Rate Analysis

The particle flow rate analysis consists of three parts. First, the uncertainty of the mass measurements are calculated, which includes the combined uncertainty of the measurement instrument, i.e. the combined uncertainty of the load cells, the LCA and the NI 9208 AI, as well as the uncertainty associated with the calibration procedure and the statistical uncertainty of the mass measurements. Secondly, the particle flow rate is then calculated as the gradient of a fitted curve through multiple measurement points. Finally, the uncertainty of the particle flow rate is then calculated as the uncertainty in the gradient of the fitted curve. The inputs, methodology and results of the analysis are given below. A copy of the detailed analysis is given in Appendix N.

7.4.1 Inputs

The uncertainty associated with the calibration of the load cells is included in the calculation of the mean particle mass flow rate and it's associated uncertainty. The analysis therefore includes fixed and variable inputs. The fixed inputs include the measured mass points during calibration, the corresponding actual mass points and their associated uncertainties. The uncertainty on the measured mass points is the design

phase uncertainty of the measuring instrument at the measured points. The uncertainty on the actual mass points then also incorporates the uncertainty associated with the calibration process. Here, each calibration mass piece of 25kg has an associated uncertainty of 1g and a confidence level of 68% is assumed.

The variable inputs were then taken as follows: For each test, a 1 second moving average of the uncalibrated mass recorded by the LIW and GIW systems are plotted against time as shown in Figure 7-5. Ten evenly distributed uncalibrated mean mass points are then taken across the same steady state period used for the gas flow rate analysis, together with their respective calibrated statistical uncertainties and the time during which they were recorded. These serve as inputs for the analysis.

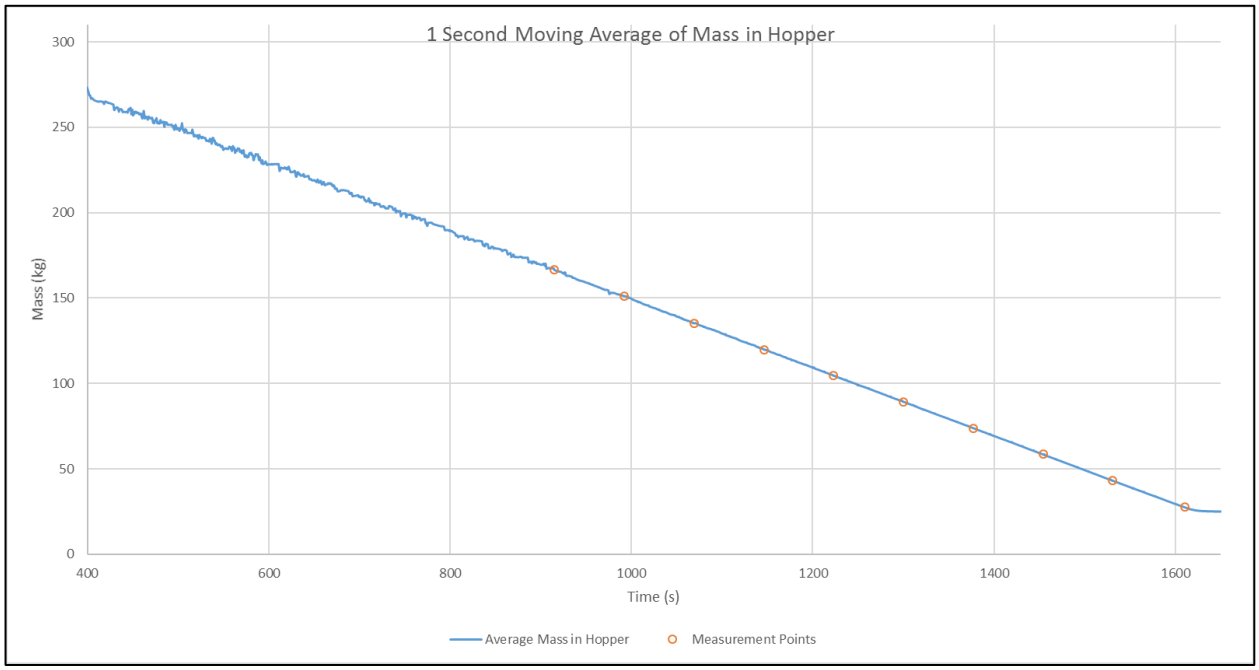

Figure 7-5 – Uncalibrated mass in bottom (LIW) hopper

7.4.2 Methodology

Calculations were performed for both the LIW and GIW system.

Calculating the Uncertainty in the Mean Mass Measurements

Initially, each uncalibrated mass measurement x is calibrated and the uncertainty in the calibrated measurement $u_y(x)$ calculated by solving Equation 7-1 to Equation 7-6 numerically. These equations are derived in Appendix G.

$$u_y(x) = \sqrt{\sum_{i=1}^{n}\left(\frac{\partial y}{\partial X_i}u_{X_i}\right)^2 + \sum_{i}^{n}\left(\frac{\partial y}{\partial Y_i}u_{Y_i}\right)^2}$$

Equation 7-1

Where:

n is the number of measurement points taken during calibration

X_i is the measured mass during calibration for an actual mass Y_i at the measured point i

u_{X_i} is the design phase uncertainty of the measuring instrument at the measured point i

u_{Y_i} is the uncertainty of the mass pieces used for the calibration process at the measured point i

y is the indicated mass after calibration for a measured mass x and is calculated as follows:

$$y = a^T F$$

Equation 7-2

where

$$a^T = (\alpha^{-1}\beta)^T = (\varepsilon\beta)^T = \beta^T \varepsilon^T$$

Equation 7-3

α and β are matrices and are calculated as follows

$$\alpha_{jk} = \sum_{i=1}^{n} \left(X_i^j X_i^k\right)$$

Equation 7-4

$$\beta_k = \sum_{i=1}^{n} \left(Y_i X_i^k\right)$$

Equation 7-5

where j and k indicate position in a m by m matrix, where m is equal to the order of the calibration curve.

Also,

$$F_k = x^k$$

Equation 7-6

u_y is therefore calculated as a function of the combined uncertainty of the measuring instrument, i.e. the combined uncertainty of the load cells, the LCA and the NI 9208 AI, as well as the uncertainty associated with the calibration procedure.

The combined uncertainty on each mass measured u_M is then calculated by summing the respective statistical uncertainty of the calibrated measurement point $u_{y.stat}$, i.e. the standard deviation of the mean calibrated measurement points over the 1 second measurement period, and u_y using the RSS method.

Calculating the Mean Particle Flow Rate

The calibrated mass measurement points $M = y$ including u_M are then plotted against the respective measurement time T_m as in Figure 7-6 (the error bands on the mass measurements are so small that they cannot be seen).

A linear curve is then fitted through the measurement points using Equation 7-2 to Equation 7-6, which yields the same results as that given by Excel's built in regression analysis. The gradient ∇ of the fitted curve is equal to the mean particle mass flow rate.

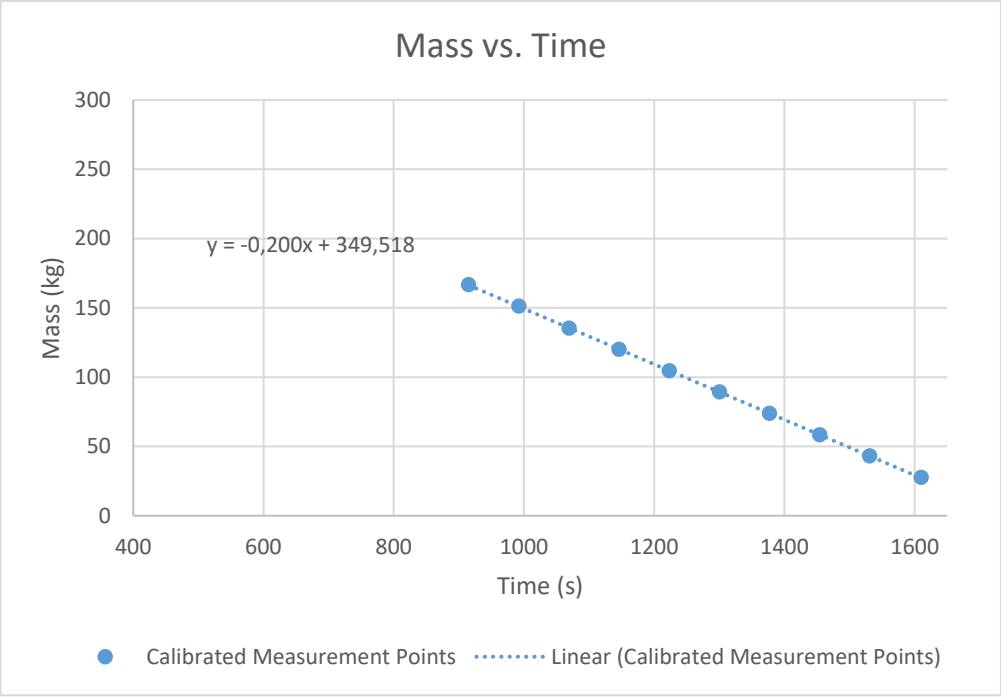

Figure 7-6 – Mass measurements (including uncertainty) vs. Time

Calculating the Uncertainty in the Mean Particle Flow Rate

Finally, the uncertainty in the mean particle mass flow rate $u_\nabla(t)$ is calculated using Equation 7-7, which is derived in Appendix G.

$$u_\nabla^2(t) = \sum_{i=1}^{n}\left(\left(\sum_{k=0}^{m}\left(T_{m_i}{}^{k}\sum_{j}^{m}\varepsilon_{kj}jt^{j-1}\right)\right)^2 u_{M_i}^2\right)$$

Equation 7-7

Where:

n is the number of measurement points taken

T_{m_i} is the time at the measured point i

u_{M_i} is the uncertainty on the measured mass at the measured point i,

and $u_{\nabla}(t)$ is constant for a linear curve.

7.4.3 Results

Figure 7-7 show graphs of the actual particle mass flow rate achieved for each test vs. the required particle mass flow rate (the error bands are so small that they cannot be seen). Tabulated results are also given in Appendix P.

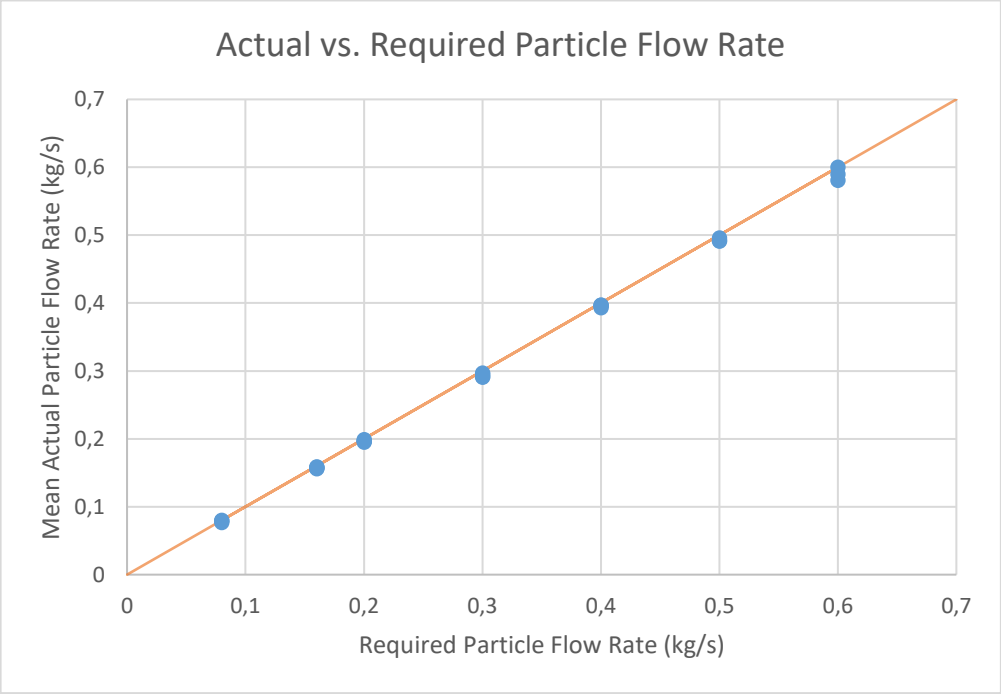

Figure 7-7 – Actual vs. required particle flow rate

7.5 Particle Loading Analysis

The actual loading during each test was easily calculated together with its uncertainty using Equation 4-18. Figure 7-8 shows a graph of the actual loading vs. it's respective set point. Tabulated results are also given in Appendix P. Furthermore, it is beneficial to evaluate if the particle flow rate affects the measurement of the gas flow rate and vice versa. Figure 7-9 shows this relationship (the error bands on the particle mass flow rates are so small that they cannot be seen).

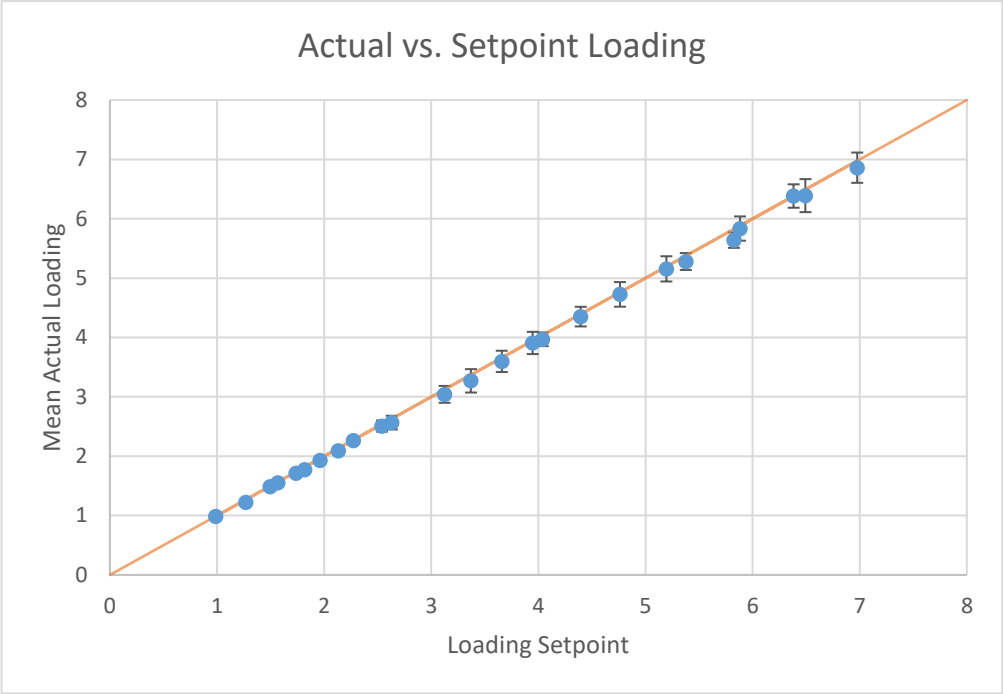

Figure 7-8 – Actual vs. set loading

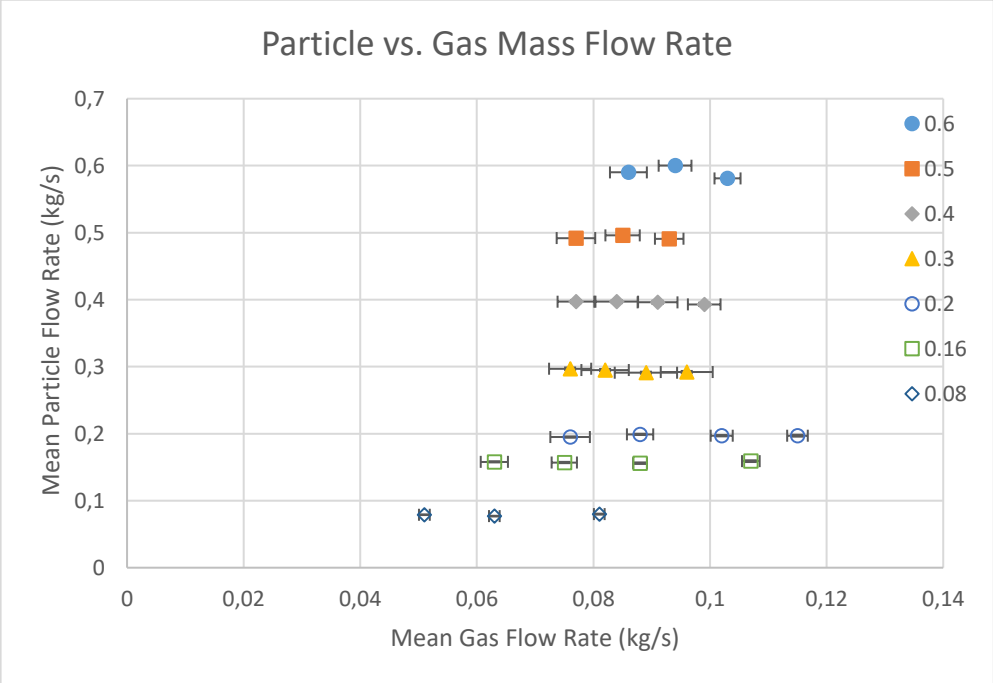

Figure 7-9 – Impact of particle flow rate on gas flow rate and vice versa

7.6 Particle Flow Rate Mass Balance

The inputs, methodology and results of the mass balance are presented below.

7.6.1 Inputs

The mass reading on the LIW and GIW system were manually recorded before and after each test. The contents of the reverse pulse jet filter were also emptied and recorded manually after each test. The recorded values are given in Appendix P.

The boundary mass values for the steady state period and their combined uncertainties, calculated in the particle flow rate analysis, are given in Appendix P and are also used as inputs for the analysis.

7.6.2 Methodology

Referring to Figure 4-12 and assuming no settling occurs in the pipe section from the cyclone outlet to the reverse pulse jet filter, the cyclone efficiency η_c is given by the following:

$$\eta_c = \frac{Mass\ collected\ by\ cyclone}{Mass\ entering\ cyclone} = \frac{GIW}{GIW + Mass\ collected\ by\ filter}$$

Equation 7-8

Assuming no particles are lost to the surroundings, a mass conservation equation for the system is given by the following:

$$LIW - GIW = Mass\ collected\ by\ filter + Settled\ mass$$

Equation 7-9

By substitution, Equation 7-9 becomes

$$LIW = GIW\left(\frac{1}{\eta_C}\right) + Settled\ mass$$

Equation 7-10

Using the manually recorded data in Appendix P, η_c is estimated using Equation 7-8.

Equation 7-10 and the boundary mass values for the steady state period are then used to determine the total mass collected during the steady state period.

7.6.3 Results

Tabulated results for the following charts are given in Appendix P.

Bar charts of the estimated cyclone efficiency and mass balance are given in Figure 7-10 and Figure 7-11. The manually recorded data for test 1 and 14 were unfortunately lost and are thus not reported here. $GIW\left(\frac{1}{\eta}\right) = GIW$ at these points.

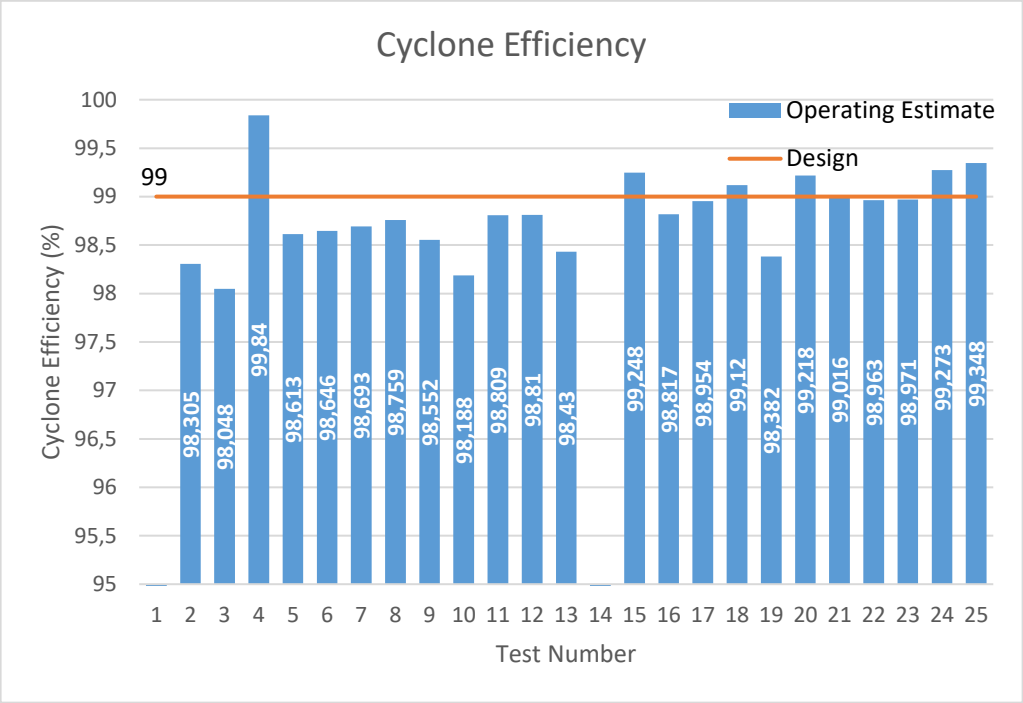

Figure 7-10 – Estimated cyclone efficiency

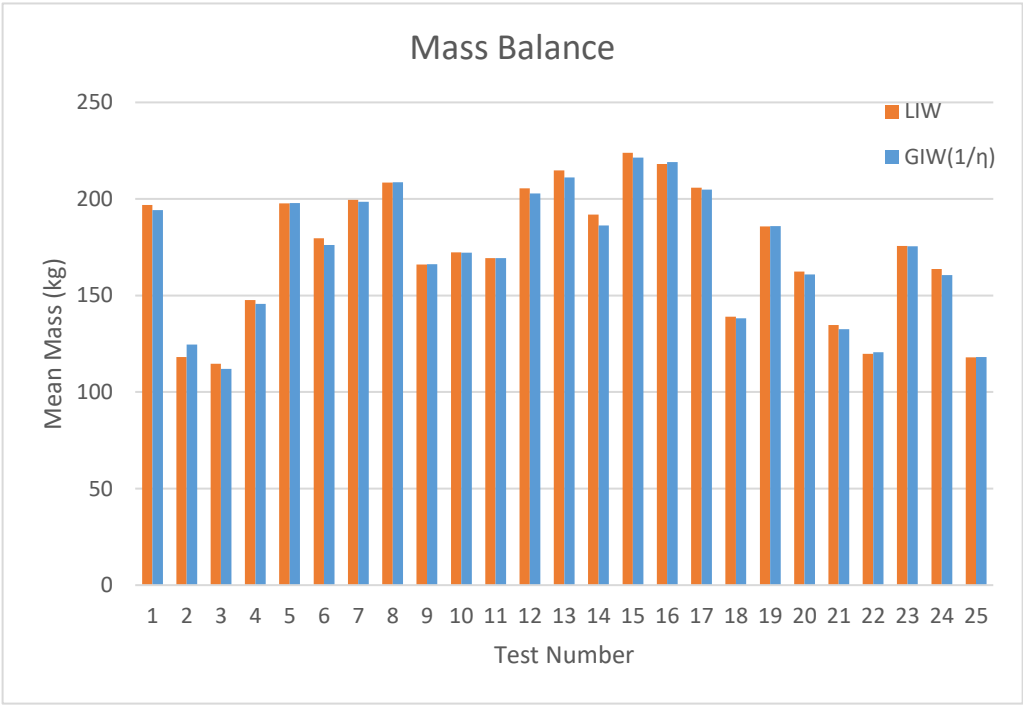

Figure 7-11 – Bar chart of mass fed vs. mass collected

Figure 7-12 shows the mass of particles fed into the system and the mass collected from the system together with the calculated uncertainty bands.

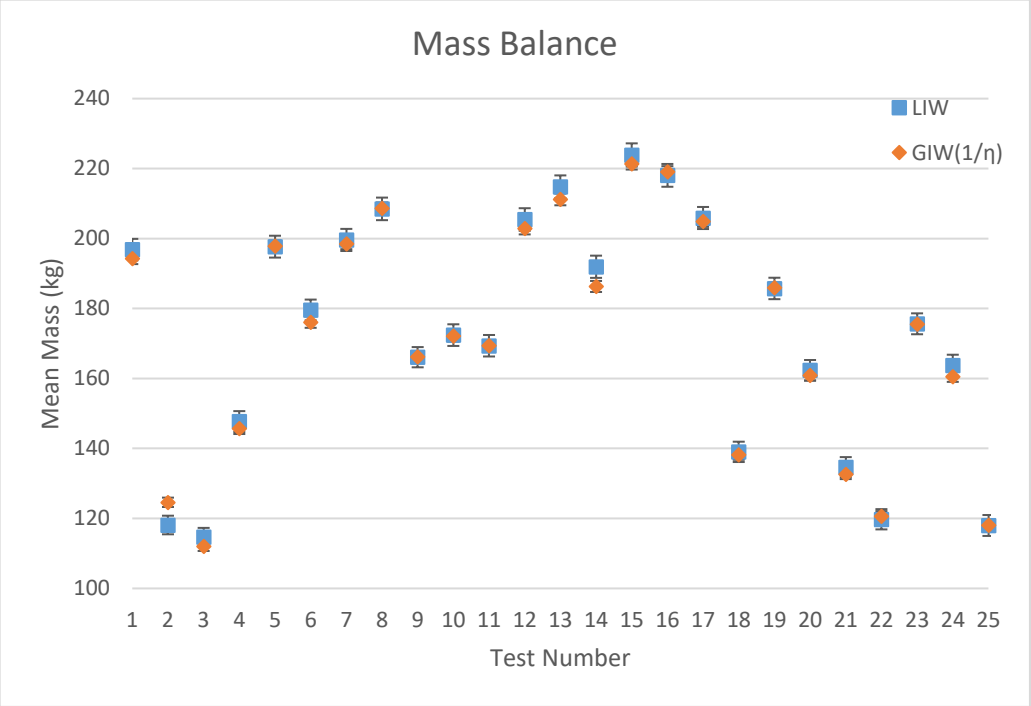

Figure 7-12 – Mass balance

7.7 Process Model Comparison

Tabulated results for the following are given in Appendix P.

The operating temperatures predicted via the process model and the actual measured values are compared in Figure 7-13.

The actual system pressure drop is estimated by subtracting atmospheric pressure from the measured orifice upstream pressure. The system pressure drops predicted via the process model and the estimated actual values are given in Figure 7-14.

Assuming that the density at the fan inlet is equal to 1.2kg/m^3, the volume flow rate at the blower inlet is easily calculated from the gas mass flow rate. The blower operating points is therefore plotted, with the model predicted operating points and the blower curve at maximum speed, in Figure 7-15.

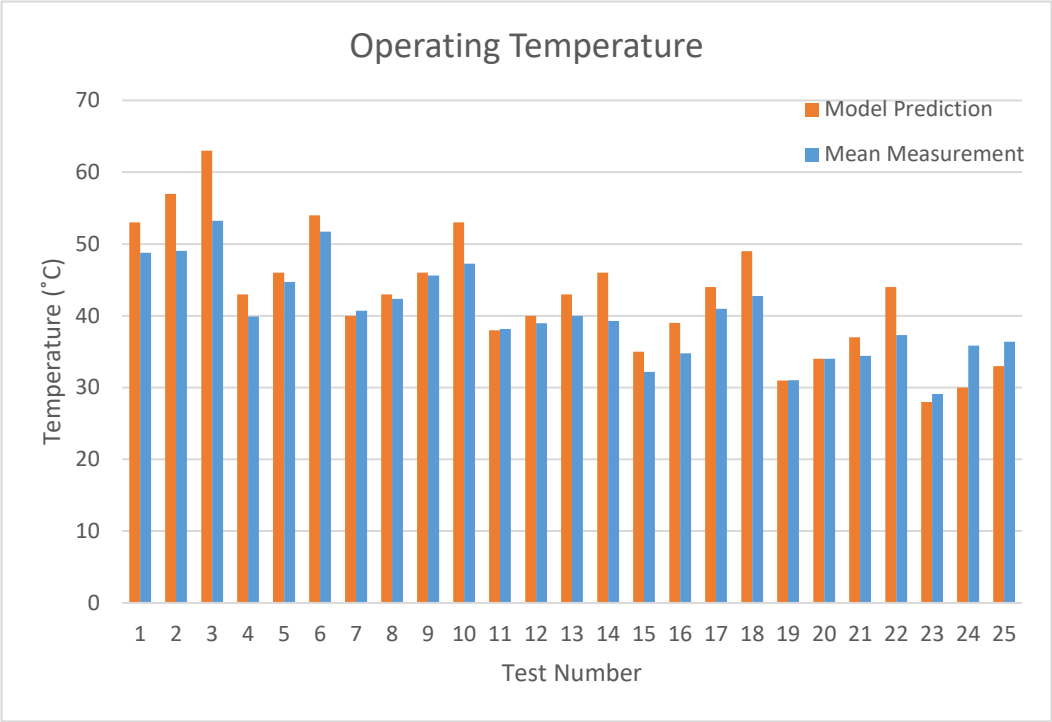

Figure 7-13 – Operating test temperatures

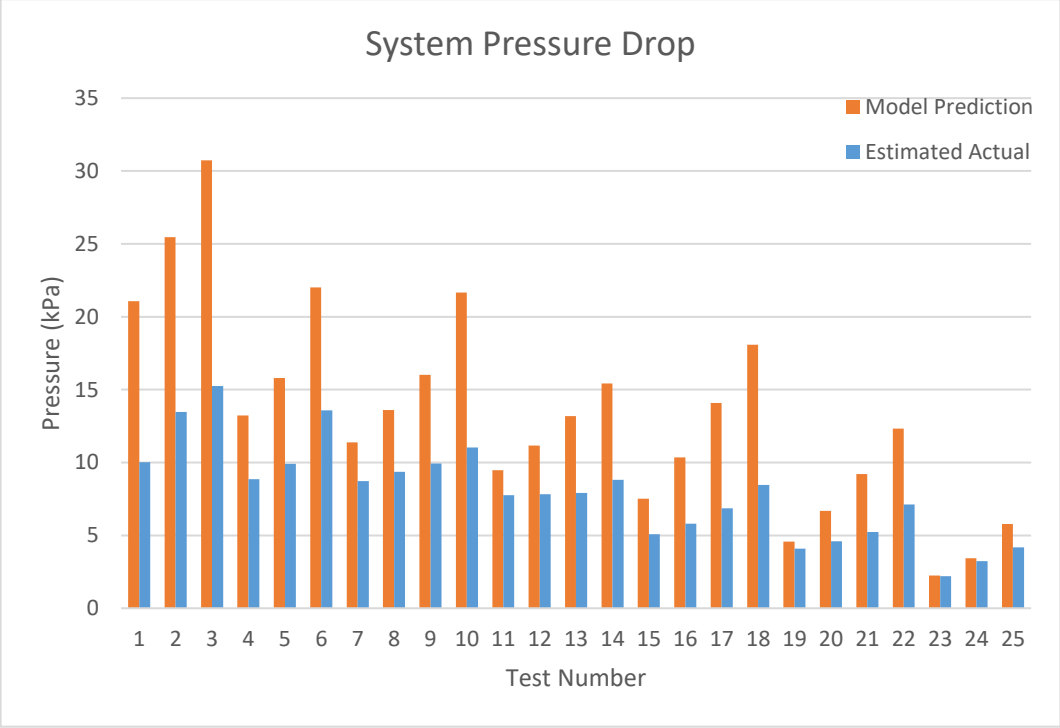

Figure 7-14 – System pressure drops

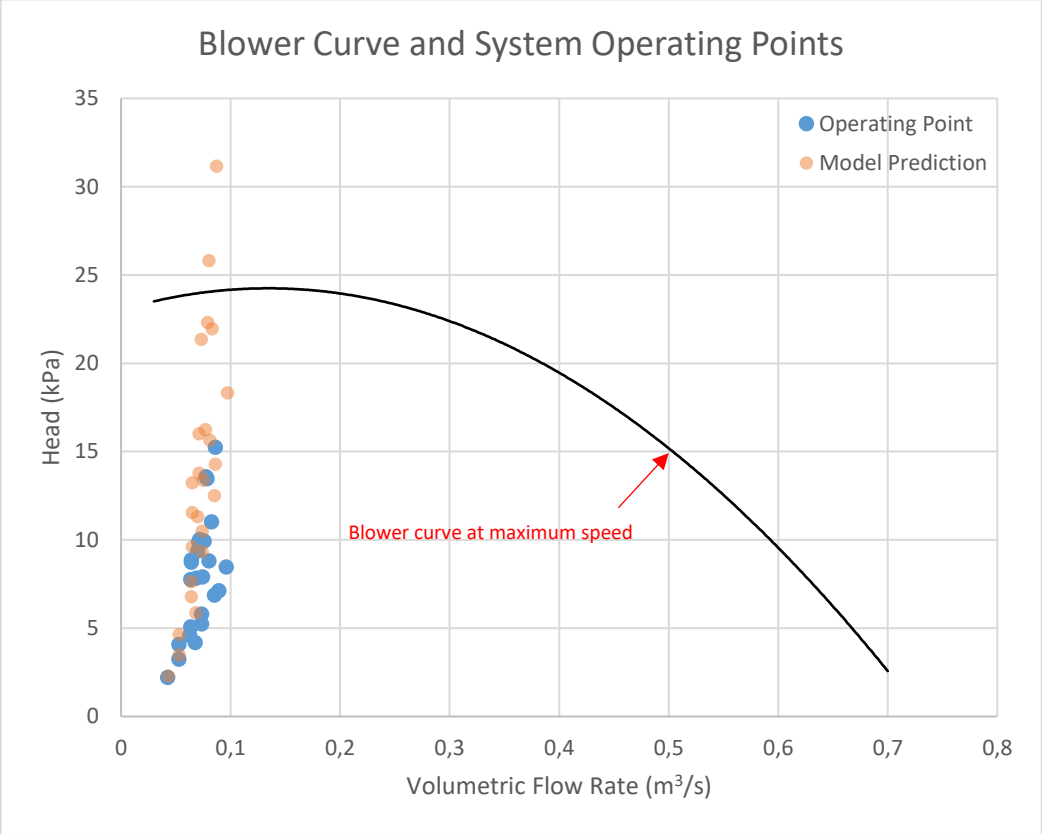

Figure 7-15 – System operating points

7.8 Discussion

Gas Flow Rate

From Appendix P, the mean measured gas mass flow rates are equal to the set points and have a maximum relative uncertainty (% uncertainty) of ±6%. For gas-only flow, it is expected that the uncertainty on a gas mass flow measurement will decrease with increasing gas mass flow rates. However, we see in Figure 7-4 that this is not strictly the case for two-phase flow and that the introduction of particles into the gas stream must therefore influence the uncertainty in the gas mass flow rate measurement. This influence is shown in Figure 7-9. Note that the uncertainty bands decrease with increasing gas mass flow rates at constant nominal particle mass flow rates of 0.08, 0.16, 0.2, 0.5 and 0.6kg/s. However, for constant nominal particle mass flow rates of 0.3 and 0.4kg/s, the uncertainty bands on the gas mass flow rate first increase with increasing gas mass flow rates, before beginning to decrease again.

From Appendix P, the relative uncertainty in the differential pressure measurements is significantly higher than that for the temperature and absolute pressure measurements. It can also be seen that the combined uncertainty for the differential pressure measurement is approximately equal to the statistical uncertainty of the differential pressure measurement. The statistical uncertainty of the differential pressure measurement therefore has a significant impact on the uncertainty of the measured gas mass

flow rate. Furthermore, the statistical uncertainties of the differential pressure measurements are elevated within the range of gas mass flow rates between 0.08 and 0.09kg/s at nominal particle mass flow rates of 0.3 and 0.4kg/s.

It is therefore postulated that the combination of gas and particle mass flow rates tested at the conditions specified above result in there being relatively higher pressure fluctuations and or vibration in the system, which adversely affected the stability of the gas mass flow rate, therefore increasing the statistical uncertainty and ultimately the total uncertainty in the measurement.

Particle Flow Rate

The method derived to calculate the uncertainty of fitting a calibration curve considers the uncertainties associated with both the indicated instrument value y and the actual value being measured x. However, the methods reviewed in literature are valid for the case where there are only errors in y, which are independent of x and which are normally distributed. Furthermore, no suitable method was found in literature to determine the particle mass flow rate and its uncertainty using a LIW or GIW system. The method used was therefore derived from basic principles.

For each test, the particle mass flow rate and its uncertainty were calculated for both the GIW and LIW systems. At the time of analysis, the uncertainty for the GIW system was found to be less than that of the LIW system for all cases. The results obtained for the GIW system is therefore reported since it represents the most reliable measurement of the two systems. Tabulated results for the LIW system are presented in Appendix P.

From Appendix P, the mean measured particle mass flow rates are slightly lower than the set points and have a maximum relative uncertainty of less than ±1%. The accuracy of the measurements is better seen on Figure 7-7, where the uncertainty bands on the measurement points are not visible on the chosen scale.

It is noted that the measured values are slightly lower than the set points, as some particles are not collected by the cyclone. Therefore, the particle mass flow rate is effectively split, at the cyclone, between the GIW system and the reverse pulse jet filter. The measurements taken by the LIW should therefore be considered as a more accurate reflection of the true values obtained during testing.

Loading

From Appendix P, the measured values for the loading are again slightly lower than the set points. This is expected as the loading is dependent on the particle mass flow rate. Figure 7-8 shows the measured values with uncertainty bands vs. the set points. Here, it can be seen that the actual uncertainty on the loading increases with increasing loading. However, it is better to consider the relative uncertainty i.e. the

uncertainty as a percentage of the measured value. The maximum relative uncertainty for the loadings during testing was ±6%. This corresponds to the maximum relative uncertainty of the gas mass flow rate, which is significantly higher than that of the particle mass flow rate.

The mean measured loadings achieved during testing correspond to AF ratios between 0.146 and 1.012. It is noted that this is outside the range of 1.5 and 2.5 required for power plant similarity. However, a limitation is imposed on the loading based on the maximum design gas volume flow rate of the cyclone. From Figure 7-9, it is postulated that an increase in the gas mass flow rate at the lowest particle mass flow rate tested, will give accurate measurement and control of the gas and particle mass flow rates at AF ratios between 1.5 and 2.5.

CYCLONE EFFICIENCY

The method used to calculate the cyclone efficiency is crude due to the test procedures followed. The results given in Figure 7-10 is therefore only an estimate and not necessarily a true reflection of the cyclone performance. Regardless, it is estimated that the cyclone operated at efficiencies greater that 98% for the tests conducted. This is within 1% of the 99% design efficiency. With regards to the particle flow rate, it is interesting to note that the particle flow rate measured by the GIW system is no less than 2% of the set point.

Mass Balance

Referring to Figure 7-11, the uncertainty bands overlap in all but one test, namely test 2. Therefore, it can be deduced that settling occurred in test 2 only. The reason for settling is not clear, as no settling occurred in test 1, where the loading was higher and the gas velocity lower than that in test 2. Regardless, the results are encouraging, as it shows that design methodology followed was successful in preventing settling from occurring in 1 out of 25 tests.

Comparison of Theoretical and Practical Results

Figure 7-14 and Figure 7-15 show that the model over-predicts the system pressure drop. Noting the order of tests conducted in Table 7-3, this over-prediction increases with both increasing gas and particle mass flow rates. The model is therefore conservative, as desired. However, for high gas and particle mass flow rates, the model is perhaps too conservative. The model therefore requires refinement to better to estimate the blower operating points at high gas and particle mass flow rates.

Figure 7-13 shows that the prototype process model, on average, over predicts the actual operating temperatures by no more than 5˚C. A contributor to this is the assumption in the model that the blower isentropic efficiency is equal to 60%. According to (Liptak, 2005), a value between 65 and 75% is common for a two-stage centrifugal blower with a VSD. The use of a higher isentropic efficiency in the model would

have therefore yielded lower temperatures. As the blower temperature rise is directly related to the pressure rise delivered, another contributor is the over-prediction of the required blower operating points.

Practical Observations

It was observed during testing that:

- The noise emitted by the blower at high loading and gas mass flow rates is well above safe working conditions, if personal protective equipment (PPE) is not used.
- Any leaks where a gas-particle mixture is present discharge dust at concentrations well above safe working conditions, if personal protective equipment (PPE) is not used.
- The sight glass provides a good visual indication of the flow within the pipeline. For example, the roping phenomenon, where particles moving around a bend cling to the bend, was clearly observed through the sight glass at low loadings and is shown in Figure 7-16.

Figure 7-16 – Roping phenomenon visualised during testing

8 Revised Test Facility Concept Design

An objective of this project is to recommend an overall system layout and instrumentation design for the final test facility. Recommendations are therefore presented in this chapter, together with a revised final test facility system layout and future developments required for the DAC system.

8.1 Revised Final Test Facility System Layout

Based on the lessons learned during the construction, commissioning and operation of the prototype facility, a revised overall system layout was developed for the envisaged final test facility. Figure 8-1 to Figure 8-3 presents the P&ID for the system. Additionally, a functional analysis and allocation for the system are presented in Figure 8-4 and Table 8-1 respectively. Differences between the initial and revised concept are given in the proceeding text.

Ball valves are now used in the flow measurement section, therefore reducing the need for two differential pressure transducers at this section to only one. Furthermore, the temperature measurement is now taken after the orifice, as in the prototype facility. This is repeated for the test sections.

The feeding system now incorporates a blow through rotary valve as in the prototype facility. A single horizontal pipeline is therefore used instead of two.

Choking tests require low gas velocities, which would require low gas mass flow rates if the initial layout is used. This would reduce the cyclone efficiency, which decreases with decreasing gas mass flow rates. The pressure drop across the orifice plate also decreases with decreasing gas mass flow rates, which in turn affects the accuracy of the measured gas mass flow rate. Therefore, the vertical test section now features an interchangeable testing pipe, where the 100NB pipe is used for saltation and similarity tests and the 250NB pipe is used for choking tests. This larger diameter pipe reduces the gas velocity at the test section, allowing choking tests to be conducted at higher gas mass flow rates.

Due to there being only one vertical pipe, the receiving system now features only two cyclones as opposed to three. As in the prototype facility, a reverse pulse jet filter replaces the cartridge filter built into the heat exchanger. Finally, a compression load cell allows the weight of the reverse pulse jet filter to be monitored online. This allows for a more detailed mass balance to be performed.

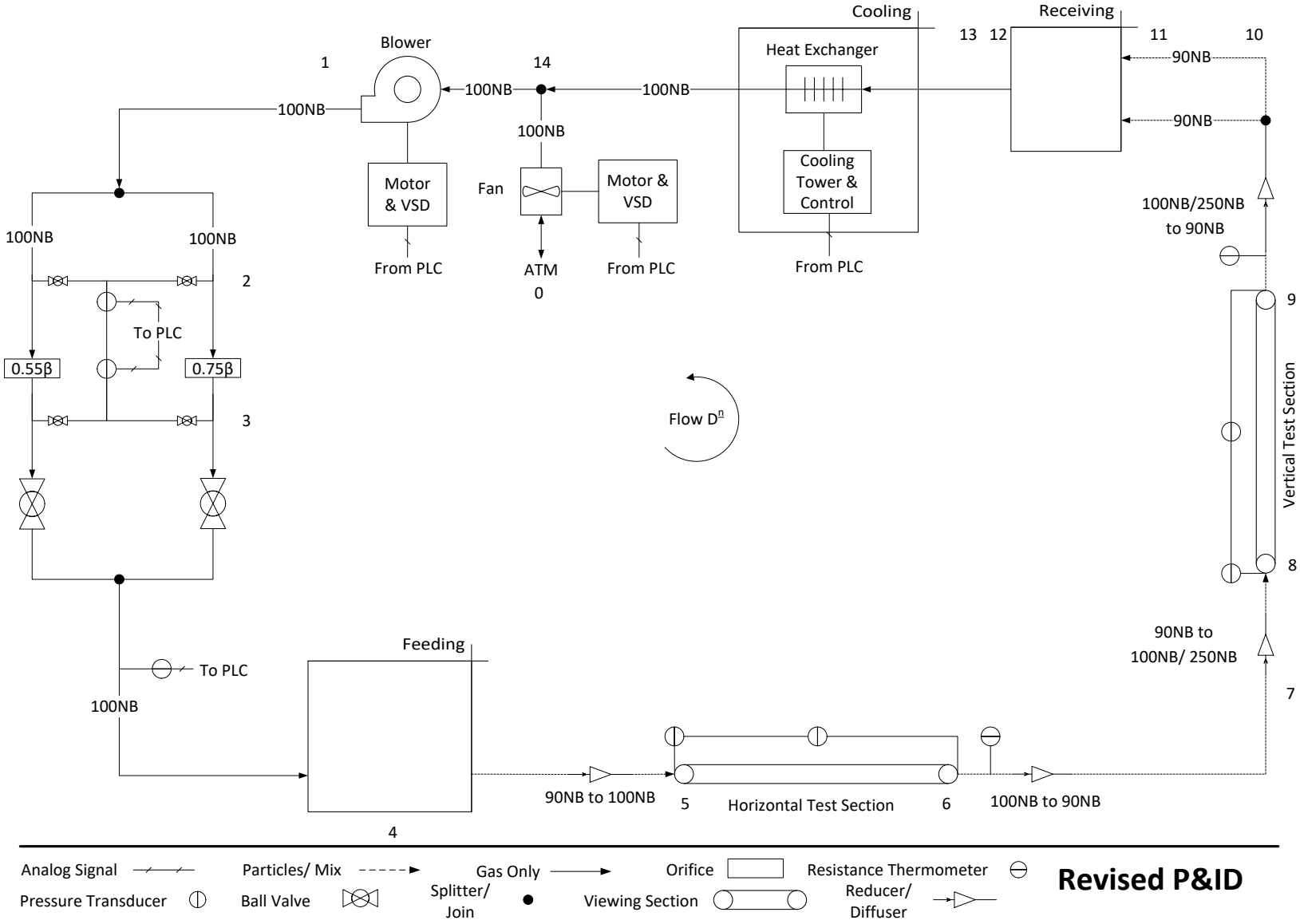

Figure 8-1 – Revised test rig schematic Part A

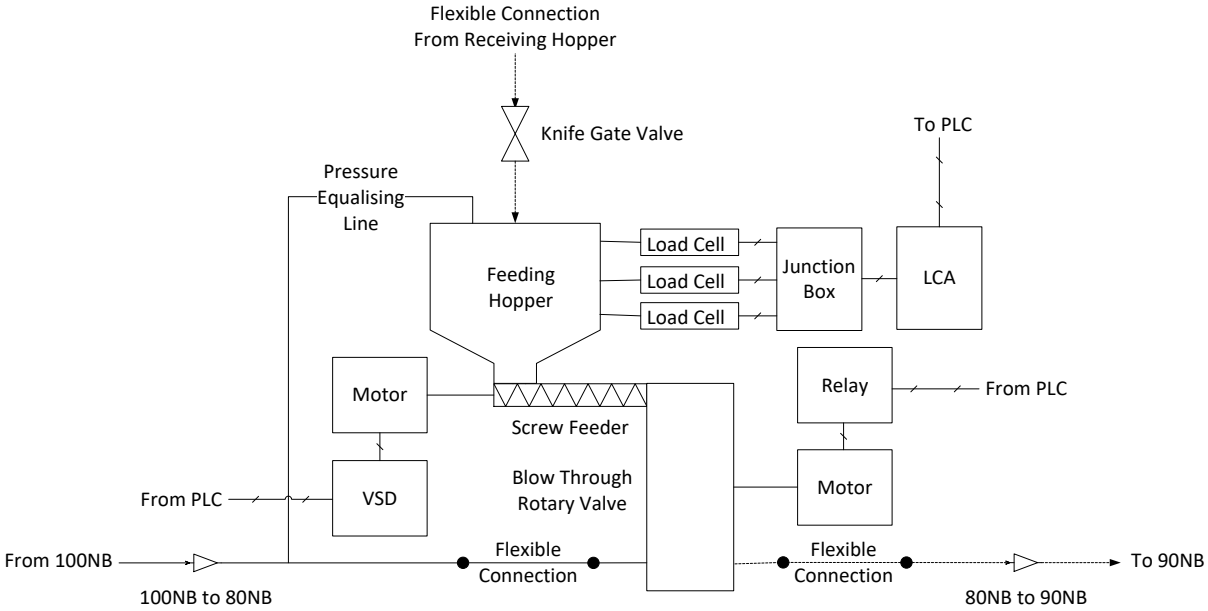

Feeding System

Figure 8-2 – Revised test rig schematic Part B

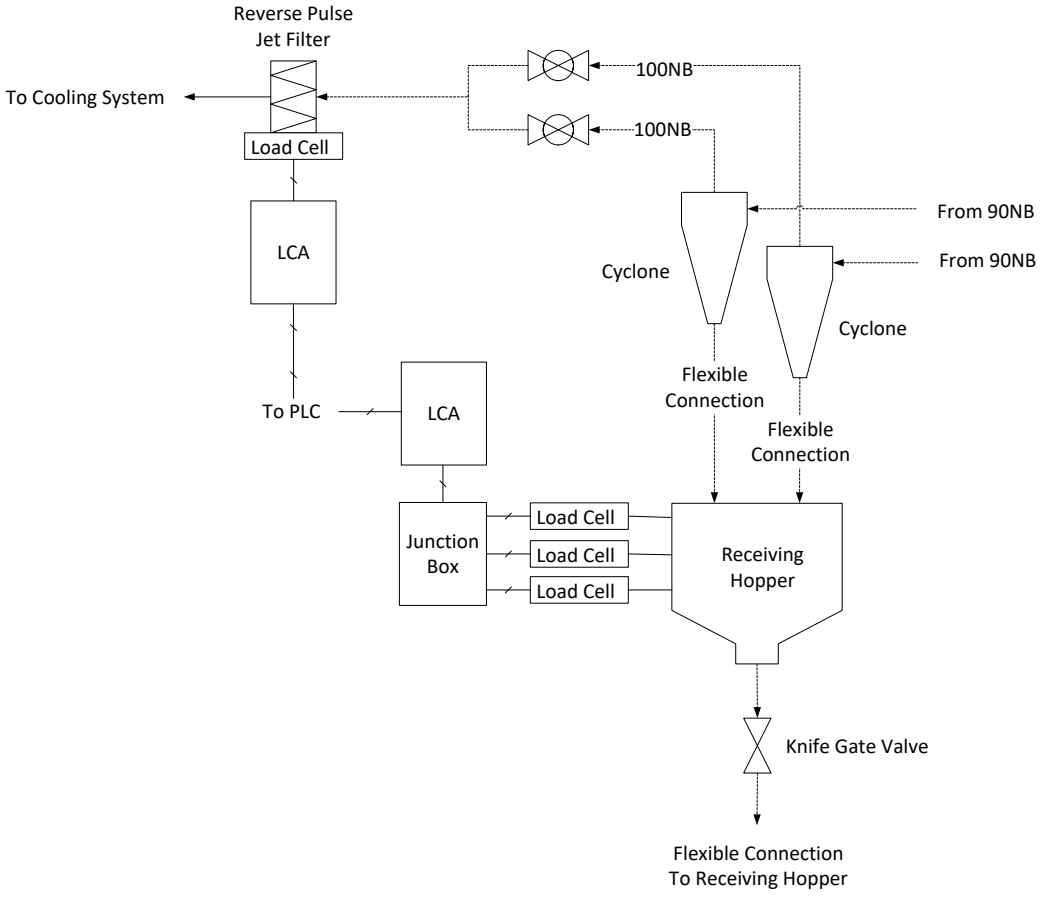

Receiving System

Figure 8-3 – Revised test rig schematic Part C

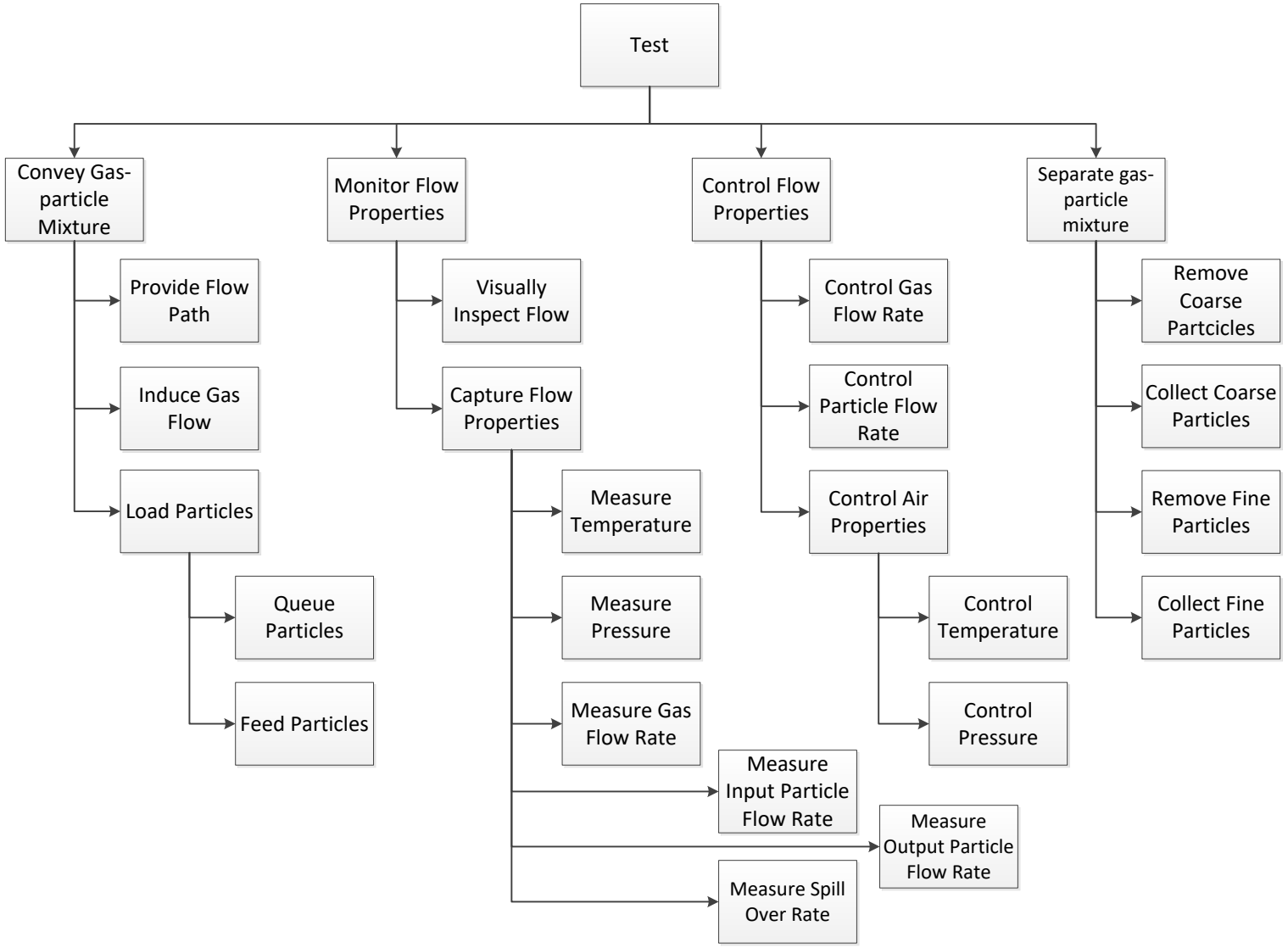

Figure 8-4 – Functional analysis for revised test rig concept

	Functions	Piping & Isolation Valves	Blower with speed control	Feeding hopper assembly	Rotary Feeder	Screw feeder with speed control	Heat exchanger assembly	Pressure regulating assembly	Sight Glass	Resistance Thermometer	Absolute Pressure Transducer	Orifice assembly	Receiving hopper assembly	Reverse pulse jet filter assembly	Cyclones
	Primary Components														
1	**Convey gas-particle mixture**														
1.1	Provide flow path	X													
1.2	Induce gas flow		X												
1.3	Queue particles			X											
1.4	Feed particles				X										
2	**Control flow properties**														
2.1	Control gas flow rate		X												
2.2	Control particle flow rate					X									
2.3	Control temperature						X								
2.4	Control pressure							X							
3	**Monitor Flow Properties**														
3.1	Visually Inspect Flow								X						
3.2	Measure temperature									X					
3.3	Measure pressure										X				
3.4	Measure gas flow rate											X			
3.5	Measure input particle flow rate			X											
3.6	Measure output particle flow rate												X		
3.7	Measure spill over particle flow rate													X	
4	**Separate gas-particle mixture**														
4.1	Remove coarse particles														X
4.2	Collect coarse particles												X		
4.3	Remove fine particles													X	
4.4	Collect fine particles													X	

Table 8-1 – Functional allocation of revised test rig concept

8.2 DAC System Future Developments

For the proposed final test facility, three absolute, differential and RTD sensors are to be included in the system. The NI 9208 AI module caters for this expansion through the unused input channels. The use of the PMP131 pressure transducer is to be replaced by the PMC51 (see Appendix S), which is an explosion-proof absolute pressure transducer. Additionally, a compression load cell with a LCA is to be included to allow for an online mass measurement of the reverse pulse jet unit. A proposed load cell and reverse pulse jet unit is given in Appendix S.

Furthermore, the C-DAQ 9174 can house up to four modules, allowing additional analog input and output modules to be added to the system if necessary. There is also the potential to include digital modules, which would allow the PLC to communicate with instruments connected to it. For example, this would allow the PLC to receive error messages from malfunctioning instruments, or to receive detailed information from the VSD's such as the actual motor speeds amongst other things.

Also, although the NI PS-14 power supply was initially oversized to allow for further expansion of the DAC system, the inclusion of an additional LCA (which requires 18W) implies that separate power supplies should be procured for the additional LCAs.

Finally, the electrical cabinet needs to isolated from the explosive atmosphere (the process and its immediate surroundings) in accordance with regulatory requirements. SANS 10108:2014 (South African Bureau of Standards (SABS), 2014) and ARP 0108:2014 (South African Bureau of Standards (SABS), 2014) provide further information.

8.3 Recommendations

- If a different cyclone design is to be used in the final test facility, further develop the cyclone model to size and calculate efficiency and pressure drops for other standard cyclone designs. Subsequently use the cyclone model to determine the geometry of the cyclone.
- If necessary, use the orifice model developed to select suitable orifice to pipe bore diameters.
- Further develop the prototype facility so that pressure drop tests can be conducted across pipe lengths, bend sections and the cyclone. Subsequently run the prototype model for varying inputs and compare the results output by the model with pressure drop data obtained from physical tests. Also, conduct a sensitivity analysis to determine how the process model outputs are affected by each input variable. Subsequently improve the prototype model to better predict the actual pressure drops measured.
- Obtain a suitable site and develop a physical layout of the final test facility accordingly. Consider a double volume room and positioning the blower outside to reduce noise pollution.

- Identify and implement methods to minimise dust generation during the detail design of the final test facility.
- Conduct an in-depth study to determine the horizontal and vertical acceleration lengths required for the final test facility, so that tests are conducted at fully developed flow conditions.
- Determine the bend radii required to minimise the effects of roping. Consider installing a rope breaker.
- Develop a process model for the final test facility, using the already developed process models as a basis.
- Determine the required blower operating envelope for the final test facility using the methodology presented in this thesis.
- Construct and commission the final test facility using explosive rated equipment.
- Conduct tests at power-plant similarity conditions to obtain knowledge of the flow properties associated with PF conveying.
- Obtain pressure drop, visual and mass balance data using the final test facility to evaluate saltation, choking, acceleration length and pressure drop data in literature. Subsequently develop new correlations.
- Use the final test facility to test and calibrate commercially available equipment.
- Use the final test facility to validate or improve CFD models.
- During testing, keep in mind that particle degradation may occur over time. Monitor the PSD of the material being conveyed to ensure consistency with model inputs.
- Use the methodology presented in this thesis to determine the values of the measured gas and particle mass flow rates and its associated uncertainties.
- Install digital modules on the DAC system to improve its functionality.

9 Summary and Conclusions

This chapter presents a summary of the work completed and conclusions made based on the preceding text.

9.1 Summary

- A prototype facility was developed and used to demonstrate the process of feeding and removing particles from a gas stream and controlling the gas and particle mass flow rates during a dilute gas-particle conveying process. The control of the gas mass flow rate is achieved by measuring the pressure drop over an orifice plate and subsequently using a DAC system to control the blower speed via a VSD. The control of the particle mass flow rate is achieved by measuring the LIW of a feed hopper over time and subsequently using a DAC system to control the auger speed via a VSD.
- A DAC system was developed and allows flow properties to measured, recorded, viewed and controlled online. The system communicates with instrumentation via analog signals only. However, the system contains modular hardware components, which can easily be upgraded for further development of the system.
- A system layout for a gas-particle test facility, including the instrumentation design, was developed. The design allows for the control of the gas and particle mass flow rates as well as the gas temperature and pressure. The design allows for pressure drop, mass balance and visual tests to be conducted. The design in its standard configuration allows saltation and power plant similarity testing to be conducted. To allow for choking tests to be conducted, the design requires only one pipe section to be swapped out. Furthermore, tests can be conducted with actual PC if the explosive proof variants of the proposed instrumentation are purchased.
- A cyclone model was developed and verified during testing. The model outputs, given particle and gas properties, the cyclone dimensions for a standard Stairmand type cyclone required to achieve a 99% theoretical gas-particle separation efficiency. During testing, an efficiency of 99 ±1% was observed.
- An orifice model was developed and can be used as a tool to select an appropriately sized orifice plate for gas mass flow measurement systems.
- A process model was developed and used to design the prototype facility. The model is developed exclusively for the physical geometry of the prototype facility and provides a conservative estimate of the required blower operating points. The methodology used to develop the model can therefore be adopted, or the model adjusted, to design similar dilute phase gas-particle transport facilities.
- Tests were conducted for loadings between 0.988 and 6.860 at gas mass flow rates between 0.051 and 0.115kg/s and particle mass flow rates between 0.077 and 0.600kg/s. The relative uncertainties calculated on the measured particle mass flow rates are less than ±1% for all tests. The maximum

relative uncertainties calculated on the measured gas mass flow rates and loadings are approximately ±6%.

- Rizk's correlation and Yang's choking theory were used, without safety factors, in the design of the prototype facility and the selection of test parameters to prevent settling from occurring. The analysis of test data shows that settling occurred in only 1 of 25 tests conducted.

9.2 Conclusions

- A literature review of the different correlations applicable to dilute phase gas-particle transport phenomena was conducted. From practical tests conducted, the Rizk correlation and Yang's choking theory can be used to calculate the superficial gas velocities required to prevent saltation and choking from occurring. Safety factors need not to be used with these correlations.
- A theoretical process model and a methodology was developed which can be used to design a dilute phase-gas particle transport facility and to determine the required operating envelope of the blower. The model provides conservative estimates of the required pressure rise through the blower and the blower outlet temperature when compared to empirical data.
- A concept layout design, an overall system layout and an instrumentation design for a gas-particle transport test facility was developed and a prototype facility, of reduced complexity but consisting of the most important components of the proposed final test facility, was designed, constructed and operated. From the results of practical tests conducted using the prototype facility, it is concluded that the design approach taken was successful and the methodologies developed in this thesis may be applied in the detail design and operation of such a facility.
- A DAC system for the prototype facility was developed which allows for accurate control of the gas and particle mass flow rates. The DAC system may be further developed for use in the proposed final facility. All explosion-proof instruments used for the prototype facility may also be used in the proposed final facility. Non-explosion proof instruments need to be isolated from the explosive atmosphere or the explosive-proof variants of these instruments procured.
- Data analysis methodologies were successfully developed to determine the values of the measured gas and particle mass flow rates and their associated uncertainties. These methodologies may be adopted for the analysis of gas and particle mass flow rates when taking pressure drop measurements over an orifice plate or when using a LIW or GIW system respectively.

10 Bibliography

Anderson, R. B., 2002. *CleanTech.pdf.* [Online] Available at: http://www.vortron.com/pdf/CleanTech.pdf [Accessed 20 February 2017].

Cabrejos, F. J. & Klinzing, G. E., 1994. Pickup and saltation mechanisms of solid particles in horizontal pneumatic transport. *Powder Technology,* Volume 79, pp. 173 - 186.

Casal, J. & Martinez-Benet, J. M., 1983. A better way to calculate cyclone pressure drop. *Chemical Engineering,* Volume January, pp. 99-100.

Cengel, Y. A., 2006. *Heat and Mass Transfer: A Practical Approach.* 3rd ed. s.l.:McGraw-Hill.

Chong, Y. O. & Leung, L. S., 1986. Comparison of Choking Velocity Correlations in Vertical Pneumatic Conveying. *Powder Technology,* Volume 47, pp. 43-50.

Chuah, T. G., Gimbun, J., Choong, T. S. Y. & Fakhru'L-Razi, A., 2003. Numerical Prediction of Cyclone Pressure Drop. *Journal of Chemical Engineering and Environment,* 2(2), pp. 67-71.

Crowe, C., Sommerfield, M. & Tsuji, Y., 1998. *Multiphase flow with droplets and particles.* 1st ed. Boca Raton: CRC Press.

Dhodapkar, S. & Zaltash, A., 1989. Acceleration zone studies in pneumatic conveying systems at various inclinations. *Fluidization and Fluid-Particle Systems - Fundamentaks and Applications, AIChE Symposium Series,* 85(270), pp. 1-8.

Dirgo, J. & Leith, D., 1985. Cyclone Collection Efficiency: Comparison of Experimental Results with Theoretical Predictions. *Aerosol Science and Technology,* 4(4), pp. 401-415.

Eskom Power Plant Engineering Institute (EPPEI), 2014. *2012-2016 Five-year Strategic Plan.* Midrand: N/A.

Fan, L.-S. & Zhu, C., 1998. *Principles of Gas-Solid Flows.* Cambridge: Cambridge University Press.

Faulkner, W. B. & Shaw, B. W., 2006. Efficiency and Pressure Drop of Cyclones Across a Wide Range of Inlet Velocities. *Applied Engineering in Agriculture,* 22(1), pp. 155-161.

Figliola, R. S. & Beasley, D. E., 2011. *Theory and Design for Mechanical Measurerments.* 5th ed. Hoboken: John Wiley & Sons.

Flagan, R. C. & Seinfeld, J. H., 1988. *Fundamentals of Air Pollution Engineering.* Englewood Cliffs, NJ: Prentice Hall.

Geldart, D. & Ling, S. J., 1992. Saltation velocities in high pressure conveying of fine coal. *Powder Technology,* Volume 69, pp. 157 - 162.

Hinkle, B. L., 1953. *Acceleration of Particles and Pressure Drops Encountered in Horizontal Penumatic Conveying.* Georgia: PhD Thesis: Georgia Institute of Technology.

International Organization for Standardization (ISO), 2003. *ISO 5167-1:2003 Measurement of fluid flow by means of pressure differential devices inserted in circular cross-section conduits running full - Part 1: General principles and requirements.* s.l.:s.n.

International Organization for Standardization (ISO), 2003. *ISO 5167-2:2003 Measurement of fluid flow by means of pressure differential devices inserted in circular cross-section conduits running full - Part 2: Orifice plates (ISO 5167-2:2003).* s.l.:s.n.

Kalen, B. & Zenz, F. A., 1974. Theoretical-Emperical Approach to Saltation Velocity in Cyclone Design. *AIChE Symposium Series: Recent Advances in Air Pollution Control,* 70(137), pp. 388-396.

Klinzing, G. E., Marcus, R. D., Rizk, F. & Leung, L. S., 1997. *Pneumatic Conveying of Solids: A Theoretical and Practical Approach.* 2nd ed. London: Chapman & Hall.

Koch, W. H. & Licht, W., 1977. New design approach boosts cyclone efficiency. *Chemical Engineering Journal,* Volume November, pp. 80-88.

Leith, D. & Licht, W., 1972. The collection efficiency of cyclone type particle collectors - A new theoretical approach. *AIChe Symposium Series: Air Pollution and Its Control,* 68(126), pp. 196-206.

Leung, L. S., Wiles, R. J. & Nicklin, D. J., 1971. Correlation for Predicting Choking Flowrates in Vertical Pneumatic Conveying. *Industrial & Engineering Chemistry,* 10(2), pp. 183-189.

Liptak, B. G., 2005. *Instrument Engineers' Handbook: Process Control and Optimization.* 4th ed. Boca Raton: CRC Press.

Matsumoto, S., Kikuta, M. & Maeda, S., 1977. Effect of particle size on the minimum transport velocity for horizontal pneumatic conveying of solids. *Journal of Chemical Engineering of Japan,* 10(4), pp. 273 - 279.

Matsumoto, S. & Saito, S., 1970. On the Mechanism of Suspension of Particles in Horizontal Pneumatic Conveying: Monte Carlo Simulation Based on the Irregular Bouncing Model. *Jorunal of Chemical Engineering of Japan,* 3(1), pp. 83-92.

Modi, M. V., Talwalkar, A. T. & Punwani, D. V., 1978. *International Powder and Bulk Solids Handling and Processing Conference - Pressure Drop Correlation for Designing Vertical Dilute-Phase Gas-Solid Lift-Lines for Materials Used in Coal Conversion Processes.* Chicago, Institute of Gas Technology.

Punwani, D. V., Modi, M. V. & Tarman, P. B., 1976. *International Powder and Bulk Solids Handling and Processing Conference - A generalized correlation for estimating choking velocity in vertical solids transport.* Chicago, Institute of Gas Technology.

Rabinovich, E. & Kalman, H., 2008. Boundary saltation and minimum pressure velocities in particle–gas systems. *Powder Technology,* Volume 185, pp. 67 - 79.

Rabinovich, E. & Kalman, H., 2011. Flow regime diagram for vertical pneumatic conveying and fluidized bed systems. *Powder Technology,* 207(1-3), pp. 119-133.

Rhodes, M., 2008. *Introduction to Particle Technology.* 2nd ed. Chichester: John Wiley & Sons Ltd.

Rizk, F., 1982. Pneumatic Transport in Dilute and Dense Phase. *Bulk Solids Handling,* 2(2), pp. 235-241.

Rose, H. E. & Duckworth, R. A., 1969. Transport of Solid Particles in Liquids and Gases. *The Engineer,* Volume 227, pp. 430-433.

Schuchart, P., 1969. Widerstandsgesetz für den hydraulischen und pneumatischen Feststofftransport in waagerechten geraden Rohren. *Chemie Ingenieur Technik,* 41(23), pp. 1251-1259.

South African Bureau of Standards (SABS), 2014. *ARP 0108:2014 Regulatory requirements for explosion-protected apparatus.* Pretoria: SABS Standards Division.

South African Bureau of Standards (SABS), 2014. *SANS 10108:2014 The classification of hazardous locations and the selection of equipment for use in such locations.* Pretoria: SABS Standards Division.

Sutherland, W., 1893. The Viscosity of Gases and Molecular Force. *Philosophical Magazine Series 5,* 36(223), pp. 507-531.

Van der Merwe, J. C., 2014. *Pulverized fuel transport and balancing using 2-phase flow modelling and testing,* Johannesburg: s.n.

Wei, W. et al., 2011. Experimental study on the solid velocity in horizontal dilute phase pneumatic. *Powder Technology,* 212(3), pp. 403-409.

Wen, C. Y. & Yu, Y. H., 1966. Mechanics of Fluidization. *Chemical Engineering Progress Symposium Series,* 62(62), pp. 100-111.

Yang, W.-C., 1973. Estimating the Solid Particle Velocity in Vertical Pneumatic Conveying Lines. *Industrial & Engineering Chemistry Fundamentals,* 12(3), pp. 349-352.

Yang, W.-C., 1974. Correlations for Solid Friction Factors in Vertical and Horizontal Pneumatic Conveyings. *AIChE Journal,* 20(3), pp. 605-607.

Yang, W.-C., 1975. A Mathematical Definition of Choking Phenomenon and a Mathematical Model for Predicting Choking Velocity and Choking Voidage. *American Institute of Chemical Engineers,* 21(5), pp. 1013-1015.

Yang, W.-C., 1977. A unified theory on dilute phase pneumatic transport. *Journal of Powder & Bulk Solids Technology,* Volume 1, pp. 89-95.

Yang, W.-C., 1978. A Correlation for Solid Friction Factor in Vertical Pneumatic Conveying Lines. *AIChE Journal,* 24(3), pp. 548-552.

Yang, W.-C., 2004. "Choking" Revisited. *Industrial & Engineering Chemistry,* Volume 43, pp. 5496-5506.

Yang, W.-C., Keairns, D. L. & Archer, D. H., 1973. Estimating the Solid Particle Velocity in Horizontal Pneuamtic Conveying Lines. *The Canadian Journal of Chemical Engineering,* Volume 51, pp. 779-781.

Zenz, F. A., 1949. Two-phase fluid-solid flow. *Industrial & Enegineering Chemistry,* 41(12), pp. 2801-2806.

Zenz, F. A., 1964. Conveyability of materials of mixed particle size. *Industrial & Engineering Chemistry Fundamentals,* 3(1), pp. 65 - 75.

List of Appendices

Appendix A. Bend Pressure Drop Theory

When analysing the pressure drop over a bend in gas-solid flow, the first step is to calculate the straight pipe equivalent bend length. The length can be assumed the same way as in single phase flow for any concentration (Klinzing, et al., 1997), therefore

$$L_b = \frac{2\pi R_b}{4}$$

Where L_b and R_b are the bend length and radius in m respectively.

The pressure drop over the bend is then calculated by summing the gas only pressure drop and the solids contribution. Klinzing, et al. (1997) recommends the use of a correlation developed by Ito in 1959 and 1960 to calculate the gas only pressure drop, and Schuchart's (1969) correlation to calculate the solids contribution. It is worth noting that Schuchart's (1969) correlation was developed using relatively large particles (1-2mm) and volumetric concentrations up to only 5%.

Itto

Itto's gas pressure drop correlation for fully developed turbulent flow across a bend is given by Klinzing, et al. (1997) as

$$\Delta P_{bg} = \left(\frac{0.029 + 0.304 \left[Re_{pipe} \left(\frac{D_{pipe}}{2R_b} \right)^2 \right]^{-0.25}}{\left(\frac{2R_b}{D_{pipe}} \right)^{0.5}} \right) \frac{L_b \rho_g U_g^2}{2D_{pipe}}$$

where ΔP_{bg} is the gas pressure drop across a bend in Pa. Here $Re_{pipe} \left(\frac{D_{pipe}}{2R_b} \right)^2$ is known as the Dean number. The equation is valid for $300 > Re_{pipe} \left(\frac{D_{pipe}}{2R_b} \right)^2 > 0.034$. For Dean numbers less than 0.034, the pressure drop is equal to the straight pipe section loss.

Schuchart

Using Schuchart's (1969) correlation, the solids contribution to pressure drop over a bend is

$$\frac{\Delta P_{bp}}{\Delta P_p} = 210 \left(\frac{2R_b}{D_{pipe}} \right)^{-1.15}$$

where ΔP_{bp} is the solids pressure drop across a bend in Pa. Here, ΔP_p is the solids contribution to pressure drop over a straight pipe of equivalent bend length i.e.

$$\Delta P_p = \Delta P_p \; per \; meter \times L_b$$

Appendix B. Cyclone Theory

Introduction

Cyclone separators are gas cleaning devices which separate dispersed particles within a gas through centrifugal forces (Flagan & Seinfeld, 1988). Cyclones are widely used in industry as they provide a cleaning solution low in capital and maintenance costs and are adaptable to a wide range of operating conditions (Dirgo & Leith, 1985). Cyclones are also "efficient in removing particles greater than 5µm" and are able to "handle heavy particle loads" according to Casal & Martinez-Benet (1983). A variety of cyclone designs exist and can be categorized, according to Flagan & Seinfeld (1988), into either reverse-flow cyclones (axial or tangential), straight-through-flow cyclones, or impeller cyclones. From literature, tangential reverse-flow cyclones are the most widely used cyclones in industry. The design, efficiency, and pressure drops associated with tangential reverse-flow cyclones are presented. The figure below, taken from Fan & Zhu (1998), illustrates a tangential reverse-flow cyclone in operation.

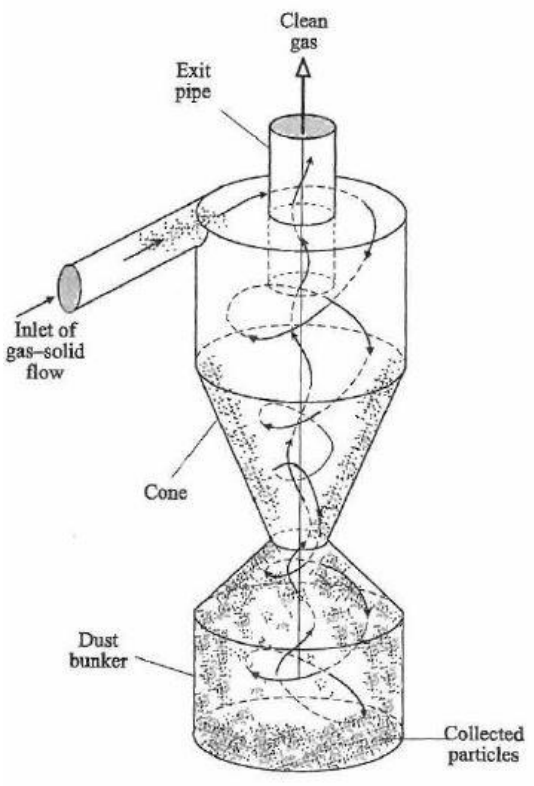

Design

The design of a cyclone is a compromise between the required collection efficiency and pressure drop allowed (Flagan & Seinfeld, 1988). The physical size is of course also relevant and affects both the

collection efficiency and pressure drop of the cyclone. From the literature reviewed, cyclones are usually designed for a fixed inlet gas velocity.

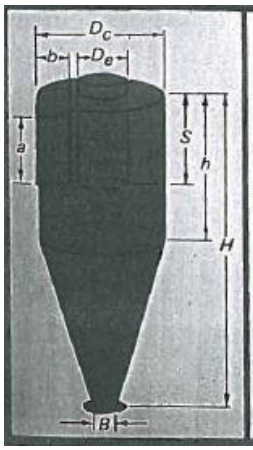

Nomenclature		High-efficiency		General-purpose		
		Stairmand [12]	Swift [15]	Lapple [4]	Swift [15]	Peterson & Whitby [8]
D_c	body dia.	1.0	1.0	1.0	1.0	1.0
a	inlet height	0.5	0.44	0.5	0.5	0.583
b	inlet width	0.2	0.21	0.25	0.25	0.208
S	outlet length	0.5	0.5	0.625	0.6	0.583
D_e	outlet dia.	0.5	0.4	0.5	0.5	0.5
h	cylinder height	1.5	1.4	2.0	1.75	1.333
H	overall height	4.0	3.9	4.0	3.75	3.17
B	dust outlet dia.	0.375	0.4	0.25	0.4	0.5
l	natural length	2.48	2.04	2.30	2.30	1.8
G	$8\,K_c/K_a^2/K_b^2$	551.3	699.2	402.9	381.8	324.8
N_H	$16\,ab/D_e^2$	6.40	9.24	8.0	8.0	7.76
	G/N_H	86.14	75.67	50.36	47.7	41.86

When sizing a cyclone, the dimensions are specified relative to the cyclone's body diameter D. Koch & Licht (1977) provide broadly cited design configurations for tangential reverse-flow cyclones, given in the figure above which was taken from Koch & Licht (1977). Additionally, Koch & Licht (1977) provide the following geometrical constraints to obtain a workable design:

1. $a < S$
2. $b < \frac{1}{2}(D - D_e)$
3. $S + l \leq H$
4. $S < h$
5. $h < H$

Fractional Efficiency

The fractional or grade efficiency η_i of a cyclone is presented in various literature. This is the measure of the cyclones ability to remove particulates of a certain size. Leith & Licht (1972) define the fractional efficiency as a function of the particle diameter

$$\eta_i(D_p) = \frac{N_1 - N_2}{N_1}$$

where N_1 and N_2 are the number of particles of diameter D_p before and after the cyclone respectively.

Leith & Licht (1972) developed a theoretical correlation to predict cyclone fractional efficiency for the purposes of design. The correlation is cited in numerous literature and is presented in the following form by Koch & Licht (1977)

$$\eta_i = 1 - \exp\left\{-2\left[\frac{G\tau_i \dot{V}_g}{D_c^3}(n+1)\right]^{\frac{1}{2(n+1)}}\right\}$$

where τ_i is the relaxation time in seconds, defined as

$$\tau_i(D_p) = \frac{\rho_p D_p^2}{18\mu_g}$$

n is the vortex exponent, which may be calculated using the following correlation

$$n = 1 - \left[1 - \frac{(12D_c)^{0.14}}{2.5}\right]\left[\frac{T+460}{530}\right]^{0.3}$$

and G is the dimensionless cyclone configuration factor, which may be calculated using the method presented in Leith & Licht (1972), or the value taken for the configurations given in the figure above.

Note that the correlations above are valid for imperial units only i.e. $\dot{V}_g$ is in ft^3/s; D_c is in ft; ρ_p is in lb/ft^3; μ_g is in lb/ft-s; and T is in °F.

Overall Efficiency

The overall efficiency of the cyclone for a given particle size distribution (PSD) can then be calculated as follows

$$\eta_T = \sum m_i \eta_i$$

where m_i is the mass fraction of particles within size range i.

It is noted that Dirgo & Leith (1985) compared experimental curves with fractional efficiency curves generated using published theories. They found the Leith & Licht (1972) theory to both under and over predict the fractional efficiency over a range of particle sizes. However, for particles larger than 5µm the theory under predicted the fractional efficiency, and can therefore be regarded as a conservative estimate for design. Furthermore, Dirgo & Leith (1985) mention that experiments were performed using a Stairmand type cyclone and therefore the results may not be applicable to other cyclone configurations.

Other definitions for cyclone efficiency are also given in literature. For example, Flagan & Seinfeld (1988) provide a collection efficiency in terms of mass

$$\eta_m = \frac{m_{p1} - m_{p2}}{m_{p1}} \times 100\ \%$$

where m_{p1} and m_{p2} are the mass of particles before and after the cyclone respectively. This efficiency is easy to determine experimentally and was employed in a study by Faulkner & Shaw (2006).

Another example is taken from Klinzing, et al. (1997), who define collection efficiency in terms of dust concentration

$$\eta_C = \frac{\overline{\rho_{p1}} - \overline{\rho_{p2}}}{\overline{\rho_{p1}}} \times 100\ \%$$

where $\overline{\rho_{p1}}$ and $\overline{\rho_{p2}}$ are the dust concentrations (or bulk densities) before and after the separation device respectively.

Improving Cyclone Efficiency

According to various literature, cyclone efficiency increases with:

- Increasing particle density.
- Increasing inlet velocity (up to a point).
- Increasing cyclone body height.
- Increasing outlet to inlet area ratios.

and decreases with:

- Increasing fluid viscosity i.e. higher temperatures.
- Increasing cyclone diameter, outlet diameter and inlet width i.e. larger cyclones.

Particle Re-entrainment

Kalen & Zenz (1974) and Koch & Licht (1977) quantify the inlet velocity at which particle re-entrainment occurs i.e. the maximum inlet velocity until efficiency starts to decrease. Kalen & Zenz (1974) did this by applying the saltation mechanism to cyclone design to hypothesise that efficiency will reduce if the spiralling velocity exceeds the saltation velocity. Koch & Licht (1977) cite the work of Kalen & Zenz (1974) and incorporate the results in their design guidelines, where they recommend an optimum inlet to saltation velocity ratio of 1.25. However, aaccording to Kalen & Zenz (1974), the optimum inlet to saltation velocity ratio is approximately 2. The figure below is an extract from Kalen & Zenz (1974), which shows efficiency curves approaching an optimal point between an inlet to saltation ratio of 1.5 and 2. A value of 1.5 is therefore recommended as a conservative estimate for design.

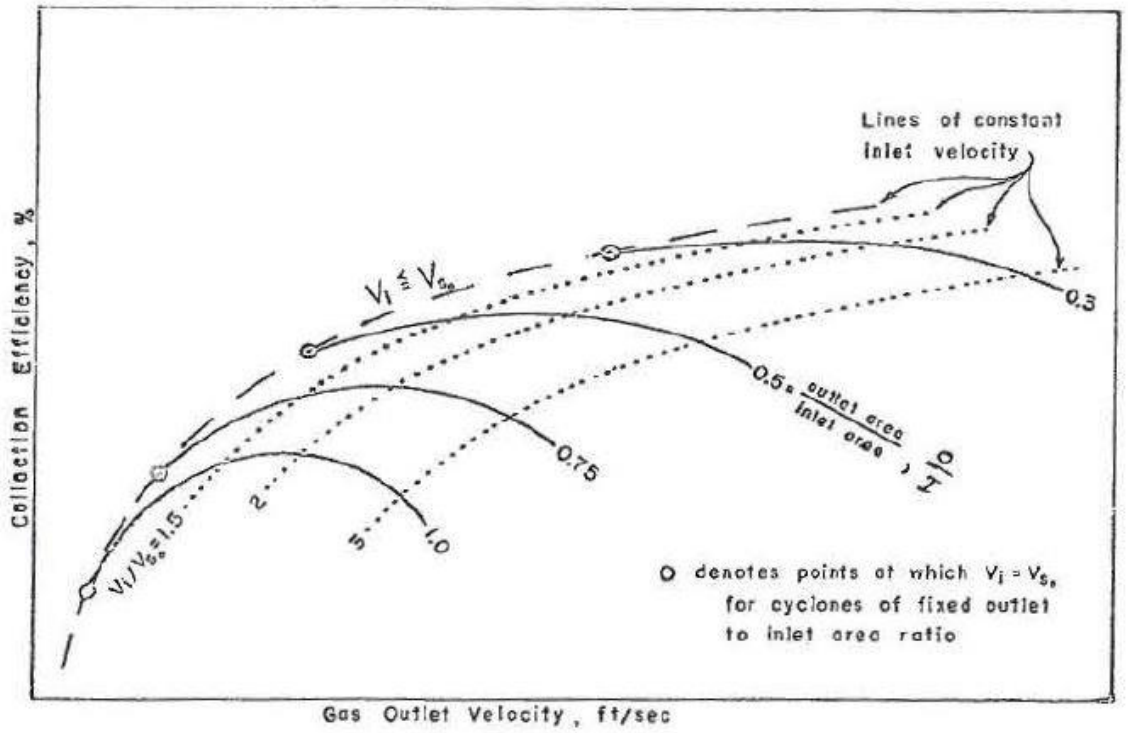

For a known inlet velocity v_i, the saltation velocity v_s can be estimated using the following (simplified) semi-empirical correlation developed by Kalen & Zenz (1974)

$$v_s = 2.055\omega \left[\frac{\left(\frac{b}{D}\right)^{0.4}}{\left(1-\frac{b}{D}\right)^{\frac{1}{3}}} \right] D^{0.067} v_i^{\frac{2}{3}}$$

Where

$$\omega = \left[\frac{4g\mu_g(\rho_p - \rho_g)}{3\rho_g^2} \right]^{\frac{1}{3}}$$

Note that the correlations above are valid for imperial units only.

Pressure Drop

Chuah, et al. (2003) compare empirical pressure drop correlations with experimental results from published literature. The results show that the Shepard & Lapple correlation shows good prediction over a range of inlet velocities. The correlation is commonly presented in literature because of its ease of use and accuracy, and is given as follows:

$$\Delta P_c = \frac{1}{2}\rho_g v_i^2 N_H$$

where N_H is the number of inlet velocity heads and is calculated as follows:

$$N_H = K\left(\frac{ab}{D_e^2}\right)$$

where K = 16 for standard inlet cyclones and 7.5 for cyclones with volute inlets. N_H is dimensionless and therefore SI units may be used.

Minimising Cyclone Pressure Drop

The factors which increase cyclone efficiency also increase cyclone pressure drop and similarly, the factors which decrease cyclone efficiency also decrease cyclone pressure drop. Koch & Licht (1977) have noted that higher cyclone configuration factors facilitate increased efficiencies and that a lower velocity heads facilitate decreased pressure drops. Since both these variables depend on cyclone geometry, Koch & Licht (1977) propose that the ratio $\frac{G}{N_H}$ be maximised for optimum cyclone design.

Effects of Loading

The efficiency and pressure drop theory presented above are applicable for relatively low dust concentrations. However, the consensus from the various literature reviewed is that cyclone efficiency and pressure drop increase and decrease respectively with increased loading. The use of the correlations presented above are therefore advised for conservative design.

Appendix C. Design Theory Derivations

Voidage

A relationship for α_g is obtained as follows:

$$z = \frac{\dot{m}_p}{\dot{m}_g} = \frac{\alpha_p \rho_p u_p A_{pipe}}{\alpha_g \rho_g u_g A_{pipe}} = \frac{\alpha_p \rho_p u_p}{\rho_g U_g}$$

therefore

$$\alpha_p = \frac{\rho_g U_g z}{\rho_p u_p}$$

and by definition

$$\alpha_p + \alpha_g = 1$$

therefore

$$\alpha_g = 1 - \frac{\rho_g U_g z}{\rho_p u_p}$$

Taking $z = Z$ gives

$$\alpha_p = \frac{\rho_g U_g Z}{\rho_p u_p}$$

and

$$\alpha_g = 1 - \frac{\rho_g U_g Z}{\rho_p u_p}$$

Particle Phase EOM

A particle phase EOM was derived by taking a 1-D Lagrange approach for a representative particle and incorporating Eulerian elements, to simplify the analysis of friction and to account for the effects of neighbouring particles on drag. The following assumptions were made in the derivation of the equation:

1. The flow is dilute and homogenous.
2. All particles are spherical and are of the same size.
3. The particle velocity is the average velocity over the CV.
4. Mass and energy are not transferred between phases.
5. Mach number, turbulence, and rotation effects on particle drag are neglected.
6. Virtual mass and Basset force effects on particle motion are neglected.

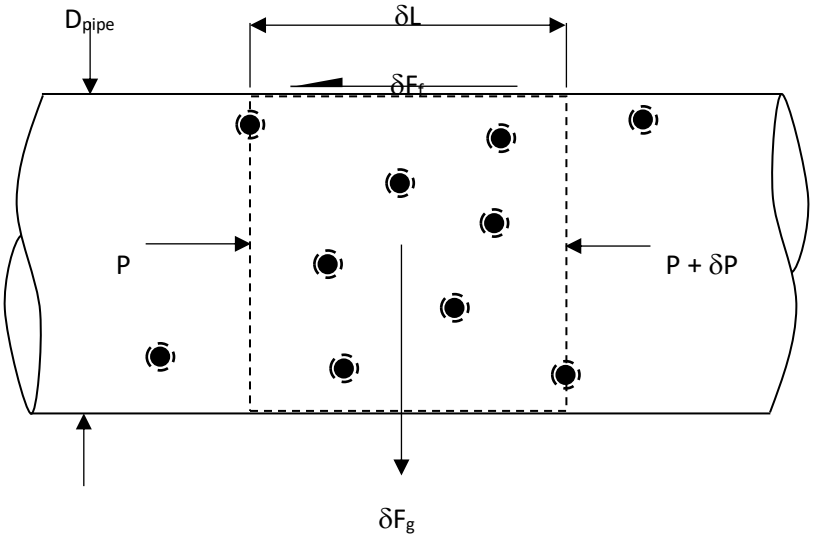

Consider the mixture flow through the CV given above, the number of particles in element δL is given by

$$\delta N = \frac{\delta M_p}{\rho_p \left(\frac{\pi D_p^3}{6}\right)}$$

The above equation is manipulated to obtain the mass δM_p of a representative particle and subsequently, the friction force opposing particle motion in element δL, which is given by

$$\delta F_{fp} = \frac{\lambda_{Dp} u_p^2}{2D_{pipe}} \delta M_p$$

The following free body diagram (FBD) is then constructed

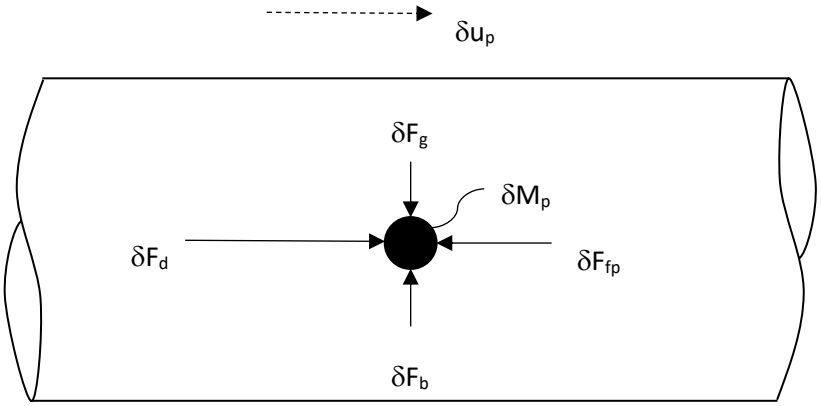

Applying Newton's Second Law, the following particle phase EOM for vertical flow is finally derived

$$\frac{\delta u_p}{\delta t} = \frac{3}{4} C_{D\infty} \alpha_g^{-4.7} \frac{\rho_g (u_g - u_p)^2}{\rho_p D_p} - g\left(1 - \frac{\rho_g}{\rho_p}\right) - \frac{\lambda_{Dp} u_p^2}{2 D_{pipe}}$$

Drag Gravity & Buoyancy Friction

where α_g may be expressed as

$$\alpha_g = 1 - \frac{\rho_g U_g}{\rho_p u_p}\left(\frac{\dot{M}_p}{\rho_g U_g A_{pipe}}\right) = 1 - \frac{4\dot{M}_p}{\rho_p \pi D_{pipe}^2 u_p}$$

For horizontal flow, the gravity/ buoyancy term is equal to zero.

Appendix D. Dimensionless Number Groups

Dimensionless number groups were used to design for similarity of PF conveying systems in South African coal-fired power plants. The following section presents the dimensionless numbers considered and selected for scaling of the prototype and proposed final test facility.

Dimensionless Number Groups in Literature

The amount of dimensionless number groups related to gas-solid flows are abundant. They also apply for different phenomena i.e. the groups associated with saltation are not necessarily the same as those that apply for choking. For example, Cabrejos & Klinzing (1994) identified seven groups related to the saltation phenomenon alone. The number groups found in various literature are presented below.

Geometric Similarity

For geometric similarity, the following groups apply:

1. The ratio of particle to pipe diameter $D_p/D_{pipe.}$
2. The relative pipe roughness $\varepsilon_r = \varepsilon/D_{pipe.}$
3. The pipe geometry and particle shape.

Flow Similarity

For flow similarity, the following groups apply:

1. The loading Z i.e. the ratio of mass flow rates of particles and gas.
2. The solids mass concentration C_M and/ or
3. the solids volume concentration or volume fraction α_d.

Dynamic Similarity

For dynamic similarity, the following groups apply:

1. The Reynolds number i.e. inertial force/ viscous force. Four types of Reynolds numbers are found in literature, these include the pipe, particle, terminal velocity, and relative particle Reynolds numbers.

$$Re = \frac{\rho_g D_{pipe} U_g}{\mu_g}; Re_p = \frac{\rho_g D_p U_g}{\mu_g}; Re_{t0} = \frac{\rho_g D_p u_{t0}}{\mu_g}; Re_r = \frac{\rho_g D_p (u_g - u_p)}{\mu_g}$$

2. The Froude number i.e. inertia force/ gravitational force. Froude numbers based on pipe and particle diameters are found in literature, with the former being the most commonly used. Additionally, Froude numbers based on the particle terminal velocity, and the superficial gas velocity at saltation U_{salt} have been found in literature.

$$Fr = \frac{U_g}{\sqrt{D_{pipe} g}};\ Fr_p = \frac{U_g^2}{\sqrt{D_p g}}; Fr_{t0} = \frac{u_{t0}^2}{\sqrt{D_p g}};\ Fr_{salt} = \frac{U_{salt}}{\sqrt{D_{pipe} g}}$$

3. Fan & Zhu (1998) show that the similarity of the Stokes number St can be achieved by ensuring the similarity of the "pseudoparticle Reynolds number" Re_p^* and the "inertia parameter" ψ. By definition

$$St = \frac{V\tau_v}{l}; Re_p^* = \frac{\rho_g V D_p}{\mu_g};\ \psi = \frac{\rho_p V D_p^2}{18\mu_g l}$$

Where V is a reference velocity in m/s, l a reference length in m, and τ_v is the momentum response time in s and is given by

$$\tau_v = \frac{\rho_p D_p^2}{18\mu_g}$$

4. The ratio of particle and gas densities ρ_p/ρ_g as well as the Archimedes number Ar are also found in literature.

$$Ar = \frac{\rho_g(\rho_p - \rho_g) g D_p^3}{\mu_g^2}$$

Dimensional Analysis

Noting that the drag coefficient $C_{D\infty}$ is a function of the relative particle Reynolds number Re_r, The equation of motion for δN particles in a differential section of pipe length δL can be written as

$$\frac{\delta u_p}{\delta t} = \frac{3}{4}[C_{D\infty}(\rho_g, u_g, u_p, D_p, \mu_g)]\left(1 - \frac{U_g \rho_g Z}{\rho_p u_p}\right)^{-4.7} \frac{\rho_g(u_g - u_p)^2}{\rho_p D_p} - g\left(1 - \frac{\rho_g}{\rho_p}\right) - \frac{\lambda_{Dp} u_p^2}{2D_{pipe}}$$

Furthermore, it is noted that the gas and particle velocities $u_g\ and\ u_p$ are functions of the superficial gas velocity U_g. U_g is therefore be used in place of both u_g and u_p in the subsequent analysis. Also, although empirical correlations exist for estimating the solids friction factor λ_{Dp}, it is widely accepted in literature that λ_{Dp} depends on the combination of pipe and particle materials. It is therefore excluded as a variable in the subsequent analysis with Z, which is deemed a co-requisite for flow similarity.

The table below lists the unique variables together with their corresponding MLT dimensions:

Variable	**Symbol**	**SI Units**	**MLT Dimensions**
Geometric			
Particle diameter	$\boldsymbol{D_p}$	m	L
Pipe diameter	$\boldsymbol{D_{pipe}}$	m	L

Kinematic			
Superficial gas velocity	$\boldsymbol{U_g}$	m/s	LT^{-1}
Gravitational acc.	$\boldsymbol{g}$	m/s^2	LT^{-2}
Dynamic			
Gas density	$\boldsymbol{\rho_g}$	kg/m^3	ML^{-3}
Particle density	$\boldsymbol{\rho_p}$	kg/m^3	ML^{-3}
Gas viscosity	$\boldsymbol{\mu_g}$	kg/ms	$ML^{-1}T^{-1}$

Using the Buckingham Π Theorem, the following π groups (dimensionless numbers) are obtained by selecting U_g, ρ_g *or* ρ_p, and D_p *or* D_{pipe} as repeating variables:

$$\frac{U_g D_p \rho_p}{\mu_g}; \frac{U_g D_p \rho_g}{\mu_g}; \frac{U_g D_{pipe} \rho_p}{\mu_g}; \frac{U_g D_{pipe} \rho_g}{\mu_g}$$

$$\frac{U_g}{\sqrt{g D_p}}; \frac{U_g}{\sqrt{g D_{pipe}}}$$

$$\frac{D_p}{D_{pipe}}$$

$$\frac{\rho_p}{\rho_g}$$

Selection of scaling parameters

Taking into consideration the numbers given in literature and the results of the dimensional analysis performed, similarity is achieved as follows:

Geometric Similarity

1. The pipe geometry and particle shape are similar i.e. the pipe cross section is circular and the particles the same.
2. The ratio of particle to pipe diameter D_p/D_{pipe} and the relative pipe roughness ε_r are not used for scaling. The exclusion of these numbers is justified as follows:
   2.1. It is apparent from literature that particles used in models are usually the same as in the scaled-up plant. This is confirmed by Klinzing, et al. (1997).
   2.2. Satisfying D_p/D_{pipe} would require the use of extremely fine particles and of a narrow size range.

2.3. According to Zenz (1964), extremely fine particles require higher conveying velocities as they get trapped in the viscid boundary layer. Tests conducted for extremely fine particles would therefore result in biased data points.

2.4. ε_r is likely to vary with time due to erosion. It is therefore uneconomical to keep ε_r constant.

Flow Similarity

1. The loading Z is kept within the ranges required for low NOx burner ignition.

$$1.5 < \frac{1}{Z} < 2.5$$

2. The volume fraction α_d is kept below 0.01. This is a criterion for dilute flow as given in various literature.

Dynamic Similarity

1. The particle Reynolds number is used for scaling

$$Re_p = \frac{\rho_g D_p U_g}{\mu_g}$$

2. The particle Froude number is used for scaling

$$Fr_p = \frac{U_g}{\sqrt{g D_p}}$$

3. The inertia parameter is used for scaling

$$\psi = \frac{\rho_p D_p U_g}{\mu_g}$$

Note that numbers containing D_{pipe} were not selected, as It was deemed too difficult to satisfy them without having to use a D_{pipe} of the same size as a those found in coal-fired power plants.

Kinematic Boundary Condition Similarity

Although not explicitly accounted for, the similarity of flow around the system boundaries (particle and pipe wall) is deemed similar because of the use of similar particles. A form of the Reynolds number is also included in the dynamic similarity scaling.

Appendix E. Conversion from Bits to Current

NI 9208 AI

The NI 9208 AI has 24-bit resolution. However, current is measured indirectly using an internal shunt resistor of 85Ω ∴ the span of the voltage drop within the 4-20mA measuring range is

$V = I{\times}R = 0.020(85) - 0.004(85) = 1.7 - 0.34 = 1.36V.$

The measurement supply voltage is $\pm 30V$ ∴ the voltage consumed by the current loop is $\frac{1.36}{60} = 2.267\%$ of the measurement supply voltage.

24-bits equates to $2^{24} = 16777216$ counts ∴ the voltage resolution is 16777216 counts or $\frac{60}{16777216} = 3.58\mu V$.

The corresponding current resolution is $\frac{1.36}{60}{\times}16777216 = 380283$ counts or $\frac{20-4}{380283} = 42\mu A$.

LCA

The LCA has 16-bit resolution on the output of 4-20mA. This equates to $2^{16} = 65536$ counts ∴ the current resolution is 65536 counts or $\frac{20-4}{65536} = 244\mu A$.

Appendix F. Embedded Scilab Script

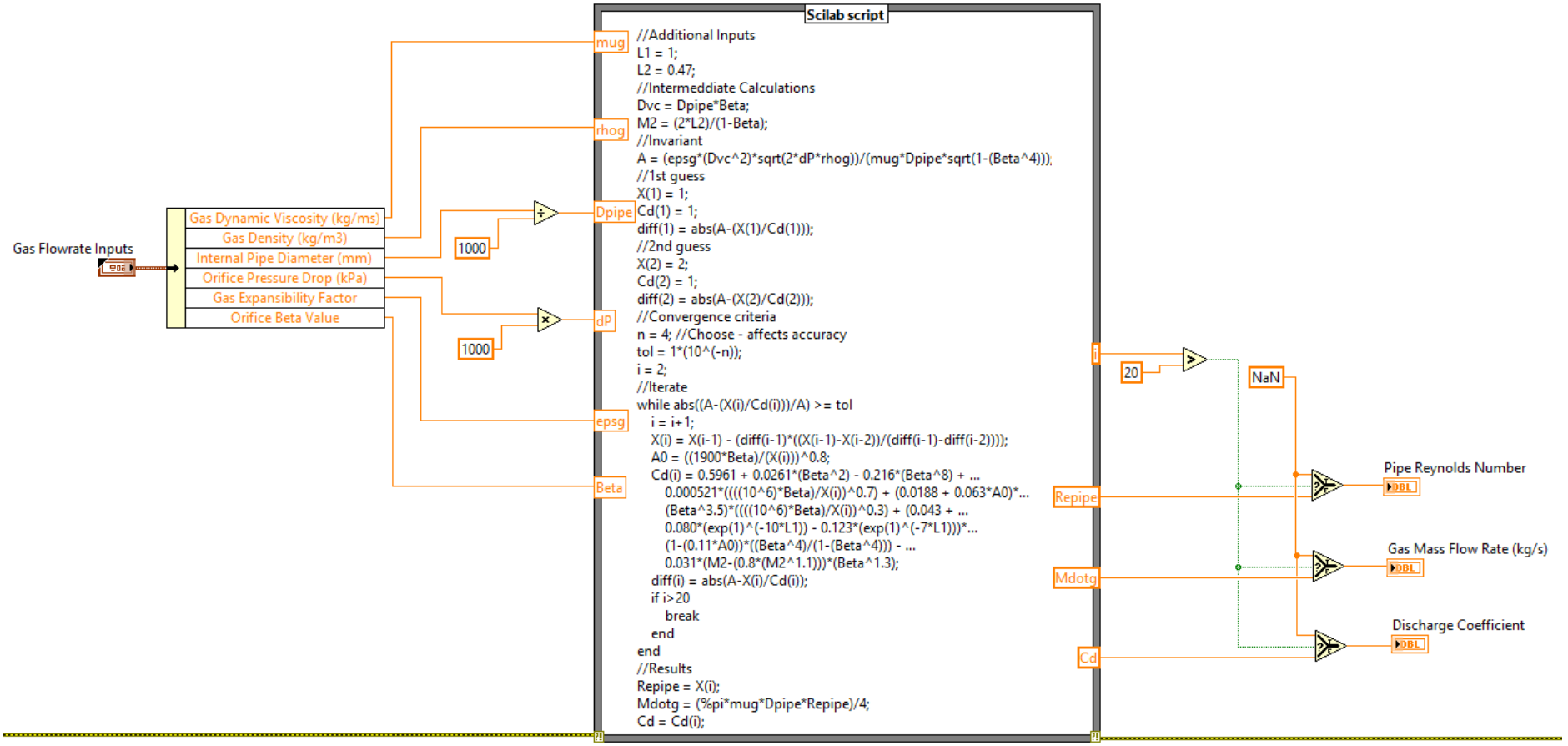

Appendix G. Hand Derivations

NUMERICAL INTEGRATION OF EOM

from $a = \frac{\delta u}{\delta t} = f(\dots)$

Want

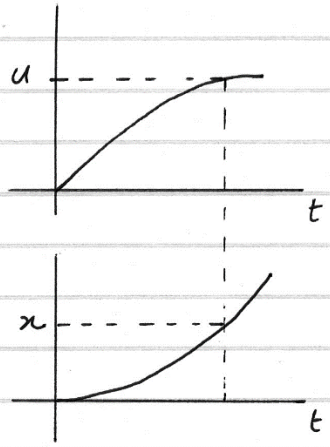

$\therefore$ let $t_{i+1} = t_i + \delta t$

$u_{i+1} = u_i + Su_i \delta t$

$x_{i+1} = x_i + Sx_i \delta t$

$i \in 1, 2, \dots, n$

where $Su_{i+1} = \alpha u \, u_{i+1} + (1 - \alpha u) u_i$

$Sx_{i+1} = \alpha x \, x_{i+1} + (1 - \alpha x) x_i$

& $Su_1 = a_1 = f_1(\dots)$

To solve, must choose $t_1 ; x_1 ; u_1 ; \delta t ; \alpha x ; \alpha u$ & end criteria

Where $\alpha = 0 \rightarrow$ fully explicit

$\alpha = 1 \rightarrow$ fully implicit

$\alpha = 0.5 \rightarrow$ Crank-Nicolson method

$\alpha = 0.7 \rightarrow$ { faster than implicit
greater stability than C-N

//

LEAST SQUARES REGRESSION

Want $y_i(x_i) = a_0 + a_1 x_i + a_2 x_i^2 + \dots + a_m x_i^m$

S.t. $\sum_{i=1}^{n} e^2 = \left[y_i(X_i) - Y_i \right]^2$ is minimised

where e is the error in predicting y from x
& Y is the actual value at a known X value

$$\therefore \text{let } g(a_0; a_1; \dots; a_m) = \sum_{i=1}^{n} e^2$$

$$= \sum_{i=1}^{n} \left(a_0 + a_1 X_i + a_2 X_i^2 + \dots + a_m X_i^m - Y_i \right)^2$$

$$= \left(a_0 + a_1 X_1 + a_2 X_1^2 + \dots + a_m X_1^m - Y_1 \right)^2$$
$$+ \left(a_0 + a_1 X_2 + a_2 X_2^2 + \dots + a_m X_2^m - Y_2 \right)^2$$
$$+ \left(a_0 + a_1 X_3 + a_2 X_3^2 + \dots + a_m X_3^m - Y_3 \right)^2$$
$$+ \dots$$
$$+ \left(a_0 + a_1 X_n + a_2 X_n^2 + \dots + a_m X_n^m - Y_n \right)^2$$

to minimise $g(a_0; a; \dots; a_m)$

$$\text{let } f_0 = \frac{\partial g}{\partial a_0} = 0 \; ; \; f_1 = \frac{\partial g}{\partial a_1} = 0 \; ; \dots ; \; f_m = \frac{\partial g}{\partial a_m} = 0$$

$$f_0(a_0; a_1; \dots; a_m) = \frac{\partial g}{\partial a_0} = 2\left(a_0 + a_1 X_1 + a_2 X_1^2 + \dots + a_m X_1^m - Y_1 \right)$$
$$+ 2\left(a_0 + a_1 X_2 + a_2 X_2^2 + \dots + a_m X_2^m - Y_2 \right)$$
$$+ \dots$$
$$+ 2\left(a_0 + a_1 X_n + a_2 X_n^2 + \dots + a_m X_n^m - Y_n \right)$$

$$f_1(a_0; a_1; \dots; a_m) = \frac{\partial g}{\partial a_1} = 2(a_0 + a_1 X_1 + a_2 X_1^2 + \dots + a_m X_1^m - Y_1) X_1$$
$$+ 2(a_0 + a_1 X_2 + a_2 X_2^2 + \dots + a_m X_2^m - Y_2) X_2$$
$$+ \dots$$
$$+ 2(a_0 + a_1 X_n + a_2 X_n^2 + \dots + a_m X_n^m - Y_n) X_n$$

$$f_2(a_0; a_1; \dots; a_m) = \frac{\partial g}{\partial a_2} = 2(\dots) X_1^2 + \dots + 2(\dots) X_n^2$$

$$f_m(\dots) = \frac{\partial g}{\partial a_m} = 2(\dots) X_1^m + \dots + 2(\dots) X_n^m$$

$$\therefore f_0(\dots) = 2\left[a_0 \sum_{i=1}^{n} X_i^0 + a_1 \sum_{i=1}^{n} X_i^1 + \dots + a_m \sum_{i=1}^{n} X_i^m - \sum_{i=1}^{n} Y_i\right] = 0$$

$$f_1(\dots) = 2\left[a_0 \sum_{i=1}^{n} X_i^1 + a_1 \sum_{i=1}^{n} X_i^2 + \dots + a_m \sum_{i=1}^{n} X_i^{m+1} - \sum_{i=1}^{n} (Y_i X_i)\right] =$$

$$f_2(\dots) = 2\left[a_0 \sum_{i=1}^{n} X_i^2 + a_1 \sum_{i=1}^{n} X_i^3 + \dots + a_m \sum_{i=1}^{n} X_i^{m+2} - \sum_{i=1}^{n} (Y_i X_i^2)\right] =$$
$$\vdots$$
$$f_n(\dots) = 2\left[a_0 \sum_{i=1}^{n} X_i^m + a_1 \sum_{i=1}^{n} X_i^{m+1} + \dots + a_m \sum_{i=1}^{n} X_i^{m+m} - \sum_{i=1}^{n} (Y_i X_i^m)\right] =$$

$$\therefore a_0 \sum_{i=1}^{n} X_i^0 + a_1 \sum_{i=1}^{n} X_i^1 + \dots + a_m \sum_{i=1}^{n} X_i^m = \sum_{i=1}^{n} (Y_i X_i^0)$$

$$a_0 \sum_{i=1}^{n} X_i^1 + a_1 \sum_{i=1}^{n} X_i^2 + \dots + a_m \sum_{i=1}^{n} X_i^{m+1} = \sum_{i=1}^{n} (Y_i X_i^1)$$
$$\vdots$$
$$a_0 \sum_{i=1}^{n} X_i^m + a_1 \sum_{i=1}^{n} X_i^{m+1} + \dots + a_m \sum_{i=1}^{n} X_i^{m+m} = \sum_{i=1}^{n} (Y_i X_i^m)$$

re-write in matrix form : $\alpha a = \beta$

$$\begin{bmatrix} \sum_{i=1}^{n}(X_i^0 X_i^0) & \sum_{i=1}^{n}(X_i^0 X_i^1) & \cdots & \sum_{i=1}^{n}(X_i^0 X_i^m) \\ \sum_{i=1}^{n}(X_i^1 X_i^0) & \sum_{i=1}^{n}(X_i^1 X_i^1) & \cdots & \sum_{i=1}^{n}(X_i^1 X_i^m) \\ \vdots & & & \\ \sum_{i=1}^{n}(X_i^m X_i^0) & \sum_{i=1}^{n}(X_i^m X_i^2) & \cdots & \sum_{i=1}^{n}(X_i^m X_i^m) \end{bmatrix} \begin{bmatrix} a_0 \\ a_1 \\ \vdots \\ a_m \end{bmatrix}$$

$$= \begin{bmatrix} \sum_{i=1}^{n}(Y_i X_i^0) \\ \sum_{i=1}^{n}(Y_i X_i^1) \\ \vdots \\ \sum_{i=1}^{n}(Y_i X_i^m) \end{bmatrix}$$

$$\therefore \alpha_{jk} = \sum_{i=1}^{n}(X_i^j X_i^k) \quad \text{and} \quad \beta_k = \sum_{i=1}^{n}(Y_i X_i^k)$$

let $\varepsilon = \alpha^{-1}$ $\therefore$ from $\alpha a = \beta$

$$a = \alpha^{-1}\beta = \varepsilon\beta$$

$$\therefore \quad a^T = \beta^T \varepsilon^T$$

$$\therefore \quad y = a^T F \quad \text{where} \quad F_k = x^k$$

//

CALIBRATION UNCERTAINTY

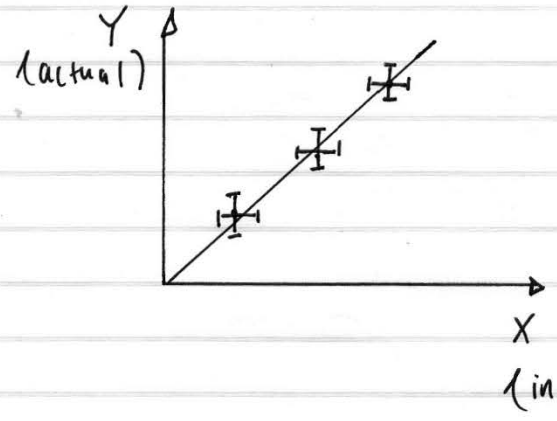

from $y = a^T F$; $y = f(X; Y)$

$$\therefore \quad u_y(x) = \sqrt{\sum \left(\frac{\partial y}{\partial X_i} u_{X_i}\right)^2 + \sum \left(\frac{\partial y}{\partial Y_i} u_{Y_i}\right)^2}$$

where

$$\frac{\partial y}{\partial X} = \begin{bmatrix} \frac{\partial y}{\partial X_0} \\ \frac{\partial y}{\partial X_1} \\ \vdots \\ \frac{\partial y}{\partial X_{n-1}} \end{bmatrix} = \begin{bmatrix} \frac{y(1.01X_0) - y(0.99X_0)}{0.02X_0} \\ \frac{y(1.01X_1) - y(0.99X_1)}{0.02X_1} \\ \vdots \end{bmatrix}$$

&

$$\frac{\partial y}{\partial Y} = \begin{bmatrix} \frac{\partial y}{\partial Y_0} \\ \frac{\partial y}{\partial Y_1} \\ \vdots \\ \frac{\partial y}{\partial Y_{n-1}} \end{bmatrix} = \begin{bmatrix} \frac{y(1.01Y_0) - y(0.99Y_0)}{0.02Y_0} \\ \frac{y(1.01Y_1) - y(0.99Y_1)}{0.02Y_1} \\ \vdots \end{bmatrix} //$$

UNCERTAINTY IN GRADIENT OF FITTED CURVE

from $y = a^T F$

let $b(x) = \frac{\delta y_1(x)}{\delta x}$

$$= \frac{\delta}{\delta x} \left\{ \begin{bmatrix} Y_1 X_1^{\,0} + Y_2 X_2^{\,0} + \ldots + Y_n X_n^{\,0} \\ Y_1 X_1^{\,1} + Y_2 X_2^{\,1} + \ldots + Y_n X_n^{\,1} \\ Y_1 X_1^{\,m} + Y_2 X_2^{\,m} + \ldots + Y_n X_n^{\,m} \end{bmatrix} \begin{bmatrix} \varepsilon \end{bmatrix} \begin{bmatrix} x^0 \\ x^1 \\ \vdots \\ x^n \end{bmatrix} \right\}$$

$$= \begin{bmatrix} \ldots \end{bmatrix} \begin{bmatrix} \varepsilon \end{bmatrix} \begin{bmatrix} 0 \\ 1x^0 \\ 2x^1 \\ \vdots \\ mx^{m-1} \end{bmatrix}$$

$$\therefore \frac{\partial b(x)}{\partial Y_1} = \begin{bmatrix} X_1^{\,0}; X_1^{\,1}; \ldots; X_1^{\,m} \end{bmatrix} \begin{bmatrix} \varepsilon \end{bmatrix} \begin{bmatrix} 0 \\ 1x^0 \\ 2x^1 \\ \vdots \\ mx^{m-1} \end{bmatrix}$$

$$\frac{\partial b(x)}{\partial Y_2} = \begin{bmatrix} X_2^{\,0}; X_2^{\,1}; \ldots; X_2^{\,m} \end{bmatrix} \begin{bmatrix} \varepsilon \end{bmatrix} \begin{bmatrix} \ldots \end{bmatrix}$$

$$\frac{\partial b(x)}{\partial Y_n} = \begin{bmatrix} X_n^{\,0}; X_n^{\,1}; \ldots; X_n^{\,m} \end{bmatrix} \begin{bmatrix} \varepsilon \end{bmatrix} \begin{bmatrix} \ldots \end{bmatrix}$$

$$\therefore \frac{\partial b}{\partial Y_i} = \begin{bmatrix} X_i^{\,0}; X_i^{\,1}; X_i^{\,m} \end{bmatrix} \begin{bmatrix} \varepsilon_{00} & \varepsilon_{01} & \cdots & \varepsilon_{0m} \\ \varepsilon_{10} & \varepsilon_{11} & \cdots & \varepsilon_{1m} \\ \vdots & & & \\ \varepsilon_{m0} & \varepsilon_{m1} & \cdots & \varepsilon_{mm} \end{bmatrix} \begin{bmatrix} 0 \\ 1x^0 \\ 2x^1 \\ mx^{m-1} \end{bmatrix}$$

$$\therefore \frac{\partial b}{\partial Y_i} = \begin{bmatrix} X_i^0 & X_i^1 & X_i^m \end{bmatrix} \begin{bmatrix} \varepsilon_{00}\cdot 0 + \varepsilon_{01}x^0 + \dots + \varepsilon_{0m}\, m x^{m-1} \\ \varepsilon_{10}\cdot 0 + \varepsilon_{11}x^0 + \dots + \varepsilon_{1m}\, m x^{m-1} \\ \vdots \\ \varepsilon_{m0}\cdot 0 + \varepsilon_{m1}x^0 + \dots + \varepsilon_{mm}\cdot m x^{m-1} \end{bmatrix}$$

$$= \begin{bmatrix} X_i^0 & X_i^1 & X_i^m \end{bmatrix} \begin{bmatrix} \sum_{j=1}^{m} \varepsilon_{0j}\, j\, x^{j-1} \\ \sum_{j=1}^{m} \varepsilon_{1j}\, j\, x^{j-1} \\ \vdots \\ \sum_{j=1}^{m} \varepsilon_{mj}\, j\, x^{j-1} \end{bmatrix}$$

$$\therefore \frac{\partial b}{\partial Y_i} = \sum_{k=0}^{m} \left(X_i^k \sum_{j=1}^{m} \varepsilon_{kj}\, j x^{j-1} \right)$$

$$\therefore u_b^2(x) = \sum_{i=1}^{n} \left[\left(\frac{\partial b}{\partial Y_i} \right)^2 u_{Y_i}^2 \right]$$

$$= \sum_{i=1}^{n} \left\{ \left[\sum_{k=0}^{m} \left(X_i^k \sum_{j=1}^{m} \varepsilon_{kj}\, j x^{j-1} \right) \right]^2 u_{Y_i}^2 \right\}$$

//

Appendix H. Process Model Flow Charts

HORIZONTAL SIMILARITY MODEL

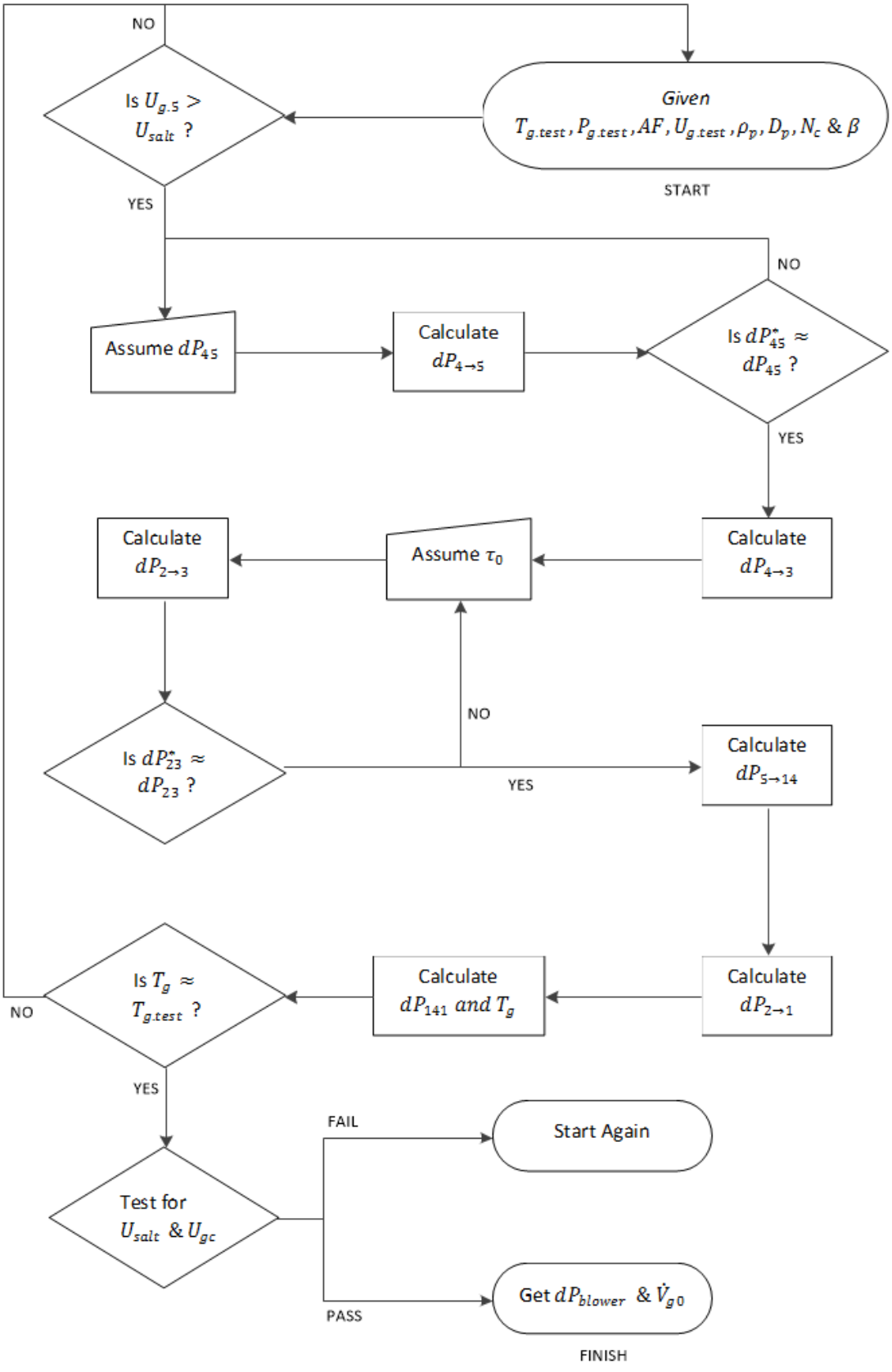

VERTICAL SIMILARITY MODEL

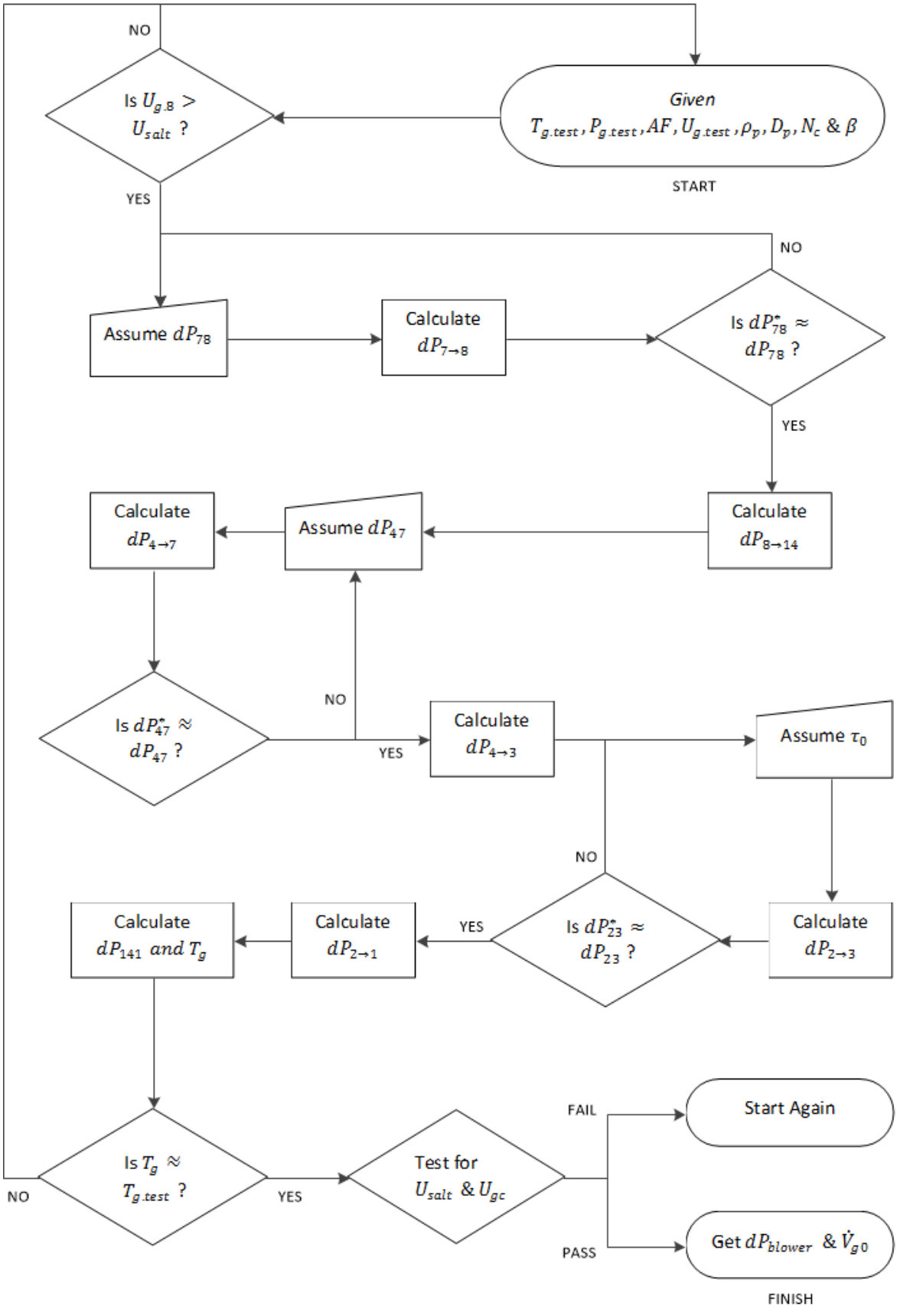

SALTATION MODEL

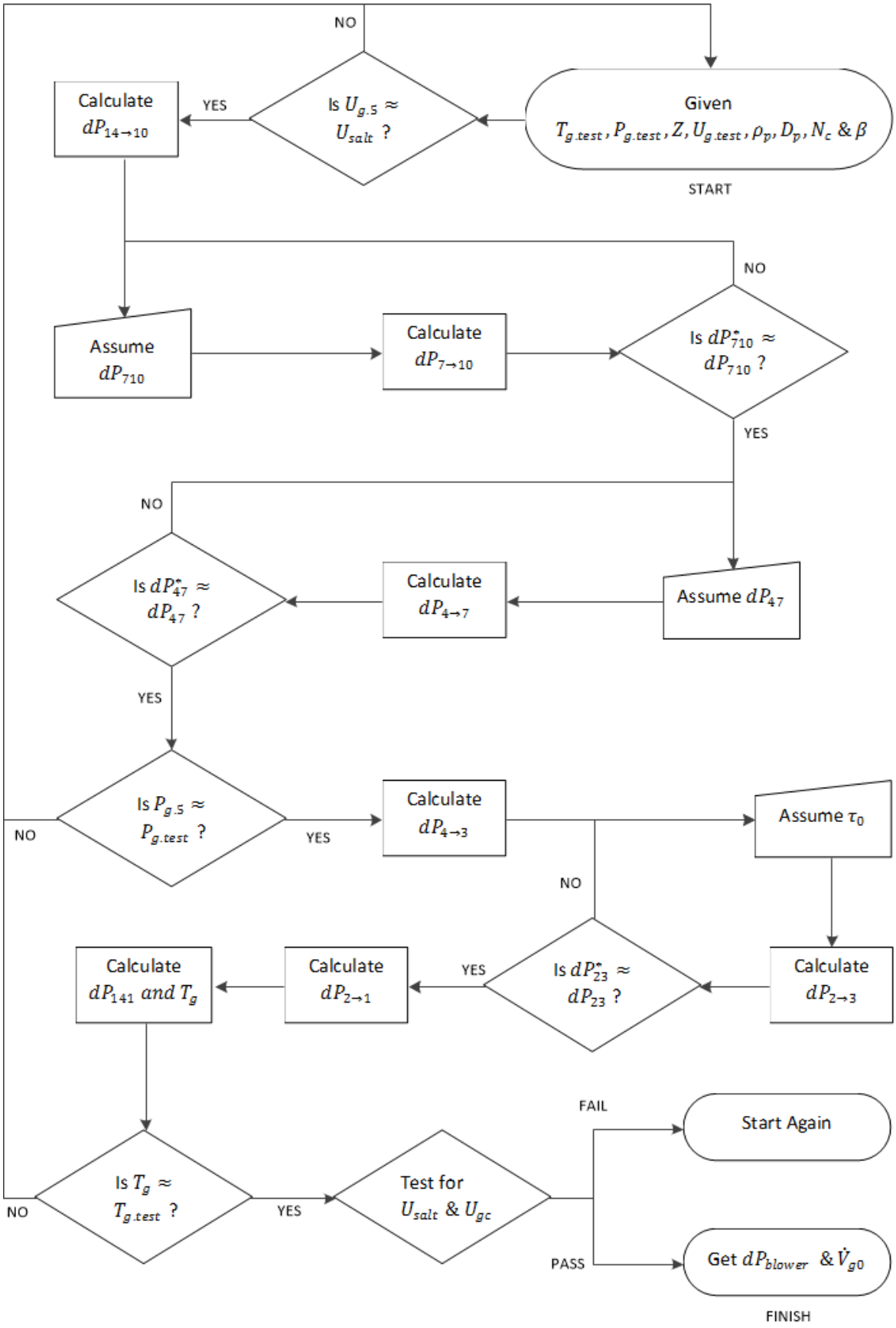

CHOKING MODEL

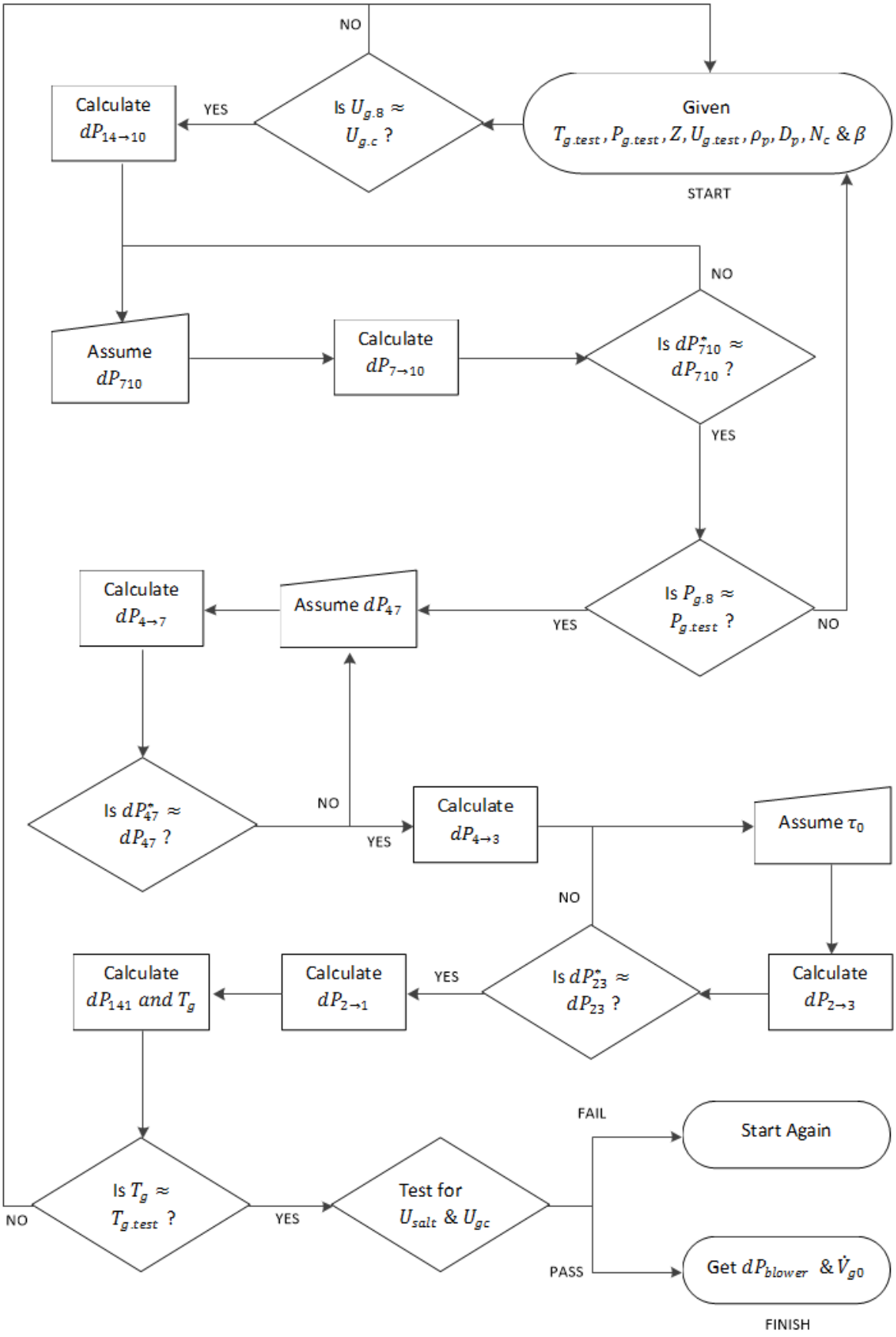

Appendix I. Prototype Process Model

Process Analysis for Prototype Tests (PFD25)

This model calculates the required blower pressure rise and process conditions at points along the prototype test facility.

Summary of assumptions made:

1. The filter loss coefficient = 0.1Pa.s/m^3
2. The blower isentropic efficiency = 60%
3. Sight glass modelled as standard pipe
4. Blow through rotary feeder inside diameter (ID) = test pipe ID
5. Temperature in pipelines constant and = Tg.test/ blower outlet temperature
6. Density across pipe sections constant and = inlet or outlet density of the respective pipe section
7. U.g. across pipe sections constant and = inlet or outlet U.g. of the respective pipe section
8. Flow properties within bends assumed constant and = inlet flow properties
9. Initial particle velocity = 0.5*U.g in vertical and return pipelines
10. Initial voidage = 0.45 in horizontal acceleration pipeline
11. No pressure recovery after orifice
12. Negiligible pressure drop in reducers/ expanders
13. Negligible pressure drop at pipe joints
14. Negligible pressure drop in gas only bends
15. Gas contributions to bend pressure drop negligible
16. No additional pressure drop due to rotary feeder blades/ buckets

Notes:

1. Conservative uncertainty factors applied to orifice, cyclcone, horizontal, vertical and return line pressure drop calculations.
2. Filter pressure drop calculation highly simplified.
3. Highlighted text indicates model inputs and comparative values for manual iteration.

1. Inputs

1.1. Test conditions

Assumed temperature $T_{g.test} := 43°C$

Assumed pressure (at feed point) $P_{g.test} := 114kPa$

Particle mass flow rate (between 0.08 and 0.8) $\dot{M}_p := 0.4\frac{kg}{s}$

Superficial gas velocity at beginning of horizontal acceleration pipeline (between 8 and 24) $U_{g.test} := 14\frac{m}{s}$

1.2. Particle properties

Particle density $\rho_p := 2300\frac{kg}{m^3}$

Particle diameter (between 125 and 180) $D_p := 65\mu m$

1.3. Ambient gas conditions

Assumed Temperature $T_{g.0} := 25\,°C$

Assumed Pressure $P_{g.0} := 101.3kPa$

1.4. Test rig properties

Orifice Beta value $\beta := 0.55$

Test pipe diameter $D_{pipe.test} := 77.92mm$

Gas only pipe diameter $D_{pipe.gas} := 102.26mm$

Relative test pipe roughness $\varepsilon_{r.test} := \frac{0.03mm}{D_{pipe.test}} = 3.85 \times 10^{-4}$

Relative gas only pipe roughness $\varepsilon_{r.gas} := \frac{0.03mm}{D_{pipe.gas}} = 2.934 \times 10^{-4}$

Assumed filter loss coefficient $k_{filter} := 0.1 \frac{Pa}{\left(\frac{m^3}{s}\right)}$

Return line length $L_{89} := 4m$

Vertical acceleration length $L_{67} := 2.5m$

Test section bend radius $R_{b.test} := 1000mm$

Horizontal acceleration length $L_{45} := 4m$

Length from orifice outlet to feed point $L_{34} := 6m$

Length from blower to orifice inlet $L_{12} := 2.5m$

2. Intermediate calculations

2.1 Test section gas properties

Specific gas constant for air

$$R_g := 287.058 \frac{J}{kg \cdot K}$$

Gas density

$$\rho_{g.test} := \left(\frac{P_{g.test}}{R_g \cdot T_{g.test}} \right) = 1.256 \frac{kg}{m^3}$$

Reference temperature

$$T_{ref} := 273.15K$$

Reference dynamic viscosity

$$\mu_{ref} := 1.716 \times 10^{-5} \frac{kg}{m \cdot s}$$

Sutherland's constant

$$S1 := 110.4K$$

Gas dynamic viscosity

$$\mu_{g.test} := \mu_{ref} \cdot \left(\frac{T_{g.test}}{T_{ref}} \right)^{\frac{3}{2}} \cdot \left(\frac{T_{ref} + S1}{T_{g.test} + S1} \right) = 1.921 \times 10^{-5} \frac{kg}{s \cdot m}$$

2.2 Loading/ Mass flow rates

Test section cross area

$$A_{pipe.test} := \frac{\pi \left(D_{pipe.test} \right)^2}{4} = 4.769 \times 10^{-3} m^2$$

Gas mass flow rate

$$\dot{M}_g := \rho_{g.test} \cdot A_{pipe.test} \cdot U_{g.test} = 0.084 \frac{kg}{s}$$

AF Ratio

$$AF := \frac{\dot{M}_g}{\dot{M}_p} = 0.21$$

Loading

$$z := \frac{1}{AF} = 4.77$$

2.3. Particle terminal velocity

For Stokes flow

$$u_{t0.stokes}(\rho_g) := \frac{(D_p)^2 \cdot (\rho_p - \rho_g) \cdot g}{18 \cdot \mu_{g.test}}$$

Corresponding Reynolds number

$$Re_{t0.stokes}(\rho_g) := \frac{\rho_g \cdot D_p \cdot u_{t0.stokes}(\rho_g)}{\mu_{g.test}}$$

For Intermediate flow

$$u_{t0.int}(\rho_g) := \left[\frac{8}{111}\cdot\frac{(\rho_g)^{0.6}\cdot(D_p)^{1.6}}{(\mu_{g.test})^{0.6}}\cdot\frac{(\rho_p-\rho_g)}{\rho_g}\cdot g\right]^{\frac{5}{7}}$$

Corresponding Reynolds number

$$Re_{t0.int}(\rho_g) := \frac{\rho_g\cdot D_p\cdot u_{t0.int}(\rho_g)}{\mu_{g.test}}$$

Particle terminal velocity

$$u_{t0}(\rho_g) := \begin{cases} u_{t0.stokes}(\rho_g) & \text{if } Re_{t0.stokes}(\rho_g) < 1 \\ u_{t0.int}(\rho_g) & \text{otherwise} \end{cases}$$

2.4. Equations of motion

Particle-wall friction factor

$$\lambda_{ph}(\alpha_g,u_g,u_p,D_{pipe},\rho_g) := \frac{0.117\cdot(1-\alpha_g)}{\alpha_g^{\,3}}\cdot\left[\frac{(1-\alpha_g)\cdot\left(\frac{\rho_g\cdot D_p\cdot u_{t0}(\rho_g)}{\mu_{g.test}}\right)\cdot\mu_{g.test}\cdot u_g}{\rho_g\cdot D_p\cdot(u_g-u_p)\cdot\sqrt{g\cdot D_{pipe}}}\right]^{-1.15}$$

$$\lambda_{pv}(\alpha_g,u_g,u_p,\rho_g) := \frac{0.0206\cdot(1-\alpha_g)}{\alpha_g^{\,3}}\cdot\left[\frac{(1-\alpha_g)\cdot\left(\frac{\rho_g\cdot D_p\cdot u_{t0}(\rho_g)}{\mu_{g.test}}\right)\cdot\mu_{g.test}}{\rho_g\cdot D_p\cdot(u_g-u_p)}\right]^{-0.869}$$

Infinately dilute drag coefficient

$$C_{Dinf}(u_g,u_p,\rho_g) := 18.5\cdot\left[\frac{\rho_g\cdot D_p\cdot(u_g-u_p)}{\mu_{g.test}}\right]^{-0.6}$$

Particle acceleration

$$a_{ph}(\alpha_g,u_g,u_p,D_{pipe},\rho_g) := \frac{3}{4}\cdot C_{Dinf}(u_g,u_p,\rho_g)\cdot\alpha_g^{-4.7}\cdot\frac{\rho_g\cdot(u_g-u_p)^2}{\rho_p\cdot D_p} - \frac{\lambda_{ph}(\alpha_g,u_g,u_p,D_{pipe},\rho_g)\cdot u_p^{\,2}}{2\cdot D_{pipe}}$$

$$a_{pv}(\alpha_g,u_g,u_p,D_{pipe},\rho_g) := \frac{3}{4}\cdot C_{Dinf}(u_g,u_p,\rho_g)\cdot\alpha_g^{-4.7}\cdot\frac{\rho_g\cdot(u_g-u_p)^2}{\rho_p\cdot D_p} - g\cdot\left(1-\frac{\rho_g}{\rho_p}\right) - \frac{\lambda_{pv}(\alpha_g,u_g,u_p,\rho_g)\cdot u_p^{\,2}}{2\cdot D_{pipe}}$$

2.5. Colebrook friction correlation

$$B\left(\lambda_g, \varepsilon_r, Re_{pipe}\right) := \frac{1}{\sqrt{\lambda_g}} + 2 \cdot \log\left(\frac{\varepsilon_r}{3.7} + \frac{2.51}{Re_{pipe} \cdot \sqrt{\lambda_g}}\right)$$

3. Across filter (10 to 11)

3.1. Intermediate calculations

Pressure at filter outlet

$$P_{g.11} := P_{g.0} = 101.3 \cdot kPa$$

Density across filter (assumed same as at outlet)

$$\rho_{g.1011} := \frac{P_{g.11}}{R_g \cdot T_{g.test}} = 1.116 \frac{kg}{m^3}$$

Volume flow rate through filter

$$Vdot_{g.1011} := \frac{\dot{M}_g}{\rho_{g.1011}} = 0.075 \frac{m^3}{s}$$

3.2. Pressure drop

Pressure drop across filter

$$dP_{1011} := k_{filter} \cdot Vdot_{g.1011} = 7.513 \times 10^{-3} \cdot Pa$$

Pressure at filter inlet

$$P_{g.10} := P_{g.11} + dP_{1011} = 101.3 \cdot kPa$$

4. Across cyclone (9 to 10)

4.1. Additional inputs (Stairmand Type Cyclone)

Cyclone diameter $D_c := 0.682\,ft = 0.208\,m$

Cyclone inlet height $a := 0.341\,ft = 0.104\,m$

Cyclone inlet width $b := 0.136\,ft = 0.041\,m$

Number of velocity heads $N_H := 6.4$

Configuration factor $G_c := 551.3$

4.2. Intermediate calculations

Pressure at cyclone outlet $P_{g.10} = 101.3\cdot kPa$

Gas density across cyclone (assumed same as outlet) $\rho_{g.910} := \frac{P_{g.10}}{R_g\cdot T_{g.test}} = 1.116\,\frac{kg}{m^3}$

Volume flow rate through cyclone $Vdot_{g.910} := \frac{\dot{M}_g}{\rho_{g.910}} = 0.075\,\frac{m^3}{s}$

Particle relaxtion time $\tau := \frac{\rho_p\cdot D_p^{\,2}}{18\cdot\mu_{g.test}} = 0.028\,s$

Cyclone vortex exponent $n := 1 - \left[1 - \frac{\left[12\left(\frac{D_c}{ft}\right)\right]^{0.14}}{2.5}\right]\cdot\left[\frac{\left(\frac{T_{g.test}}{K}\cdot\frac{9}{5} - 459.89\right) + 460}{530}\right]^{0.3} = 0.527$

Inlet area $A_i := a\cdot b = 4.308\times 10^{-3}\,m^2$

Effective radius $r := \frac{1}{2}\cdot\left(D_c - b\right) = 0.083\,m$

Kalen & Zenz parameter

$$\omega := \left[\frac{4 \cdot g \cdot \mu_{g.test} \cdot \left(\rho_p - \rho_{g.910}\right)}{3 \cdot \rho_{g.910}^{\,2}}\right]^{\frac{1}{3}} = 0.774\,\frac{m}{s}$$

4.3. Fractional efficiency

Fractional efficiency correlation

$$\eta := 1 - \exp\left[-2\left[\frac{G_c \cdot \tau \cdot Vdot_{g.910}}{D_c^{\,3}} \cdot (n+1)\right]^{\frac{0.5}{n+1}}\right] = 0.999988$$

Inlet velocity over saltation correlation
(SHOULD BE LESS THAN 1.5
to avoid re-entrainment)

$$R_{salt} := \frac{\left(\frac{Vdot_{g.910}}{A_i}\right)}{\left[2.1 \cdot \left(9.6 \cdot \frac{b}{ft}\right)^{0.4} \cdot \omega \cdot \left[\frac{\left(\frac{Vdot_{g.910}}{A_i}\right)^2}{32.2\,\frac{ft}{s^2} \cdot r}\right]^{\frac{1}{3}}\right]} = 1.341$$

4.4. Pressure drop

Pressure drop across cyclone

$$dP_{910} := 0.5 \cdot \rho_{g.910} \cdot \left(\frac{Vdot_{g.910}}{A_i}\right)^2 \cdot N_H = 1.086 \times 10^3\,Pa$$

Pressure at cyclone inlet

$$P_{g.9} := P_{g.10} + dP_{910} = 102.386 \cdot kPa$$

5. Return line (8 to 9)

5.1. Additional inputs

Time step

$\Delta t := 0.000001\,s$

Finite difference method constant

$FDM := 0.7$

5.2. Intermediate calculations

Pipe diameter

$D_{pipe.89} := D_{pipe.test} = 77.92\cdot mm$

Pipe cross section area

$A_{pipe.89} := \frac{\pi \cdot D_{pipe.89}^{2}}{4} = 4.769 \times 10^{-3}\,m^2$

Pipe relative roughness

$\varepsilon_{r.89} := \varepsilon_{r.test} = 3.85 \times 10^{-4}$

Pressure at section outlet

$P_{g.9} = 1.024 \times 10^{5}\,Pa$

Gas density across section (assumed same as outlet)

$\rho_{g.89} := \frac{P_{g.9}}{R_g \cdot T_{g.test}} = 1.128\,\frac{kg}{m^3}$

Superficial gas velocity

$U_{g.89} := \frac{\dot{M}_g}{\rho_{g.89} \cdot A_{pipe.89}} = 15.588\,\frac{m}{s}$

Pipe Reynolds number

$Re_{pipe.89} := \frac{\rho_{g.89} \cdot D_{pipe.89} \cdot U_{g.89}}{\mu_{g.test}} = 7.132 \times 10^{4}$

Assumed particle velocity at beginning of section

$u_{p.8} := \frac{U_{g.89}}{2} = 7.794\,\frac{m}{s}$

Voidage at start of section

$\alpha_{g.8} := 1 - \frac{\rho_{g.89} \cdot U_{g.89} \cdot z}{\rho_p \cdot u_{p.8}} = 0.995321$

Gas friction factor

Guess

$\lambda_{g.89} := 0.05$

Given

$$B\left(\lambda_{g.89}, \varepsilon_{r.89}, Re_{pipe.89}\right) = 0$$

Solution

$$\lambda_{g.89} := \text{Find}\left(\lambda_{g.89}\right)$$

Gas friction factor (Darcy-Weisbach type) $\lambda_{g.89} = 0.021$

5.3. Flow calculations

Solve loop

$$\text{Results} := \left| \begin{array}{l} i \leftarrow 0 \\ \alpha g_0 \leftarrow \alpha_{g.8} \\ up_0 \leftarrow u_{p.8} \\ x_0 \leftarrow 0 \\ ug_0 \leftarrow \dfrac{U_{g.89}}{\alpha g_0} \\ ap_0 \leftarrow a_{ph}\left(\alpha g_0, ug_0, up_0, D_{pipe.89}, \rho_{g.89}\right) \\ S_0 \leftarrow ap_0 \\ \text{while } x_i \le L_{89} \\ \quad \left| \begin{array}{l} up_{i+1} \leftarrow up_i + S_i \cdot \Delta t \\ x_{i+1} \leftarrow x_i + 0.5 \cdot \left(up_i + up_{i+1}\right) \cdot \Delta t \\ \alpha g_{i+1} \leftarrow 1 - \dfrac{U_{g.89} \cdot \rho_{g.89} \cdot z}{\rho_p \cdot up_{i+1}} \\ ug_{i+1} \leftarrow \dfrac{U_{g.89}}{\alpha g_{i+1}} \\ ap_{i+1} \leftarrow a_{ph}\left(\alpha g_{i+1}, ug_{i+1}, up_{i+1}, D_{pipe.89}, \rho_{g.89}\right) \\ S_{i+1} \leftarrow FDM \cdot ap_{i+1} + (1 - FDM) \cdot ap_i \\ i \leftarrow i + 1 \end{array} \right. \\ \begin{bmatrix} x \cdot m^{-1} \\ up \cdot \left(\dfrac{m}{s}\right)^{-1} \\ ug \cdot \left(\dfrac{m}{s}\right)^{-1} \\ \alpha g \end{bmatrix} \end{array} \right.$$

Displacement array $x_{89} := Results_0 \cdot m$

Particle velocity array $u_{p.89} := Results_1 \cdot \frac{m}{s}$

Gas velocity array $u_{g.89} := Results_2 \cdot \frac{m}{s}$

Voidage array $\alpha_{g.89} := Results_3$

Number of elements $n_{89} := last(x_{89})$ $i := 0 .. n_{89}$

Time array $t_{89_i} := i \cdot \Delta t$

Horizontal steady state particle velocity $u_{p.9} := u_{p.89_{n_{89}}} = 14.367 \frac{m}{s}$

Horizontal steady state gas velocity $u_{g.9} := u_{g.89_{n_{89}}} = 15.628 \frac{m}{s}$

Horizontal steady state voidage $\alpha_{g.9} := \alpha_{g.89_{n_{89}}} = 0.997462$

Horizontal steady state friction factor

$$\lambda_{p.9} := \lambda_{ph}\left(\alpha_{g.89_{n_{89}}}, u_{g.89_{n_{89}}}, u_{p.89_{n_{89}}}, D_{pipe.89}, \rho_{g.89}\right) = 0.049491$$

5.4. Plot

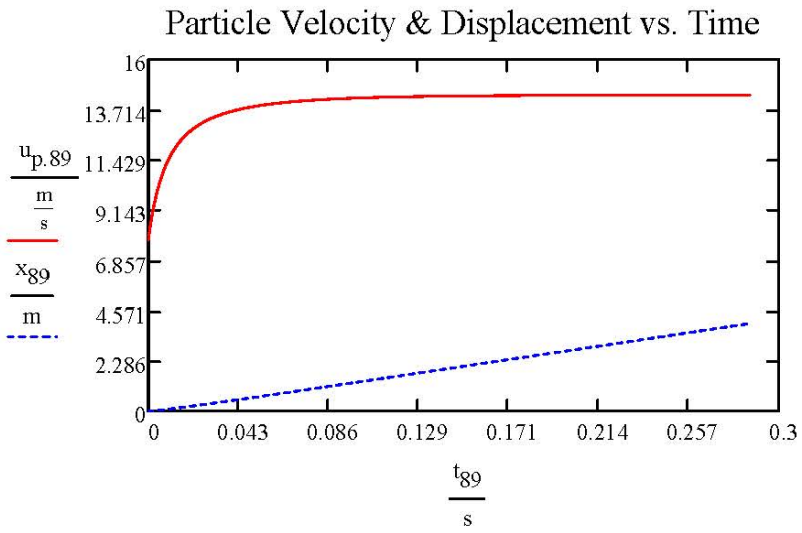

5.5. Pressure drop

Pressure drop across section

$$dP_{89} := \left[\frac{\lambda_{g.89}\cdot\rho_{g.89}\cdot\left(u_{g.9}\right)^2}{2\cdot D_{pipe.89}} + \frac{\lambda_{p.9}\cdot\rho_p\cdot\left(1-\alpha_{g.9}\right)\cdot\left(u_{p.9}\right)^2}{2\cdot D_{pipe.89}}\right]\cdot L_{89} \ldots = 2.23\times10^{3}\,\text{Pa}$$
$$+\rho_p\cdot\left(1-\alpha_{g.9}\right)\cdot\left(u_{p.9}\right)^2 - \rho_p\cdot\left(1-\alpha_{g.8}\right)\cdot\left(u_{p.8}\right)^2$$

incl. uncertainty $dP_{89} := dP_{89}\cdot 1.3 = 2.899\times10^{3}\,\text{Pa}$

Pressure at section inlet $P_{g.8} := P_{g.9} + dP_{89} = 105.285\cdot\text{kPa}$

6. Vertical acceleration section (6 to 7)

6.1. Additional inputs

Assumed pressure drop from 6 to 8 $dP_{68} := 2.864\ \text{kPa}$

6.2. Intermediate calculations

Pipe diameter $D_{pipe.67} := D_{pipe.test} = 77.92\cdot\text{mm}$

Pipe cross section area $A_{pipe.67} := \frac{\pi\cdot D_{pipe.67}^{2}}{4} = 4.769\times10^{-3}\,\text{m}^2$

Pipe relative roughness $\varepsilon_{r.67} := \varepsilon_{r.test} = 3.85\times10^{-4}$

Pressure at section inlet $P_{g.6} := P_{g.8} + dP_{68} = 108.149\cdot\text{kPa}$

Gas density across section (assumed same as inlet) $\rho_{g.67} := \frac{P_{g.6}}{R_g\cdot T_{g.test}} = 1.192\,\frac{\text{kg}}{\text{m}^3}$

Superficial gas velocity $U_{g.67} := \frac{\dot{M}_g}{\rho_{g.67}\cdot A_{pipe.67}} = 14.757\,\frac{\text{m}}{\text{s}}$

Pipe Reynolds number $Re_{pipe.67} := \frac{\rho_{g.67}\cdot D_{pipe.67}\cdot U_{g.67}}{\mu_{g.test}} = 7.132\times10^{4}$

Assumed particle velocity at 6 $u_{p.6} := \frac{U_{g.67}}{2} = 7.379\,\frac{\text{m}}{\text{s}}$

Voidage at start of section $\alpha_{g.6} := 1 - \frac{\rho_{g.67} \cdot U_{g.67} \cdot z}{\rho_p \cdot u_{p.6}} = 0.995057$

Gas friction factor

Guess $\lambda_{g.67} := 0.05$

Given

$$B\left(\lambda_{g.67}, \varepsilon_{r.67}, Re_{pipe.67}\right) = 0$$

Solution

$$\lambda_{g.67} := \text{Find}\left(\lambda_{g.67}\right)$$

Gas friction factor (Darcy-Weisbach type) $\lambda_{g.67} = 0.021$

6.3. Flow properties

Solve loop

$$\text{Results} := \left| \begin{array}{l} i \leftarrow 0 \\ \alpha g_0 \leftarrow \alpha_{g.6} \\ up_0 \leftarrow u_{p.6} \\ x_0 \leftarrow 0 \\ ug_0 \leftarrow \frac{U_{g.67}}{\alpha g_0} \\ ap_0 \leftarrow a_{pv}\left(\alpha g_0, ug_0, up_0, D_{pipe.67}, \rho_{g.67}\right) \\ S_0 \leftarrow ap_0 \\ \text{while } x_i \le L_{67} \\ \quad \left| \begin{array}{l} up_{i+1} \leftarrow up_i + S_i \cdot \Delta t \\ x_{i+1} \leftarrow x_i + 0.5 \cdot \left(up_i + up_{i+1}\right) \cdot \Delta t \\ \alpha g_{i+1} \leftarrow 1 - \frac{U_{g.67} \cdot \rho_{g.67} \cdot z}{\rho_p \cdot up_{i+1}} \\ ug_{i+1} \leftarrow \frac{U_{g.67}}{\alpha g_{i+1}} \\ ap_{i+1} \leftarrow a_{pv}\left(\alpha g_{i+1}, ug_{i+1}, up_{i+1}, D_{pipe.67}, \rho_{g.67}\right) \\ S_{i+1} \leftarrow FDM \cdot ap_{i+1} + (1 - FDM) \cdot ap_i \\ i \leftarrow i + 1 \end{array} \right. \\ \begin{bmatrix} x \cdot m^{-1} \\ up \cdot \left(\frac{m}{s}\right)^{-1} \\ ug \cdot \left(\frac{m}{s}\right)^{-1} \\ \alpha g \end{bmatrix} \end{array} \right.$$

Displacement array $x_{67} := Results_0 \cdot m$

Particle velocity array $u_{p.67} := Results_1 \cdot \frac{m}{s}$

Gas velocity array $u_{g.67} := Results_2 \cdot \frac{m}{s}$

Voidage array $\alpha_{g.67} := Results_3$

Number of elements $n_{67} := last(x_{67}) \qquad i := 0 .. n_{67}$

Time array $t_{67_i} := i \cdot \Delta t$

Vertical steady state particle velocity $u_{p.7} := u_{p.67_{n_{67}}} = 13.975 \frac{m}{s}$

Vertical steady state gas velocity $u_{g.7} := u_{g.67_{n_{67}}} = 14.796 \frac{m}{s}$

Vertical steady state voidage $\alpha_{g.7} := \alpha_{g.67_{n_{67}}} = 0.99739$

Vertical steady state friction factor $\lambda_{p.7} := \lambda_{pv}\left(\alpha_{g.67_{n_{67}}}, u_{g.67_{n_{67}}}, u_{p.67_{n_{67}}}, \rho_{g.67}\right) = 0.021478$

6.4. Plot

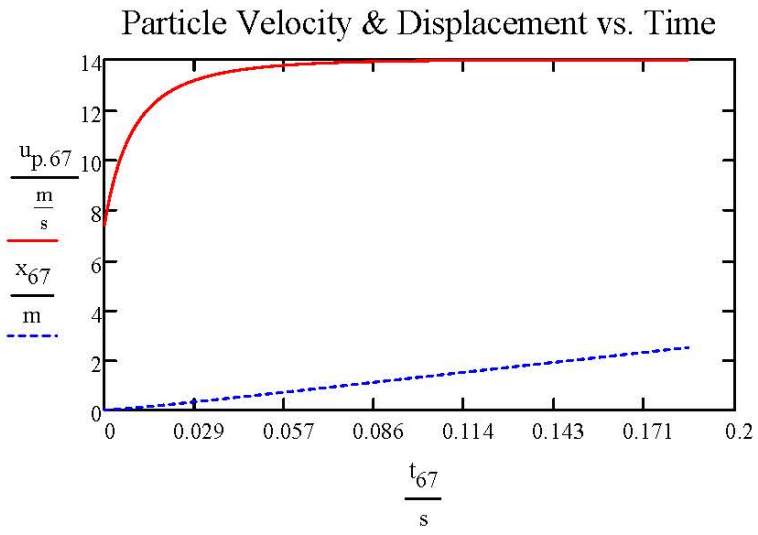

6.5. Pressure drop

Pressure drop across section

$$dP_{67} := \left[\left(1 - \alpha_{g.7}\right)\cdot\rho_p\cdot g + \alpha_{g.7}\cdot\rho_{g.67}\cdot g \ldots + \frac{\lambda_{g.67}\cdot\rho_{g.67}\cdot\left(u_{g.7}\right)^2}{2\cdot D_{pipe.67}} + \frac{\lambda_{p.7}\cdot\rho_p\cdot\left(1 - \alpha_{g.7}\right)\cdot\left(u_{p.7}\right)^2}{2\cdot D_{pipe.67}} \right]\cdot L_{67} \ldots + \rho_p\cdot\left(1 - \alpha_{g.7}\right)\cdot\left(u_{p.7}\right)^2 - \rho_p\cdot\left(1 - \alpha_{g.6}\right)\cdot\left(u_{p.6}\right)^2 = 1.221 \times 10^3\,\text{Pa}$$

incl. uncertainty $dP_{67} := dP_{67}\cdot 1.3 = 1.587 \times 10^3\,\text{Pa}$

Pressure at section outlet $P_{g.7} := P_{g.6} - dP_{67} = 1.066 \times 10^5\,\text{Pa}$

7. Top bend (7 to 8)

7.1. Intermediate calculations

Particle velocity $u_{p.78} := u_{p.7} = 13.975\,\frac{\text{m}}{\text{s}}$

Gas velocity $u_{g.78} := u_{g.7} = 14.796\,\frac{\text{m}}{\text{s}}$

Voidage $\alpha_{g.78} := \alpha_{g.7} = 0.99739$

Solids friction factor $\lambda_{p.78} := \lambda_{p.7} = 0.021$

Pipe diamater $D_{pipe.78} := D_{pipe.test} = 0.078\,\text{m}$

Bend radius $R_{b.78} := R_{b.test} = 1\,\text{m}$

Solids only pressure drop per meter $dP_{solids.v} := \frac{\lambda_{p.78}\cdot\rho_p\cdot\left(1 - \alpha_{g.78}\right)\cdot u_{p.78}^2}{2\cdot D_{pipe.78}} = 161.57\cdot\frac{\text{Pa}}{\text{m}}$

Equivalent bend lengths $L_{78} := \frac{2\pi\cdot R_{b.78}}{4} = 1.571\,\text{m}$

Equivalent solids only pressure losses $dP_{solids.78} := dP_{solids.v} \cdot L_{78} = 253.794\,Pa$

7.2. Pressure drop

Bend pressure losses $dP_{78} := 210 \cdot \left(\frac{2 \cdot R_{b.78}}{D_{pipe.78}}\right)^{-1.15} \cdot dP_{solids.78} = 1.276 \times 10^{3}\,Pa$

Pressure section outlet $P_{g.8} := P_{g.7} - dP_{78} = 105.286 \cdot kPa$

Pressure drop from 6 to 8 $dP_{68} := dP_{67} + dP_{78} = 2.864 \cdot kPa$

8. Horizontal acceleration section (4 to 5)

8.1. Additional inputs

Assumed pressure drop from 4 to 6 $dP_{46} := 5.51\ kPa$

8.2. Intermediate calculations

Pipe diameter $D_{pipe.45} := D_{pipe.test} = 77.92 \cdot mm$

Pipe cross section area $A_{pipe.45} := \frac{\pi \cdot D_{pipe.45}^{2}}{4} = 4.769 \times 10^{-3}\,m^{2}$

Pipe relative roughness $\varepsilon_{r.45} := \varepsilon_{r.test} = 3.85 \times 10^{-4}$

Pressure at section inlet $P_{g.4} := P_{g.6} + dP_{46} = 113.659 \cdot kPa$

Gas density across section (assumed same as inlet) $\rho_{g.45} := \frac{P_{g.4}}{R_g \cdot T_{g.test}} = 1.252\,\frac{kg}{m^{3}}$

Superficial gas velocity $U_{g.45} := \frac{\dot{M}_g}{\rho_{g.45} \cdot A_{pipe.45}} = 14.042\,\frac{m}{s}$

Pipe Reynolds number $Re_{pipe.45} := \frac{\rho_{g.45} \cdot D_{pipe.45} \cdot U_{g.45}}{\mu_{g.test}} = 7.132 \times 10^{4}$

Gas friction factor

Guess $\lambda_{g.45} := 0.05$

Given

$$B\left(\lambda_{g.45}, \varepsilon_{r.45}, Re_{pipe.45}\right) = 0$$

Solution

$$\lambda_{g.45} := \text{Find}\left(\lambda_{g.45}\right)$$

Gas friction factor (Darcy-Weisbach type) $\lambda_{g.45} = 0.021$

8.3. Flow calculations

Solve loop

$$\text{Results} := \left| \begin{array}{l} i \leftarrow 0 \\ \alpha g_0 \leftarrow 0.45 \\ up_0 \leftarrow \dfrac{U_{g.45} \cdot \rho_{g.45} \cdot z}{\left(1 - \alpha g_0\right) \cdot \rho_p} \\ x_0 \leftarrow 0 \\ ug_0 \leftarrow \dfrac{U_{g.45}}{\alpha g_0} \\ ap_0 \leftarrow a_{ph}\left(\alpha g_0, ug_0, up_0, D_{pipe.45}, \rho_{g.45}\right) \\ S_0 \leftarrow ap_0 \\ \text{while } x_i \le L_{45} \\ \quad \left| \begin{array}{l} up_{i+1} \leftarrow up_i + S_i \cdot \Delta t \\ x_{i+1} \leftarrow x_i + 0.5 \cdot \left(up_i + up_{i+1}\right) \cdot \Delta t \\ \alpha g_{i+1} \leftarrow 1 - \dfrac{U_{g.45} \cdot \rho_{g.45} \cdot z}{\rho_p \cdot up_{i+1}} \\ ug_{i+1} \leftarrow \dfrac{U_{g.45}}{\alpha g_{i+1}} \\ ap_{i+1} \leftarrow a_{ph}\left(\alpha g_{i+1}, ug_{i+1}, up_{i+1}, D_{pipe.45}, \rho_{g.45}\right) \\ S_{i+1} \leftarrow FDM \cdot ap_{i+1} + (1 - FDM) \cdot ap_i \\ i \leftarrow i + 1 \end{array} \right. \\ \begin{bmatrix} x \cdot m^{-1} \\ up \cdot \left(\dfrac{m}{s}\right)^{-1} \\ ug \cdot \left(\dfrac{m}{s}\right)^{-1} \\ \alpha g \end{bmatrix} \end{array} \right.$$

Displacement array $x_{45} := Results_0 \cdot m$

Particle velocity array $u_{p.45} := Results_1 \cdot \frac{m}{s}$

Gas velocity array $u_{g.45} := Results_2 \cdot \frac{m}{s}$

Voidage array $\alpha_{g.45} := Results_3$

Number of elements $n_{45} := last(x_{45}) \qquad i := 0 .. n_{45}$

Time array $t_{45_i} := i \cdot \Delta t$

Horizontal steady state particle velocity $u_{p.5} := u_{p.45_{n_{45}}} = 13.155 \frac{m}{s}$

Horizontal steady state gas velocity $u_{g.5} := u_{g.45_{n_{45}}} = 14.081 \frac{m}{s}$

Horizontal steady state voidage $\alpha_{g.5} := \alpha_{g.45_{n_{45}}} = 0.997228$

Horizontal steady state friction factor

$$\lambda_{p.5} := \lambda_{ph}\left(\alpha_{g.45_{n_{45}}}, u_{g.45_{n_{45}}}, u_{p.45_{n_{45}}}, D_{pipe.45}, \rho_{g.45}\right) = 0.040001$$

8.4. Plot

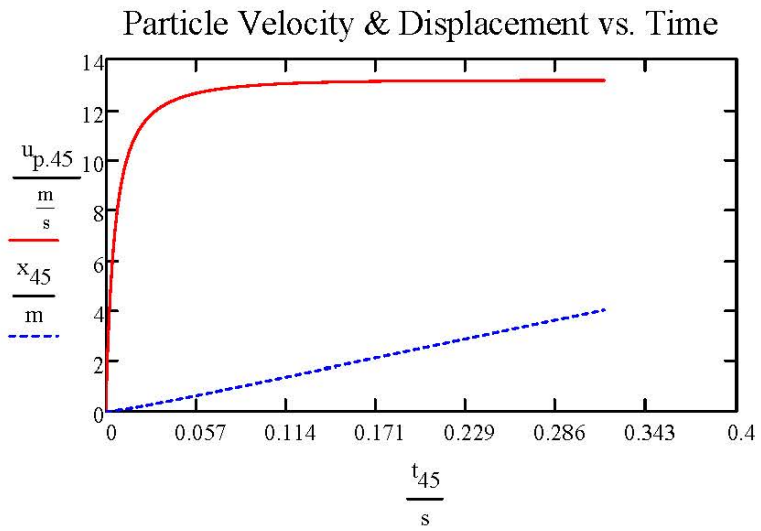

8.5. Pressure drop

Pressure drop across section

$$dP_{45} := \left[\frac{\lambda_{g.45}\cdot\rho_{g.45}\cdot\left(u_{g.5}\right)^2}{2\cdot D_{pipe.45}} + \frac{\lambda_{p.5}\cdot\rho_p\cdot\left(1-\alpha_{g.5}\right)\cdot\left(u_{p.5}\right)^2}{2\cdot D_{pipe.45}}\right]\cdot L_{45} + \rho_p\cdot\left(1-\alpha_{g.5}\right)\cdot\left(u_{p.7}\right)^2 = 2.512\times 10^3\,\text{Pa}$$

incl. uncertainty $dP_{45} := dP_{45}\cdot 1.3 = 3.265\times 10^3\,\text{Pa}$

Pressure at section outlet $P_{g.5} := P_{g.4} - dP_{45} = 1.104\times 10^5\,\text{Pa}$

9. Bottom bend (5 to 6)

9.1. Intermediate calculations

Particle velocity $u_{p.56} := u_{p.5} = 13.155\,\frac{\text{m}}{\text{s}}$

Gas velocity $u_{g.56} := u_{g.5} = 14.081\,\frac{\text{m}}{\text{s}}$

Voidage $\alpha_{g.56} := \alpha_{g.5} = 0.997228$

Solids friction factor $\lambda_{p.56} := \lambda_{p.5} = 0.04$

Pipe diamater $D_{pipe.56} := D_{pipe.test} = 0.078\,\text{m}$

Bend radius $R_{b.56} := R_{b.test} = 1\,\text{m}$

Solids only pressure drop per meter $dP_{solids.h} := \frac{\lambda_{p.56}\cdot\rho_p\cdot\left(1-\alpha_{g.56}\right)\cdot u_{p.56}^2}{2\cdot D_{pipe.56}} = 283.243\cdot\frac{\text{Pa}}{\text{m}}$

Equivalent bend length $L_{b.56} := \frac{2\pi\cdot R_{b.56}}{4} = 1.571\,\text{m}$

Equivalent solids only pressure loss $dP_{solids.56} := dP_{solids.h}\cdot L_{b.56} = 444.917\,\text{Pa}$

9.2. Pressure drop

Bend pressure loss $dP_{56} := 210 \cdot \left(\frac{2 \cdot R_{b.56}}{D_{pipe.56}}\right)^{-1.15} \cdot dP_{solids.56} = 2.237 \times 10^{3}\,Pa$

Pressure loss from 4 to 6 $dP_{46} := dP_{45} + dP_{56} = 5.502 \cdot kPa$

10. Orifice outlet to feed point (3 to 4)

10.1. Intermediate calculations

Pipe diameter $D_{pipe.34} := D_{pipe.gas} = 102.26 \cdot mm$

Pipe cross section area $A_{pipe.34} := \frac{\pi \cdot D_{pipe.34}^{2}}{4} = 8.213 \times 10^{-3}\,m^{2}$

Pipe relative roughness $\varepsilon_{r.34} := \varepsilon_{r.gas} = 2.934 \times 10^{-4}$

Pressure at section inlet $P_{g.4} = 113.659 \cdot kPa$

Gas density across section (assumed same as inlet) $\rho_{g.34} := \left(\frac{P_{g.4}}{R_g \cdot T_{g.test}}\right) = 1.252\,\frac{kg}{m^{3}}$

Superficial gas velocity $U_{g.34} := \frac{\dot{M}_g}{(\rho_{g.34} \cdot A_{pipe.34})} = 8.153\,\frac{m}{s}$

Pipe Reynolds number $Re_{pipe.34} := \frac{\rho_{g.34} \cdot D_{pipe.34} \cdot U_{g.34}}{\mu_{g.test}} = 5.434 \times 10^{4}$

Gas friction factor

Guess $\lambda_{g.34} := 0.05$

Given

$$B\left(\lambda_{g.34}, \varepsilon_{r.34}, Re_{pipe.34}\right) = 0$$

Solution

$\lambda_{g.34} := \text{Find}(\lambda_{g.34})$

Gas friction factor (Darcy-Weisbach type) $\lambda_{g.34} = 0.022$

10.2. Pressure drop

Pressure drop across section $dP_{34} := \frac{\lambda_{g.34} \cdot \rho_{g.34} \cdot (U_{g.34})^2}{2 \cdot D_{pipe.34}} \cdot L_{34} = 52.67\ \text{Pa}$

Pressure at section inlet $P_{g.3} := P_{g.4} + dP_{34} = 113.712 \cdot \text{kPa}$

11. Across orifice (2 to 3)

11.1. Additional inputs

Pressure ratio $\tau_o := 98.991\%$

Length constant 1 $L_1 := 1$

Length constant 2 $L_2 := 0.47$

Gas isentropic exponent $\kappa := 1.4$

Pressure drop confidence $\eta_o := 95\%$

11.2. Intermediate calculations

Pressure at orifice outlet $P_{g.3} = 113.712 \cdot \text{kPa}$

Assumed pressure at orifice inlet $P_{g.2} := \frac{P_{g.3}}{\tau_o} = 114.871 \cdot \text{kPa}$

Gas density at orifice inlet $\rho_{g.2} := \frac{P_{g.2}}{R_g \cdot T_{g.test}} = 1.266\ \frac{\text{kg}}{\text{m}^3}$

Diameter of pipe $D_{pipe.2} := D_{pipe.gas} = 0.102\ \text{m}$

Diamater at vena contracta

$$D_{vc} := \beta \cdot D_{pipe.2} = 0.056\,m$$

Pipe cross section area

$$A_{pipe.2} := \frac{\pi \cdot D_{pipe.2}^{2}}{4} = 8.213 \times 10^{-3}\,m^{2}$$

Superficial gas velocity

$$U_{g.2} := \frac{\dot{M}_g}{\left(\rho_{g.2} \cdot A_{pipe.2}\right)} = 8.067\,\frac{m}{s}$$

Pipe Reynolds number

$$Re_{pipe.2} := \frac{\rho_{g.2} \cdot D_{pipe.2} \cdot U_{g.2}}{\mu_{g.test}} = 5.434 \times 10^{4}$$

Constant 3

$$M_2 := \frac{2 \cdot L_2}{1 - \beta} = 2.089$$

Constant 4

$$A_o := \left(\frac{19000 \cdot \beta}{Re_{pipe.2}}\right)^{0.8} = 0.267$$

Gas expansibility factor

$$\varepsilon_g := 1 - \left(0.351 + 0.256 \cdot \beta^{4} + 0.93 \cdot \beta^{8}\right) \cdot \left[1 - \left(\tau_o\right)^{\frac{1}{\kappa}}\right] = 0.997$$

Discharge coefficient

$$C_d := 0.5961 + 0.0261 \cdot (\beta)^{2} - 0.216 \cdot (\beta)^{8} + 0.000521 \cdot \left(\frac{10^{6} \cdot \beta}{Re_{pipe.2}}\right)^{0.7} \ldots = 0.611$$
$$+ \left[\left(0.0188 + 0.0063 \cdot A_o\right) \cdot (\beta)^{3.5} \cdot \left(\frac{10^{6}}{Re_{pipe.2}}\right)^{0.3}\right] \ldots$$
$$+ \left(0.043 + 0.080 \cdot e^{-10 \cdot L_1} - 0.123 \cdot e^{-7 \cdot L_1}\right) \cdot \left(1 - 0.11 \cdot A_o\right) \cdot \frac{(\beta)^{4}}{1 - (\beta)^{4}} \ldots$$
$$+ 0 - 0.031 \cdot \left[M_2 - 0.8 \cdot \left(M_2\right)^{1.1}\right] \cdot (\beta)^{1.3}$$

11.3. Pressure drop

Pressure drop across orifice

$$dP_{23} := -\frac{8 \cdot \dot{M}_g^{2} \cdot \left(\beta^{4} - 1\right)}{\pi^{2} \cdot C_d^{2} \cdot D_{vc}^{4} \cdot \rho_{g.2} \cdot \varepsilon_g^{2}} = 1.102 \times 10^{3}\,Pa$$

Adjusted for uncertainty

$$dP_{23} := \frac{dP_{23}}{\eta_o} = 1.16 \times 10^{3}\,Pa$$

Pressure at orfice inlet

$$P_{g.2} := P_{g.3} + dP_{23} = 114.871 \cdot kPa$$

12. Blower outlet to orifice inlet (1 to 2)

12.1. Intermediate calculations

Pipe diameter

$$D_{pipe.12} := D_{pipe.gas} = 102.26 \cdot mm$$

Pipe cross section area

$$A_{pipe.12} := \frac{\pi \cdot D_{pipe.12}^{2}}{4} = 8.213 \times 10^{-3}\ m^{2}$$

Pipe relative roughness

$$\varepsilon_{r.12} := \varepsilon_{r.gas} = 2.934 \times 10^{-4}$$

Pressure at section outlet

$$P_{g.2} = 114.871 \cdot kPa$$

Gas density across section (assumed same as outlet)

$$\rho_{g.12} := \left(\frac{P_{g.2}}{R_g \cdot T_{g.test}} \right) = 1.266 \frac{kg}{m^{3}}$$

Superficial gas velocity

$$U_{g.12} := \frac{\dot{M}_g}{\left(\rho_{g.12} \cdot A_{pipe.12}\right)} = 8.067 \frac{m}{s}$$

Pipe Reynolds number

$$Re_{pipe.12} := \frac{\rho_{g.12} \cdot D_{pipe.12} \cdot U_{g.12}}{\mu_{g.test}} = 5.434 \times 10^{4}$$

Gas friction factor

Guess $\lambda_{g.12} := 0.05$

Given

$$B\left(\lambda_{g.12}, \varepsilon_{r.12}, Re_{pipe.12}\right) = 0$$

Solution

$$\lambda_{g.12} := Find\left(\lambda_{g.12}\right)$$

Gas friction factor (Darcy-Weisbach type)

$$\lambda_{g.12} = 0.022$$

12.2. Pressure drop

Pressure drop across section

$$dP_{12} := \frac{\lambda_{g.12} \cdot \rho_{g.12} \cdot \left(U_{g.12}\right)^2}{2 \cdot D_{pipe.12}} \cdot L_{12} = 21.714\,Pa$$

Pressure at section inlet

$$P_{g.1} := P_{g.2} + dP_{12} = 114.893 \cdot kPa$$

13. Blower sizing

13.1. Additional Inputs

Standard density

$$\rho_{g.std} := 1.2 \frac{kg}{m^3}$$

Assumed blower isentropic efficiency

$$\eta_{blower} := 60\%$$

Specific heat capacity

$$kJ := 1000J = 1 \times 10^3 J \qquad C_p := 1 \frac{kJ}{kg \cdot K}$$

Specific heat ratio

$$\gamma := 1.4$$

13.2. Blower sizing

Pressure at blower inlet

$$P_{g.0} = 101.3 \cdot kPa$$

Pressure head required

$$dP_{01} := P_{g.1} - P_{g.0} = 13.593 \cdot kPa$$

Gas density at blower inlet

$$\rho_{g.0} := \left(\frac{P_{g.0}}{R_g \cdot T_{g.0}}\right) = 1.184 \frac{kg}{m^3}$$

Volume flow rate at blower inlet

$$Vdot_{g.0} := \frac{\dot{M}_g}{\rho_{g.0}} = 0.071 \frac{m^3}{s}$$

Pressure head required at std conditions

$$dP_{blower} := dP_{01} \cdot \left(\frac{\rho_{g.std}}{\rho_{g.0}}\right) = 13.781 \cdot kPa$$

13.3. Blower temperature rise

Pressure Ratio $PR := \frac{P_{g.1}}{P_{g.0}} = 1.134$

Gas temperature rise $dT := \frac{1}{\eta_{blower}} \cdot T_{g.0} \cdot \left(PR^{\frac{\gamma - 1}{\gamma}} - 1 \right) = 18.203K$

Outlet gas temperature $T_g := T_{g.0} + dT = 43.203°C$

14. Pressure Map

$P_{g.0} = 101.3kPa$

$P_{g.1} = 114.893kPa$

$P_{g.2} = 114.871 \cdot kPa$

$P_{g.3} = 113.712 \cdot kPa$

$P_{g.4} = 113.659 \cdot kPa$

$P_{g.5} = 110.394 \cdot kPa$

$P_{g.6} = 108.149 \cdot kPa$

$P_{g.7} = 106.562 \cdot kPa$

$P_{g.8} = 105.286 \cdot kPa$

$P_{g.9} = 102.386 \cdot kPa$

$P_{g.10} = 101.3 \cdot kPa$

$P_{g.11} = 101.3 \cdot kPa$

$dP_{01} = 13.593kPa$

$dP_{12} = 21.714Pa$

$dP_{23} = 1.16 \cdot kPa$

$dP_{34} = 52.67\ Pa$

$dP_{45} = 3.265 \cdot kPa$

$dP_{56} = 2.237 \times 10^{3} Pa$

$dP_{67} = 1.587 \times 10^{3} Pa$

$dP_{78} = 1.276 \times 10^{3} Pa$

$dP_{89} = 2.899 \times 10^{3} Pa$

$dP_{910} = 1.086 \times 10^{3} Pa$

$dP_{1011} = 7.513 \times 10^{-3} Pa$

Appendix J.Estimating the Required Filter Area

Filter sizing

Method adopted from Pneumatic Conveying of Solids, Pages 407-409/ Example 10.6

Inputs

Particle flow rate	$\dot{M}_p := \begin{pmatrix} 0.6 \\ 0.6 \\ 0.08 \end{pmatrix} \frac{kg}{s}$	ref: Max particle flow rate/ PFD30/ PFD16
Gas flow rate FAD	$Vdot_g := \begin{pmatrix} 0.123 \\ 0.073 \\ 0.098 \end{pmatrix} \frac{m^3}{s}$	ref: Max cyclone flow rate/ PFD30/ PFD16
Gas density at ATM	$\rho_{g.} := 1.2 \frac{kg}{m^3}$	ref: Assumption
Seperation efficiency	$\eta_c := 99\%$	ref: Reference cyclone efficiency

Calculations

Gas mass flow rate	$\dot{M}_g := \rho_{g.} \cdot Vdot_g = \begin{pmatrix} 0.148 \\ 0.088 \\ 0.118 \end{pmatrix} \frac{kg}{s}$
Loading	$z := \overrightarrow{\left(\frac{\dot{M}_p}{\dot{M}_g}\right)} = \begin{pmatrix} 4.065 \\ 6.849 \\ 0.68 \end{pmatrix}$
Loading after seperation	$z_c := \left(1 - \eta_c\right) \cdot z = \begin{pmatrix} 0.041 \\ 0.068 \\ 6.803 \times 10^{-3} \end{pmatrix}$
Particle flow rate after seperation	$\dot{M}_{pc} := \left(1 - \eta_c\right) \cdot \dot{M}_p = \begin{pmatrix} 21.6 \\ 21.6 \\ 2.88 \end{pmatrix} \cdot \frac{kg}{hr}$
Dust concentration after seperation	$\rho_c := \overrightarrow{\left[z_c \cdot \left(\dot{M}_{pc} \cdot \frac{hr}{kg}\right)\right]} \cdot \frac{mg}{m^3} = \begin{pmatrix} 0.878 \\ 1.479 \\ 0.02 \end{pmatrix} \cdot \frac{mg}{m^3}$

Graph

Case 1 and 2 indistinguishable on graph, therefore size for minimum & mean particle sizes i.e. 37 and 65 micron using a dust concentration of 1mg/m3.

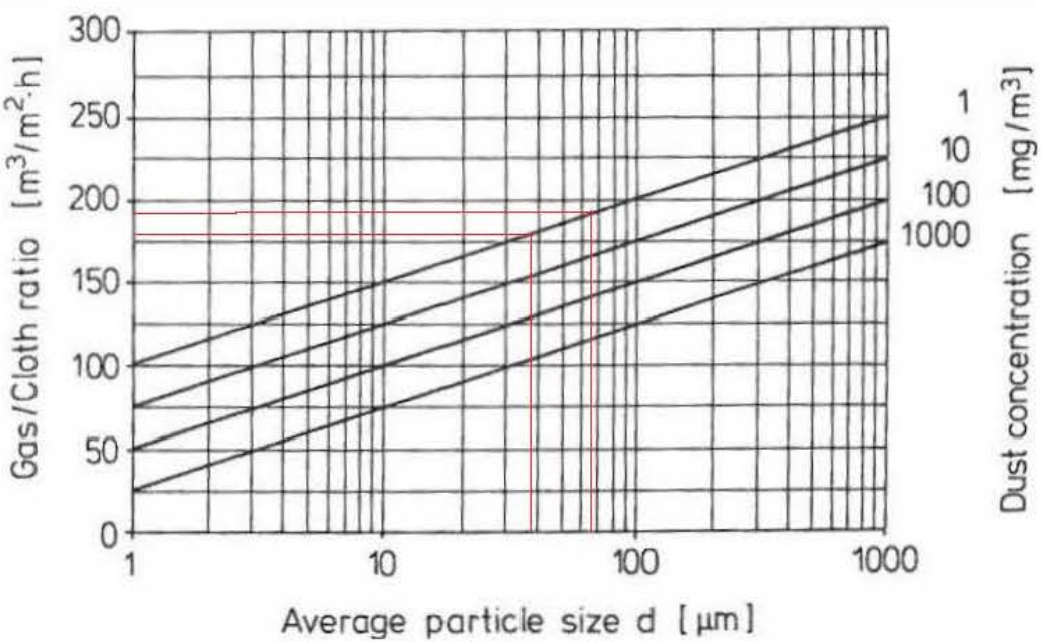

Approximate gas/cloth ratio is 180 and 190

$$\gamma := \begin{pmatrix} 180 \\ 190 \end{pmatrix} \frac{m}{hr} = \begin{pmatrix} 0.05 \\ 0.053 \end{pmatrix} \frac{m}{s}$$

Fabric filter area required for case 1

$$A_{F1} := \frac{Vdot_{g_0}}{\gamma} = \begin{pmatrix} 2.46 \\ 2.331 \end{pmatrix} m^2$$

Fabric filter area required for case 2

$$A_{F2} := \frac{Vdot_{g_1}}{\gamma} = \begin{pmatrix} 1.46 \\ 1.383 \end{pmatrix} m^2$$

If we oversize by 30%

$$A_F := A_{F1_0} \cdot 1.3 = 3.198\ m^2$$

Appendix K. Design Phase Uncertainty Analysis

Design Phase Uncertainty Analysis

Hopper := Loss in Weight / Gain in Weight

1. Temperature

Measured temperature $T_g := \begin{pmatrix} 28 \\ 49 \end{pmatrix} °C$ Scenarios from process analysis 31 & 28

Unitless function for uncertainty calculations $T\_ := \frac{T_g - 273.15K}{K} = \begin{pmatrix} 28 \\ 49 \end{pmatrix}$

RTD

RTD instrument uncertainty at T.g

$$u_{c.RTD\_} := [0.1 + 0.0017(T\_)]\Delta°C = \begin{pmatrix} 0.148 \\ 0.183 \end{pmatrix} \cdot \Delta°C \quad (95\%)$$

$$u_{c.RTD} := \frac{1}{2} \cdot u_{c.RTD\_} = \begin{pmatrix} 0.074 \\ 0.092 \end{pmatrix} \cdot \Delta°C \quad (68\%)$$

RTD design stage uncertainty $u_{d.RTD} := u_{c.RTD} = \begin{pmatrix} 0.074 \\ 0.092 \end{pmatrix} \cdot \Delta°C$ (68%)

Transmitter

Transmitter instrument uncertainty $u_{c.Trans\_} := 0.2\Delta°C$ (95%)

$$u_{c.Trans} := \frac{1}{2} \cdot u_{c.Trans\_} = 0.1 \cdot \Delta°C \quad (68\%)$$

Transmitter design stage uncertainty $u_{d.Trans} := u_{c.Trans} = 0.1 \cdot \Delta°C$ (68%)

Combined RTD & Transmitter uncerta $u_{d.TR15} := \sqrt{u_{d.RTD}^2 + u_{d.Trans}^2} = \begin{pmatrix} 0.124 \\ 0.136 \end{pmatrix} \cdot \Delta°C$ (68%)

Converted to mA $u_{d.TR15} := \frac{u_{d.TR15}}{5} \cdot \frac{mA}{\Delta°C} = \begin{pmatrix} 0.025 \\ 0.027 \end{pmatrix} \cdot mA$ (68%)

NI9208 AI

NI9208 zero-order uncertainty $u_{0.AI\_} := \frac{1}{2}\cdot(42\mu A) = 21\cdot\mu A$ (95%)

$u_{0.AI} := \frac{1}{2}u_{0.AI\_} = 10.5\cdot\mu A$ (68%)

Measured signal assuming no error $T_{mA} := \frac{T\_ + 20}{5}\cdot mA = \begin{pmatrix} 9.6 \\ 13.8 \end{pmatrix}\cdot mA$

NI9208 gain error on T.mA $u_{1\_} := T_{mA}\cdot 0.76\% = \begin{pmatrix} 72.96 \\ 104.88 \end{pmatrix}\cdot\mu A$ (95%)

$u_1 := \frac{1}{2}\cdot u_{1\_} = \begin{pmatrix} 36.48 \\ 52.44 \end{pmatrix}\cdot\mu A$ (68%)

NI9208 offset error $u_{2\_} := 22mA\cdot 0.04\% = 8.8\cdot\mu A$ (95%)

$u_2 := \frac{1}{2}\cdot u_{2\_} = 4.4\cdot\mu A$ (68%)

NI9208 noise error $u_{3\_} := 200nA = 200\cdot nA$ (95%)

$u_3 := \frac{1}{2}\cdot u_{3\_} = 100\cdot nA$ (68%)

N9208 instrument uncertainty $u_{c.AI} := \sqrt{(u_1)^2 + (u_2)^2 + u_3{}^2} = \begin{pmatrix} 0.037 \\ 0.053 \end{pmatrix}\cdot mA$ (68%)

NI9208 design stage uncertainty $u_{d.AI} := \sqrt{u_{0.AI}{}^2 + u_{c.AI}{}^2} = \begin{pmatrix} 0.038 \\ 0.054 \end{pmatrix}\cdot mA$ (68%)

System design stage uncertainty $u_{d.T.g} := \sqrt{u_{d.TR15}{}^2 + u_{d.AI}{}^2} = \begin{pmatrix} 0.046 \\ 0.06 \end{pmatrix}\cdot mA$ (68%)

Converted to Temp $u_{d.T.g} := 5\cdot u_{d.T.g}\cdot\frac{\Delta°C}{mA} = \begin{pmatrix} 0.228 \\ 0.301 \end{pmatrix}\cdot\Delta°C$ (68%)

% Error $\%Error_{d.T.g} := \frac{\overrightarrow{u_{d.T.g}}}{T\_\cdot\Delta°C} = \begin{pmatrix} 0.814 \\ 0.614 \end{pmatrix}\cdot\%$ (68%)

2. Absolute Pressure

Measured Pressure	$P_1 := \begin{pmatrix} 103.534 \\ 119.338 \end{pmatrix} kPa$	Scenarios from process analysis 31 & 28

PMP131

PMP131 instrument uncertainty	$u_{c.PMP\_} := 160kPa \cdot 0.5\% = 800\,Pa$	(95%)
	$u_{c.PMP} := \frac{1}{2} \cdot u_{c.PMP\_} = 400\,Pa$	(68%)
PMP131 design stage uncertainty	$u_{d.PMP} := u_{c.PMP} = 400\,Pa$	(68%)
Converted to mA	$u_{d.PMP} := \frac{u_{d.PMP}}{10} \cdot \frac{mA}{kPa} = 0.04 \cdot mA$	(68%)

NI9208 AI

NI9208 zero-order uncertainty	$u_{0.AI} = 10.5 \cdot \mu A$	(68%)
Measured signal assuming no error	$P_{mA} := \frac{P_1 + 40kPa}{10} \cdot \frac{mA}{kPa} = \begin{pmatrix} 14.353 \\ 15.934 \end{pmatrix} \cdot mA$	
NI9208 gain error on P.mA	$u_{4\_} := P_{mA} \cdot 0.76\% = \begin{pmatrix} 109.086 \\ 121.097 \end{pmatrix} \cdot \mu A$	(95%)
	$u_4 := \frac{1}{2} \cdot u_{4\_} = \begin{pmatrix} 54.543 \\ 60.548 \end{pmatrix} \cdot \mu A$	(68%)
NI9208 offset error	$u_2 = 4.4 \cdot \mu A$	(68%)
NI9208 noise error	$u_3 = 100 \cdot nA$	(68%)
N9208 instrument uncertainty	$u_{c.AI} := \sqrt{(u_4)^2 + (u_2)^2 + u_3^2} = \begin{pmatrix} 0.055 \\ 0.061 \end{pmatrix} \cdot mA$	(68%)
NI9208 design stage uncertainty	$u_{d.AI} := \sqrt{u_{0.AI}^2 + u_{c.AI}^2} = \begin{pmatrix} 0.056 \\ 0.062 \end{pmatrix} \cdot mA$	(68%)

System design stage uncertainty $u_{d.P.1} := \sqrt{u_{d.PMP}^{2} + u_{d.AI}^{2}} = \begin{pmatrix} 0.069 \\ 0.073 \end{pmatrix} \cdot mA$ (68%)

Converted to Pressure $u_{d.P.1} := 10 \cdot u_{d.P.1} \cdot \frac{kPa}{mA} = \begin{pmatrix} 0.686 \\ 0.735 \end{pmatrix} \cdot kPa$ (68%)

% Error $\%Error_{d.P.1} := \frac{\overrightarrow{u_{d.P.1}}}{P_1} = \begin{pmatrix} 0.662 \\ 0.616 \end{pmatrix} \cdot \%$ (68%)

3. Pressure drop

Measured pressure $dP := -\begin{pmatrix} 0.429 \\ 2.035 \end{pmatrix} kPa$ Scenarios from process analysis 31 & 28

Upper range value $URV := 0kPa$

Lower range value $LRV := -5kPa$

Turn down $TD := \frac{10kPa}{|LRV|} = 2$

Set span $Span := URV - LRV = 5 \cdot kPa$

PMD55

PMD55 zero-oder uncertainty $u_{0.PMD\_} := \frac{1}{2}(1\,\mu A) = 0.5 \cdot \mu A$ (95%)

$u_{0.PMD} := \frac{1}{2} \cdot u_{0.PMD\_} = 0.25 \cdot \mu A$ (68%)

PMD55 instrument uncertainty $u_{c.PMD\_} := \begin{cases} (Span \cdot 0.1\%) & \text{if } TD \le 4 \\ [Span \cdot (0.012 \cdot TD + 0.052)\%] & \text{otherwise} \end{cases} = 5\,Pa$ (95%)

$u_{c.PMD} := \frac{1}{2} \cdot u_{c.PMD\_} = 2.5\,Pa$ (68%)

Converted to mA $u_{c.PMD} := \frac{u_{c.PMD}}{Span} \cdot 16mA = 8 \times 10^{-3} \cdot mA$ (68%)

PMD55 design stage uncertainty

$$u_{d.PMD} := \sqrt{u_{0.PMD}^{2} + u_{c.PMD}^{2}} = 8.004 \cdot \mu A \quad (68\%)$$

NI9208 AI

NI9208 zero-order uncertainty

$$u_{0.AI} - 10.5 \cdot \mu A \quad (68\%)$$

Measured signal assuming no error

$$dP_{mA} := \frac{\left(dP - URV + \frac{20}{16} \cdot Span\right) \cdot 16mA}{Span} = \begin{pmatrix} 18.627 \\ 13.488 \end{pmatrix} \cdot mA$$

NI9208 gain error on dP.mA

$$u_{5\_} := dP_{mA} \cdot 0.76\% = \begin{pmatrix} 141.567 \\ 102.509 \end{pmatrix} \cdot \mu A \quad (95\%)$$

$$u_5 := \frac{1}{2} \cdot u_{5\_} = \begin{pmatrix} 70.783 \\ 51.254 \end{pmatrix} \cdot \mu A \quad (68\%)$$

NI9208 offset error

$$u_2 = 4.4 \cdot \mu A \quad (68\%)$$

NI9208 noise error

$$u_3 = 100 \cdot nA \quad (68\%)$$

N9208 instrument uncertainty

$$u_{c.AI} := \sqrt{(u_5)^2 + (u_2)^2 + u_3^{2}} = \begin{pmatrix} 70.92 \\ 51.443 \end{pmatrix} \cdot \mu A \quad (68\%)$$

NI9208 design stage uncertainty

$$u_{d.AI} := \sqrt{u_{0.AI}^{2} + u_{c.AI}^{2}} = \begin{pmatrix} 71.693 \\ 52.504 \end{pmatrix} \cdot \mu A \quad (68\%)$$

System design stage uncertainty

$$u_{d.dP} := \sqrt{u_{d.PMD}^{2} + u_{d.AI}^{2}} = \begin{pmatrix} 72.139 \\ 53.11 \end{pmatrix} \cdot \mu A \quad (68\%)$$

Converted to Pressure

$$u_{d.dP} := \frac{Span}{16mA} \cdot u_{d.dP} = \begin{pmatrix} 22.543 \\ 16.597 \end{pmatrix} Pa \quad (68\%)$$

% Error

$$\%Error_{d.dP} := \frac{\overrightarrow{u_{d.dP}}}{|dP|} = \begin{pmatrix} 5.255 \\ 0.816 \end{pmatrix} \cdot \% \quad (68\%)$$

4. Gas Flow Rate

Mass flow rate $\dot{M}_g := \begin{pmatrix} 0.051 \\ 0.115 \end{pmatrix} \frac{kg}{s}$

Discharge coefficient $C_d := \begin{pmatrix} 0.613 \\ 0.610 \end{pmatrix}$ Scenarios from process analysis 31 & 28

Gas expansibilty factor $\varepsilon_g := \begin{pmatrix} 0.999 \\ 0.995 \end{pmatrix}$

Specific gas constant for air $R_g := 287.058 \frac{J}{kg \cdot K}$

Orifice beta value $\beta := 0.55$

Gas only pipe diameter $D_{pipe} := 102.26mm$

Vena contracta $D_{vc} := \beta \cdot D_{pipe} = 0.056\,m$

Pressure drop across orifice $dP := -dP = \begin{pmatrix} 0.429 \\ 2.035 \end{pmatrix} \cdot kPa$

Gas density at upstream face $\rho_1 := \begin{pmatrix} 1.198 \\ 1.290 \end{pmatrix} \frac{kg}{m^3}$ Scenarios from process analysis 31 & 28

Specific heat ratio $\kappa := 1.4$

Uncertainty on discharge coefficient

$$u_{d.C.d\_} := 0.5\% \cdot C_d = \begin{pmatrix} 3.065 \times 10^{-3} \\ 3.05 \times 10^{-3} \end{pmatrix} \quad (95\%)$$

Uncertainty on pipe diameter

$$u_{D.pipe\_} := 0.4\% \cdot D_{pipe} = 0.409 \cdot mm \quad (95\%)$$

Uncertainty on vena contracta

$$u_{D.vc\_} := 0.1\% \cdot D_{vc} = 0.056 \cdot mm \quad (95\%)$$

Uncertainty on gas expansibilty factor

$$u_{d.\varepsilon.g\_} := \overrightarrow{\left[\left(\frac{3.5 \cdot dP}{\kappa \cdot P_1}\%\right) \cdot \varepsilon_g\right]} = \begin{pmatrix} 1.035 \times 10^{-4} \\ 4.242 \times 10^{-4} \end{pmatrix} \quad (95\%)$$

Uncertainty on density

Uncertainty on gas temperature

$$u_{d.T.g\_} := 2u_{d.T.g} = \begin{pmatrix} 0.456 \\ 0.601 \end{pmatrix} \cdot \Delta°C \quad (95\%)$$

Uncertainty on gas pressure

$$u_{d.P1\_} := 2u_{d.P.1} = \begin{pmatrix} 1.372 \\ 1.469 \end{pmatrix} \cdot kPa \quad (95\%)$$

Uncertainty on pressure drop

$$u_{d.dP\_} := 2 \cdot u_{d.dP} = \begin{pmatrix} 45.087 \\ 33.194 \end{pmatrix} Pa \quad (95\%)$$

Uncertainty on density

$$u_{d.\rho1\_} := \overrightarrow{\sqrt{\left[\left(\frac{1}{R_g \cdot T_g}\right) \cdot u_{d.P1\_}\right]^2 + \left[\left(\frac{-P_1}{R_g \cdot T_g^{\,2}}\right) \cdot u_{d.T.g\_}\right]^2}} = \begin{pmatrix} 0.016 \\ 0.016 \end{pmatrix} \frac{kg}{m^3} \quad (95\%)$$

Uncertainty on mass flow rate

$$u_{d.Mdot.g\_} := \left[\dot{M}_g \cdot \overrightarrow{\sqrt{\left(\frac{u_{d.C.d\_}}{C_d}\right)^2 + \left(\frac{u_{d.\varepsilon.g\_}}{\varepsilon_g}\right)^2 + \left(\frac{2\beta^4}{1-\beta^4}\right)^2 \cdot \left(\frac{u_{D.pipe\_}}{D_{pipe}}\right)^2 \ldots + \left(\frac{2}{1-\beta^4}\right)^2 \cdot \left(\frac{u_{D.vc\_}}{D_{vc}}\right)^2 + \frac{1}{4} \cdot \left(\frac{u_{d.dP\_}}{dP}\right)^2 + \left(\frac{u_{d.\rho1\_}}{\rho_1}\right)^2}}\right] = \begin{pmatrix} 2.779 \times 10^{-3} \\ 1.827 \times 10^{-3} \end{pmatrix} \frac{kg}{s} \quad (95\%)$$

$$u_{d.Mdot.g} := \frac{1}{2} u_{d.Mdot.g\_} = \begin{pmatrix} 1.39 \times 10^{-3} \\ 9.134 \times 10^{-4} \end{pmatrix} \frac{kg}{s} \quad (68\%)$$

% Error

$$\%Error_{d.Mdot.g} := \frac{\overrightarrow{u_{d.Mdot.g}}}{\dot{M}_g} = \begin{pmatrix} 2.725 \\ 0.794 \end{pmatrix} \cdot \% \quad (68\%)$$

5. Gain in weight

Excitation voltage $V_E := 10V$

LCA Max $LCA := 310kg$

Applied mass $Mass := \begin{pmatrix} 50 \\ 250 \end{pmatrix} kg$ Approximate boundary values of steady state data

Single load cell

200kg load cell zero-order uncertainty $u_{0.200\_} := \frac{1}{2}\left(\frac{200}{3000}\right)kg = 0.033\,kg$ (95%)

$u_{0.200} := \frac{1}{2}u_{0.200\_} = 0.017\,kg$ (68%)

Converted to mV $u_{0.200} := \frac{V_E\left(\frac{2mV}{V}\right)}{200kg} \cdot u_{0.200} = 1.667 \times 10^{-3} \cdot mV$ (68%)

200kg load cell %FS uncertainty $u_{1.200\_} := 200kg \cdot 0.020\% = 0.04\,kg$ (95%)

$u_{1.200} := \frac{1}{2} \cdot u_{1.200\_} = 0.02\,kg$ (68%)

Converted to mV $u_{1.200} := \frac{V_E\left(\frac{2mV}{V}\right)}{200kg} \cdot u_{1.200} = 2 \times 10^{-3} \cdot mV$ (68%)

200kg load cell offset uncertainty $u_{2.200\_} := V_E \cdot \left(\frac{0.02mV}{V}\right) = 0.2 \cdot mV$ (95%)

$u_{2.200} := \frac{1}{2} \cdot u_{2.200\_} = 0.1 \cdot mV$ (68%)

200kg load cell instrument uncetainty $u_{c.200} := \sqrt{u_{1.200}^{\,2} + u_{2.200}^{\,2}} = 0.1 \cdot mV$ (68%)

200kg load cell design stage uncertainty $u_{d.200} := \sqrt{u_{0.200}^{\,2} + u_{c.200}^{\,2}} = 0.1 \cdot mV$ (68%)

Converted to kg

$$u_{d.200} := \frac{200\text{kg}}{V_E \cdot \left(\frac{2\text{mV}}{\text{V}}\right)} \cdot u_{d.200} = 1\ \text{kg} \quad (68\%)$$

Junction box

600kg load cell design stage uncertainty

$$u_{d.600} := \sqrt{3 \cdot \left(u_{d.200}\right)^2} = 1.733\ \text{kg} \quad (68\%)$$

Converted to mA

$$u_{d.600} := \frac{16\text{mA}}{\text{LCA}} \cdot u_{d.600} = 89.426 \cdot \mu\text{A} \quad (68\%)$$

LCA

LCA zero-order uncertainty

$$u_{0.LCA\_} := \frac{1}{2}(244\mu\text{A}) = 122 \cdot \mu\text{A} \quad (95\%)$$

$$u_{0.LCA} := \frac{1}{2} u_{0.LCA\_} = 61 \cdot \mu\text{A} \quad (68\%)$$

LCA instrument error

$$u_{c.LCA\_} := \text{Mass} \cdot 0.01\% = \begin{pmatrix} 5 \times 10^{-3} \\ 0.025 \end{pmatrix} \text{kg} \quad (95\%)$$

$$u_{c.LCA} := \frac{1}{2} u_{c.LCA\_} = \begin{pmatrix} 2.5 \times 10^{-3} \\ 0.013 \end{pmatrix} \text{kg} \quad (68\%)$$

Converted to mA

$$u_{c.LCA} := \frac{16\text{mA}}{\text{LCA}} \cdot u_{c.LCA} = \begin{pmatrix} 0.129 \\ 0.645 \end{pmatrix} \cdot \mu\text{A} \quad (68\%)$$

LCA design stage uncertainty

$$u_{d.LCA} := \sqrt{u_{0.LCA}^2 + u_{c.LCA}^2} = \begin{pmatrix} 61 \\ 61.003 \end{pmatrix} \cdot \mu\text{A} \quad (68\%)$$

NI9208 AI

NI9208 zero-order uncertainty

$$u_{0.AI} = 10.5 \cdot \mu\text{A} \quad (68\%)$$

Measured signal assuming no error

$$\text{Mass}_{mA} := \frac{(\text{Mass} + 0.25 \cdot \text{LCA}) \cdot 16\text{mA}}{\text{LCA}} = \begin{pmatrix} 6.581 \\ 16.903 \end{pmatrix} \cdot \text{mA}$$

NI9208 gain error on Mass.mA

$$u_{6\_} := \text{Mass}_{mA} \cdot 0.76\% = \begin{pmatrix} 50.013 \\ 128.465 \end{pmatrix} \cdot \mu\text{A} \quad (95\%)$$

$$u_6 := \frac{1}{2} \cdot u_{6\_} = \begin{pmatrix} 25.006 \\ 64.232 \end{pmatrix} \cdot \mu\text{A} \quad (68\%)$$

NI9208 offset error $u_2 = 4.4 \cdot \mu A$ (68%)

NI9208 noise error $u_3 = 100 \cdot nA$ (68%)

N9208 instrument uncertainty $u_{0.AI} := \sqrt{(u_6)^2 + (u_2)^2 + u_3^2} = \begin{pmatrix} 25.391 \\ 64.383 \end{pmatrix} \cdot \mu A$ (68%)

NI9208 design stage uncertainty $u_{d.AI} := \sqrt{u_{0.AI}^2 + u_{c.AI}^2} = \begin{pmatrix} 27.476 \\ 65.233 \end{pmatrix} \cdot \mu A$ (68%)

System design stage uncertainty $u_{d.Mass.GIW} := \sqrt{u_{d.600}^2 + u_{d.LCA}^2 + u_{d.AI}^2} = \begin{pmatrix} 111.683 \\ 126.388 \end{pmatrix} \cdot \mu A$ (68%)

Converted to Mass $u_{d.Mass.GIW} := \frac{LCA}{16mA}\left(u_{d.Mass.GIW}\right) = \begin{pmatrix} 2.164 \\ 2.449 \end{pmatrix} kg$ (68%)

% Error $\%Error_{d.Mass.GIW} := \frac{\overrightarrow{u_{d.Mass.GIW}}}{Mass} = \begin{pmatrix} 4.328 \\ 0.98 \end{pmatrix} \cdot \%$ (68%)

6. Loss in Weight

Single load cell

500kg load cell zero-order uncertainty $u_{0.500} := \frac{1}{2}\left(\frac{500}{3000}\right) kg = 0.083\ kg$ (95%)

$u_{0.500} := \frac{1}{2} u_{0.500} = 0.042\ kg$ (68%)

Converted to mV $u_{0.500} := \frac{V_E\left(\frac{2mV}{V}\right)}{500kg} \cdot u_{0.500} = 1.667 \times 10^{-3} \cdot mV$ (68%)

500kg load cell %FS uncertainty $u_{1.500\_} := 500kg \cdot 0.023\% = 0.115\ kg$ (95%)

$u_{1.500} := \frac{1}{2} \cdot u_{1.500\_} = 0.058\ kg$ (68%)

Converted to mV

$$u_{1.500\_} := \frac{V_E\left(\frac{2mV}{V}\right)}{500kg} \cdot u_{1.500} = 2.3 \times 10^{-3} \cdot mV \quad (68\%)$$

500kg load cell offset uncertainty

$$u_{2.500\_} := V_E \cdot \left(\frac{0.02mV}{V}\right) = 0.2 \cdot mV \quad (95\%)$$

$$u_{2.500} := \frac{1}{2} \cdot u_{2.500\_} = 0.1 \cdot mV \quad (68\%)$$

500kg load cell instrument uncetainty

$$u_{c.500} := \sqrt{u_{1.500}^{\ 2} + u_{2.500}^{\ 2}} = 0.1 \cdot mV \quad (68\%)$$

500kg load cell design stage uncertainty

$$u_{d.500} := \sqrt{u_{0.500}^{\ 2} + u_{c.500}^{\ 2}} = 0.1 \cdot mV \quad (68\%)$$

Converted to kg

$$u_{d.500\_} := \frac{500kg}{V_E \cdot \left(\frac{2mV}{V}\right)} \cdot u_{d.500} = 2.501\,kg \quad (68\%)$$

Junction box

1500kg load cell design stage uncertainty

$$u_{d.1500} := \sqrt{3 \cdot \left(u_{d.500}\right)^2} = 4.332\,kg \quad (68\%)$$

Converted to mA

$$u_{d.1500\_} := \frac{16mA}{LCA} \cdot u_{d.1500} = 223.581 \cdot \mu A \quad (68\%)$$

LCA

LCA design stage uncertainty

$$u_{d.LCA} = \begin{pmatrix} 61 \\ 61.003 \end{pmatrix} \cdot \mu A \quad (68\%)$$

NI9208 AI

NI9208 design stage uncertainty

$$u_{d.AI} = \begin{pmatrix} 27.476 \\ 65.233 \end{pmatrix} \cdot \mu A \quad (68\%)$$

System design stage uncertainty

$$u_{d.Mass.LIW} := \sqrt{u_{d.1500}^{\ 2} + u_{d.LCA}^{\ 2} + u_{d.AI}^{\ 2}} = \begin{pmatrix} 233.376 \\ 240.759 \end{pmatrix} \cdot \mu A \quad (68\%)$$

Converted to Mass

$$u_{d.Mass.LIW\_} := \frac{LCA}{16mA}\left(u_{d.Mass.LIW}\right) = \begin{pmatrix} 4.522 \\ 4.665 \end{pmatrix} kg \quad (68\%)$$

% Error

$$\%Error_{d.Mass.LIW} := \frac{\overrightarrow{u_{d.Mass.LIW}}}{Mass} = \begin{pmatrix} 9.043 \\ 1.866 \end{pmatrix} \cdot \% \quad (68\%)$$

7. Particle Flow Rate

Mass at beginning and end of test

$$Mass = \begin{pmatrix} 50 \\ 250 \end{pmatrix} kg$$

Approximate boundary values of steady state data

Particle flow rate

$$\dot{M}_p := \begin{pmatrix} 0.07 \\ 0.8 \end{pmatrix} \frac{kg}{s}$$

Minimum and maximum design flow rates

Uncertainty on mass flow rate

Time taken per test

$$\Delta t := \frac{Mass_0 - Mass_1}{\dot{M}_p} = \begin{pmatrix} -2.857 \times 10^3 \\ -250 \end{pmatrix} s$$

Uncertainty on boundary masses (using LIW or GIW)

$$u_{d.Mass} := \begin{cases} u_{d.Mass.LIW} & \text{if Hopper = 1} \\ u_{d.Mass.GIW} & \text{otherwise} \end{cases} = \begin{pmatrix} 4.522 \\ 4.665 \end{pmatrix} kg \quad (68\%)$$

Uncertainty on flow rate

$$u_{d.Mdot.p} := \sqrt{\left(\frac{1}{\Delta t} \cdot u_{d.Mass_1}\right)^2 + \left(\frac{-1}{\Delta t} \cdot u_{d.Mass_0}\right)^2} = \begin{pmatrix} 2.274 \times 10^{-3} \\ 0.026 \end{pmatrix} \frac{kg}{s} \quad (68\%)$$

% Error

$$\%Error_{d.Mdot.p} := \frac{\overrightarrow{u_{d.Mdot.p}}}{\dot{M}_p} = \begin{pmatrix} 3.248 \\ 3.248 \end{pmatrix} \cdot \% \quad (68\%)$$

8. Summary of uncertainties

Intermediate uncertainties

Temperature	$T_g = \begin{pmatrix} 28 \\ 49 \end{pmatrix} \cdot °C$	±	$u_{d.T.g} = \begin{pmatrix} 0.228 \\ 0.301 \end{pmatrix} \cdot \Delta °C$	(68%)
		or	$\%Error_{d.T.g} = \begin{pmatrix} 0.814 \\ 0.614 \end{pmatrix} \cdot \%$	
Pressure	$P_1 = \begin{pmatrix} 103.534 \\ 119.338 \end{pmatrix} \cdot kPa$	±	$u_{d.P.1} = \begin{pmatrix} 685.897 \\ 734.557 \end{pmatrix} Pa$	(68%)
		or	$\%Error_{d.P.1} = \begin{pmatrix} 0.662 \\ 0.616 \end{pmatrix} \cdot \%$	
Delta Pressure	$dP = \begin{pmatrix} 429 \\ 2.035 \times 10^3 \end{pmatrix} \cdot Pa$	±	$u_{d.dP} = \begin{pmatrix} 22.543 \\ 16.597 \end{pmatrix} Pa$	(68%)
		or	$\%Error_{d.dP} = \begin{pmatrix} 5.255 \\ 0.816 \end{pmatrix} \cdot \%$	
Loss in Weight Mass	$Mass = \begin{pmatrix} 50 \\ 250 \end{pmatrix} kg$	±	$u_{d.Mass.LIW} = \begin{pmatrix} 4.522 \\ 4.665 \end{pmatrix} kg$	(68%)
		or	$\%Error_{d.Mass.LIW} = \begin{pmatrix} 9.043 \\ 1.866 \end{pmatrix} \cdot \%$	
Gain in Weight Mass	$Mass = \begin{pmatrix} 50 \\ 250 \end{pmatrix} kg$	±	$u_{d.Mass.GIW} = \begin{pmatrix} 2.164 \\ 2.449 \end{pmatrix} kg$	(68%)
		or	$\%Error_{d.Mass.GIW} = \begin{pmatrix} 4.328 \\ 0.98 \end{pmatrix} \cdot \%$	

Mass flow rates

Gas mass flow rate $\dot{M}_g = \begin{pmatrix} 183.6 \\ 414 \end{pmatrix} \cdot \frac{kg}{hr}$ ± $u_{d.Mdot.g} = \begin{pmatrix} 5.003 \\ 3.288 \end{pmatrix} \cdot \frac{kg}{hr}$ (68%)

or $\%Error_{d.Mdot.g} = \begin{pmatrix} 2.725 \\ 0.794 \end{pmatrix} \cdot \%$

Particle mass flow rate $\dot{M}_p = \begin{pmatrix} 252 \\ 2.88 \times 10^3 \end{pmatrix} \cdot \frac{kg}{hr}$ ± $u_{d.Mdot.p} = \begin{pmatrix} 8.186 \\ 93.55 \end{pmatrix} \cdot \frac{kg}{hr}$ (68%)

or $\%Error_{d.Mdot.p} = \begin{pmatrix} 3.248 \\ 3.248 \end{pmatrix} \cdot \%$

Appendix L. Test Rig Scaling

Part A - Plant Flow Properties Analysis

An analysis performed to determine power plant flow properties at low and high load conditions, using averaged data from a dissertation by Van der Merwe (2013).

1. Inputs

1.1. Plant conditions

Gas pressure $P_g := 85kPa$

Gas temperature $T_g := 90\,°C$

Pipe diameter $D_{pipe} := 450mm$

Mass flow rate of gas $\dot{M}_g := \begin{pmatrix} 3.12 \\ 3.93 \end{pmatrix} \frac{kg}{s}$

Mass flow rate of particles $\dot{M}_p := \begin{pmatrix} 1.28 \\ 2.50 \end{pmatrix} \frac{kg}{s}$

1.2 Particle properties

Particle diameter $D_p := \begin{pmatrix} 37 \\ 300 \end{pmatrix} \mu m$

Particle density $\rho_p := 1550 \frac{kg}{m^3}$

2. Intermediate calculations

2.1 Gas properties

Calculate gas density

Specific gas constant for air $R_g := 287.058 \frac{J}{kg \cdot K}$

Gas density $\rho_g := \frac{P_g}{R_g \cdot T_g} = 0.815 \frac{kg}{m^3}$

Calculate gas dynamic viscosity

Reference temperature

$$T_{ref} := 273.15K$$

Reference dynamic viscosity

$$\mu_{ref} := 1.716 \times 10^{-5} \frac{kg}{m \cdot s}$$

Sutherland's constant

$$S1 := 110.4K$$

Gas dynamic viscosity

$$\mu_g := \mu_{ref} \cdot \left(\frac{T_g}{T_{ref}}\right)^{\frac{3}{2}} \cdot \left(\frac{T_{ref} + S1}{T_g + S1}\right) = 2.131 \times 10^{-5} \frac{kg}{s \cdot m}$$

2.2 Flow properties

Loading

$$z := \frac{\overrightarrow{\dot{M}_p}}{\dot{M}_g} = \begin{pmatrix} 0.41 \\ 0.636 \end{pmatrix}$$

Air fuel ratio

$$AF := \frac{1}{z} = \begin{pmatrix} 2.438 \\ 1.572 \end{pmatrix}$$

Pipe cross section area

$$A_{pipe} := \frac{\pi D_{pipe}^{2}}{4} = 0.159\,m^2$$

Superficial gas velocity

$$U_g := \frac{\overrightarrow{\dot{M}_g}}{A_{pipe} \cdot \rho_g} = \begin{pmatrix} 24.059 \\ 30.305 \end{pmatrix} \frac{m}{s}$$

Superficial particle velocity

$$U_p := \frac{\overrightarrow{\dot{M}_p}}{A_{pipe} \cdot \rho_p} = \begin{pmatrix} 5.192 \times 10^{-3} \\ 0.01 \end{pmatrix} \frac{m}{s}$$

2.3 Particle terminal velocity

For Stokes flow

$$u_{t0.stokes} := \frac{D_p^{2} \cdot (\rho_p - \rho_g) \cdot g}{18 \cdot \mu_g} = \begin{pmatrix} 0.054 \\ 3.565 \end{pmatrix} \frac{m}{s}$$

Corresponding Reynolds number

$$Re_{t0.stokes} := \frac{\overrightarrow{\rho_g \cdot D_p \cdot u_{t0.stokes}}}{\mu_g} = \begin{pmatrix} 0.077 \\ 40.933 \end{pmatrix}$$

Check or change to Intermeddiate flow

$$u_{t0_0} := \begin{cases} u_{t0.stokes_0} & \text{if } Re_{t0.stokes_0} < 1 \\ \left[\frac{8}{111}\cdot\frac{\rho_g^{0.6}\cdot\left(D_{p_0}\right)^{1.6}}{\mu_g^{0.6}}\cdot\frac{\left(\rho_p-\rho_g\right)}{\rho_g}\cdot g\right]^{\frac{5}{7}} & \text{otherwise} \end{cases} = 0.054\,\frac{m}{s}$$

$$u_{t0_1} := \begin{cases} u_{t0.stokes_1} & \text{if } Re_{t0.stokes_1} < 1 \\ \left[\frac{8}{111}\cdot\frac{\rho_g^{0.6}\cdot\left(D_{p_1}\right)^{1.6}}{\mu_g^{0.6}}\cdot\frac{\left(\rho_p-\rho_g\right)}{\rho_g}\cdot g\right]^{\frac{5}{7}} & \text{otherwise} \end{cases} = 1.487\,\frac{m}{s}$$

Corresponding Reynolds number

$$Re_{t0} := \frac{\overrightarrow{\rho_g\cdot D_p\cdot u_{t0}}}{\mu_g} = \begin{pmatrix} 0.077 \\ 17.07 \end{pmatrix}$$

3. Horizontal flow

3.1. Flow properties

Particle velocity (Hinkle correlation)

$$u_{ph} := \left[\overrightarrow{U_g\cdot\left[1-0.044\cdot\left(\frac{D_p}{m}\right)^{0.3}\cdot\left(\frac{\rho_p}{\frac{kg}{m^3}}\right)^{0.5}\right]}\right] = \begin{pmatrix} 22.107 \\ 25.7 \end{pmatrix}\frac{m}{s}$$

Voidage

$$\alpha_{gh} := 1 - \frac{\overrightarrow{U_g\cdot\rho_g\cdot z}}{\rho_p\cdot u_{ph}} = \begin{pmatrix} 0.99977 \\ 0.99961 \end{pmatrix}$$

Particle volume fraction

$$\alpha_{ph} := 1 - \alpha_{gh} = \begin{pmatrix} 2.349\times10^{-4} \\ 3.946\times10^{-4} \end{pmatrix}$$

Gas velocity

$$u_{gh} := \frac{U_g}{\alpha_{gh}} = \begin{pmatrix} 24.065 \\ 30.317 \end{pmatrix}\frac{m}{s}$$

Slip velocity

$$u_{rh} := u_{gh} - u_{ph} = \begin{pmatrix} 1.957 \\ 4.617 \end{pmatrix}\frac{m}{s}$$

3.2. Flow regime

Relative Reynolds number

$$Re_{rh} := \frac{\overrightarrow{\rho_g \cdot D_p \cdot u_{rh}}}{\mu_g} = \begin{pmatrix} 2.771 \\ 53.013 \end{pmatrix}$$

Drag coefficient

$$C_{D\infty h_0} := \begin{cases} 24 \cdot \left(Re_{rh_0}\right)^{-1} & \text{if } Re_{rh_0} < 1 \\ \left[18.5 \cdot \left(Re_{rh_0}\right)^{-0.6}\right] & \text{otherwise} \end{cases} = 10.036$$

$$C_{D\infty h_1} := \begin{cases} 24 \cdot \left(Re_{rh_1}\right)^{-1} & \text{if } Re_{rh_1} < 1 \\ \left[18.5 \cdot \left(Re_{rh_1}\right)^{-0.6}\right] & \text{otherwise} \end{cases} = 1.708$$

4. Vertical flow

4.1. Flow properties

Slip velocity (terminal velocity assumption)

$$u_{rv} := u_{t0}$$

Particle velocity

$$u_{pv} := U_g - u_{rv} = \begin{pmatrix} 24.005 \\ 28.818 \end{pmatrix} \frac{m}{s}$$

Voidage

$$\alpha_{gv} := 1 - \frac{\overrightarrow{U_g \cdot \rho_g \cdot z}}{\rho_p \cdot u_{pv}} = \begin{pmatrix} 0.99978 \\ 0.99965 \end{pmatrix}$$

Particle volume fraction

$$\alpha_{pv} := 1 - \alpha_{gv} = \begin{pmatrix} 2.163 \times 10^{-4} \\ 3.519 \times 10^{-4} \end{pmatrix}$$

4.2. Flow regime

Relative Reynolds number

$$Re_{rv} := \frac{\overrightarrow{\rho_g \cdot D_p \cdot u_{rv}}}{\mu_g} = \begin{pmatrix} 0.077 \\ 17.07 \end{pmatrix}$$

Drag coefficient

$$C_{D\infty v_0} := \begin{cases} 24 \cdot \left(Re_{rv_0}\right)^{-1} & \text{if } Re_{rv_0} < 1 \\ \left[18.5 \cdot \left(Re_{rv_0}\right)^{-0.6}\right] & \text{otherwise} \end{cases} = 312.531$$

$$C_{D\infty v_1} := \begin{cases} 24 \cdot \left(Re_{rv_1}\right)^{-1} & \text{if } Re_{rv_1} < 1 \\ \left[18.5 \cdot \left(Re_{rv_1}\right)^{-0.6}\right] & \text{otherwise} \end{cases} = 3.372$$

5. Saltation

Rizk constant 1

$$R1 := \frac{1440}{m} \cdot D_p + 1.96 = \begin{pmatrix} 2.013 \\ 2.392 \end{pmatrix}$$

Rizk constant 2

$$R2 := \frac{1100}{m} \cdot D_p + 2.5 = \begin{pmatrix} 2.541 \\ 2.83 \end{pmatrix}$$

Saltation velocity

$$U_{salt} := \left[\frac{4 \cdot \frac{\dot{M}_p}{\frac{kg}{s}} \cdot 10^{R1} \cdot \left(\frac{g}{\frac{m}{s^2}}\right)^{\frac{R2}{2}} \cdot \left(\frac{D_{pipe}}{m}\right)^{\frac{R2}{2}-2}}{\pi \cdot \frac{\rho_g}{\frac{kg}{m^3}}} \right]^{\frac{1}{R2+1}} \cdot \frac{m}{s} = \begin{pmatrix} 12.044 \\ 15.786 \end{pmatrix} \frac{m}{s}$$

6. Choking

Solid friction factor at choking

$$B(\alpha_{gc}, u_{gc}) := \frac{2 \cdot g \cdot D_{pipe} \cdot \left(\alpha_{gc}^{-4.7} - 1\right)}{\left(u_{gc} - u_{t0}\right)^2} - 0.01$$

Slip velocity = Terminal velocity

$$D(\alpha_{gc}, u_{gc}) := \frac{U_p}{1 - \alpha_{gc}} - u_{gc} - u_{t0}$$

Guess $\alpha_{gc} := \begin{pmatrix} 0.99 \\ 0.99 \end{pmatrix}$ $u_{gc} := \begin{pmatrix} 5 \\ 5 \end{pmatrix} \frac{m}{s}$

Given

$B(\alpha_{gc}, u_{gc}) = 0$

$D(\alpha_{gc}, u_{gc}) = 0$

Solve $\begin{pmatrix} \alpha_{gc} \\ u_{gc} \end{pmatrix} := \text{Find}(\alpha_{gc}, u_{gc})$

Voidage at choking

$$\alpha_{gc} = \begin{pmatrix} 0.998184 \\ 0.99822 \end{pmatrix}$$

Gas velocity at choking

$$u_{gc} = \begin{pmatrix} 2.806 \\ 4.211 \end{pmatrix} \frac{m}{s}$$

Choking velocity

$$U_{gc} := \overrightarrow{(\alpha_{gc} \cdot u_{gc})} = \begin{pmatrix} 2.801 \\ 4.203 \end{pmatrix} \frac{m}{s}$$

7. Similarity Conditions

7.1. Gas flow regime

Pipe Reynolds number

$$Re_{pipe} := \frac{\overrightarrow{\rho_g \cdot D_{pipe} \cdot U_g}}{\mu_g} = \begin{pmatrix} 4.143 \times 10^5 \\ 5.219 \times 10^5 \end{pmatrix}$$

Note: Turbulent Flow

7.2. Non dimensional numbers for a representative particle

Representative particle diameter

$$D_{rp} := 300\,\mu m$$

Superficial velocity range

$$U_g = \begin{pmatrix} 24.059 \\ 30.305 \end{pmatrix} \frac{m}{s}$$

Vectorise

$$U_{rg} := 24\frac{m}{s}, 25\frac{m}{s} .. 30\frac{m}{s} =$$

24	m/s
25	
26	
27	
28	
29	
30	

Particle Reynolds number

$$Re_p := \frac{\rho_g \cdot D_{rp} \cdot U_{rg}}{\mu_g}$$

Particle Froude number

$$Fr_p := \frac{U_{rg}}{\sqrt{D_{rp} \cdot g}}$$

Inertia parameter

$$\psi := \frac{\rho_p \cdot U_{rg} \cdot D_{rp}}{\mu_g}$$

Similarity table

$$ST^{\langle 0 \rangle} := \frac{U_{rg}}{\frac{m}{s}} \qquad ST^{\langle 1 \rangle} := Re_p \qquad ST^{\langle 2 \rangle} := Fr_p \qquad ST^{\langle 3 \rangle} := \psi$$

$$ST = \begin{pmatrix} 24 & 275.547 & 442.477 & 5.238 \times 10^5 \\ 25 & 287.028 & 460.913 & 5.456 \times 10^5 \\ 26 & 298.509 & 479.35 & 5.674 \times 10^5 \\ 27 & 309.99 & 497.786 & 5.893 \times 10^5 \\ 28 & 321.471 & 516.223 & 6.111 \times 10^5 \\ 29 & 332.952 & 534.659 & 6.329 \times 10^5 \\ 30 & 344.433 & 553.096 & 6.547 \times 10^5 \end{pmatrix}$$

Part B - Test Rig Flow Properties

The following model specifies required test rig operating conditions and particle properties to attain power plant similarity

1. Inputs

1.1. Fixed inputs

Gas temperature $T_g := 20°C$

Specific gas constant for air $R_g := 287.058 \frac{J}{kg \cdot K}$

1.2. Particle properties

Particle density $\rho_p := 1550 \frac{kg}{m^3}$

1.3. Similarity condition

Particle Reynolds number $Re_{p.req} := 344.433$

Particle Froude number $Fr_{p.req} := 553.096$

Inertia parameter $\psi_{req} := 6.547 \times 10^5$

2. Intermediate calculations

Reference temperature $T_{ref} := 273.15K$

Reference dynamic viscosity $\mu_{ref} := 1.716 \times 10^{-5} \frac{kg}{m \cdot s}$

Sutherland's constant $S1 := 110.4K$

Gas dynamic viscosity $\mu_g := \mu_{ref} \cdot \left(\frac{T_g}{T_{ref}} \right)^{\frac{3}{2}} \cdot \left(\frac{T_{ref} + S1}{T_g + S1} \right) = 1.813 \times 10^{-5} \frac{kg}{s \cdot m}$

3. Required operating conditions

3.1. Calculations

$$Re_p(P_g, U_g, D_p) := \frac{\left(\frac{P_g}{R_g \cdot T_g}\right) \cdot D_p \cdot U_g}{\mu_g}$$

$$Fr_p(P_g, U_g, D_p) := \frac{U_g}{\sqrt{D_p \cdot g}}$$

$$\psi(P_g, U_g, D_p) := \frac{\rho_p \cdot U_g \cdot D_p}{\mu_g}$$

Guess $P_g := 85kPa$ $U_g := 30\frac{m}{s}$ $D_p := 300\mu m$

Given

$$Re_p(P_g, U_g, D_p) = Re_{p.req}$$

$$Fr_p(P_g, U_g, D_p) = Fr_{p.req}$$

$$\psi(P_g, U_g, D_p) = \psi_{req}$$

Solve

$$\begin{pmatrix} P_g \\ U_g \\ D_p \end{pmatrix} := Find(P_g, U_g, D_p)$$

3.2. Results

Gas Pressure $P_g = 68.62 \cdot kPa$

Superficial gas velocity $U_g = 28.429 \frac{m}{s}$

Particle diameter $D_p = 269.412 \cdot \mu m$

3.3. Check

Particle Reynolds number $\frac{\left(\frac{P_g}{R_g \cdot T_g}\right) \cdot D_p \cdot U_g}{\mu_g} = 344.433$ $Re_{p.req} = 344.433$

Particle Froude number $\frac{U_g}{\sqrt{D_p \cdot g}} = 553.096$ $Fr_{p.req} = 553.096$

Inertia Parameter $\frac{\rho_p \cdot U_g \cdot D_p}{\mu_g} = 6.547 \times 10^5$ $\psi_{req} = 6.547 \times 10^5$

Appendix M. Component Models

Cyclone Basic Sizing

This model determines the required cyclone dimensions for a gas-particle seperation efficiency greater or equal to 99%. The model also calculates the corresponding efficiencies and pressure drops over a range of gas volume flow rates.

Section A - Sizing

1. Inputs

1.1. Gas and particle properties

Gas temperature	$T_g := 60\,°C = 140\,°F$
Minimum gas pressure	$P_{g.min} := 70kPa = 10.153\,psi$
Maximum gas pressure	$P_{g.max} := 125kPa = 18.13\,psi$
Pipe diameter	$D_{pipe} := 102.26mm = 0.335\,ft$
Minimum gas velocity	$U_{g.min} := 3\frac{m}{s} = 9.843\frac{ft}{s}$
Minimum particle diameter	$D_p := 37\mu m = 1.214 \times 10^{-4}\,ft$
Minimum particle density	$\rho_p := 1400\frac{kg}{m^3} = 87.399\frac{lb}{ft^3}$

1.2 Stairmand type cyclone specific inputs

Configuration factor	$G_c := 551.3$
Number of inlet velocity heads	$N_H := 6.40$
Required fractional efficiency	$\eta_{req} := 99\%$

2. Cyclone sizing

2.1. Intermeddiate calculations

Calculate gas density

Specific gas constant for air

$$R_g := 287.058 \frac{J}{kg \cdot K} = 3.09 \times 10^3 \frac{ft^2}{K \cdot s^2}$$

Minimum gas density (T.g.max & P.g.min)

$$\rho_{g.min} := \frac{P_{g.min}}{R_g \cdot T_g} = 0.046 \frac{lb}{ft^3}$$

Maximum gas density (T.g.min & P.g.max)

$$\rho_{g.max} := \frac{P_{g.max}}{R_g \cdot T_g} = 0.082 \frac{lb}{ft^3}$$

Calculate gas dynamic viscosity

Reference temperature

$$T_{ref} := 273.15K$$

Reference dynamic viscosity

$$\mu_{ref} := 1.716 \times 10^{-5} \frac{kg}{m \cdot s} = 1.153 \times 10^{-5} \frac{lb}{ft \cdot s}$$

Sutherland's constant

$$S1 := 110.4K$$

Maximum gas dynamic viscosity

$$\mu_g := \mu_{ref} \cdot \left(\frac{T_g}{T_{ref}} \right)^{\frac{3}{2}} \cdot \left(\frac{T_{ref} + S1}{T_g + S1} \right) = 1.343 \times 10^{-5} \frac{lb}{ft \cdot s}$$

Pipe cross section area

$$A_{pipe} := \frac{\pi \cdot D_{pipe}^2}{4} = 0.088\, ft^2$$

Minimum gas flowrate

$$Vdot_{g.min} := U_{g.min} \cdot A_{pipe} = 0.87 \cdot \frac{ft^3}{s}$$

2.2. Solve for cyclone diameter

Inlet gas flowrate

$$Vdot_c := Vdot_{g.min}$$

Relaxation time

$$\tau := \frac{\rho_p \cdot D_p^2}{18 \cdot \mu_g} = 5.327 \times 10^{-3}\, s$$

Fractional efficiency correlation $$B(D_c,n) := 1 - \exp\left[-2\left[\frac{G_c\cdot\tau\cdot Vdot_c}{D_c^{\,3}}\cdot(n+1)\right]^{\frac{0.5}{n+1}}\right]$$

Vortex exponent correlation $$D(D_c,n) := 1 - \left[1 - \frac{\left[12\left(\frac{D_c}{ft}\right)\right]^{0.14}}{2.5}\right]\cdot\left[\frac{\left(\frac{T_g}{K}\cdot\frac{9}{5} - 459.67\right) + 460}{530}\right]^{0.3} - n$$

Guess $D_c := 1\,ft$ $n := 0.6$

Given

$B(D_c,n) = \eta_{req}$

$D(D_c,n) = 0$

Solve

$$\begin{pmatrix} D_c \\ n \end{pmatrix} := \text{Find}(D_c,n)$$

Cyclone diameter $D_c = 0.675\cdot ft$

Vortex exponent $n = 0.519$

2.2 Cyclone dimensions

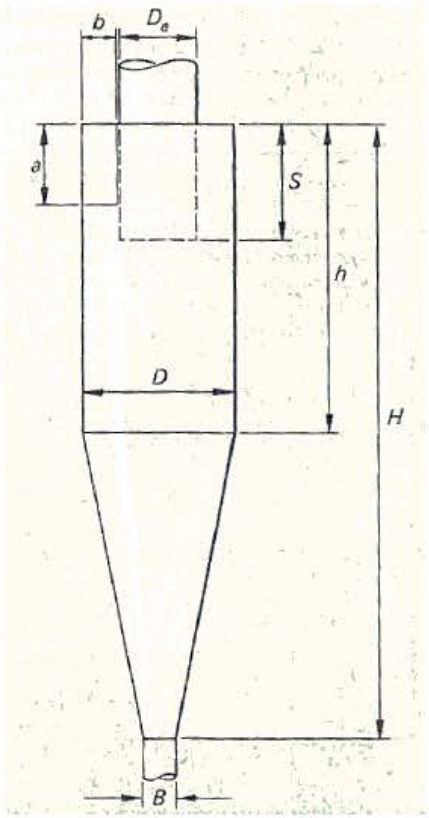

$D_c = 0.206 \cdot m$

$a := 0.5 \cdot D_c = 0.103 \cdot m$

$b := 0.2 \cdot D_c = 0.041 \cdot m$

$S\_ := 0.5 \cdot D_c = 0.103 \cdot m$

$D_e := 0.5 \cdot D_c = 0.103 \cdot m$

$h := 1.5 \cdot D_c = 0.309 \cdot m$

$H\_ := 4 \cdot D_c = 0.824 \cdot m$

$B\_ := 0.375 \cdot D_c = 0.077 \cdot m$

Natural length

$l\_ := 2.48 \cdot D_c = 0.511 \cdot m$

3. Check

1. $a < S$ (to prevent short-circuiting).
2. $b < 1/2(D_c - D_e)$ (to avoid sudden contraction).
3. $S + l \leq H$ (to keep the vortex inside the cyclone).
4. $S < h$.
5. $h < H$.
6. $\Delta P < 10$ in. H_2O.
7. $v_i/v_s \leq 1.35$ (to prevent reentrainment).
8. $v_i/v_s \simeq 1.25$ (for optimum efficiency).

1 $a = 0.103 \cdot m$ $S\_ = 0.103\,m$

2 $b = 0.041 \cdot m$ $\frac{1}{2} \cdot (D_c - D_e) = 0.051 \cdot m$

3 $S\_ + l\_ = 0.614 \cdot m$ $H\_ = 0.824 \cdot m$

4	$S\_ = 0.103 \cdot m$	$h = 0.309 \cdot m$
5	$h = 0.309 \cdot m$	$H\_ = 0.824 \cdot m$
6	N/A	
7, 8	See proceeding section	

Section B - Performance Characterisation

4. Calculations

4.1. Volume flowrate

Pipe gas velocity

$$U_g := 3\frac{m}{s}, 4\frac{m}{s} .. 30\frac{m}{s} =$$

3	$\cdot\frac{m}{s}$
4	
5	
6	
7	
8	
9	
10	
11	
12	
13	
14	
15	
16	
17	
...	

Gas volume flowrate

$$Vdot_g := U_g \cdot A_{pipe}$$

4.2. Fractional efficiency

Fractional efficiency correlation

$$\eta\left(Vdot_g\right) := 1 - \exp\left[-2\left[\frac{G_c \cdot \tau \cdot Vdot_g}{D_c^{\,3}} \cdot (n+1)\right]^{\frac{0.5}{n+1}}\right]$$

4.3. Saltation ratio

Inlet area

$$A_i := a \cdot b$$

Effective radius

$$r := \frac{1}{2} \cdot \left(D_c - b\right)$$

Kalen & Zenz parameter

$$\omega := \left[\frac{4 \cdot g \cdot \mu_g \cdot \left(\rho_p - \rho_{g.min}\right)}{3 \cdot \rho_{g.min}^{\,2}}\right]^{\frac{1}{3}}$$

Inlet velocity over saltation correlation

$$R_{salt}\left(Vdot_g\right) := \frac{\left(\frac{Vdot_g}{A_i}\right)}{\left[2.1 \cdot \left(9.6 \cdot \frac{b}{ft}\right)^{0.4} \cdot \omega \cdot \left[\frac{\left(\frac{Vdot_g}{A_i}\right)^2}{32.2 \frac{ft}{s^2} \cdot r}\right]^{\frac{1}{3}}\right]}$$

4.4. Pressure drop

Non-volute cyclone pressure drop (Max density)

$$dP_c\left(Vdot_g\right) := 0.5 \cdot \rho_{g.max} \cdot \left(\frac{Vdot_g}{A_i}\right)^2 \cdot N_H$$

5. Performace Curves

5.1. Efficiency (Min density)

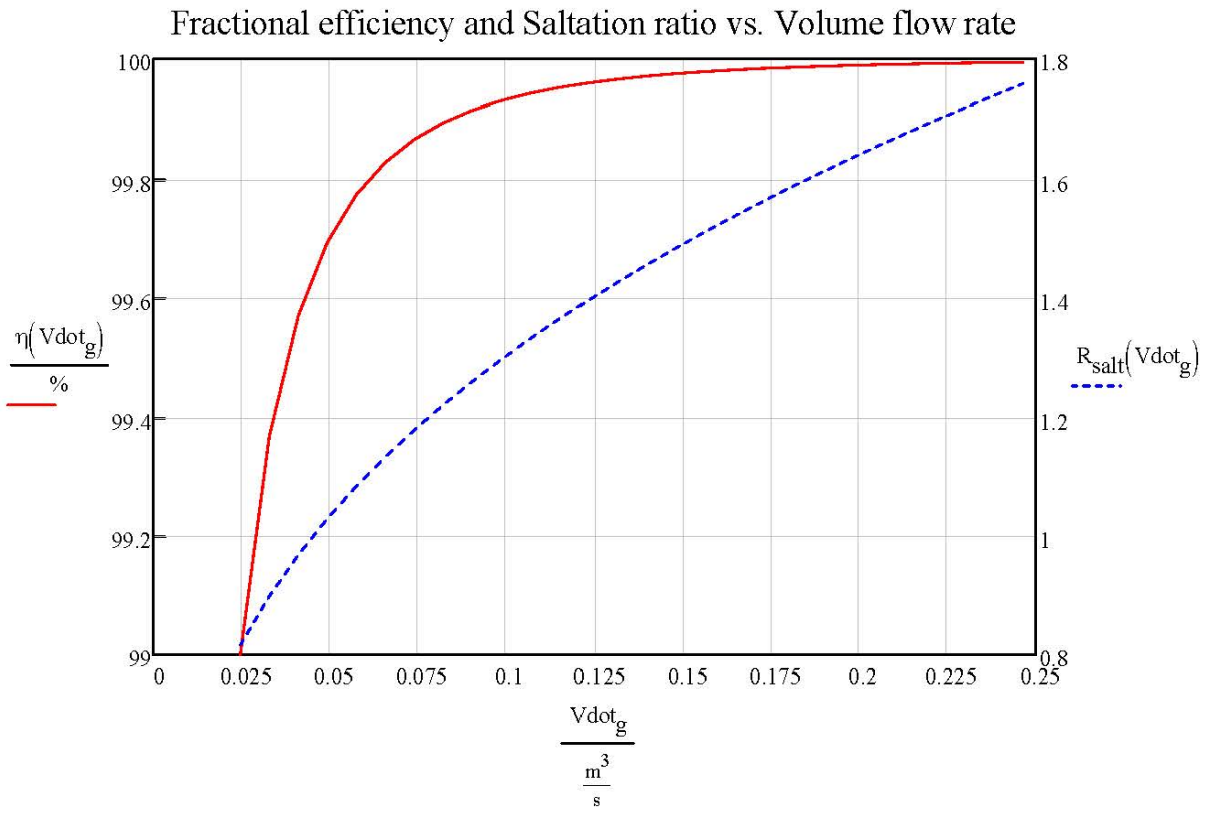

Read Vdot.g appox. 0.150m3/s @ R.salt = 1.5

Note maximum flowrate is $\mathrm{Vdot_{g.max}} := 30\frac{\mathrm{m}}{\mathrm{s}} \cdot \mathrm{A_{pipe}} = 0.246 \cdot \frac{\mathrm{m}^3}{\mathrm{s}}$

Therefore use 2 cyclones in parallel from 50% of flowrate to prevent re-entrainment (and also to limit pressure drop)

2nd cyclone kick in flowrate $\mathrm{Vdot_{g.kickin}} := \frac{\mathrm{Vdot_{g.max}}}{2} = 0.123 \cdot \frac{\mathrm{m}^3}{\mathrm{s}}$

Fractional efficiency at minimum flowrate $\eta(\mathrm{Vdot_{g.min}}) = 0.99$

Fractional efficiency at kick in flowrate $\eta(\mathrm{Vdot_{g.kickin}}) = 1$

5.2. Pressure drop (Max density)

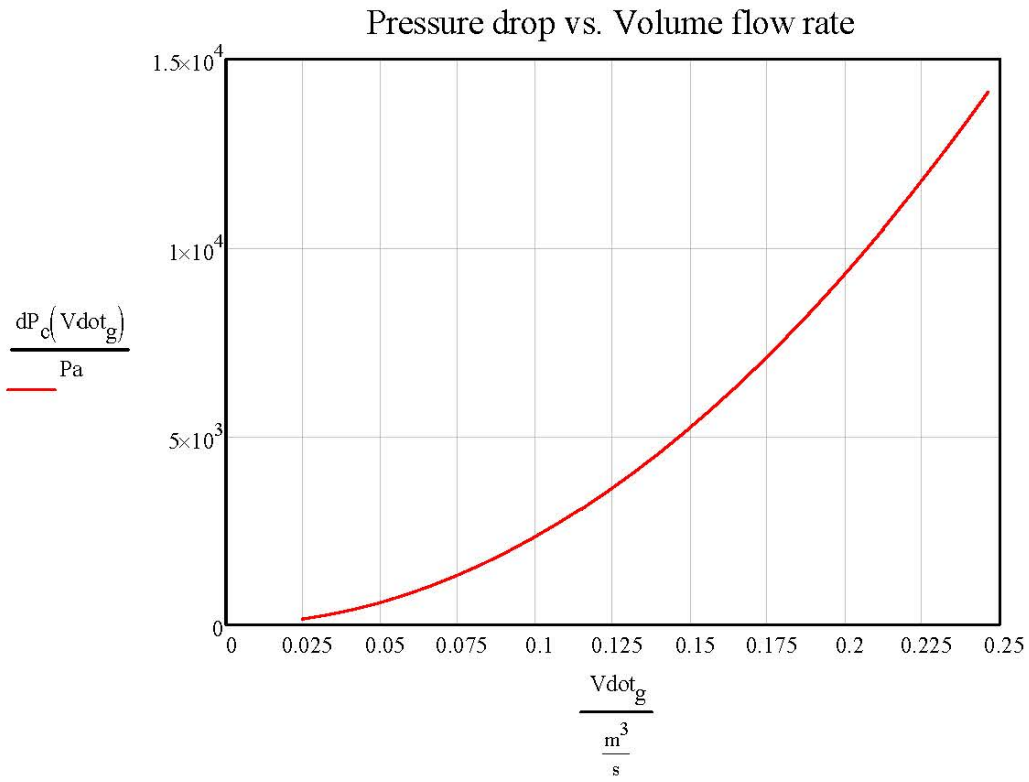

Pressure drop at kick in flowrate $dP_c(Vdot_{g.kickin}) = 3.533 \cdot kPa$

Orifice Basic Sizing

The following model calculates the expected pressure drops for orifices of varying pipe to orifice bore diameter ratios over a range of flow conditions.

1. Inputs

Gas temperature

$$T_g := \begin{pmatrix} 60 \\ 60 \end{pmatrix} °C$$

Gas absolute pressure

$$P_g := \begin{pmatrix} 70 \\ 125 \end{pmatrix} kPa$$

Pipe diameter

$$D_{pipe} := 102.26mm$$

Pressure ratio (assumed)

$$\tau := 95\%$$

Pipe to diameter ratio

$$\beta := \begin{pmatrix} 0.35 \\ 0.45 \\ 0.55 \\ 0.65 \\ 0.75 \end{pmatrix}$$

Velocity range

$$U_g := 6\frac{m}{s}, 7\frac{m}{s} .. 30\frac{m}{s} =$$

6	m/s
7	
8	
9	
10	
11	
12	
13	
14	
15	
16	
17	
18	
19	
20	
...	

2. Calculations

2.1. Intermediate calculations

Specific gas constant for air

$$R_g := 287.058 \frac{J}{kg \cdot K}$$

Gas density

$$\rho_g := \left(\frac{\overrightarrow{P_g}}{R_g \cdot T_g} \right) = \begin{pmatrix} 0.732 \\ 1.307 \end{pmatrix} \frac{kg}{m^3}$$

Reference temperature

$$T_{ref} := 273.15K$$

Reference dynamic viscosity

$$\mu_{ref} := 1.716 \times 10^{-5} \frac{kg}{m \cdot s}$$

Sutherland's constant

$$S1 := 110.4K$$

Gas dynamic viscosity

$$\mu_g := \left[\overrightarrow{\mu_{ref} \cdot \left(\frac{T_g}{T_{ref}} \right)^{\frac{3}{2}} \cdot \left(\frac{T_{ref} + S1}{T_g + S1} \right)} \right] = \begin{pmatrix} 1.999 \times 10^{-5} \\ 1.999 \times 10^{-5} \end{pmatrix} \frac{kg}{s \cdot m}$$

Pipe cross section area

$$A_{pipe} := \pi \cdot \frac{D_{pipe}^2}{4}$$

Diameter at vena contracta

$$D_{vc} := \beta \cdot D_{pipe} = \begin{pmatrix} 0.036 \\ 0.046 \\ 0.056 \\ 0.066 \\ 0.077 \end{pmatrix} m$$

Reynolds number in pipe

$$Re_D := \begin{pmatrix} \frac{\rho_{g_0} \cdot D_{pipe} \cdot U_g}{\mu_{g_0}} \\ \frac{\rho_{g_1} \cdot D_{pipe} \cdot U_g}{\mu_{g_1}} \end{pmatrix}$$

Length constant 1

$$L_1 := 1$$

Length constant 2

$$L_2 := 0.47$$

Constant 3 $$M_2 := \frac{2 \cdot L_2}{1 - \beta}$$

Constant 4 $$A_0 := \begin{bmatrix} \left(\frac{19000 \cdot \beta_0}{Re_{D_0}}\right)^{0.8} \\ \left(\frac{19000 \cdot \beta_1}{Re_{D_0}}\right)^{0.8} \\ \left(\frac{19000 \cdot \beta_2}{Re_{D_0}}\right)^{0.8} \\ \left(\frac{19000 \cdot \beta_3}{Re_{D_0}}\right)^{0.8} \\ \left(\frac{19000 \cdot \beta_4}{Re_{D_0}}\right)^{0.8} \end{bmatrix} \quad A_1 := \begin{bmatrix} \left(\frac{19000 \cdot \beta_0}{Re_{D_1}}\right)^{0.8} \\ \left(\frac{19000 \cdot \beta_1}{Re_{D_1}}\right)^{0.8} \\ \left(\frac{19000 \cdot \beta_2}{Re_{D_1}}\right)^{0.8} \\ \left(\frac{19000 \cdot \beta_3}{Re_{D_1}}\right)^{0.8} \\ \left(\frac{19000 \cdot \beta_4}{Re_{D_1}}\right)^{0.8} \end{bmatrix}$$

Gas isentropic exponent (at standard conditions) $\kappa := 1.4$

Gas expansibility factor $$\varepsilon_g := 1 - \left(0.351 + 0.256 \cdot \beta^4 + 0.93 \cdot \beta^8\right) \cdot \left[1 - (\tau)^{\frac{1}{\kappa}}\right]$$

Gas mass flow rate $$\dot{M}_g := \begin{pmatrix} \rho_{g_0} \cdot A_{pipe} \cdot U_g \\ \rho_{g_1} \cdot A_{pipe} \cdot U_g \end{pmatrix}$$

2.2. Discharge coefficient

Discharge coefficient at lower gas density

$$C_{d0_0} := 0.5961 + 0.0261 \cdot \left(\beta_0\right)^2 - 0.216 \cdot \left(\beta_0\right)^8 + 0.000521 \cdot \left(\frac{10^6 \cdot \beta_0}{Re_{D_0}}\right)^{0.7} \ldots$$
$$+ \left[\left(0.0188 + 0.0063 \cdot A_{0_0}\right) \cdot \left(\beta_0\right)^{3.5} \cdot \left(\frac{10^6}{Re_{D_0}}\right)^{0.3}\right] \ldots$$
$$+ \left(0.043 + 0.080 \cdot e^{-10 \cdot L_1} - 0.123 \cdot e^{-7 \cdot L_1}\right) \cdot \left(1 - 0.11 \cdot A_{0_0}\right) \cdot \frac{\left(\beta_0\right)^4}{1 - \left(\beta_0\right)^4} \ldots$$
$$+ 0 - 0.031 \cdot \left[M_{2_0} - 0.8 \cdot \left(M_{2_0}\right)^{1.1}\right] \cdot \left(\beta_0\right)^{1.3}$$

$$C_{d0_1} := 0.5961 + 0.0261\cdot(\beta_1)^2 - 0.216\cdot(\beta_1)^8 + 0.000521\cdot\left(\frac{10^6\cdot\beta_1}{Re_{D_0}}\right)^{0.7} \dots$$
$$+ \overrightarrow{\left[\left(0.0188 + 0.0063\cdot A_{0_1}\right)\cdot(\beta_1)^{3.5}\cdot\left(\frac{10^6}{Re_{D_0}}\right)^{0.3}\right]} \dots$$
$$+ \left(0.043 + 0.080\cdot e^{-10\cdot L_1} - 0.123\cdot e^{-7\cdot L_1}\right)\cdot\left(1 - 0.11\cdot A_{0_1}\right)\cdot\frac{(\beta_1)^4}{1-(\beta_1)^4} \dots$$
$$+ 0 - 0.031\cdot\left[M_{2_1} - 0.8\cdot\left(M_{2_1}\right)^{1.1}\right]\cdot(\beta_1)^{1.3}$$

$$C_{d0_2} := 0.5961 + 0.0261\cdot(\beta_2)^2 - 0.216\cdot(\beta_2)^8 + 0.000521\cdot\left(\frac{10^6\cdot\beta_2}{Re_{D_0}}\right)^{0.7} \dots$$
$$+ \overrightarrow{\left[\left(0.0188 + 0.0063\cdot A_{0_2}\right)\cdot(\beta_2)^{3.5}\cdot\left(\frac{10^6}{Re_{D_0}}\right)^{0.3}\right]} \dots$$
$$+ \left(0.043 + 0.080\cdot e^{-10\cdot L_1} - 0.123\cdot e^{-7\cdot L_1}\right)\cdot\left(1 - 0.11\cdot A_{0_2}\right)\cdot\frac{(\beta_2)^4}{1-(\beta_2)^4} \dots$$
$$+ 0 - 0.031\cdot\left[M_{2_2} - 0.8\cdot\left(M_{2_2}\right)^{1.1}\right]\cdot(\beta_2)^{1.3}$$

$$C_{d0_3} := 0.5961 + 0.0261\cdot(\beta_3)^2 - 0.216\cdot(\beta_3)^8 + 0.000521\cdot\left(\frac{10^6\cdot\beta_3}{Re_{D_0}}\right)^{0.7} \dots$$
$$+ \overrightarrow{\left[\left(0.0188 + 0.0063\cdot A_{0_3}\right)\cdot(\beta_3)^{3.5}\cdot\left(\frac{10^6}{Re_{D_0}}\right)^{0.3}\right]} \dots$$
$$+ \left(0.043 + 0.080\cdot e^{-10\cdot L_1} - 0.123\cdot e^{-7\cdot L_1}\right)\cdot\left(1 - 0.11\cdot A_{0_3}\right)\cdot\frac{(\beta_3)^4}{1-(\beta_3)^4} \dots$$
$$+ 0 - 0.031\cdot\left[M_{2_3} - 0.8\cdot\left(M_{2_3}\right)^{1.1}\right]\cdot(\beta_3)^{1.3}$$

$$C_{d0_4} := 0.5961 + 0.0261\cdot(\beta_4)^2 - 0.216\cdot(\beta_4)^8 + 0.000521\cdot\left(\frac{10^6\cdot\beta_4}{Re_{D_0}}\right)^{0.7} \dots$$
$$+\sqrt{\left[\left(0.0188 + 0.0063\cdot A_{0_4}\right)\cdot(\beta_4)^{3.5}\cdot\left(\frac{10^6}{Re_{D_0}}\right)^{0.3}\right]} \dots$$
$$+\left(0.043 + 0.080\cdot e^{-10\cdot L_1} - 0.123\cdot e^{-7\cdot L_1}\right)\cdot\left(1 - 0.11\cdot A_{0_4}\right)\cdot\frac{(\beta_4)^4}{1-(\beta_4)^4} \dots$$
$$+0 - 0.031\cdot\left[M_{2_4} - 0.8\cdot\left(M_{2_4}\right)^{1.1}\right]\cdot(\beta_4)^{1.3}$$

Discharge coefficient at higher gas density

$$C_{d1_0} := 0.5961 + 0.0261\cdot(\beta_0)^2 - 0.216\cdot(\beta_0)^8 + 0.000521\cdot\left(\frac{10^6\cdot\beta_0}{Re_{D_1}}\right)^{0.7} \dots$$
$$+\sqrt{\left[\left(0.0188 + 0.0063\cdot A_{1_0}\right)\cdot(\beta_0)^{3.5}\cdot\left(\frac{10^6}{Re_{D_1}}\right)^{0.3}\right]} \dots$$
$$+\left(0.043 + 0.080\cdot e^{-10\cdot L_1} - 0.123\cdot e^{-7\cdot L_1}\right)\cdot\left(1 - 0.11\cdot A_{1_0}\right)\cdot\frac{(\beta_0)^4}{1-(\beta_0)^4} \dots$$
$$+0 - 0.031\cdot\left[M_{2_0} - 0.8\cdot\left(M_{2_0}\right)^{1.1}\right]\cdot(\beta_0)^{1.3}$$

$$C_{d1_1} := 0.5961 + 0.0261\cdot(\beta_1)^2 - 0.216\cdot(\beta_1)^8 + 0.000521\cdot\left(\frac{10^6\cdot\beta_1}{Re_{D_1}}\right)^{0.7} \dots$$
$$+\sqrt{\left[\left(0.0188 + 0.0063\cdot A_{1_1}\right)\cdot(\beta_1)^{3.5}\cdot\left(\frac{10^6}{Re_{D_1}}\right)^{0.3}\right]} \dots$$
$$+\left(0.043 + 0.080\cdot e^{-10\cdot L_1} - 0.123\cdot e^{-7\cdot L_1}\right)\cdot\left(1 - 0.11\cdot A_{1_1}\right)\cdot\frac{(\beta_1)^4}{1-(\beta_1)^4} \dots$$
$$+0 - 0.031\cdot\left[M_{2_1} - 0.8\cdot\left(M_{2_1}\right)^{1.1}\right]\cdot(\beta_1)^{1.3}$$

$$C_{dl_2} := 0.5961 + 0.0261\cdot(\beta_2)^2 - 0.216\cdot(\beta_2)^8 + 0.000521\cdot\left(\frac{10^6\cdot\beta_2}{Re_{D_1}}\right)^{0.7} \dots$$
$$+ \overrightarrow{\left[\left(0.0188 + 0.0063\cdot A1_2\right)\cdot(\beta_2)^{3.5}\cdot\left(\frac{10^6}{Re_{D_1}}\right)^{0.3}\right]} \dots$$
$$+ \left(0.043 + 0.080\cdot e^{-10\cdot L_1} - 0.123\cdot e^{-7\cdot L_1}\right)\cdot\left(1 - 0.11\cdot A1_2\right)\cdot\frac{(\beta_2)^4}{1-(\beta_2)^4} \dots$$
$$+ 0 - 0.031\cdot\left[M2_2 - 0.8\cdot(M2_2)^{1.1}\right]\cdot(\beta_2)^{1.3}$$

$$C_{dl_3} := 0.5961 + 0.0261\cdot(\beta_3)^2 - 0.216\cdot(\beta_3)^8 + 0.000521\cdot\left(\frac{10^6\cdot\beta_3}{Re_{D_1}}\right)^{0.7} \dots$$
$$+ \overrightarrow{\left[\left(0.0188 + 0.0063\cdot A1_3\right)\cdot(\beta_3)^{3.5}\cdot\left(\frac{10^6}{Re_{D_1}}\right)^{0.3}\right]} \dots$$
$$+ \left(0.043 + 0.080\cdot e^{-10\cdot L_1} - 0.123\cdot e^{-7\cdot L_1}\right)\cdot\left(1 - 0.11\cdot A1_3\right)\cdot\frac{(\beta_3)^4}{1-(\beta_3)^4} \dots$$
$$+ 0 - 0.031\cdot\left[M2_3 - 0.8\cdot(M2_3)^{1.1}\right]\cdot(\beta_3)^{1.3}$$

$$C_{dl_4} := 0.5961 + 0.0261\cdot(\beta_4)^2 - 0.216\cdot(\beta_4)^8 + 0.000521\cdot\left(\frac{10^6\cdot\beta_4}{Re_{D_1}}\right)^{0.7} \dots$$
$$+ \overrightarrow{\left[\left(0.0188 + 0.0063\cdot A1_4\right)\cdot(\beta_4)^{3.5}\cdot\left(\frac{10^6}{Re_{D_1}}\right)^{0.3}\right]} \dots$$
$$+ \left(0.043 + 0.080\cdot e^{-10\cdot L_1} - 0.123\cdot e^{-7\cdot L_1}\right)\cdot\left(1 - 0.11\cdot A1_4\right)\cdot\frac{(\beta_4)^4}{1-(\beta_4)^4} \dots$$
$$+ 0 - 0.031\cdot\left[M2_4 - 0.8\cdot(M2_4)^{1.1}\right]\cdot(\beta_4)^{1.3}$$

2.3. Pressure drop across orifice

Mass flow correlation

$$\dot{M}_g = \frac{C_d}{\sqrt{1-\beta^4}} \cdot \varepsilon_g \cdot \frac{\pi}{4} \cdot D_{vc}^{\ 2} \cdot \sqrt{2 \cdot dPorifice \cdot \rho_g}$$

Re-arranged for pressure drop

$$-\frac{8 \cdot \dot{M}_g^{\ 2} \cdot \left(\beta^4 - 1\right)}{\pi^2 \cdot C_d^{\ 2} \cdot D_{vc}^{\ 4} \cdot \rho_g \cdot \varepsilon_g^{\ 2}}$$

Pressure drop confidence

$\eta_o := 95\%$

Pressure drop at lower gas density

$$dP_{orifice.0} := \left[\begin{array}{l} -\frac{8 \cdot \left(\dot{M}_{g_0}\right)^2 \cdot \left[\left(\beta_0\right)^4 - 1\right]}{\pi^2 \cdot \left(C_{d0_0}\right)^2 \cdot \left(D_{vc_0}\right)^4 \cdot \rho_{g_0} \cdot \left(\varepsilon_{g_0}\right)^2} \\ -\frac{8 \cdot \left(\dot{M}_{g_0}\right)^2 \cdot \left[\left(\beta_1\right)^4 - 1\right]}{\pi^2 \cdot \left(C_{d0_1}\right)^2 \cdot \left(D_{vc_1}\right)^4 \cdot \rho_{g_0} \cdot \left(\varepsilon_{g_1}\right)^2} \\ -\frac{8 \cdot \left(\dot{M}_{g_0}\right)^2 \cdot \left[\left(\beta_2\right)^4 - 1\right]}{\pi^2 \cdot \left(C_{d0_2}\right)^2 \cdot \left(D_{vc_2}\right)^4 \cdot \rho_{g_0} \cdot \left(\varepsilon_{g_2}\right)^2} \\ -\frac{8 \cdot \left(\dot{M}_{g_0}\right)^2 \cdot \left[\left(\beta_3\right)^4 - 1\right]}{\pi^2 \cdot \left(C_{d0_3}\right)^2 \cdot \left(D_{vc_3}\right)^4 \cdot \rho_{g_0} \cdot \left(\varepsilon_{g_3}\right)^2} \\ -\frac{8 \cdot \left(\dot{M}_{g_0}\right)^2 \cdot \left[\left(\beta_4\right)^4 - 1\right]}{\pi^2 \cdot \left(C_{d0_4}\right)^2 \cdot \left(D_{vc_4}\right)^4 \cdot \rho_{g_0} \cdot \left(\varepsilon_{g_4}\right)^2} \end{array} \right]$$

Pressure drop at higher gas density

$$dP_{orifice.1} := \begin{bmatrix} -\frac{8\cdot\left(\dot{M}_{g_1}\right)^2\cdot\left[\left(\beta_0\right)^4-1\right]}{\pi^2\cdot\left(C_{dl_0}\right)^2\cdot\left(D_{vc_0}\right)^4\cdot\rho_{g_1}\cdot\left(\varepsilon_{g_0}\right)^2} \\ -\frac{8\cdot\left(\dot{M}_{g_1}\right)^2\cdot\left[\left(\beta_1\right)^4-1\right]}{\pi^2\cdot\left(C_{dl_1}\right)^2\cdot\left(D_{vc_1}\right)^4\cdot\rho_{g_1}\cdot\left(\varepsilon_{g_1}\right)^2} \\ -\frac{8\cdot\left(\dot{M}_{g_1}\right)^2\cdot\left[\left(\beta_2\right)^4-1\right]}{\pi^2\cdot\left(C_{dl_2}\right)^2\cdot\left(D_{vc_2}\right)^4\cdot\rho_{g_1}\cdot\left(\varepsilon_{g_2}\right)^2} \\ -\frac{8\cdot\left(\dot{M}_{g_1}\right)^2\cdot\left[\left(\beta_3\right)^4-1\right]}{\pi^2\cdot\left(C_{dl_3}\right)^2\cdot\left(D_{vc_3}\right)^4\cdot\rho_{g_1}\cdot\left(\varepsilon_{g_3}\right)^2} \\ -\frac{8\cdot\left(\dot{M}_{g_1}\right)^2\cdot\left[\left(\beta_4\right)^4-1\right]}{\pi^2\cdot\left(C_{dl_4}\right)^2\cdot\left(D_{vc_4}\right)^4\cdot\rho_{g_1}\cdot\left(\varepsilon_{g_4}\right)^2} \end{bmatrix}$$

2.3. Pressure loss

Pressure loss at lower gas density (after recovery)

$$d\omega_0 := \overrightarrow{\begin{bmatrix} \frac{\sqrt{1-\left(\beta_0\right)^4\cdot\left[1-\left(C_{d0_0}\right)^2\right]}-C_{d0_0}\cdot\left(\beta_0\right)^2}{\sqrt{1-\left(\beta_0\right)^4\cdot\left[1-\left(C_{d0_0}\right)^2\right]}+C_{d0_0}\cdot\left(\beta_0\right)^2}\cdot dP_{orifice.0_0} \\ \frac{\sqrt{1-\left(\beta_1\right)^4\cdot\left[1-\left(C_{d0_1}\right)^2\right]}-C_{d0_1}\cdot\left(\beta_1\right)^2}{\sqrt{1-\left(\beta_1\right)^4\cdot\left[1-\left(C_{d0_1}\right)^2\right]}+C_{d0_1}\cdot\left(\beta_1\right)^2}\cdot dP_{orifice.0_1} \\ \frac{\sqrt{1-\left(\beta_2\right)^4\cdot\left[1-\left(C_{d0_2}\right)^2\right]}-C_{d0_2}\cdot\left(\beta_2\right)^2}{\sqrt{1-\left(\beta_2\right)^4\cdot\left[1-\left(C_{d0_2}\right)^2\right]}+C_{d0_2}\cdot\left(\beta_2\right)^2}\cdot dP_{orifice.0_2} \\ \frac{\sqrt{1-\left(\beta_3\right)^4\cdot\left[1-\left(C_{d0_3}\right)^2\right]}-C_{d0_3}\cdot\left(\beta_3\right)^2}{\sqrt{1-\left(\beta_3\right)^4\cdot\left[1-\left(C_{d0_3}\right)^2\right]}+C_{d0_3}\cdot\left(\beta_3\right)^2}\cdot dP_{orifice.0_3} \\ \frac{\sqrt{1-\left(\beta_4\right)^4\cdot\left[1-\left(C_{d0_4}\right)^2\right]}-C_{d0_4}\cdot\left(\beta_4\right)^2}{\sqrt{1-\left(\beta_4\right)^4\cdot\left[1-\left(C_{d0_4}\right)^2\right]}+C_{d0_4}\cdot\left(\beta_4\right)^2}\cdot dP_{orifice.0_4} \end{bmatrix}}$$

Pressure loss at higher gas density (after recovery)

$$d\omega_1 := \left[\frac{\sqrt{1-(\beta_0)^4\cdot\left[1-\left(C_{dl_0}\right)^2\right]}-C_{dl_0}\cdot(\beta_0)^2}{\sqrt{1-(\beta_0)^4\cdot\left[1-\left(C_{dl_0}\right)^2\right]}+C_{dl_0}\cdot(\beta_0)^2}\cdot dP_{orifice.1_0} \quad \frac{\sqrt{1-(\beta_1)^4\cdot\left[1-\left(C_{dl_1}\right)^2\right]}-C_{dl_1}\cdot(\beta_1)^2}{\sqrt{1-(\beta_1)^4\cdot\left[1-\left(C_{dl_1}\right)^2\right]}+C_{dl_1}\cdot(\beta_1)^2}\cdot dP_{orifice.1_1} \right.$$
$$\left. \frac{\sqrt{1-(\beta_2)^4\cdot\left[1-\left(C_{dl_2}\right)^2\right]}-C_{dl_2}\cdot(\beta_2)^2}{\sqrt{1-(\beta_2)^4\cdot\left[1-\left(C_{dl_2}\right)^2\right]}+C_{dl_2}\cdot(\beta_2)^2}\cdot dP_{orifice.1_2} \quad \frac{\sqrt{1-(\beta_3)^4\cdot\left[1-\left(C_{dl_3}\right)^2\right]}-C_{dl_3}\cdot(\beta_3)^2}{\sqrt{1-(\beta_3)^4\cdot\left[1-\left(C_{dl_3}\right)^2\right]}+C_{dl_3}\cdot(\beta_3)^2}\cdot dP_{orifice.1_3} \right.$$
$$\left. \frac{\sqrt{1-(\beta_4)^4\cdot\left[1-\left(C_{dl_4}\right)^2\right]}-C_{dl_4}\cdot(\beta_4)^2}{\sqrt{1-(\beta_4)^4\cdot\left[1-\left(C_{dl_4}\right)^2\right]}+C_{dl_4}\cdot(\beta_4)^2}\cdot dP_{orifice.1_4} \right]$$

2.4 Adjust dP for uncertainty

Adjusted for uncertainty $$dP_{orifice.1} := \frac{dP_{orifice.1}}{\eta_o}$$

Adjusted for uncertainty $$dP_{orifice.0} := \eta_o \cdot dP_{orifice.0}$$

3. Selection

3.1. Pressure drop at lower gas density - uncertainty

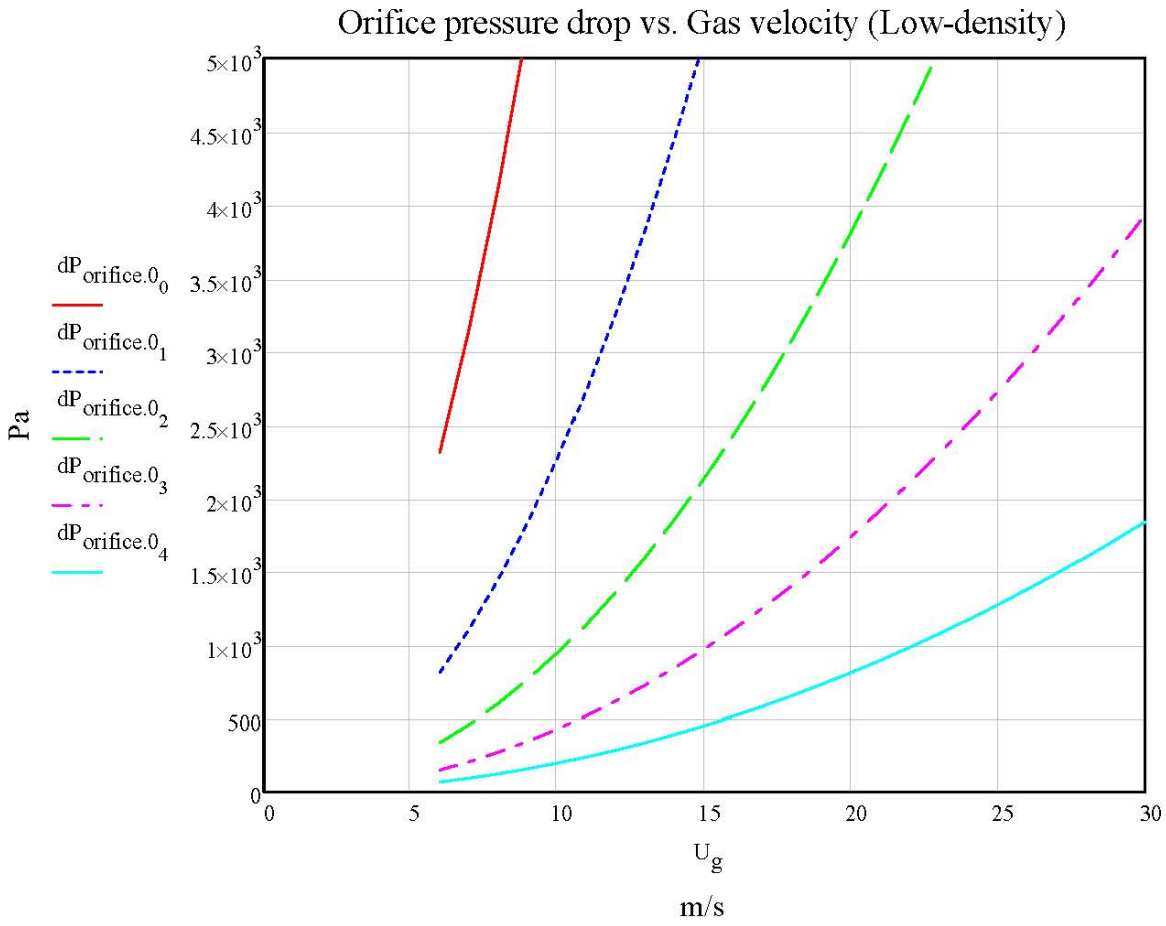

3.2 Pressure drop at higher gas density + uncertainty

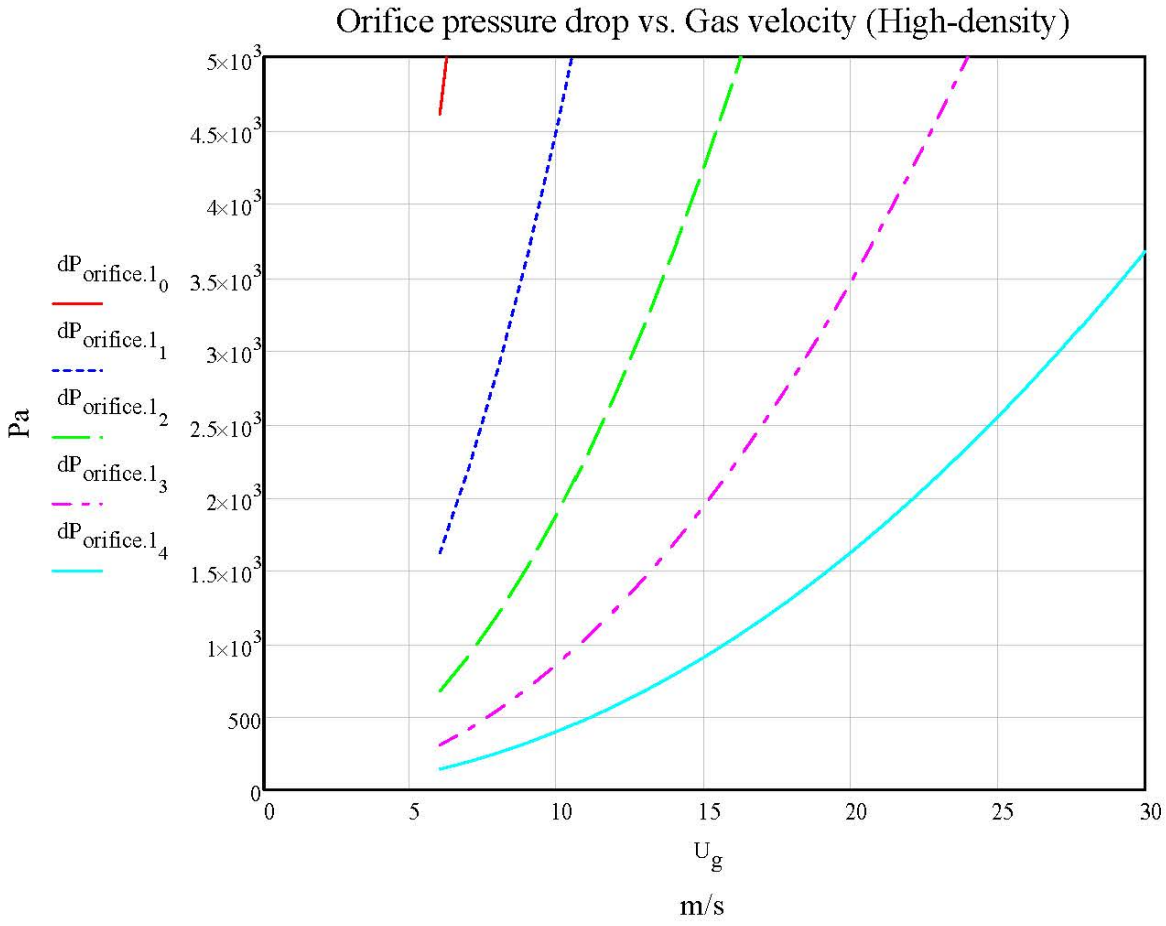

3.3. Plausible solutions

Orifice vena contracta to pipe diameter ratio

$$\beta = \begin{pmatrix} 0.35 \\ 0.45 \\ 0.55 \\ 0.65 \\ 0.75 \end{pmatrix}$$

Consider installing 2 orifices in parallel:

Operate 1 x β = 0.55 for 6 <= Ug <= 15 m/s

Operate 1 x β = 0.75 for 15 < Ug <= 30 m/s

4. Pressure drops

4.1. For dP Transducer

Minimum pressure drop

$$dP_{min} := \left(dP_{orifice.0_2}{}^{T}\right)^{\langle 0 \rangle} = (337.162)\,Pa$$

Maximum pressure drop

$$dP_{max} := \left(dP_{orifice.1_2}{}^{T}\right)^{\langle 9 \rangle} = (4.261)\cdot kPa$$

4.2. For System Pressure

Minimum pressure drop after recovery

$$d\omega_{min} := \left(d\omega_{0_2}{}^{T}\right)^{\langle 0 \rangle} = (240.707)\,Pa$$

Maximum pressure drop after recovery

$$d\omega_{max} := \left(d\omega_{1_2}{}^{T}\right)^{\langle 9 \rangle} = (2.757)\cdot kPa$$

Pipe, Feeder & Hopper Sizing

Particles :=

PC
FA

1. Inputs

1.1. Input particle flow rates

Min. mass flow rate of PC with rhobar of 750kg/m3 - 0.07kg/s (Auger Spec)
Min. mass flow rate of FA with rhobar of 860kg/m3 - 0.08kg/s (Auger Spec)
Max. mass flow rate of PC - 0.697kg/s (Auger Spec)
Max. mass flow rate of FA - 0.8kg/s (Auger Spec)

Min. mass flow rate

$$\dot{M}_{p_0} := \begin{cases} 0.07 & \text{if Particles} = 1 \\ 0.08 & \text{otherwise} \end{cases} \frac{kg}{s}$$

Max. mass flow rate

$$\dot{M}_{p_1} := \begin{cases} 0.697 & \text{if Particles} = 1 \\ 0.8 & \text{otherwise} \end{cases} \frac{kg}{s}$$

1.2. Input gas conditions

Gas pressure

$P_g := 70kPa$

Gas temperature

$T_g := 60°C$

1.3. Input particle properties

Particle density (PC - 1550kg/m3; FA - 2300kg/m3)

$$\rho_p := \begin{cases} 1550 & \text{if Particles} = 1 \\ 2300 & \text{otherwise} \end{cases} \frac{kg}{m^3}$$

Particle bulk density (PC - 750kg/m3; FA - 860kg/m3)

$$\rho bar_p := \begin{cases} 750 & \text{if Particles} = 1 \\ 860 & \end{cases} \frac{kg}{m^3}$$

Particle diameter

$D_p := 37\mu m$

1.4. Input test rig dimensions

Horiznotal test pipe diameter $D_{pipe.100} := 102.26mm$

Vertical test pipe diamater $D_{pipe.250} := 242.88mm$

Feed line pipe diameter $D_{pipe.80} := 77.92mm$

Acceleration line pipe diameter $D_{pipe.90} := 90.12mm$

2. Intermediate calculations

2.1 Gas properties

Calculate gas density

Specific gas constant for air $R_g := 287.058 \frac{J}{kg \cdot K}$

Gas density $\rho_g := \frac{P_g}{R_g \cdot T_g} = 0.731962 \frac{kg}{m^3}$

Calculate gas dynamic viscosity

Reference temperature $T_{ref} := 273.15K$

Reference dynamic viscosity $\mu_{ref} := 1.716 \times 10^{-5} \frac{kg}{m \cdot s}$

Sutherland's constant $S1 := 110.4K$

Gas dynamic viscosity $\mu_g := \left[\mu_{ref} \cdot \left(\frac{T_g}{T_{ref}} \right)^{\frac{3}{2}} \cdot \left(\frac{T_{ref} + S1}{T_g + S1} \right) \right] = 1.999 \times 10^{-5} \frac{kg}{s \cdot m}$

2.2 Superficial particle velocity

Cross section area of horziontal test pipe

$$A_{pipe.100} := \frac{\pi D_{pipe.100}^{2}}{4} = 8.213 \times 10^{-3}\,m^2$$

Cross section area of vertical test pipe

$$A_{pipe.250} := \frac{\pi D_{pipe.250}^{2}}{4} = 0.046\,m^2$$

Cross section area of feed pipe

$$A_{pipe.80} := \frac{\pi D_{pipe.80}^{2}}{4} = 4.769 \times 10^{-3}\,m^2$$

Cross section area of acceleration pipe

$$A_{pipe.90} := \frac{\pi D_{pipe.90}^{2}}{4} = 6.379 \times 10^{-3}\,m^2$$

Superficial particle velocities

$$U_{p.100} := \frac{\dot{M}_p}{A_{pipe.100} \cdot \rho_p} = \begin{pmatrix} 5.498762 \times 10^{-3} \\ 0.054752 \end{pmatrix} \frac{m}{s}$$

$$U_{p.250} := \frac{\dot{M}_p}{A_{pipe.250} \cdot \rho_p} = \begin{pmatrix} 9.747493 \times 10^{-4} \\ 9.705718 \times 10^{-3} \end{pmatrix} \frac{m}{s}$$

$$U_{p.80} := \frac{\dot{M}_p}{A_{pipe.80} \cdot \rho_p} = \begin{pmatrix} 9.470624 \times 10^{-3} \\ 0.0943 \end{pmatrix} \frac{m}{s}$$

$$U_{p.90} := \frac{\dot{M}_p}{A_{pipe.90} \cdot \rho_p} = \begin{pmatrix} 7.080014 \times 10^{-3} \\ 0.070497 \end{pmatrix} \frac{m}{s}$$

2.3 Particle terminal velocity

For Stokes flow

$$u_{t0.stokes} := \frac{D_p^{2} \cdot (\rho_p - \rho_g) \cdot g}{18 \cdot \mu_g} = 0.058\,\frac{m}{s}$$

Corresponding Reynolds number

$$Re_{t0.stokes} := \frac{\rho_g \cdot D_p \cdot u_{t0.stokes}}{\mu_g} = 0.078$$

Check or change to Intermeddiate flow

$$u_{t0} := \begin{cases} u_{t0.stokes} & \text{if } Re_{t0.stokes} < 1 \\ \left[\frac{8}{111}\cdot\frac{(\rho_g)^{0.6}\cdot(D_p)^{1.6}}{(\mu_g)^{0.6}}\cdot\frac{(\rho_p-\rho_g)}{\rho_g}\cdot g\right]^{\frac{5}{7}} & \text{otherwise} \end{cases} = 0.057813\,\frac{m}{s}$$

Corresponding Reynolds number $Re_{t0} := \frac{\rho_g \cdot D_p \cdot u_{t0}}{\mu_g} = 0.078$

3. Saltation calculations

Rizk constant 1 $R1 := \frac{1440}{m}\cdot D_p + 1.96 = 2.013$

Rizk constant 2 $R2 := \frac{1100}{m}\cdot D_p + 2.5 = 2.541$

Saltation velocities

$$U_{salt.100} := \left[\frac{4\cdot\frac{\dot{M}_p}{\frac{kg}{s}}\cdot 10^{R1}\cdot\left(\frac{g}{\frac{m}{s^2}}\right)^{\frac{R2}{2}}\cdot\left(\frac{D_{pipe.100}}{m}\right)^{\frac{R2}{2}-2}}{\pi\cdot\frac{\rho_g}{\frac{kg}{m^3}}}\right]^{\frac{1}{R2+1}}\cdot\frac{m}{s}$$

$$U_{salt.80} := \left[\frac{4\cdot\frac{\dot{M}_p}{\frac{kg}{s}}\cdot 10^{R1}\cdot\left(\frac{g}{\frac{m}{s^2}}\right)^{\frac{R2}{2}}\cdot\left(\frac{D_{pipe.80}}{m}\right)^{\frac{R2}{2}-2}}{\pi\cdot\frac{\rho_g}{\frac{kg}{m^3}}}\right]^{\frac{1}{R2+1}}\cdot\frac{m}{s}$$

$$U_{salt.90} := \left[\frac{4 \cdot \frac{\dot{M}_p}{\frac{kg}{s}} \cdot 10^{R1} \cdot \left(\frac{g}{\frac{m}{s^2}} \right)^{\frac{R2}{2}} \cdot \left(\frac{D_{pipe.90}}{m} \right)^{\frac{R2}{2}-2}}{\pi \cdot \frac{\rho_g}{\frac{kg}{m^3}}} \right]^{\frac{1}{R2+1}} \cdot \frac{m}{s}$$

Gas mass flow rates at saltation

$$\dot{M}_{g.salt.100} := \rho_g \cdot A_{pipe.100} \cdot U_{salt.100}$$

$$\dot{M}_{g.salt.80} := \rho_g \cdot A_{pipe.80} \cdot U_{salt.80}$$

$$\dot{M}_{g.salt.90} := \rho_g \cdot A_{pipe.90} \cdot U_{salt.90}$$

loading at saltation

$$z_{salt.100} := \frac{\dot{M}_p}{\dot{M}_{g.salt.100}}$$

$$z_{salt.80} := \frac{\dot{M}_p}{\dot{M}_{g.salt.80}}$$

$$z_{salt.90} := \frac{\dot{M}_p}{\dot{M}_{g.salt.90}}$$

4. Choking calculations

4.1. Vertical Test Pipe

Solid friction factor at choking

$$B\left(\alpha_{gc.250}, u_{gc.250}\right) := \frac{2 \cdot g \cdot D_{pipe.250} \cdot \left(\alpha_{gc.250}^{-4.7} - 1 \right)}{\left(u_{gc.250} - u_{t0} \right)^2} - 0.0$$

Slip velocity = Terminal velocity

$$D\left(\alpha_{gc.250}, u_{gc.250}\right) := \frac{U_{p.250}}{1 - \alpha_{gc.250}} - u_{gc.250} - u_{t0}$$

Guess $\alpha_{gc.250} := \begin{pmatrix} 0.99 \\ 0.99 \end{pmatrix}$ $u_{gc.250} := \begin{pmatrix} 5 \\ 5 \end{pmatrix} \frac{m}{s}$

Given

$$B(\alpha_{gc.250}, u_{gc.250}) = 0$$

$$D(\alpha_{gc.250}, u_{gc.250}) = 0$$

Voidage at choking Gas velocity at choking

Solve $\begin{pmatrix} \alpha_{gc.250} \\ u_{gc.250} \end{pmatrix} := \text{Find}(\alpha_{gc.250}, u_{gc.250})$

Choking velocity $U_{gc.250} := \overrightarrow{(\alpha_{gc.250} \cdot u_{gc.250})}$

Gas mass flow rate at choking $\dot{M}_{gc.250} := \rho_g \cdot A_{pipe.250} \cdot U_{gc.250}$

loading at choking $z_{c.250} := \dfrac{\dot{M}_p}{\dot{M}_{gc.250}}$

4.2. Acceleration Pipe

Solid friction factor at choking $E(\alpha_{gc.90}, u_{gc.90}) := \dfrac{2 \cdot g \cdot D_{pipe.90} \cdot \left(\alpha_{gc.90}^{-4.7} - 1\right)}{(u_{gc.90} - u_{t0})^2} - 0.01$

Slip velocity = Terminal velocity $I(\alpha_{gc.90}, u_{gc.90}) := \dfrac{U_{p.90}}{1 - \alpha_{gc.90}} - u_{gc.90} - u_{t0}$

Guess $\alpha_{gc.90} := \begin{pmatrix} 0.99 \\ 0.99 \end{pmatrix}$ $u_{gc.90} := \begin{pmatrix} 5 \\ 5 \end{pmatrix} \frac{m}{s}$

Given

$$E(\alpha_{gc.90}, u_{gc.90}) = 0$$

$$I(\alpha_{gc.90}, u_{gc.90}) = 0$$

Voidage at choking Gas velocity at choking

Solve $\begin{pmatrix} \alpha_{gc.90} \\ u_{gc.90} \end{pmatrix} := \text{Find}(\alpha_{gc.90}, u_{gc.90})$

Choking velocity $U_{gc.90} := \overrightarrow{\left(\alpha_{gc.90} \cdot u_{gc.90}\right)}$

Gas mass flow rate at choking $\dot{M}_{gc.90} := \rho_g \cdot A_{pipe.90} \cdot U_{gc.90}$

loading at choking $z_{c.90} := \frac{\dot{M}_p}{\dot{M}_{gc.90}}$

5. Check pipe sizes

5.1. Saltation Tests

HORIZONTAL TEST PIPE

Saltation velocity $U_{salt.100} = \begin{pmatrix} 7.416 \\ 14.192 \end{pmatrix} \frac{m}{s}$

Loading at saltation $z_{salt.100} = \begin{pmatrix} 1.57 \\ 8.169 \end{pmatrix}$

CHECK ACCELERATION PIPE

Saltation velocity $U_{salt.90} = \begin{pmatrix} 7.611 \\ 14.567 \end{pmatrix} \frac{m}{s}$

Loading at saltation $z_{salt.90} = \begin{pmatrix} 1.97 \\ 10.248 \end{pmatrix}$ must be > z.salt.100

Velocity in pipe during saltation tests

$U_{g.90} := \frac{\dot{M}_{g.salt.100}}{\left(\rho_g \cdot A_{pipe.90}\right)} = \begin{pmatrix} 9.548 \\ 18.274 \end{pmatrix} \frac{m}{s}$ must be > U.salt.90

CHECK FEED PIPE

Saltation velocity $U_{salt.80} = \begin{pmatrix} 7.843 \\ 15.01 \end{pmatrix} \frac{m}{s}$

Loading at saltation $z_{salt.80} = \begin{pmatrix} 2.557 \\ 13.304 \end{pmatrix}$ must be > z.salt.100

Velocity in pipe during saltation tests

$$U_{g.80} := \frac{\dot{M}_{g.salt.100}}{(\rho_g \cdot A_{pipe.80})} = \begin{pmatrix} 12.772 \\ 24.444 \end{pmatrix} \frac{m}{s}$$ must be > U.salt.80

CHECK IF CHOKING OCCURS IN 250NB VERTICAL TEST PIPE

Choking velocity $$U_{gc.250} = \begin{pmatrix} 1.317 \\ 2.81 \end{pmatrix} \frac{m}{s}$$

Loading at choking $$z_{c.250} = \begin{pmatrix} 1.567 \\ 7.315 \end{pmatrix}$$ must be > z.salt.100

Velocity in pipe during saltation tests $$U_{g.250s} := \frac{\dot{M}_{g.salt.100}}{(\rho_g \cdot A_{pipe.250})} = \begin{pmatrix} 1.315 \\ 2.516 \end{pmatrix} \frac{m}{s}$$ must be > U.gc.250

Not satisfied! Choking will occur if the 250NB test pipe is used during saltation tests

CHECK IF CHOKING OCCURS IN VERTICALACCELERATION PIPE

Choking velocity $$U_{gc.90} = \begin{pmatrix} 1.825 \\ 3.9 \end{pmatrix} \frac{m}{s}$$

Loading at choking $$z_{c.90} = \begin{pmatrix} 8.216 \\ 38.281 \end{pmatrix}$$ must be > z.salt.100

Velocity in pipe during saltation tests

$$U_{g.90s} := \frac{\dot{M}_{g.salt.100}}{(\rho_g \cdot A_{pipe.90})} = \begin{pmatrix} 9.548 \\ 18.274 \end{pmatrix} \frac{m}{s}$$ must be > U.gc.90

5.2. Choking Test Conditions

VERTICAL TEST PIPE

Choking velocity $$U_{gc.250} = \begin{pmatrix} 1.317 \\ 2.81 \end{pmatrix} \frac{m}{s}$$

Loading at choking $$z_{c.250} = \begin{pmatrix} 1.567 \\ 7.315 \end{pmatrix}$$

CHECK VERTICAL ACCELERATION PIPE

Choking velocity $U_{gc.90} = \begin{pmatrix} 1.825 \\ 3.9 \end{pmatrix} \frac{m}{s}$

Loading at choking $z_{c.90} = \begin{pmatrix} 8.216 \\ 38.281 \end{pmatrix}$ must be > z.c.250

Velocity in pipe during choking tests

$$U_{g.90c} := \frac{\dot{M}_{gc.250}}{(\rho_g \cdot A_{pipe.90})} = \begin{pmatrix} 9.569 \\ 20.409 \end{pmatrix} \frac{m}{s}$$ must be > U.gc.90

CHECK IF SALTATION OCCURS IN HORIZONTAL TEST PIPE

Saltation velocity $U_{salt.100} = \begin{pmatrix} 7.416 \\ 14.192 \end{pmatrix} \frac{m}{s}$

Loading at saltation $z_{salt.100} = \begin{pmatrix} 1.57 \\ 8.169 \end{pmatrix}$ must be > z.c.250

Velocity in pipe during choking tests

$$U_{g.100c} := \frac{\dot{M}_{gc.250}}{(\rho_g \cdot A_{pipe.100})} = \begin{pmatrix} 7.432 \\ 15.851 \end{pmatrix} \frac{m}{s}$$ must be > U.salt.100

CHECK IF SALTATION OCCURS IN HORIZONTAL ACCELERATION PIPE

Saltation velocity $U_{salt.90} = \begin{pmatrix} 7.611 \\ 14.567 \end{pmatrix} \frac{m}{s}$

Loading at saltation $z_{salt.90} = \begin{pmatrix} 1.97 \\ 10.248 \end{pmatrix}$ must be > z.c.250

Velocity in pipe during choking tests

$$U_{g.90c\_} := \frac{\dot{M}_{gc.250}}{(\rho_g \cdot A_{pipe.90})} = \begin{pmatrix} 9.569 \\ 20.409 \end{pmatrix} \frac{m}{s}$$ must be > U.salt.90

CHECK IF SALTATION OCCURS IN FEED PIPE

Saltation velocity $U_{salt.80} = \begin{pmatrix} 7.843 \\ 15.01 \end{pmatrix} \frac{m}{s}$

Loading at saltation $z_{salt.80} = \begin{pmatrix} 2.557 \\ 13.304 \end{pmatrix}$ must be > z.c.250

Velocity in pipe during choking tests

$U_{g.80c} := \frac{\dot{M}_{gc.250}}{(\rho_g \cdot A_{pipe.80})} = \begin{pmatrix} 12.8 \\ 27.3 \end{pmatrix} \frac{m}{s}$ must be > U.salt.80

6. Feed Rates & Basic Hopper Sizing

6.1. Feed Rates

Mass flow rate range $\dot{M}_p = \begin{pmatrix} 0.07 \\ 0.697 \end{pmatrix} \frac{kg}{s}$ $\dot{M}_p = \begin{pmatrix} 0.278 \\ 2.766 \end{pmatrix} \cdot \frac{ton}{hr}$

Volume flow rate range $Vdot_p := \frac{\dot{M}_p}{\rho_p} = \begin{pmatrix} 4.516 \times 10^{-5} \\ 4.497 \times 10^{-4} \end{pmatrix} \frac{m^3}{s}$ $Vdot_p = \begin{pmatrix} 2.71 \\ 26.981 \end{pmatrix} \cdot \frac{L}{min}$

6.2. Basic hopper sizing

Test time $t := 5min$

Calculations

Hopper mass capacity $M_p := \dot{M}_p \cdot t = \begin{pmatrix} 21 \\ 209.1 \end{pmatrix} kg$

Volume of hopper (must be less than 300L) $V_{hopper} := \frac{M_p}{\rho bar_p} = \begin{pmatrix} 24.419 \\ 243.14 \end{pmatrix} L$ $V_{hopper} = \begin{pmatrix} 0.024 \\ 0.243 \end{pmatrix} \cdot m^3$

Appendix N. Gas and Particle Flow Rate Analysis

Gas Mass Flow Rate Uncertainty Analysis

1. Temperature (Design stage)

Mean Temperature $T_g := EXCEL_8\,°C = 315.914\,K$

Unitless function for uncertainty calulations $T\_ := \frac{T_g - 273.15K}{K} = 42.764$

RTD

RTD instrument uncertainty at T.g $u_{c.RTD} := (0.1 + 0.0017T\_)\Delta°C = 0.173\cdot\Delta°C$ (95%)

$u_{0.RTD} := \frac{1}{2}\cdot u_{c.RTD} = 0.086\cdot\Delta°C$ (68%)

RTD design stage uncertainty $u_{d.RTD} := u_{c.RTD} = 0.086\cdot\Delta°C$ (68%)

Transmitter

Transmitter instrument uncertainty $u_{c.Trans} := 0.2\Delta°C$ (95%)

$u_{0.Trans} := \frac{1}{2}\cdot u_{c.Trans} = 0.1\cdot\Delta°C$ (68%)

Transmitter design stage uncertainty $u_{d.Trans} := u_{c.Trans} = 0.1\cdot\Delta°C$ (68%)

Combined RTD & Transmitter uncerta $u_{d.TR15} := \sqrt{u_{d.RTD}^2 + u_{d.Trans}^2} = 0.132\cdot\Delta°C$ (68%)

Converted to mA $u_{d.TR15} := \frac{u_{d.TR15}}{5}\cdot\frac{mA}{\Delta°C} = 0.026\cdot mA$ (68%)

NI9208 AI

NI9208 zero-order uncertainty $u_{0.AI} := \frac{1}{2}\cdot(42\mu A) = 21\cdot\mu A$ (95%)

$u_{0.AI} := \frac{1}{2}u_{0.AI} = 10.5\cdot\mu A$ (68%)

Measured signal assuming no error $T_{mA} := \frac{T\_ + 20}{5} \cdot mA = 12.553 \cdot mA$

NI9208 gain error on T.mA $u_1 := T_{mA} \cdot 0.76\% = 95.401 \cdot \mu A$ (95%)

$u_{1s} := \frac{1}{2} \cdot u_1 = 47.7 \cdot \mu A$ (68%)

NI9208 offset error $u_2 := 22mA \cdot 0.04\% = 8.8 \cdot \mu A$ (95%)

$u_{2s} := \frac{1}{2} \cdot u_2 = 4.4 \cdot \mu A$ (68%)

NI9208 noise error $u_3 := 200nA = 200 \cdot nA$ (95%)

$u_{3s} := \frac{1}{2} \cdot u_3 = 100 \cdot nA$ (68%)

N9208 instrument uncertainty $u_{c.AI} := \sqrt{(u_1)^2 + (u_2)^2 + u_3{}^2} = 0.048 \cdot mA$ (68%)

NI9208 design stage uncertainty $u_{d.AI} := \sqrt{u_{0.AI}{}^2 + u_{c.AI}{}^2} = 0.049 \cdot mA$ (68%)

System design stage uncertainty $u_{d.T.g} := \sqrt{u_{d.TR15}{}^2 + u_{d.AI}{}^2} = 0.056 \cdot mA$ (68%)

Converted to Temp $u_{d.T.g} := 5 \cdot u_{d.T.g} \cdot \frac{\Delta°C}{mA} = 0.279 \cdot \Delta°C$ (68%)

% Error $\%Error_{d.T.g} := \frac{u_{d.T.g}}{T\_ \cdot \Delta°C} = 0.651 \cdot \%$ (68%)

2. Absolute Pressure (Design stage)

Mean Pressure $P_1 := EXCEL_6\,kPa = 1.098 \times 10^5\,Pa$

PMP131

PMP131 instrument uncertainty $u_{c.PMP} := 160kPa \cdot 0.5\% = 800\,Pa$ (95%)

$u_{0.PMP} := \frac{1}{2} \cdot u_{c.PMP} = 400\,Pa$ (68%)

PMP131 design stage uncertainty $u_{d.PMP} := u_{c.PMP} = 400\,Pa$ (68%)

Converted to mA $u_{1.PMP} := \frac{u_{d.PMP}}{10} \cdot \frac{mA}{kPa} = 0.04 \cdot mA$ (68%)

NI9208 AI

NI9208 zero-order uncertainty $u_{0.AI} = 10.5 \cdot \mu A$ (68%)

Measured signal assuming no error $P_{mA} := \frac{P_1 + 40kPa}{10} \cdot \frac{mA}{kPa} = 14.977 \cdot mA$

NI9208 gain error on P.mA $u_4 := P_{mA} \cdot 0.76\% = 113.824 \cdot \mu A$ (95%)

$u_4 := \frac{1}{2} \cdot u_4 = 56.912 \cdot \mu A$ (68%)

NI9208 offset error $u_2 = 4.4 \cdot \mu A$ (68%)

NI9208 noise error $u_3 = 100 \cdot nA$ (68%)

N9208 instrument uncertainty $u_{0.AI} := \sqrt{(u_4)^2 + (u_2)^2 + u_3{}^2} = 0.057 \cdot mA$ (68%)

NI9208 design stage uncertainty $u_{1.AI} := \sqrt{u_{0.AI}{}^2 + u_{c.AI}{}^2} = 0.058 \cdot mA$ (68%)

System design stage uncertainty $u_{d.P.1} := \sqrt{u_{d.PMP}^{2} + u_{d.AI}^{2}} = 0.07 \cdot mA$ (68%)

Converted to Pressure $u_{d.P.1} := 10 \cdot u_{d.P.1} \cdot \frac{kPa}{mA} = 0.705 \cdot kPa$ (68%)

% Error $\%Error_{d.P.1} := \frac{u_{d.P.1}}{P_1} = 0.642 \cdot \%$ (68%)

3. Pressure drop (Design stage)

Mean pressure drop $dP := -EXCEL_4 \, kPa = -2.191 \times 10^{3} \, Pa$

Upper range value $URV := 0kPa$

Lower range value $LRV := -5kPa$

Turn down $TD := \frac{10kPa}{|LRV|} = 2$

Set span $Span := URV - LRV = 5 \cdot kPa$

PMD55

PMD55 zero-oder uncertainty $u_{0.PMD} := \frac{1}{2}(1 \mu A) = 0.5 \cdot \mu A$ (95%)

$u_{0.PMD} := \frac{1}{2} \cdot u_{0.PMD} = 0.25 \cdot \mu A$ (68%)

PMD55 instrument uncertainty $u_{c.PMD} := \begin{cases} (Span \cdot 0.1\%) & \text{if } TD \le 4 \\ [Span \cdot (0.012 \cdot TD + 0.052)\%] & \text{otherwise} \end{cases} = 5 \, Pa$ (95%)

$u_{o.PMD} := \frac{1}{2} \cdot u_{c.PMD} = 2.5 \, Pa$ (68%)

Converted to mA $u_{o.PMD} := \frac{u_{c.PMD}}{Span} \cdot 16mA = 8 \times 10^{-3} \cdot mA$ (68%)

PMD55 design stage uncertainty

$$u_{d.PMD} := \sqrt{u_{0.PMD}^{2} + u_{c.PMD}^{2}} = 8.004 \cdot \mu A \quad (68\%)$$

NI9208 AI

NI9208 zero-order uncertainty

$$u_{0.AI} = 10.5 \cdot \mu A \quad (68\%)$$

Measured signal assuming no error

$$dP_{mA} := \frac{\left(dP - URV + \frac{20}{16} \cdot Span\right) \cdot 16mA}{Span} = 12.989 \cdot mA$$

NI9208 gain error on dP.mA

$$u_5 := dP_{mA} \cdot 0.76\% = 98.713 \cdot \mu A \quad (95\%)$$

$$u_5 := \frac{1}{2} \cdot u_4 = 28.456 \cdot \mu A \quad (68\%)$$

NI9208 offset error

$$u_2 = 4.4 \cdot \mu A \quad (68\%)$$

NI9208 noise error

$$u_3 = 100 \cdot nA \quad (68\%)$$

N9208 instrument uncertainty

$$u_{c.AI} := \sqrt{(u_5)^2 + (u_2)^2 + u_3^{2}} = 28.794 \cdot \mu A \quad (68\%)$$

NI9208 design stage uncertainty

$$u_{d.AI} := \sqrt{u_{0.AI}^{2} + u_{c.AI}^{2}} = 30.649 \cdot \mu A \quad (68\%)$$

System design stage uncertainty

$$u_{d.dP} := \sqrt{u_{d.PMD}^{2} + u_{d.AI}^{2}} = 31.677 \cdot \mu A \quad (68\%)$$

Converted to Pressure

$$u_{d.dP} := \frac{Span}{16mA} \cdot u_{d.dP} = 9.899\,Pa \quad (68\%)$$

% Error

$$\%Error_{d.dP} := \frac{u_{d.dP}}{|dP|} = 0.452 \cdot \% \quad (68\%)$$

4. Combined design and statistical uncertainties of measured values

Statistical uncertainties of measured variables

Temperature	$u_{s.T.g} := EXCEL_9 \cdot \Delta°C = 0.675\,K$	(68%)
Pressure	$u_{s.P.1} := EXCEL_7\,kPa = 182.771\,Pa$	(68%)
Pessure drop	$u_{s.dP} := EXCEL_5\,kPa = 57.889\,Pa$	

Combined uncertainties of measured variables

Temperature	$u_{T.g} := \sqrt{u_{d.T.g}^2 + u_{s.T.g}^2} = 0.731 \cdot \Delta°C$	(68%)
Pressure	$u_{P.1} := \sqrt{u_{d.P.1}^2 + u_{s.P.1}^2} = 728.193\,Pa$	(68%)
Pressure drop	$u_{dP} := \sqrt{u_{d.dP}^2 + u_{s.dP}^2} = 58.729\,Pa$	(68%)

5. Gas flow rate uncertainty

Inputs

Specific gas constant for air	$R_g := 287.058\,\frac{J}{kg \cdot K}$
Orifice beta value	$\beta := 0.55$
Gas only pipe diameter	$D_{pipe} := 102.26mm$
Vena contracta	$D_{vc} := \beta \cdot D_{pipe} = 0.056\,m$
Pressure drop across orifice	$dP := -dP = 2.191 \cdot kPa$
Specific heat ratio	$\kappa := 1.4$

Mean calculated discharge coefficient $C_d := EXCEL_0 = 0.609$

Statistical uncertainty $u_{s.C.d} := EXCEL_1 = 4.25 \times 10^{-5}$ (68%)

Mean calculated gas expansibilty factor $\varepsilon_g := EXCEL_2 = 0.995$

Statistical uncertainty $u_{s.\varepsilon.g} := EXCEL_3 = 1.451 \times 10^{-4}$ (68%)

Uncertainty on density

Calculated density $\rho_1 := \frac{P_1}{R_g \cdot T_g} = 1.21 \frac{kg}{m^3}$

Uncertainty on gas temperature $u_{T.g\_} := 2u_{T.g} = 1.461 \cdot \Delta°C$ (95%)

Uncertainty on gas pressure $u_{P.1\_} := 2u_{P.1} = 1.456 \cdot kPa$ (95%)

Uncertainty on pressure drop $u_{dP\_} := 2 \cdot u_{dP} = 117.459\,Pa$ (95%)

Uncertainty on density

$$u_{\rho 1\_} := \sqrt{\left[\left(\frac{1}{R_g \cdot T_g}\right) \cdot u_{P.1\_}\right]^2 + \left[\left(\frac{-P_1}{R_g \cdot T_g^{\,2}}\right) \cdot u_{T.g\_}\right]^2} = 0.017 \frac{kg}{m^3} \quad (95\%)$$

Uncertainty on discharge coefficient

Design based uncertainty $u_{d.C.d\_} := 0.5\% \cdot C_d = 3.046 \times 10^{-3}$ (95%)

$u_{s.C.d\_} := 2 \cdot u_{s.C.d} = 8.5 \times 10^{-5}$ (95%)

Combined uncertainty $u_{C.d\_} := \sqrt{u_{d.C.d\_}^{\,2} + u_{s.C.d\_}^{\,2}} = 3.047 \times 10^{-3}$ (95%)

Uncertainty on gas expansibilty factor

Design based uncertainty

$$u_{d.\varepsilon.g\_} := \left(\frac{3.5 \cdot dP}{\kappa \cdot P_1}\%\right) \cdot \varepsilon_g = 4.963 \times 10^{-4} \quad (95\%)$$

$$u_{s.\varepsilon.g\_} := 2 \cdot u_{s.\varepsilon.g} = 2.902 \times 10^{-4} \quad (95\%)$$

Combined uncertainty

$$u_{\varepsilon.g\_} := \sqrt{u_{d.\varepsilon.g\_}^{\ 2} + u_{s.\varepsilon.g\_}^{\ 2}} = 5.749 \times 10^{-4} \quad (95\%)$$

Uncertainty on pipe diameter

$$u_{D.pipe\_} := 0.4\% \cdot D_{pipe} = 0.409 \cdot mm \quad (95\%)$$

Uncertainty on vena contracta

$$u_{D.vc\_} := 0.1\% \cdot D_{vc} = 0.056 \cdot mm \quad (95\%)$$

Uncertainty on mass flow rate

Calculated mass flow rate

$$\dot{M}_g := \frac{C_d}{\sqrt{1 - \beta^4}} \cdot \varepsilon_g \cdot \frac{\pi}{4} \cdot D_{vc}^{\ 2} \cdot \sqrt{2 \cdot dP \cdot \rho_1} = 0.115 \frac{kg}{s}$$

Uncertainty

$$u_{Mdot.g\_} := \dot{M}_g \cdot \sqrt{\left(\frac{u_{C.d\_}}{C_d}\right)^2 + \left(\frac{u_{\varepsilon.g\_}}{\varepsilon_g}\right)^2 + \left(\frac{2\beta^4}{1 - \beta^4}\right)^2 \cdot \left(\frac{u_{D.pipe\_}}{D_{pipe}}\right)^2 \ldots + \left(\frac{2}{1 - \beta^4}\right)^2 \cdot \left(\frac{u_{D.vc\_}}{D_{vc}}\right)^2 + \frac{1}{4} \cdot \left(\frac{u_{dP\_}}{dP}\right)^2 + \left(\frac{u_{\rho 1\_}}{\rho_1}\right)^2} = 3.539 \times 10^{-3} \frac{kg}{s} \quad (95\%)$$

$$u_{Mdot.g} := \frac{1}{2} u_{Mdot.g\_} = 1.769 \times 10^{-3} \frac{kg}{s} \quad (68\%)$$

% Error

$$\%Error_{Mdot.g} := \frac{u_{Mdot.g}}{\dot{M}_g} = 1.538 \cdot \% \quad (68\%)$$

Loss/ Gain in weight calibration, uncertainty and flow rate analysis

All values in kg unless otherwise stated

Hopper :=

Loss in Weight
Gain in Weight

Calibration data and curve fitting calculations

Calibration data

$$X_{LIW} := \begin{pmatrix} 0.110 \\ 20.191 \\ 60.125 \\ 119.989 \\ 180.081 \\ 240.091 \\ 280.181 \\ 300.550 \end{pmatrix} \quad u_{X.LIW} := \begin{pmatrix} 4.505 \\ 4.511 \\ 4.526 \\ 4.558 \\ 4.601 \\ 4.655 \\ 4.696 \\ 4.719 \end{pmatrix} \quad X_{GIW} := \begin{pmatrix} -0.075 \\ 20.427 \\ 62.749 \\ 123.672 \\ 186.055 \\ 244.795 \\ 283.459 \\ 304.650 \end{pmatrix} \quad u_{X.GIW} := \begin{pmatrix} 2.129 \\ 2.141 \\ 2.173 \\ 2.238 \\ 2.325 \\ 2.43 \\ 2.509 \\ 2.551 \end{pmatrix}$$

Indicated mass at calibration points (statistical uncertainty not recorded, therefore ignored)

$$X := \begin{cases} X_{LIW} & \text{if Hopper} = 1 \\ X_{GIW} & \text{otherwise} \end{cases} = \begin{pmatrix} -0.075 \\ 20.427 \\ 62.749 \\ 123.672 \\ 186.055 \\ 244.795 \\ 283.459 \\ 304.65 \end{pmatrix}$$

Instrument uncertainty (from design stage uncertainty analysis)

$$u_X := \begin{cases} u_{X.LIW} & \text{if Hopper} = 1 \\ u_{X.GIW} & \text{otherwise} \end{cases} = \begin{pmatrix} 2.129 \\ 2.141 \\ 2.173 \\ 2.238 \\ 2.325 \\ 2.43 \\ 2.509 \\ 2.551 \end{pmatrix}$$

Actual mass at calibration points

$$Y := \begin{pmatrix} 0 \\ 20 \\ 60 \\ 120 \\ 180 \\ 240 \\ 280 \\ 300 \end{pmatrix}$$

Uncertainty of mass pieces (1g per 20kg)

$$u_Y := \begin{pmatrix} 0 \\ 0.001 \\ 3\sqrt{0.001} \\ 6\sqrt{0.001} \\ 9\sqrt{0.001} \\ 12\sqrt{0.001} \\ 14\sqrt{0.001} \\ 15\sqrt{0.001} \end{pmatrix} = \begin{pmatrix} 0.000 \\ 0.001 \\ 0.095 \\ 0.190 \\ 0.285 \\ 0.379 \\ 0.443 \\ 0.474 \end{pmatrix}$$

Curve fitting calculations

Alpha matrix

$$\text{alpha\_matrix}(m\_,n\_,X\_) := \left| \begin{array}{l} \text{for } j \in 0..m\_ \\ \quad \text{for } k \in 0..m\_ \\ \quad\quad \alpha'_{j,k} \leftarrow 0 \\ \quad\quad \text{for } i \in 0..n\_ - 1 \\ \quad\quad\quad \alpha'_{j,k} \leftarrow \alpha'_{j,k} + \left(X_{\_i}\right)^{j} \cdot \left(X_{\_i}\right)^{k} \\ \alpha' \end{array} \right.$$

Beta vector

$$\text{beta\_vector}(m\_,n\_,X\_,Y\_) := \left| \begin{array}{l} \text{for } k \in 0..m\_ \\ \quad \beta'_k \leftarrow 0 \\ \quad \text{for } i \in 0..n\_ - 1 \\ \quad\quad \beta'_k \leftarrow \beta'_k + Y_{\_i} \cdot \left(X_{\_i}\right)^{k} \\ \beta' \end{array} \right.$$

Curve fitting constants

$$a(m\_,n,X\_,Y\_) := \left(\text{alpha\_matrix}(m\_,n,X\_)^{-1}\right) \cdot \text{beta\_vector}(m\_,n,X\_,Y\_)$$

Calibration equation

$$y\_poly(m\_,n,x\_,X\_,Y\_) := \left| \begin{array}{l} \text{for } k \in 0..m\_ \\ \quad F_k \leftarrow x\_^{k} \\ y \leftarrow a(m\_,n,X\_,Y\_)^{T} F \end{array} \right.$$

System uncertainty calculations (includes instrument, calibration weights and calibration curve fitting uncertainties)

%/100 change in X $\Delta X := 0.01$

%/100 change in Y $\Delta Y := 0.01$

Change in Y if zero $\Delta Y_0 := 0.01$

Perturbed Vectors

$$X_{pf}(n,i) := \begin{| for\ I \in 0..n-1 \\ \quad X_{pf_I} \leftarrow X_I \\ X_{pf_i} \leftarrow X_i + \Delta X \cdot X_i \\ X_{pf}} \qquad X_{pb}(n,i) := \begin{| for\ I \in 0..n-1 \\ \quad X_{pb_I} \leftarrow X_I \\ X_{pb_i} \leftarrow X_i - \Delta X \cdot X_i \\ X_{pb}}$$

$$Y_{pf}(n,i) := \begin{| for\ I \in 0..n-1 \\ \quad Y_{pf_I} \leftarrow Y_I \\ Y_{pf_i} \leftarrow Y_i + \Delta Y \ \text{if}\ Y_i = 0 \\ Y_{pf_i} \leftarrow Y_i + \Delta Y \cdot Y_i \ \text{otherwise} \\ Y_{pf}} \qquad Y_{pb}(n,i) := \begin{| for\ I \in 0..n-1 \\ \quad Y_{pb_I} \leftarrow Y_I \\ Y_{pb_i} \leftarrow Y_i + \Delta Y \ \text{if}\ Y_i = 0 \\ Y_{pb_i} \leftarrow Y_i + \Delta Y \cdot Y_i \ \text{otherwise} \\ Y_{pb}}$$

Partial derivative of y wrt X

$$dydXi(m\_,x\_,n,i) := \frac{y\_poly(m\_,n,x\_,X_{pf}(n,i),Y) - y\_poly(m\_,n,x\_,X_{pb}(n,i),Y)}{2 \cdot \Delta X \cdot X_i}$$

In vector form

$$dydX\_vector(m\_,x\_,n) := \begin{| for\ i \in 0..n-1 \\ \quad dydX_i \leftarrow dydXi(m\_,x\_,n,i) \\ dydX}$$

Uncertainty in y wrt X

$$uy_X(m\_,x,n) := \begin{| dydX \leftarrow dydX\_vector(m\_,x,n) \\ uy_X \leftarrow 0 \\ for\ i \in 0..n-1 \\ \quad uy_X \leftarrow uy_X + \left(dydX_i \cdot u_{X_i}\right)^2 \\ uy_X \leftarrow \sqrt{uy_X}}$$

Partial derivative of y wrt Y

$$dydYi(m\_,x\_,n,i) := \begin{cases} \dfrac{y\_poly\left(m\_,n,x\_,X,Y_{pf}(n,i)\right) - y\_poly\left(m\_,n,x\_,X,Y_{pb}(n,i)\right)}{2\cdot\Delta Y} & \text{if } Y_i = 0 \\ \dfrac{y\_poly\left(m\_,n,x\_,X,Y_{pf}(n,i)\right) - y\_poly\left(m\_,n,x\_,X,Y_{pb}(n,i)\right)}{2\cdot\Delta Y\cdot Y_i} & \text{otherwise} \end{cases}$$

In vector form

$$dydY\_vector(m\_,x\_,n) := \left| \begin{array}{l} \text{for } i \in 0..n-1 \\ \quad dydY_i \leftarrow dydYi(m\_,x\_,n,i) \\ dydY \end{array} \right.$$

Uncertainty in y wrt Y

$$uy_Y(m\_,x,n) := \left| \begin{array}{l} dydY \leftarrow dydY\_vector(m\_,x,n) \\ uy_Y \leftarrow 0 \\ \text{for } i \in 0..n-1 \\ \quad uy_Y \leftarrow uy_Y + \left(dydY_i\cdot u_{Y_i}\right)^2 \\ uy_Y \leftarrow \sqrt{uy_Y} \end{array} \right.$$

Total uncertainty

$$uy(m\_,x,n) := \sqrt{uy_X(m\_,x,n)^2 + uy_Y(m\_,x,n)^2}$$

In vector form

$$y\_vector(m\_,n,x\_,X\_,Y\_,points\_) := \left| \begin{array}{l} \text{for } l \in 0..points\_-1 \\ \quad y_{\_l} \leftarrow y\_poly\left(m\_,n,x_{\_l},X\_,Y\_\right) \\ y\_ \end{array} \right.$$

$$uy\_vector(m\_,x\_,n,points\_) := \left| \begin{array}{l} \text{for } l \in 0..points\_-1 \\ \quad u_{\_l} \leftarrow uy\left(m\_,x_{\_l},n\right) \\ u\_ \end{array} \right.$$

Test data

Time at measured datapoints (from test data) (s)

$$Tm := \begin{pmatrix} 915 \\ 992 \\ 1069 \\ 1146 \\ 1223 \\ 1300 \\ 1377 \\ 1454 \\ 1531 \\ 1610 \end{pmatrix}$$

Mean values of measured uncalibrated datapoints (from test data)

$$x\_LIW := \begin{pmatrix} 166.765 \\ 151.423 \\ 135.464 \\ 120.056 \\ 104.729 \\ 89.394 \\ 73.998 \\ 58.569 \\ 43.125 \\ 27.634 \end{pmatrix} \quad x\_GIW := \begin{pmatrix} 112.497 \\ 128.008 \\ 143.822 \\ 159.404 \\ 174.737 \\ 190.321 \\ 205.649 \\ 220.832 \\ 236.085 \\ 251.407 \end{pmatrix}$$

$$x\_vector := \begin{cases} x\_LIW & \text{if } Hopper = 1 \\ x\_GIW & \text{otherwise} \end{cases}$$

Statistical uncertainty of calibrated datapoints (from test data)

$$uy\_stat\_LIW := \begin{pmatrix} 0.122393055 \\ 0.008688824 \\ 0.010701773 \\ 0.009337144 \\ 0.074027335 \\ 0.006247901 \\ 0.005899187 \\ 0.069816103 \\ 0.007420909 \\ 0.005608277 \end{pmatrix} \quad uy\_stat\_GIW := \begin{pmatrix} 0.066169326 \\ 0.081314155 \\ 0.060966541 \\ 0.042492681 \\ 0.580041499 \\ 0.055393997 \\ 0.063836 \\ 0.551692606 \\ 0.093173085 \\ 0.047612318 \end{pmatrix}$$

$$uy\_stat := \begin{cases} uy\_stat\_LIW & \text{if } Hopper = 1 \\ uy\_stat\_GIW & \text{otherwise} \end{cases}$$

Results: Combined system and statistical uncertainty of data

Calculations

Number of calibration points $n := \text{length}(X) = 8$

Order of calibration polynomial $mn := 1$

no. of measured datapoints $points := \text{length}(x\_vector) = 10$

Combined uncertainty

$$uy\_combined(m\_, x\_, n, points\_) := \sqrt{(uy\_vector(m\_, x\_, n, points\_))^2 + uy\_stat^2}$$

Results

Calibrated values

$$y\_vector(mn, n, x\_vector, X, Y, points) = \begin{pmatrix} 109.849 \\ 125.144 \\ 140.737 \\ 156.101 \\ 171.22 \\ 186.586 \\ 201.7 \\ 216.671 \\ 231.711 \\ 246.819 \end{pmatrix}$$

Combined uncertainty

$$uy\_combined(mn, x\_vector, n, points) = \begin{pmatrix} 0.825 \\ 0.808 \\ 0.804 \\ 0.816 \\ 1.023 \\ 0.887 \\ 0.941 \\ 1.143 \\ 1.075 \\ 1.149 \end{pmatrix}$$

System uncertainty component

$$uy\_vector(mn, x\_vector, n, points) = \begin{pmatrix} 0.823 \\ 0.804 \\ 0.802 \\ 0.815 \\ 0.843 \\ 0.885 \\ 0.939 \\ 1.001 \\ 1.071 \\ 1.148 \end{pmatrix}$$

Statistical uncertainty component

$$uy\_stat = \begin{pmatrix} 0.066 \\ 0.081 \\ 0.061 \\ 0.042 \\ 0.580 \\ 0.055 \\ 0.064 \\ 0.552 \\ 0.093 \\ 0.048 \end{pmatrix}$$

Mass flow rate calculations

Data

Calibrated mass at measured points

$$M := y\_vector(mn, n, x\_vector, X, Y, points) = \begin{pmatrix} 109.849 \\ 125.144 \\ 140.737 \\ 156.101 \\ 171.22 \\ 186.586 \\ 201.7 \\ 216.671 \\ 231.711 \\ 246.819 \end{pmatrix}$$

Uncertainty of mass at measured points

$$u_M := uy\_combined(mn, x\_vector, n, points) = \begin{pmatrix} 0.825 \\ 0.808 \\ 0.804 \\ 0.816 \\ 1.023 \\ 0.887 \\ 0.941 \\ 1.143 \\ 1.075 \\ 1.149 \end{pmatrix}$$

Curve fitting calculations

Alpha matrix

$$\begin{aligned} &Alpha\_matrix(m\_, points\_) := \\ &\quad \text{for } j \in 0..m\_ \\ &\quad\quad \text{for } k \in 0..m\_ \\ &\quad\quad\quad \alpha'_{j,k} \leftarrow 0 \\ &\quad\quad\quad \text{for } i \in 0..points\_ - 1 \\ &\quad\quad\quad\quad \alpha'_{j,k} \leftarrow \alpha'_{j,k} + \left(Tm_i\right)^j \cdot \left(Tm_i\right)^k \\ &\quad \alpha' \end{aligned}$$

Beta vector

$$\begin{aligned} &Beta\_vector(m\_, points\_) := \\ &\quad \text{for } k \in 0..m\_ \\ &\quad\quad \beta'_k \leftarrow 0 \\ &\quad\quad \text{for } i \in 0..points\_ - 1 \\ &\quad\quad\quad \beta'_k \leftarrow \beta'_k + M_i \cdot \left(Tm_i\right)^k \\ &\quad \beta' \end{aligned}$$

Order of curve fit

$$Mn := 1$$

Curve fitting constants

$$\alpha := Alpha\_matrix(Mn, points)$$

$$\beta := Beta\_vector(Mn, points)$$

$$\varepsilon := \alpha^{-1}$$

$$a2 := \varepsilon \cdot \beta$$

Gradient of curve fit i.e. avg. mass flow rate

$$Mdot := a2_1$$

Let the gradient be "a", then the partial derivative of a wrt M

$$dadMi(m\_, i, t\_) := \begin{array}{l} dadMi\_ \leftarrow 0 \\ \text{for } k \in 0 .. m\_ \\ \quad dummy \leftarrow 0 \\ \quad \text{for } j \in 0 .. m\_ \\ \quad\quad dummy \leftarrow dummy + \varepsilon_{k,j} \cdot j \cdot t\_^{j-1} \\ \quad dadMi\_ \leftarrow dadMi\_ + \left(Tm_i\right)^k \cdot dummy \\ dadMi\_ \end{array}$$

In vector form

$$dadM\_vector(m\_, t\_) := \begin{array}{l} \text{for } i \in 0 .. points - 1 \\ \quad dadM_i \leftarrow dadMi(m\_, i, t\_) \\ dadM \end{array}$$

uncertainty in a wrt M

$$u\_a\_function(m\_, t\_) := \begin{array}{l} dadM \leftarrow dadM\_vector(m\_, t\_) \\ u\_a \leftarrow 0 \\ \text{for } i \in 0 .. points - 1 \\ \quad u\_a \leftarrow u\_a + \left(dadM_i \cdot u_{M_i}\right)^2 \\ u\_a \leftarrow \sqrt{u\_a} \end{array}$$

In vector form

$$u\_a\_vector(m\_, points\_, t\_) := \left| \begin{array}{l} \text{for } 1 \in 0 .. points\_ - 1 \\ \quad u_{1} \leftarrow u\_a\_function(m\_, t_{1}) \\ u\_ \end{array} \right.$$

Results: Average mass flow rate and uncertainty

Average mass flow rate (kg/s)

$$Mdot = 0.197$$

Uncertainty in mass flow rate at measured points (kg/s)

$$u_{Mdot} := u\_a\_vector(Mn, points, Tm) = \begin{pmatrix} 1.396 \times 10^{-3} \\ 1.396 \times 10^{-3} \\ 1.396 \times 10^{-3} \\ 1.396 \times 10^{-3} \\ 1.396 \times 10^{-3} \\ 1.396 \times 10^{-3} \\ 1.396 \times 10^{-3} \\ 1.396 \times 10^{-3} \\ 1.396 \times 10^{-3} \\ 1.396 \times 10^{-3} \end{pmatrix}$$

Average uncertainty in mass flow rate (kg/s)

$$u_{Mdot\_avg} := \frac{1}{points} \left(\sum_{i=0}^{points-1} u_{Mdot_i} \right) = 1.396 \times 10^{-3}$$

%

$$\%u_{Mdot} := \frac{u_{Mdot\_avg}}{Mdot} = 0.708 \cdot \%$$

Appendix O. Similarity Matrix

For the given power-plant conditions on the LEFT, similarity can be obtained in the test facility by operating at the conditions on the RIGHT. Highlighted conditions correspond to using particles with densities approximately equal to PC.

Plant Conditions					Test Conditions				
Particle Diameter (μm)	Superficial Gas Velocity (m/s)	Particle Reynolds Number	Particle Froude Number	Inertia Parameter	Gas Temperature (°C)	Particle Density (kg/m^3)	Gas Pressure (kPa)	Superficial Gas Velocity (m/s)	Particle Diameter (μm)
300	24	275.547	442.477	523800	20	650	28.774	30.386	480.895
300	24	275.547	442.477	523800	20	1100	48.695	25.499	338.634
300	24	275.547	442.477	523800	20	1400	64.975	23.529	288.342
300	24	275.547	442.477	523800	20	1550	68.615	22.744	269.425
300	24	275.547	442.477	523800	20	1700	75.256	22.055	253.334
300	24	275.547	442.477	523800	20	2000	88.536	20.892	227.321
300	24	275.547	442.477	523800	20	2450	108.457	19.525	198.556
300	26	298.509	479.786	567400	20	650	29.927	32.51	468.186
300	26	298.509	479.786	567400	20	1100	48.699	27.639	338.409
300	26	298.509	479.786	567400	20	1400	61.981	25.505	288.15
300	26	298.509	479.786	567400	20	1550	68.621	24.654	269.246
300	26	298.509	479.786	567400	20	1700	75.262	23.906	253.166
300	26	298.509	479.786	567400	20	2000	88.544	22.646	227.17
300	26	298.509	479.786	567400	20	2450	108.466	21.164	198.424
300	28	321.471	516.223	611100	20	650	28.774	35.451	480.896
300	28	321.471	516.223	611100	20	1100	48.695	29.748	338.635
300	28	321.471	516.223	611100	20	1400	61.975	27.451	288.342
300	28	321.471	516.223	611100	20	1550	68.615	26.535	269.425
300	28	321.471	516.223	611100	20	1700	75.255	25.73	253.334
300	28	321.471	516.223	611100	20	2000	88.536	24.373	227.321
300	28	321.471	516.223	611100	20	2450	108.456	22.779	198.556
300	30	344.433	553.096	654700	20	650	28.776	37.982	480.871
300	30	344.433	553.096	654700	20	1100	48.698	31.872	338.617
300	30	344.433	553.096	654700	20	1400	61.98	29.411	288.327
300	30	344.433	553.096	654700	20	1550	68.62	28.429	269.412
300	30	344.433	553.096	654700	20	1700	75.261	27.567	253.321
300	30	344.433	553.096	654700	20	2000	88.543	26.114	227.31
300	30	344.433	553.096	654700	20	2450	108.465	24.406	198.546

Plant Conditions					Test Conditions				
Particle Diameter (μm)	Superficial Gas Velocity (m/s)	Particle Reynolds Number	Particle Froude Number	Inertia Parameter	Gas Temperature (°C)	Particle Density (kg/m^3)	Gas Pressure (kPa)	Superficial Gas Velocity (m/s)	Particle Diameter (μm)
150	24	137.773	625.756	261900	20	650	28.774	30.386	240.448
150	24	137.773	625.756	261900	20	1100	48.695	25.499	169.317
150	24	137.773	625.756	261900	20	1400	61.975	23.529	144.171
150	24	137.773	625.756	261900	20	1550	68.615	22.744	134.713
150	24	137.773	625.756	261900	20	1700	75.255	22.055	126.667
150	24	137.773	625.756	261900	20	2000	88.536	20.892	113.661
150	24	137.773	625.756	261900	20	2450	108.456	19.925	99.278
150	26	149.254	677.903	283700	20	650	28.777	32.917	240.434
150	26	149.254	677.903	283700	20	1100	48.699	27.623	169.307
150	26	149.254	677.903	283700	20	1400	61.98	25.489	144.162
150	26	149.254	677.903	283700	20	1550	68.621	24.639	134.705
150	26	149.254	677.903	283700	20	1700	75.262	23.892	126.66
150	26	149.254	677.903	283700	20	2000	88.543	22.632	113.654
150	26	149.254	677.903	283700	20	2450	108.466	21.152	99.272
150	28	160.736	730.049	305500	20	650	28.779	35.449	240.422
150	28	160.736	730.049	305500	20	1100	48.703	29.747	169.299
150	28	160.736	730.049	305500	20	1400	61.985	27.449	144.155
150	28	160.736	730.049	305500	20	1550	68.627	26.533	134.698
150	28	160.736	730.049	305500	20	1700	75.268	25.729	126.653
150	28	160.736	730.049	305500	20	2000	88.551	24.372	113.648
150	28	160.736	730.049	305500	20	2450	108.474	22.778	99.267
150	30	172.217	782.195	327400	20	650	28.772	37.984	240.46
150	30	172.217	782.195	327400	20	1100	48.691	31.874	169.326
150	30	172.217	782.195	327400	20	1400	61.97	29.412	144.178
150	30	172.217	782.195	327400	20	1550	68.61	28.431	134.72
150	30	172.217	782.195	327400	20	1700	75.25	27.569	126.674
150	30	172.217	782.195	327400	20	2000	88.529	26.115	113.666
150	30	172.217	782.195	327400	20	2450	108.448	24.407	99.283

Plant Conditions					Test Conditions				
Particle Diameter (μm)	Superficial Gas Velocity (m/s)	Particle Reynolds Number	Particle Froude Number	Inertia Parameter	Gas Temperature (°C)	Particle Density (kg/m^3)	Gas Pressure (kPa)	Superficial Gas Velocity (m/s)	Particle Diameter (μm)
37	24	33.984	1260	64600	20	650	28.775	30.3087	59.307
37	24	33.984	1260	64600	20	1100	48.696	25.499	41.763
37	24	33.984	1260	64600	20	1400	N/A	N/A	N/A
37	24	33.984	1260	64600	20	1550	68.617	22.745	33.227
37	24	33.984	1260	64600	20	1700	75.258	22.055	31.243
37	24	33.984	1260	64600	20	2000	88.538	20.892	28.035
37	24	33.984	1260	64600	20	2450	108.459	19.525	24.487
37	26	36.816	1365	69990	20	650	29.927	32.491	57.776
37	26	36.816	1365	69990	20	1100	48.691	27.625	41.765
37	26	36.816	1365	69990	20	1400	61.971	25.491	33.563
37	26	36.816	1365	69990	20	1550	68.611	24.641	33.23
37	26	36.816	1365	69990	20	1700	75.25	23.894	31.245
37	26	36.816	1365	69990	20	2000	88.53	22.634	28.037
37	26	36.816	1365	69990	20	2450	108.449	21.153	24.489
37	28	39.648	1470	75370	20	650	28.774	35.452	59.309
37	28	39.648	1470	75370	20	1100	48.694	29.749	41.764
37	28	39.648	1470	75370	20	1400	61.974	27.452	35.561
37	28	39.648	1470	75370	20	1550	68.6147	26.536	33.228
37	28	39.648	1470	75370	20	1700	75.254	25.731	31.244
37	28	39.648	1470	75370	20	2000	88.534	24.374	28.036
37	28	39.648	1470	75370	20	2450	108.455	22.78	24.488
37	30	42.48	1575	80750	20	650	28.775	37.984	59.307
37	30	42.48	1575	80750	20	1100	48.696	31.874	41.763
37	30	42.48	1575	80750	20	1400	61.977	29.412	35.56
37	30	42.48	1575	80750	20	1550	68.617	28.431	33.227
37	30	42.48	1575	80750	20	1700	75.258	27.569	31.243
37	30	42.48	1575	80750	20	2000	88.538	26.115	28.035
37	30	42.48	1575	80750	20	2450	108.459	24.407	24.487

Plant Conditions					Test Conditions				
Particle Diameter (μm)	Superficial Gas Velocity (m/s)	Particle Reynolds Number	Particle Froude Number	Inertia Parameter	Gas Temperature (°C)	Particle Density (kg/m^3)	Gas Pressure (kPa)	Superficial Gas Velocity (m/s)	Particle Diameter (μm)
300	24	275.547	442.477	523800	30	650	29.253	30.824	494.839
300	24	275.547	442.477	523800	30	1100	49.505	25.866	348.453
300	24	275.547	442.477	523800	30	1400	63.007	23.868	296.702
300	24	275.547	442.477	523800	30	1550	69.757	23.072	277.237
300	24	275.547	442.477	523800	30	1700	76.508	22.372	260.679
300	24	275.547	442.477	523800	30	2000	90.01	21.192	233.912
300	24	275.547	442.477	523800	30	2450	110.262	19.806	204.313
300	26	298.509	479.786	567400	30	650	29.758	33.222	488.925
300	26	298.509	479.786	567400	30	1100	50.36	27.879	344.289
300	26	298.509	479.786	567400	30	1400	64.095	25.725	293.156
300	26	298.509	479.786	567400	30	1550	70.962	24.867	273.924
300	26	298.509	479.786	567400	30	1700	77.83	24.113	257.564
300	26	298.509	479.786	567400	30	2000	91.564	22.841	231.117
300	26	298.509	479.786	567400	30	2450	112.166	21.347	201.871
300	28	321.471	516.223	611100	30	650	29.756	35.757	489.251
300	28	321.471	516.223	611100	30	1100	50.356	30.006	344.518
300	28	321.471	516.223	611100	30	1400	64.089	27.688	293.351
300	28	321.471	516.223	611100	30	1550	70.956	26.764	274.106
300	28	321.471	516.223	611100	30	1700	77.823	25.953	257.736
300	28	321.471	516.223	611100	30	2000	91.556	24.584	231.271
300	28	321.471	516.223	611100	30	2450	112.156	22.976	202.005
300	30	344.433	553.096	654700	30	650	29.758	38.31	489.226
300	30	344.433	553.096	654700	30	1100	50.36	32.148	344.5
300	30	344.433	553.096	654700	30	1400	64.094	29.665	293.337
300	30	344.433	553.096	654700	30	1550	70.961	28.675	274.092
300	30	344.433	553.096	654700	30	1700	77.828	27.806	257.722
300	30	344.433	553.096	654700	30	2000	91.563	26.34	231.259
300	30	344.433	553.096	654700	30	2450	112.165	24.617	201.995

Plant Conditions					Test Conditions				
Particle Diameter (μm)	Superficial Gas Velocity (m/s)	Particle Reynolds Number	Particle Froude Number	Inertia Parameter	Gas Temperature (°C)	Particle Density (kg/m^3)	Gas Pressure (kPa)	Superficial Gas Velocity (m/s)	Particle Diameter (μm)
150	24	137.773	625.756	261900	30	650	29.756	30.649	244.625
150	24	137.773	625.756	261900	30	1100	50.356	25.719	172.259
150	24	137.773	625.756	261900	30	1400	64.089	23.733	146.676
150	24	137.773	625.756	261900	30	1550	70.956	22.941	137.053
150	24	137.773	625.756	261900	30	1700	77.822	22.245	128.868
150	24	137.773	625.756	261900	30	2000	91.556	21.072	115.635
150	24	137.773	625.756	261900	30	2450	112.156	19.694	101.003
150	26	149.254	677.903	283700	30	650	29.758	33.202	244.611
150	26	149.254	677.903	283700	30	1100	50.36	27.862	172.249
150	26	149.254	677.903	283700	30	1400	64.095	25.71	146.667
150	26	149.254	677.903	283700	30	1550	70.962	24.852	137.045
150	26	149.254	677.903	283700	30	1700	77.829	24.098	128.86
150	26	149.254	677.903	283700	30	2000	91.564	22.828	115.628
150	26	149.254	677.903	283700	30	2450	112.166	21.334	100.997
150	28	160.736	730.049	305500	30	650	29.761	35.755	244.599
150	28	160.736	730.049	305500	30	1100	50.364	30.004	172.24
150	28	160.736	730.049	305500	30	1400	64.1	27.686	146.66
150	28	160.736	730.049	305500	30	1550	70.968	26.763	137.038
150	28	160.736	730.049	305500	30	1700	77.836	25.951	128.854
150	28	160.736	730.049	305500	30	2000	91.571	24.583	115.623
150	28	160.736	730.049	305500	30	2450	112.175	22.975	100.992
150	30	172.217	782.195	327400	30	650	29.753	38.312	244.638
150	30	172.217	782.195	327400	30	1100	50.352	32.15	172.268
150	30	172.217	782.195	327400	30	1400	64.084	29.666	146.683
150	30	172.217	782.195	327400	30	1550	70.951	28.677	137.06
150	30	172.217	782.195	327400	30	1700	77.817	27.807	128.874
150	30	172.217	782.195	327400	30	2000	91.549	26.341	115.641
150	30	172.217	782.195	327400	30	2450	112.148	24.618	101.008

Plant Conditions					Test Conditions				
Particle Diameter (μm)	Superficial Gas Velocity (m/s)	Particle Reynolds Number	Particle Froude Number	Inertia Parameter	Gas Temperature (°C)	Particle Density (kg/m^3)	Gas Pressure (kPa)	Superficial Gas Velocity (m/s)	Particle Diameter (μm)
37	24	33.984	1260	64600	30	650	29.757	30.65	60.338
37	24	33.984	1260	64600	30	1100	50.357	25.72	42.488
37	24	33.984	1260	64600	30	1400	64.091	23.733	36.178
37	24	33.984	1260	64600	30	1550	70.958	22.941	33.805
37	24	33.984	1260	64600	30	1700	77.825	22.246	31.786
37	24	33.984	1260	64600	30	2000	N/A	N/A	N/A
37	24	33.984	1260	64600	30	2450	112.159	19.694	24.913
37	26	36.816	1365	69990	30	650	29.754	33.205	60.342
37	26	36.816	1365	69990	30	1100	50.352	27.864	42.491
37	26	36.816	1365	69990	30	1400	64.085	25.714	36.18
37	26	36.816	1365	69990	30	1550	70.951	24.854	33.807
37	26	36.816	1365	69990	30	1700	77.817	24.1	31.788
37	26	36.816	1365	69990	30	2000	91.55	22.829	28.524
37	26	36.816	1365	69990	30	2450	112.149	21.336	24.914
37	28	39.648	1470	75370	30	650	29.755	35.758	60.34
37	28	39.648	1470	75370	30	1100	50.355	30.007	42.49
37	28	39.648	1470	75370	30	1400	64.088	27.689	36.179
37	28	39.648	1470	75370	30	1550	70.955	26.765	33.806
37	28	39.648	1470	75370	30	1700	77.821	25.954	31.787
37	28	39.648	1470	75370	30	2000	91.555	24.585	28.523
37	28	39.648	1470	75370	30	2450	112.154	22.977	24.913
37	30	42.48	1575	80750	30	650	29.757	38.312	60.338
37	30	42.48	1575	80750	30	1100	50.357	32.15	42.488
37	30	42.48	1575	80750	30	1400	64.091	29.666	36.178
37	30	42.48	1575	80750	30	1550	70.958	28.677	33.805
37	30	42.48	1575	80750	30	1700	77.825	27.807	31.786
37	30	42.48	1575	80750	30	2000	91.559	26.341	28.522
37	30	42.48	1575	80750	30	2450	112.159	24.618	24.913

Plant Conditions					Test Conditions				
Particle Diameter (μm)	Superficial Gas Velocity (m/s)	Particle Reynolds Number	Particle Froude Number	Inertia Parameter	Gas Temperature (°C)	Particle Density (kg/m^3)	Gas Pressure (kPa)	Superficial Gas Velocity (m/s)	Particle Diameter (μm)
300	24	275.547	442.477	523800	40	650	30.737	30.903	497.403
300	24	275.547	442.477	523800	40	1100	52.017	25.933	350.259
300	24	275.547	442.477	523800	40	1400	66.203	23.93	298.24
300	24	275.547	442.477	523800	40	1550	73.297	23.131	278.674
300	24	275.547	442.477	523800	40	1700	80.39	22.43	262.03
300	24	275.547	442.477	523800	40	2000	94.576	21.247	235.124
300	24	275.547	442.477	523800	40	2450	115.856	19.857	205.371
300	26	298.509	479.786	567400	40	650	30.74	33.498	497.072
300	26	298.509	479.786	567400	40	1100	52.021	28.11	350.026
300	26	298.509	479.786	567400	40	1400	66.209	25.939	298.041
300	26	298.509	479.786	567400	40	1550	73.303	25.073	278.489
300	26	298.509	479.786	567400	40	1700	80.397	24.313	261.856
300	26	298.509	479.786	567400	40	2000	94.585	23.031	234.968
300	26	298.509	479.786	567400	40	2450	115.866	21.525	205.235
300	28	321.471	516.223	611100	40	650	30.737	36.054	497.403
300	28	321.471	516.223	611100	40	1100	52.017	30.255	350.259
300	28	321.471	516.223	611100	40	1400	66.203	27.918	298.24
300	28	321.471	516.223	611100	40	1550	73.297	26.986	278.674
300	28	321.471	516.223	611100	40	1700	80.39	26.168	262.03
300	28	321.471	516.223	611100	40	2000	94.576	24.788	235.124
300	28	321.471	516.223	611100	40	2450	115.856	23.167	205.371
300	30	344.433	553.096	654700	40	650	30.74	38.628	497.378
300	30	344.433	553.096	654700	40	1100	52.021	32.415	350.241
300	30	344.433	553.096	654700	40	1400	66.208	29.911	298.224
300	30	344.433	553.096	654700	40	1550	73.302	28.913	278.66
300	30	344.433	553.096	654700	40	1700	80.396	28.037	262.017
300	30	344.433	553.096	654700	40	2000	94.583	26.558	235.112
300	30	344.433	553.096	654700	40	2450	115.865	24.821	205.361

Plant Conditions					Test Conditions				
Particle Diameter (μm)	Superficial Gas Velocity (m/s)	Particle Reynolds Number	Particle Froude Number	Inertia Parameter	Gas Temperature (°C)	Particle Density (kg/m^3)	Gas Pressure (kPa)	Superficial Gas Velocity (m/s)	Particle Diameter (μm)
150	24	137.773	625.756	261900	40	650	30.737	30.903	248.702
150	24	137.773	625.756	261900	40	1100	52.017	25.933	175.129
150	24	137.773	625.756	261900	40	1400	66.203	23.929	149.12
150	24	137.773	625.756	261900	40	1550	73.296	23.131	139.337
150	24	137.773	625.756	261900	40	1700	80.39	22.43	131.015
150	24	137.773	625.756	261900	40	2000	94.576	21.247	117.562
150	24	137.773	625.756	261900	40	2450	115.856	19.857	102.686
150	26	149.254	677.903	283700	40	650	30.74	33.478	248.687
150	26	149.254	677.903	283700	40	1100	52.021	28.093	175.119
150	26	149.254	677.903	283700	40	1400	66.209	25.923	149.111
150	26	149.254	677.903	283700	40	1550	73.303	25.058	139.329
150	26	149.254	677.903	283700	40	1700	80.397	24.298	131.007
150	26	149.254	677.903	283700	40	2000	94.584	23.017	117.555
150	26	149.254	677.903	283700	40	2450	115.866	21.511	102.68
150	28	160.736	730.049	305500	40	650	30.742	36.052	248.675
150	28	160.736	730.049	305500	40	1100	52.026	30.253	175.11
150	28	160.736	730.049	305500	40	1400	66.214	27.916	149.104
150	28	160.736	730.049	305500	40	1550	73.309	26.985	139.322
150	28	160.736	730.049	305500	40	1700	80.403	26.167	131.001
150	28	160.736	730.049	305500	40	2000	94.592	24.787	117.549
150	28	160.736	730.049	305500	40	2450	115.875	23.166	102.675
150	30	172.217	782.195	327400	40	650	30.735	38.63	248.714
150	30	172.217	782.195	327400	40	1100	52.013	32.416	175.138
150	30	172.217	782.195	327400	40	1400	66.198	29.913	149.128
150	30	172.217	782.195	327400	40	1550	73.291	28.915	139.344
150	30	172.217	782.195	327400	40	1700	80.384	28.038	131.022
150	30	172.217	782.195	327400	40	2000	94.569	26.56	117.568
150	30	172.217	782.195	327400	40	2450	115.847	24.822	102.691

Plant Conditions					Test Conditions				
Particle Diameter (μm)	Superficial Gas Velocity (m/s)	Particle Reynolds Number	Particle Froude Number	Inertia Parameter	Gas Temperature (°C)	Particle Density (kg/m^3)	Gas Pressure (kPa)	Superficial Gas Velocity (m/s)	Particle Diameter (μm)
37	24	33.984	1260	64600	40	650	30.738	30.904	61.343
37	24	33.984	1260	64600	40	1100	52.018	25.933	43.196
37	24	33.984	1260	64600	40	1400	66.205	23.93	36.781
37	24	33.984	1260	64600	40	1550	73.299	23.132	34.368
37	24	33.984	1260	64600	40	1700	80.392	22.43	32.315
37	24	33.984	1260	64600	40	2000	94.579	21.248	28.997
37	24	33.984	1260	64600	40	2450	115.859	19.858	25.328
37	26	36.816	1365	69990	40	650	30.735	33.48	61.347
37	26	36.816	1365	69990	40	1100	52.013	28.095	43.199
37	26	36.816	1365	69990	40	1400	66.199	25.925	36.783
37	26	36.816	1365	69990	40	1550	73.292	25.06	34.37
37	26	36.816	1365	69990	40	1700	80.384	24.3	32.317
37	26	36.816	1365	69990	40	2000	94.57	23.019	28.999
37	26	36.816	1365	69990	40	2450	115.848	21.513	25.329
37	28	39.648	1470	75370	40	650	30.737	36.055	61.345
37	28	39.648	1470	75370	40	1100	52.016	30.256	43.198
37	28	39.648	1470	75370	40	1400	66.202	27.919	36.782
37	28	39.648	1470	75370	40	1550	73.295	26.987	34.369
37	28	39.648	1470	75370	40	1700	80.388	26.169	32.316
37	28	39.648	1470	75370	40	2000	94.575	24.789	28.998
37	28	39.648	1470	75370	40	2450	115.854	23.168	25.329
37	30	42.48	1575	80750	40	650	30.738	38.63	61.343
37	30	42.48	1575	80750	40	1100	52.018	32.416	43.196
37	30	42.48	1575	80750	40	1400	66.205	29.912	36.781
37	30	42.48	1575	80750	40	1550	73.299	28.915	34.368
37	30	42.48	1575	80750	40	1700	80.392	28.038	32.315
37	30	42.48	1575	80750	40	2000	94.579	26.559	28.997
37	30	42.48	1575	80750	40	2450	115.859	24.822	25.328

Plant Conditions					Test Conditions				
Particle Diameter (μm)	Superficial Gas Velocity (m/s)	Particle Reynolds Number	Particle Froude Number	Inertia Parameter	Gas Temperature (°C)	Particle Density (kg/m^3)	Gas Pressure (kPa)	Superficial Gas Velocity (m/s)	Particle Diameter (μm)
300	24	275.547	442.477	523800	50	650	31.719	31.15	505.363
300	24	275.547	442.477	523800	50	1100	53.678	26.139	355.864
300	24	275.547	442.477	523800	50	1400	68.318	24.12	303.013
300	24	275.547	442.477	523800	50	1550	75.637	23.316	283.134
300	24	275.547	442.477	523800	50	1700	82.957	22.609	266.224
300	24	275.547	442.477	523800	50	2000	97.596	21.416	238.887
300	24	275.547	442.477	523800	50	2450	119.556	20.016	208.658
300	26	298.509	479.786	567400	50	650	31.722	33.765	505.028
300	26	298.509	479.786	567400	50	1100	53.683	28.334	355.628
300	26	298.509	479.786	567400	50	1400	68.323	26.145	302.811
300	26	298.509	479.786	567400	50	1550	75.644	25.273	282.946
300	26	298.509	479.786	567400	50	1700	82.964	24.507	266.047
300	26	298.509	479.786	567400	50	2000	97.605	23.215	238.728
300	26	298.509	479.786	567400	50	2450	119.566	21.696	208.519
300	28	321.471	516.223	611100	50	650	31.719	36.341	505.363
300	28	321.471	516.223	611100	50	1100	53.678	30.496	355.864
300	28	321.471	516.223	611100	50	1400	68.317	28.14	303.013
300	28	321.471	516.223	611100	50	1550	75.637	27.202	283.134
300	28	321.471	516.223	611100	50	1700	82.957	26.377	266.224
300	28	321.471	516.223	611100	50	2000	97.596	24.986	238.887
300	28	321.471	516.223	611100	50	2450	119.555	23.352	208.658
300	30	344.433	553.096	654700	50	650	31.721	38.936	505.338
300	30	344.433	553.096	654700	50	1100	53.682	32.673	355.846
300	30	344.433	553.096	654700	50	1400	68.323	30.15	302.997
300	30	344.433	553.096	654700	50	1550	75.643	29.144	283.119
300	30	344.433	553.096	654700	50	1700	82.963	28.26	266.21
300	30	344.433	553.096	654700	50	2000	97.604	26.77	238.875
300	30	344.433	553.096	654700	50	2450	119.565	25.019	208.648

Plant Conditions					Test Conditions				
Particle Diameter (μm)	Superficial Gas Velocity (m/s)	Particle Reynolds Number	Particle Froude Number	Inertia Parameter	Gas Temperature (°C)	Particle Density (kg/m^3)	Gas Pressure (kPa)	Superficial Gas Velocity (m/s)	Particle Diameter (μm)
150	24	137.773	625.756	261900	50	650	31.719	31.15	252.682
150	24	137.773	625.756	261900	50	1100	53.678	26.139	177.932
150	24	137.773	625.756	261900	50	1400	68.317	24.12	151.506
150	24	137.773	625.756	261900	50	1550	75.637	23.316	141.567
150	**24**	**137.773**	**625.756**	**261900**	**50**	**1700**	**82.957**	**22.609**	**133.112**
150	24	137.773	625.756	261900	50	2000	97.596	21.416	119.444
150	24	137.773	625.756	261900	50	2450	119.555	20.016	104.329
150	26	149.254	677.903	283700	50	650	31.722	33.744	252.667
150	26	149.254	677.903	283700	50	1100	53.638	28.317	177.922
150	26	149.254	677.903	283700	50	1400	68.323	26.129	151.497
150	26	149.254	677.903	283700	50	1550	75.644	25.258	141.559
150	26	149.254	677.903	283700	50	1700	82.964	24.492	133.104
150	26	149.254	677.903	283700	50	2000	97.605	23.2	119.437
150	26	149.254	677.903	283700	50	2450	119.566	21.683	104.323
150	28	160.736	730.049	305500	50	650	31.724	36.339	252.654
150	28	160.736	730.049	305500	50	1100	53.687	30.494	177.913
150	28	160.736	730.049	305500	50	1400	68.329	28.139	151.49
150	28	160.736	730.049	305500	50	1550	75.65	27.2	141.551
150	28	160.736	730.049	305500	50	1700	82.971	26.375	133.097
150	28	160.736	730.049	305500	50	2000	97.613	24.984	119.431
150	28	160.736	730.049	305500	50	2450	119.575	23.35	104.318
150	30	172.217	782.195	327400	50	650	31.716	38.938	252.695
150	30	172.217	782.195	327400	50	1100	53.674	32.675	177.941
150	30	172.217	782.195	327400	50	1400	68.312	30.151	151.514
150	30	172.217	782.195	327400	50	1550	75.632	29.145	141.574
150	30	172.217	782.195	327400	50	1700	82.951	28.261	133.119
150	30	172.217	782.195	327400	50	2000	97.589	26.771	119.45
150	30	172.217	782.195	327400	50	2450	119.547	25.02	104.334

Plant Conditions					Test Conditions				
Particle Diameter (μm)	Superficial Gas Velocity (m/s)	Particle Reynolds Number	Particle Froude Number	Inertia Parameter	Gas Temperature (°C)	Particle Density (kg/m^3)	Gas Pressure (kPa)	Superficial Gas Velocity (m/s)	Particle Diameter (μm)
37	24	33.984	1260	64600	50	650	31.72	31.15	62.325
37	24	33.984	1260	64600	50	1100	53.68	26.14	43.888
37	24	33.984	1260	64600	50	1400	68.319	24.121	37.37
37	24	33.984	1260	64600	50	1550	75.639	23.316	34.918
37	24	33.984	1260	64600	50	1700	82.959	22.609	32.833
37	24	33.984	1260	64600	50	2000	97.599	21.417	29.461
37	24	33.984	1260	64600	50	2450	119.559	20.016	25.733
37	26	36.816	1365	69990	50	650	31.717	33.747	62.329
37	26	36.816	1365	69990	50	1100	53.674	28.319	43.89
37	26	36.816	1365	69990	50	1400	68.313	26.132	37.372
37	26	36.816	1365	69990	50	1550	75.632	25.26	34.92
37	26	36.816	1365	69990	50	1700	82.951	24.494	32.835
37	26	36.816	1365	69990	50	2000	97.59	23.202	29.463
37	26	36.816	1365	69990	50	2450	119.548	21.685	25.735
37	28	39.648	1470	75370	50	650	31.718	36.343	62.327
37	28	39.648	1470	75370	50	1100	53.677	30.497	43.889
37	28	39.648	1470	75370	50	1400	68.316	28.141	37.371
37	28	39.648	1470	75370	50	1550	75.636	27.203	34.919
37	28	39.648	1470	75370	50	1700	82.956	26.378	32.834
37	28	39.648	1470	75370	50	2000	97.595	24.987	29.465
37	28	39.648	1470	75370	50	2450	119.554	23.352	25.734
37	30	42.48	1575	80750	50	650	31.72	38.938	62.325
37	30	42.48	1575	80750	50	1100	53.68	32.675	43.888
37	30	42.48	1575	80750	50	1400	68.319	30.151	37.37
37	30	42.48	1575	80750	50	1550	75.639	29.145	34.918
37	30	42.48	1575	80750	50	1700	82.959	28.261	32.833
37	30	42.48	1575	80750	50	2000	97.599	26.771	29.461
37	30	42.48	1575	80750	50	2450	119.559	25.02	25.733

Plant Conditions					Test Conditions				
Particle Diameter (μm)	Superficial Gas Velocity (m/s)	Particle Reynolds Number	Particle Froude Number	Inertia Parameter	Gas Temperature (°C)	Particle Density (kg/m^3)	Gas Pressure (kPa)	Superficial Gas Velocity (m/s)	Particle Diameter (μm)
300	24	275.547	442.477	523800	60	650	32.7	31.388	513.141
300	24	275.547	442.477	523800	60	1100	55.339	26.34	361.341
300	24	275.547	442.477	523800	60	1400	70.432	24.305	307.676
300	24	275.547	442.477	523800	60	1550	77.978	23.494	287.491
300	24	275.547	442.477	523800	60	1700	85.524	22.782	270.321
300	24	275.547	442.477	523800	60	2000	100.617	21.581	242.564
300	24	275.547	442.477	523800	60	2450	123.255	20.169	211.87
300	26	298.509	479.786	567400	60	650	32.703	34.024	512.801
300	26	298.509	479.786	567400	60	1100	55.344	28.551	361.101
300	26	298.509	479.786	567400	60	1400	70.438	26.346	307.472
300	26	298.509	479.786	567400	60	1550	77.985	25.467	287.3
300	26	298.509	479.786	567400	60	1700	85.532	24.695	270.142
300	26	298.509	479.786	567400	60	2000	100.625	23.392	242.403
300	26	298.509	479.786	567400	60	2450	123.266	21.862	211.729
300	28	321.471	516.223	611100	60	650	32.7	36.62	513.142
300	28	321.471	516.223	611100	60	1100	55.339	30.73	361.341
300	28	321.471	516.223	611100	60	1400	70.432	28.356	307.676
300	28	321.471	516.223	611100	60	1550	77.978	27.41	287.491
300	28	321.471	516.223	611100	60	1700	85.524	26.579	270.321
300	28	321.471	516.223	611100	60	2000	100.616	25.177	242.564
300	28	321.471	516.223	611100	60	2450	123.255	23.531	211.87
300	30	344.433	553.096	654700	60	650	32.703	39.235	513.116
300	30	344.433	553.096	654700	60	1100	55.343	32.924	361.323
300	30	344.433	553.096	654700	60	1400	70.437	30.381	307.661
300	30	344.433	553.096	654700	60	1550	77.984	29.367	287.477
300	30	344.433	553.096	654700	60	1700	85.53	28.477	270.308
300	30	344.433	553.096	654700	60	2000	100.624	26.975	242.552
300	30	344.433	553.096	654700	60	2450	123.264	25.211	211.859

Plant Conditions					Test Conditions				
Particle Diameter (μm)	Superficial Gas Velocity (m/s)	Particle Reynolds Number	Particle Froude Number	Inertia Parameter	Gas Temperature (°C)	Particle Density (kg/m^3)	Gas Pressure (kPa)	Superficial Gas Velocity (m/s)	Particle Diameter (μm)
150	24	137.773	625.756	261900	60	650	32.7	31.388	256.571
150	24	137.773	625.756	261900	60	1100	55.339	26.34	180.671
150	24	137.773	625.756	261900	60	1400	70.431	24.305	153.838
150	24	137.773	625.756	261900	60	1550	77.978	23.494	143.746
150	24	137.773	625.756	261900	60	1700	85.524	22.782	135.161
150	24	137.773	625.756	261900	60	2000	100.616	21.581	121.282
150	24	137.773	625.756	261900	60	2450	123.255	20.169	105.935
150	26	149.254	677.903	283700	60	650	32.703	34.003	256.556
150	26	149.254	677.903	283700	60	1100	55.344	28.534	180.66
150	26	149.254	677.903	283700	60	1400	70.438	26.33	153.829
150	26	149.254	677.903	283700	60	1550	77.984	25.451	143.737
150	26	149.254	677.903	283700	60	1700	85.531	24.68	135.153
150	26	149.254	677.903	283700	60	2000	100.625	23.378	121.275
150	26	149.254	677.903	283700	60	2450	123.266	21.849	105.929
150	28	160.736	730.049	305500	60	650	32.706	36.618	256.543
150	28	160.736	730.049	305500	60	1100	55.348	30.728	180.651
150	28	160.736	730.049	305500	60	1400	70.443	28.354	153.821
150	28	160.736	730.049	305500	60	1550	77.991	27.409	143.73
150	28	160.736	730.049	305500	60	1700	85.538	26.577	135.146
150	28	160.736	730.049	305500	60	2000	100.633	25.176	121.269
150	28	160.736	730.049	305500	60	2450	123.276	23.529	105.923
150	30	172.217	782.195	327400	60	650	32.698	39.236	256.584
150	30	172.217	782.195	327400	60	1100	55.335	32.925	180.68
150	30	172.217	782.195	327400	60	1400	70.426	30.382	153.846
150	30	172.217	782.195	327400	60	1550	77.972	29.369	143.753
150	30	172.217	782.195	327400	60	1700	85.518	28.478	135.168
150	30	172.217	782.195	327400	60	2000	100.609	26.976	121.288
150	30	172.217	782.195	327400	60	2450	123.246	25.212	105.94

Plant Conditions					Test Conditions				
Particle Diameter (μm)	Superficial Gas Velocity (m/s)	Particle Reynolds Number	Particle Froude Number	Inertia Parameter	Gas Temperature (°C)	Particle Density (kg/m^3)	Gas Pressure (kPa)	Superficial Gas Velocity (m/s)	Particle Diameter (μm)
37	24	33.984	1260	64600	60	650	32.701	31.389	63.284
37	24	33.984	1260	64600	60	1100	55.341	26.34	44.563
37	24	33.984	1260	64600	60	1400	70.434	24.306	37.945
37	24	33.984	1260	64600	60	1550	77.98	23.495	35.455
37	24	33.984	1260	64600	60	1700	85.526	22.782	33.338
37	24	33.984	1260	64600	60	2000	100.619	21.581	29.915
37	24	33.984	1260	64600	60	2450	123.259	20.169	26.129
37	26	36.816	1365	69990	60	650	32.698	34.006	63.288
37	26	36.816	1365	69990	60	1100	55.335	28.536	44.566
37	26	36.816	1365	69990	60	1400	70.427	26.332	37.947
37	26	36.816	1365	69990	60	1550	77.973	25.454	35.458
37	26	36.816	1365	69990	60	1700	85.518	24.682	33.34
37	26	36.816	1365	69990	60	2000	100.61	23.38	29.917
37	26	36.816	1365	69990	60	2450	123.247	21.851	26.131
37	28	39.648	1470	75370	60	650	32.7	36.621	63.286
37	28	39.648	1470	75370	60	1100	55.338	30.731	44.564
37	28	39.648	1470	75370	60	1400	70.43	28.357	37.946
37	28	39.648	1470	75370	60	1550	77.977	27.411	35.456
37	28	39.648	1470	75370	60	1700	85.523	26.58	33.339
37	28	39.648	1470	75370	60	2000	100.615	25.178	29.916
37	28	39.648	1470	75370	60	2450	123.253	23.531	26.13
37	30	42.48	1575	80750	60	650	32.701	39.236	63.284
37	30	42.48	1575	80750	60	1100	55.341	32.925	44.563
37	30	42.48	1575	80750	60	1400	70.434	30.382	37.945
37	30	42.48	1575	80750	60	1550	77.98	29.369	35.455
37	30	42.48	1575	80750	60	1700	85.526	28.478	33.338
37	30	42.48	1575	80750	60	2000	100.619	26.976	29.915
37	30	42.48	1575	80750	60	2450	123.259	25.212	26.129

Appendix P. Tabulated Test Results

TEMPERATURE

Test	Mean Actual Gas Flow Rate	GIW Mean Actual Particle Flow Rate	Model Temperature	Mean Temperature	Instrument Uncertainty	Statistical Uncertainty	Combined Uncertainty	Combined Uncertainty
#	kg/s	kg/s	˚C	˚C	˚C	˚C	˚C	%
1	0.086	0.590	53	48.795	0.301	1.361	1.393	2.855
2	0.094	0.600	57	49.055	0.300	0.088	0.314	0.640
3	0.103	0.581	63	53.239	0.316	0.137	0.344	0.646
4	0.077	0.492	43	39.908	0.269	0.138	0.302	0.757
5	0.085	0.496	46	44.734	0.285	0.730	0.784	1.753
6	0.093	0.491	54	51.727	0.310	0.232	0.388	0.750
7	0.077	0.397	40	40.689	0.271	0.738	0.786	1.932
8	0.084	0.397	43	42.358	0.277	0.754	0.804	1.898
9	0.091	0.396	46	45.612	0.289	0.748	0.801	1.756
10	0.099	0.393	53	47.269	0.294	1.048	1.089	2.304
11	0.076	0.297	38	38.167	0.262	0.220	0.343	0.899
12	0.082	0.295	40	38.965	0.265	0.543	0.605	1.553
13	0.089	0.291	43	40.009	0.269	1.355	1.382	3.454
14	0.096	0.292	46	39.280	0.266	0.717	0.765	1.948
15	0.076	0.195	35	32.183	0.242	1.218	1.242	3.859
16	0.088	0.199	39	34.777	0.251	1.704	1.723	4.954
17	0.102	0.197	44	40.975	0.272	1.369	1.396	3.407
18	0.115	0.197	49	42.764	0.279	0.675	0.731	1.709
19	0.063	0.158	31	31.010	0.238	0.336	0.412	1.329
20	0.075	0.157	34	34.033	0.248	0.332	0.415	1.219
21	0.088	0.156	37	34.407	0.250	0.815	0.852	2.476
22	0.107	0.159	44	37.330	0.260	0.516	0.578	1.548
23	0.051	0.079	28	29.106	0.232	0.362	0.430	1.477
24	0.063	0.077	30	35.863	0.255	0.377	0.455	1.269
25	0.081	0.080	33	36.371	0.256	0.092	0.272	0.748

ORIFICE UPSTREAM PRESSURE & SYSTEM PRESSURE DROP

Test	Mean Actual Gas Flow Rate	GIW Mean Actual Particle Flow Rate	Mean Upstream Pressure	Instrument Uncertainty	Statistical Uncertainty	Combined Uncertainty	Combined Uncertainty	Model System Pressure Drop	Estimated System Pressure Drop
#	kg/s	kg/s	kPa	Pa	Pa	Pa	%	kPa	kPa
1	0.086	0.590	111.324	720.294	443.624	836.915	0.752	21.064	10.024
2	0.094	0.600	114.763	709.665	401.026	824.406	0.718	25.451	13.463
3	0.103	0.581	116.540	725.818	391.303	824.579	0.708	30.730	15.240
4	0.077	0.492	110.156	706.061	369.233	796.787	0.723	13.237	8.856
5	0.085	0.496	111.200	709.282	576.901	914.273	0.822	15.786	9.900
6	0.093	0.491	114.879	720.655	482.172	867.083	0.755	22.013	13.579
7	0.077	0.397	110.033	705.696	655.684	963.290	0.875	11.382	8.733
8	0.084	0.397	110.668	707.646	633.521	949.795	0.858	13.593	9.368
9	0.091	0.396	111.227	709.367	667.928	974.335	0.876	16.023	9.927
10	0.099	0.393	112.324	712.748	627.283	949.470	0.845	21.658	11.024
11	0.076	0.297	109.062	702.716	616.634	934.905	0.857	9.477	7.762
12	0.082	0.295	109.123	702.904	674.071	973.881	0.892	11.155	7.823
13	0.089	0.291	109.207	703.161	764.524	1038.716	0.951	13.192	7.907
14	0.096	0.292	110.116	705.948	682.976	982.252	0.892	15.424	8.816
15	0.076	0.195	106.374	694.510	557.850	890.809	0.837	7.524	5.074
16	0.088	0.199	107.098	696.715	288.084	753.925	0.704	10.342	5.798
17	0.102	0.197	108.161	699.959	223.536	734.786	0.679	14.079	6.861
18	0.115	0.197	109.769	704.883	182.771	728.193	0.663	18.079	8.469
19	0.063	0.158	105.378	691.482	276.152	744.585	0.707	4.568	4.078
20	0.075	0.157	105.887	693.030	282.314	748.326	0.707	6.686	4.587
21	0.088	0.156	106.534	694.996	144.363	709.831	0.666	9.210	5.234
22	0.107	0.159	108.420	700.752	155.088	717.709	0.662	12.330	7.120
23	0.051	0.079	103.510	685.824	108.910	694.418	0.671	2.244	2.210
24	0.063	0.077	104.535	688.926	113.751	698.254	0.668	3.431	3.235
25	0.081	0.080	105.478	691.787	95.569	698.357	0.662	5.785	4.178

ORIFICE PRESSURE DROP

Test	Mean Actual Gas Flow Rate	GIW Mean Actual Particle Flow Rate	Mean Orifice Pressure Drop	Instrument Uncertainty	Statistical Uncertainty	Combined Uncertainty	Combined Uncertainty
#	kg/s	kg/s	kPa	Pa	Pa	Pa	%
1	0.086	0.590	1.221	10.166	86.478	87.052	7.130
2	0.094	0.600	1.418	9.982	81.429	82.026	5.785
3	0.103	0.581	1.700	10.262	68.193	68.961	4.057
4	0.077	0.492	0.959	9.920	80.341	80.951	8.441
5	0.085	0.496	1.176	9.975	78.119	78.753	6.697
6	0.093	0.491	1.398	10.173	69.253	69.997	5.007
7	0.077	0.397	0.961	9.913	75.950	76.594	7.970
8	0.084	0.397	1.148	9.947	97.084	97.592	8.501
9	0.091	0.396	1.353	9.977	97.954	98.461	7.277
10	0.099	0.393	1.599	10.036	84.640	85.233	5.330
11	0.076	0.297	0.939	9.861	87.058	87.614	9.331
12	0.082	0.295	1.099	9.865	106.345	106.801	9.718
13	0.089	0.291	1.302	9.869	153.289	153.607	11.798
14	0.096	0.292	1.498	9.918	135.518	135.881	9.071
15	0.076	0.195	0.947	9.718	81.695	82.271	8.688
16	0.088	0.199	1.272	9.757	59.899	60.688	4.771
17	0.102	0.197	1.733	9.813	56.116	56.968	3.287
18	0.115	0.197	2.191	9.899	57.889	58.729	2.680
19	0.063	0.158	0.650	9.666	46.096	47.098	7.246
20	0.075	0.157	0.929	9.693	50.912	51.826	5.579
21	0.088	0.156	1.277	9.727	26.532	28.259	2.213
22	0.107	0.159	1.883	9.827	44.376	45.451	2.414
23	0.051	0.079	0.429	9.567	10.545	14.238	3.319
24	0.063	0.077	0.665	9.621	13.649	16.699	2.511
25	0.081	0.080	1.098	9.671	16.596	19.208	1.749

GAS FLOW RATE, MASS FLOW RATE AND LOADING

Test	Req. Gas Flow Rate	Mean Actual Gas Flow Rate	Uncertainty	Uncertainty	Req. Particle Flow Rate	Mean Actual Particle Flow Rate	Uncertainty	Uncertainty	Loading setpoint	Mean actual loading	Uncertainty	Uncertainty
#	kg/s	kg/s	kg/s	%	kg/s	kg/s	kg/s	%				%
1	0.086	0.086	0.003	3.680	0.6	0.590	0.003	0.542	6.977	6.860	0.255	3.720
2	0.094	0.094	0.003	2.996	0.6	0.600	0.005	0.756	6.383	6.383	0.197	3.090
3	0.103	0.103	0.002	2.167	0.6	0.581	0.005	0.819	5.825	5.641	0.131	2.317
4	0.077	0.077	0.003	4.292	0.5	0.492	0.004	0.723	6.494	6.390	0.278	4.353
5	0.085	0.085	0.003	3.465	0.5	0.496	0.003	0.529	5.882	5.835	0.205	3.505
6	0.093	0.093	0.002	2.632	0.5	0.491	0.003	0.600	5.376	5.280	0.143	2.700
7	0.077	0.077	0.003	4.094	0.4	0.397	0.002	0.521	5.195	5.156	0.213	4.127
8	0.084	0.084	0.004	4.354	0.4	0.397	0.002	0.518	4.762	4.726	0.207	4.384
9	0.091	0.091	0.003	3.756	0.4	0.396	0.002	0.594	4.396	4.352	0.165	3.803
10	0.099	0.099	0.003	2.828	0.4	0.393	0.002	0.618	4.040	3.970	0.115	2.895
11	0.076	0.076	0.004	4.754	0.3	0.297	0.002	0.603	3.947	3.908	0.187	4.792
12	0.082	0.082	0.004	4.957	0.3	0.295	0.002	0.546	3.659	3.598	0.179	4.987
13	0.089	0.089	0.005	6.008	0.3	0.291	0.002	0.520	3.371	3.270	0.197	6.030
14	0.096	0.096	0.004	4.640	0.3	0.292	0.002	0.560	3.125	3.042	0.142	4.673
15	0.076	0.076	0.003	4.459	0.2	0.195	0.001	0.494	2.632	2.566	0.115	4.486
16	0.088	0.088	0.002	2.564	0.2	0.199	0.001	0.486	2.273	2.261	0.059	2.609
17	0.102	0.102	0.002	1.854	0.2	0.197	0.001	0.504	1.961	1.931	0.037	1.921
18	0.115	0.115	0.002	1.538	0.2	0.197	0.001	0.709	1.739	1.713	0.029	1.694
19	0.063	0.063	0.002	3.705	0.16	0.158	0.001	0.542	2.540	2.508	0.094	3.744
20	0.075	0.075	0.002	2.895	0.16	0.157	0.001	0.610	2.133	2.093	0.062	2.958
21	0.088	0.088	0.001	1.349	0.16	0.156	0.001	0.707	1.818	1.773	0.027	1.523
22	0.107	0.107	0.002	1.416	0.16	0.159	0.001	0.814	1.495	1.486	0.024	1.633
23	0.051	0.051	0.001	1.817	0.08	0.079	0.000	0.557	1.569	1.549	0.029	1.901
24	0.063	0.063	0.001	1.456	0.08	0.077	0.000	0.622	1.270	1.222	0.019	1.583
25	0.081	0.081	0.001	1.135	0.08	0.080	0.001	0.841	0.988	0.988	0.014	1.413

LIW VS. GIW MASS FLOW RATES

Test	Req. Particle Flow Rate	GIW Mean Actual Particle Flow Rate	Uncertainty	Uncertainty	LIW Mean Actual Particle Flow Rate	Uncertainty	Uncertainty
#	kg/s	kg/s	kg/s	%	kg/s	kg/s	%
1	0.6	0.590	0.003	0.542	0.597	0.006	1.038
2	0.6	0.600	0.005	0.756	0.568	0.009	1.578
3	0.6	0.581	0.005	0.819	0.602	0.009	1.552
4	0.5	0.492	0.004	0.723	0.499	0.007	1.381
5	0.5	0.496	0.003	0.529	0.500	0.005	1.049
6	0.5	0.491	0.003	0.600	0.501	0.006	1.106
7	0.4	0.397	0.002	0.521	0.402	0.004	1.043
8	0.4	0.397	0.002	0.518	0.402	0.004	1.018
9	0.4	0.396	0.002	0.594	0.400	0.005	1.160
10	0.4	0.393	0.002	0.618	0.400	0.005	1.211
11	0.3	0.297	0.002	0.603	0.300	0.004	1.216
12	0.3	0.295	0.002	0.546	0.300	0.003	1.032
13	0.3	0.291	0.002	0.520	0.300	0.003	0.988
14	0.3	0.292	0.002	0.560	0.299	0.003	1.097
15	0.2	0.195	0.001	0.494	0.200	0.002	0.968
16	0.2	0.199	0.001	0.486	0.200	0.002	0.975
17	0.2	0.197	0.001	0.504	0.199	0.002	1.009
18	0.2	0.197	0.001	0.709	0.200	0.003	1.417
19	0.16	0.158	0.001	0.542	0.160	0.002	1.096
20	0.16	0.157	0.001	0.610	0.160	0.002	1.216
21	0.16	0.156	0.001	0.707	0.160	0.002	1.449
22	0.16	0.159	0.001	0.814	0.160	0.003	1.653
23	0.08	0.079	0.000	0.557	0.080	0.001	1.126
24	0.08	0.077	0.000	0.622	0.080	0.001	1.231
25	0.08	0.080	0.001	0.841	0.080	0.001	1.738

MANUALLY RECORDED DATA

Test	LIW Start	LIW End	GIW Start	GIW End	Filter	Estimated Cyclone Efficiency
#	kg	kg	kg	kg	kg	%
1	Lost	Lost	Lost	Lost	Lost	0.000
2	294.45	21.52	0.08	273.35	4.713	98.305
3	300.76	18.10	0.35	267.77	5.323	98.048
4	242.66	4.23	51.17	287.92	0.379	99.840
5	280.51	3.96	4.08	280.05	3.881	98.613
6	295.17	24.48	0.11	263.11	3.610	98.646
7	280.06	6.12	0.86	275.13	3.631	98.693
8	271.10	6.67	0.03	270.84	3.402	98.759
9	272.96	1.83	0.21	270.82	3.976	98.552
10	268.69	0.27	0.16	267.67	4.936	98.188
11	282.39	1.13	0.55	282.34	3.396	98.809
12	298.33	2.28	0.64	295.59	3.551	98.810
13	293.04	2.21	1.11	290.25	4.613	98.430
14	Lost	Lost	Lost	Lost	Lost	0.000
15	283.28	7.29	1.33	277.36	2.091	99.248
16	281.67	14.07	-0.49	267.63	3.210	98.817
17	280.03	28.79	-0.33	252.74	2.676	98.954
18	273.09	24.25	-0.03	248.59	2.008	99.120
19	278.08	18.58	0.51	259.07	4.251	98.382
20	271.15	25.90	-0.43	244.79	1.933	99.218
21	265.94	28.30	-0.40	236.99	2.359	99.016
22	273.65	20.42	-0.47	254.82	2.675	98.963
23	268.83	30.03	-0.42	237.63	2.476	98.971
24	276.85	13.94	0.32	261.38	1.911	99.273
25	270.96	12.97	-0.02	260.37	1.709	99.348

LIW DURING STEADY STATE TESTING PERIOD

Test	LIW Mass at Start	Uncertainty	LIW Mass at End	Uncertainty	LIW	Uncertainty	Upper Limit	Lower Limit
#	kg	kg	kg	kg	kg	kg	kg	kg
1	236.427	2.101	39.603	2.264	196.824	3.089	199.913	193.735
2	230.922	2.050	112.794	1.697	118.128	2.661	120.789	115.467
3	190.883	1.756	76.182	1.926	114.701	2.606	117.307	112.095
4	167.246	1.653	19.546	2.480	147.700	2.980	150.680	144.720
5	222.738	1.979	25.049	2.419	197.689	3.125	200.814	194.564
6	236.442	2.102	56.847	2.094	179.595	2.967	182.562	176.628
7	217.667	1.937	18.062	2.496	199.605	3.159	202.764	196.446
8	220.907	1.964	12.423	2.561	208.484	3.227	211.711	205.257
9	216.046	1.924	49.955	2.160	166.091	2.893	168.984	163.198
10	182.956	1.713	10.551	2.582	172.405	3.099	175.504	169.306
11	182.798	1.711	13.429	2.549	169.369	3.070	172.439	166.299
12	213.549	1.905	8.101	2.610	205.448	3.231	208.679	202.217
13	233.058	2.070	18.246	2.495	214.812	3.242	218.054	211.570
14	200.129	1.808	8.185	2.610	191.944	3.175	195.119	188.769
15	233.340	2.072	9.448	2.594	223.892	3.320	227.212	220.572
16	236.472	2.101	18.407	2.493	218.065	3.260	221.325	214.805
17	237.395	2.110	31.517	2.349	205.878	3.158	209.036	202.720
18	166.589	1.655	27.551	2.391	139.038	2.908	141.946	136.130
19	210.091	1.878	24.351	2.426	185.740	3.068	188.808	182.672
20	192.336	1.761	29.997	2.365	162.339	2.949	165.288	159.390
21	166.378	1.650	31.709	2.347	134.669	2.869	137.538	131.800
22	146.439	1.623	26.669	2.401	119.770	2.898	122.668	116.872
23	208.987	1.870	33.349	2.329	175.638	2.987	178.625	172.651
24	183.368	1.714	19.580	2.479	163.788	3.014	166.802	160.774
25	135.208	1.631	17.216	2.506	117.992	2.990	120.982	115.002

GIW DURING STEADY STATE TESTING PERIOD

Test	GIW Mass at Start	Uncertainty	GIW Mass at End	Uncertainty	GIW	Uncertainty	Upper Limit	Lower Limit	GIW(1/η)	Uncertainty	Upper Limit	Lower Limit
#	kg	kg	kg	kg	kg	kg	kg	kg	kg	kg	kg	kg
1	63.557	1.036	257.849	1.210	194.292	1.593	195.885	192.699	#DIV/0!	1.593	#DIV/0!	#DIV/0!
2	59.799	1.000	182.302	0.885	122.503	1.335	123.838	121.168	124.615	1.335	125.951	123.280
3	102.625	0.849	212.478	1.023	109.853	1.329	111.182	108.524	112.040	1.329	113.369	110.711
4	122.780	0.821	268.224	1.300	145.444	1.538	146.982	143.906	145.677	1.538	147.215	144.140
5	60.391	0.983	255.529	1.205	195.138	1.555	196.693	193.583	197.883	1.555	199.438	196.328
6	53.852	1.256	227.603	1.057	173.751	1.642	175.393	172.109	176.136	1.642	177.777	174.494
7	60.354	0.983	256.282	1.206	195.928	1.556	197.484	194.372	198.523	1.556	200.079	196.967
8	52.981	1.107	259.060	1.218	206.079	1.646	207.725	204.433	208.669	1.646	210.314	207.023
9	54.174	1.010	217.989	1.011	163.815	1.429	165.244	162.386	166.222	1.429	167.651	164.793
10	84.976	1.086	254.028	1.192	169.052	1.613	170.665	167.439	172.172	1.613	173.784	170.559
11	95.740	0.857	263.164	1.241	167.424	1.508	168.932	165.916	169.442	1.508	170.950	167.934
12	82.588	1.032	283.070	1.356	200.482	1.704	202.186	198.778	202.896	1.704	204.601	201.192
13	62.197	1.013	270.071	1.338	207.874	1.678	209.552	206.196	211.190	1.678	212.868	209.511
14	88.202	0.878	274.510	1.306	186.308	1.574	187.882	184.734	#DIV/0!	1.574	#DIV/0!	#DIV/0!
15	49.892	1.025	269.590	1.276	219.698	1.637	221.335	218.061	221.363	1.637	222.999	219.726
16	45.021	1.044	261.509	1.230	216.488	1.613	218.101	214.875	219.080	1.613	220.693	217.466
17	47.683	1.032	250.434	1.168	202.751	1.559	204.310	201.192	204.894	1.559	206.453	203.336
18	109.849	0.825	246.820	1.149	136.971	1.415	138.386	135.556	138.187	1.415	139.602	136.773
19	63.304	0.963	246.252	1.146	182.948	1.497	184.445	181.451	185.957	1.497	187.454	184.460
20	75.472	0.917	235.083	1.089	159.611	1.424	161.035	158.187	160.869	1.424	162.293	159.445
21	101.272	0.842	232.590	1.078	131.318	1.368	132.686	129.950	132.623	1.368	133.991	131.255
22	131.212	0.802	250.641	1.170	119.429	1.418	120.847	118.011	120.680	1.418	122.099	119.262
23	55.850	0.994	229.613	1.061	173.763	1.454	175.217	172.309	175.570	1.454	177.023	174.116
24	95.025	0.856	254.371	1.190	159.346	1.466	160.812	157.880	160.513	1.466	161.979	159.047
25	139.961	0.802	257.314	1.206	117.353	1.448	118.801	115.905	118.123	1.448	119.571	116.675

Appendix Q. Additional Literature Consulted

The following provides a list of literature containing the different components normally found in pneumatic conveying systems and test facilities built by others.

Cabrejos, F. J. & Klinzing, G. E., 1994. Pickup and saltation mechanisms of solid particles in horizontal pneumatic transport. Powder Technology, Volume 79, pp. 173 - 186.

Dhodapkar, S. & Zaltash, A., 1989. Acceleration zone studies in pneumatic conveying systems at various inclinations. *Fluidization and Fluid-Particle Systems - Fundamentaks and Applications, AIChE Symposium Series,* 85(270), pp. 1-8.

Hinkle, B. L., 1953. *Acceleration of Particles and Pressure Drops Encountered in Horizontal Penumatic Conveying.* Georgia: PhD Thesis: Georgia Institute of Technology.

Klinzing, G. E., Marcus, R. D., Rizk, F. & Leung, L. S., 1997. *Pneumatic Conveying of Solids: A Theoretical and Practical Approach.* 2nd ed. London: Chapman & Hall.

Rabinovich, E. & Kalman, H., 2008. Boundary saltation and minimum pressure velocities in particle–gas systems. *Powder Technology,* Volume 185, pp. 67 - 79.

Rose, H. E. & Duckworth, R. A., 1969. Transport of Solid Particles in Liquids and Gases. *The Engineer,* Volume 227, pp. 430-433.

Wei, W. et al., 2011. Experimental study on the solid velocity in horizontal dilute phase pneumatic. *Powder Technology,* 212(3), pp. 403-409.

Wen, C. Y. & Yu, Y. H., 1966. Mechanics of Fluidization. *Chemical Engineering Progress Symposium Series,* 62(62), pp. 100-111.

Zenz, F. A., 1949. Two-phase fluid-solid flow. *Industrial & Enegineering Chemistry,* 41(12), pp. 2801-2806.

Appendix R. Particle Density and Size Tests

RESULTS OF DENSITY TESTS MANDATED

Results of particle density tests mandated on PFA received from *POWER STATION 1*.

E032 - Colin Du Sart

Fly ash sample 1

Page 1

AccuPyc 1330 V1.02
Serial Number: 10
Density and Volume Report

Sample ID: 2016-02-22--01
Number of Purges: 10
Cell Volume: 12.0806 cc

Sample Weight: 6.5544 g
Equilibration Rate: 0.0050 psig/mir
Expansion Volume: 8.0167 cc

Run#	Volume cc	Deviation cc	Density g/cc	Deviation g/cc
1	2.9060	0.0165	2.2555	-0.0131
2	2.9036	0.0142	2.2573	-0.0113
3	2.8994	0.0099	2.2606	-0.0079
4	2.8700	-0.0194	2.2837	0.0152
5	2.9047	0.0153	2.2565	-0.0121
6	2.9126	0.0232	2.2504	-0.0182
7	2.9062	0.0168	2.2553	-0.0133
8	2.8990	0.0096	2.2609	-0.0077
9	2.8449	-0.0445	2.3039	0.0353
10	2.8477	-0.0417	2.3016	0.0330

Average Volume: 2.8894 cc
Average Density: 2.2686 g/cc

Standard Deviation: 0.0254 cc
Standard Deviation: 0.0201 g/cc

E032 - Colin Du Sart
Fly ash sample 2

AccuPyc 1330 V1.02
Serial Number: 10
Density and Volume Report

Sample ID: 2016-02-24--02
Number of Purges: 10
Cell Volume: 12.0806 cc

Sample Weight: 9.0667 g
Equilibration Rate: 0.0050 psig/min
Expansion Volume: 8.0167 cc

Run#	Volume cc	Deviation cc	Density g/cc	Deviation g/cc
1	3.9701	0.0122	2.2838	-0.0073
2	4.0314	0.0735	2.2490	-0.0420
3	4.0320	0.0741	2.2487	-0.0423
4	3.9452	-0.0127	2.2982	0.0072
5	3.9504	-0.0075	2.2951	0.0041
6	3.9253	-0.0326	2.3098	0.0188
7	3.9476	-0.0103	2.2968	0.0057
8	3.9229	-0.0350	2.3112	0.0202
9	3.9422	-0.0157	2.2999	0.0089
10	3.9119	-0.0460	2.3177	0.0267

Average Volume: 3.9579 cc
Average Density: 2.2910 g/cc

Standard Deviation: 0.0422 cc
Standard Deviation: 0.0242 g/cc

E032 - Colin Du Sart
Fly Ash sample 3

AccuPyc 1330 V1.02
Serial Number: 10
Density and Volume Report

Sample ID: 2016-02-25--03
Number of Purges: 10
Cell Volume: 12.0806 cc

Sample Weight: 8.4917 g
Equilibration Rate: 0.0050 psig/min
Expansion Volume: 8.0187 cc

Run#	Volume cc	Deviation cc	Density g/cc	Deviation g/cc
1	3.6445	-0.0733	2.3300	0.0454
2	3.7701	0.0523	2.2524	-0.0322
3	3.6863	-0.0316	2.3036	0.0191
4	3.7704	0.0525	2.2522	-0.0323

Average Volume: 3.7178 cc
Average Density: 2.2845 g/cc

Standard Deviation: 0.0629 cc
Standard Deviation: 0.0388 g/cc

E032 - Colin Du Sart
Fly ash sample 4

AccuPyc 1330 V1.02
Serial Number: 10
Density and Volume Report

Sample ID: 2016-02-23--04
Number of Purges: 10
Cell Volume: 12.0806 cc

Sample Weight: 6.4260 g
Equilibration Rate: 0.0050 psig/min
Expansion Volume: 8.0167 cc

Run#	Volume cc	Deviation cc	Density g/cc	Deviation g/cc
1	2.8372	-0.0015	2.2649	0.0012
2	2.8361	-0.0026	2.2658	0.0021
3	2.8356	-0.0031	2.2662	0.0025
4	2.8365	-0.0022	2.2654	0.0017
5	2.8480	0.0093	2.2563	-0.0074

Average Volume: 2.8387 cc
Average Density: 2.2637 g/cc

Standard Deviation: 0.0053 cc
Standard Deviation: 0.0042 g/cc

E032 - Colin Du Sart
Fly ash sample 5

AccuPyc 1330 V1.02
Serial Number: 10
Density and Volume Report

Sample ID: 2016-02-24--05
Number of Purges: 10
Cell Volume: 12.0806 cc

Sample Weight: 6.9080 g
Equilibration Rate: 0.0050 psig/mir
Expansion Volume: 8.0167 cc

Run#	Volume cc	Deviation cc	Density g/cc	Deviation g/cc
1	3.0587	0.0110	2.2585	-0.0082
2	3.0575	0.0098	2.2594	-0.0074
3	3.0556	0.0079	2.2608	-0.0059
4	3.0106	-0.0370	2.2945	0.0278
5	3.0545	0.0068	2.2616	-0.0051
6	3.0463	-0.0014	2.2677	0.0009
7	3.0633	0.0157	2.2550	-0.0117
8	3.0604	0.0127	2.2572	-0.0095
9	3.0103	-0.0374	2.2948	0.0281
10	3.0597	0.0121	2.2577	-0.0090

Average Volume: 3.0477 cc
Average Density: 2.2667 g/cc

Standard Deviation: 0.0201 cc
Standard Deviation: 0.0151 g/cc

RESULTS OF SIZE TESTS CONDUCTED

Results of particle size tests mandated on PFA received from Matla Power Station

MASTERSIZER 2000

Result Analysis Report

Sample Name: Fly Ash Sample 1 - Average	**SOP Name:** Alab_Fly Ash	**Measured:** Monday, February 22, 2016 11:32:15 AM	
Sample Source & type: Paris	**Measured by:** Unknown	**Analysed:** Monday, February 22, 2016 11:32:17 AM	
Sample bulk lot ref: 123-ABC	**Result Source:** Averaged		
Particle Name: Fly Ash	**Accessory Name:** Hydro 2000G (A)	**Analysis model:** General purpose	**Sensitivity:** Enhanced
Particle RI: 1.500	**Absorption:** 0.1	**Size range:** 0.020 to 2000.000 um	**Obscuration:** 11.68 %
Dispersant Name: Water	**Dispersant RI:** 1.330	**Weighted Residual:** 0.684 %	**Result Emulation:** Off
Concentration: 0.0185 %Vol	**Span :** 3.929	**Uniformity:** 1.28	**Result units:** Volume
Specific Surface Area: 0.757 m²/g	**Surface Weighted Mean D[3,2]:** 7.926 um	**Vol. Weighted Mean D[4,3]:** 68.096 um	

d(0.1): 5.020 um **d(0.5):** 40.922 um **d(0.9):** 165.811 um

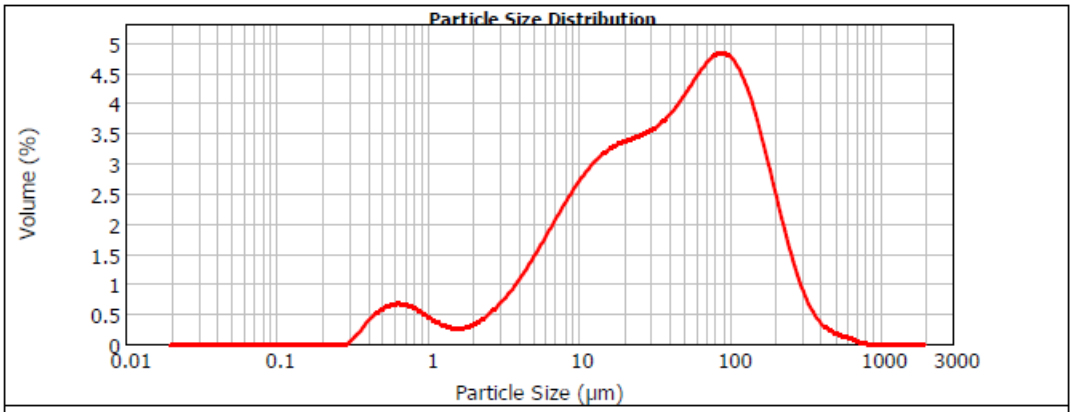

Size (µm)	Volume In %
1.000	1.39
2.000	1.27
3.000	3.44
5.000	3.86
7.000	5.59
10.000	

Size (µm)	Volume In %
10.000	7.86
15.000	6.17
20.000	4.96
25.000	9.76
38.000	8.61
53.000	

Size (µm)	Volume In %
53.000	10.19
75.000	10.84
106.000	9.83
150.000	6.93
212.000	3.60
300.000	

Size (µm)	Volume In %
300.000	1.30
425.000	0.42
600.000	0.11
850.000	0.00
1000.000	0.00
1400.000	

Size (µm)	Volume In %
1400.000	0.00
2000.000	0.00
2800.000	0.00
4000.000	0.00
5600.000	0.00
8000.000	

Size (µm)	Volume In %
8000.000	

MASTERSIZER 2000

Result Analysis Report

Sample Name: Fly Ash Sample 2 - Average
Sample Source & type: Paris
Sample bulk lot ref: 123-ABC
SOP Name: Alab_Fly Ash
Measured by: Unknown
Result Source: Averaged
Measured: Monday, February 22, 2016 11:42:36 AM
Analysed: Monday, February 22, 2016 11:42:38 AM

Particle Name: Fly Ash
Particle RI: 1.500
Dispersant Name: Water
Accessory Name: Hydro 2000G (A)
Absorption: 0.1
Dispersant RI: 1.330
Analysis model: General purpose
Size range: 0.020 to 2000.000 um
Weighted Residual: 0.674 %
Sensitivity: Enhanced
Obscuration: 10.38 %
Result Emulation: Off

Concentration: 0.0165 %Vol
Specific Surface Area: 0.745 m²/g
Span : 3.827
Surface Weighted Mean D[3,2]: 8.058 um
Uniformity: 1.23
Vol. Weighted Mean D[4,3]: 65.878 um
Result units: Volume

d(0.1): 5.151 um **d(0.5):** 40.799 um **d(0.9):** 161.269 um

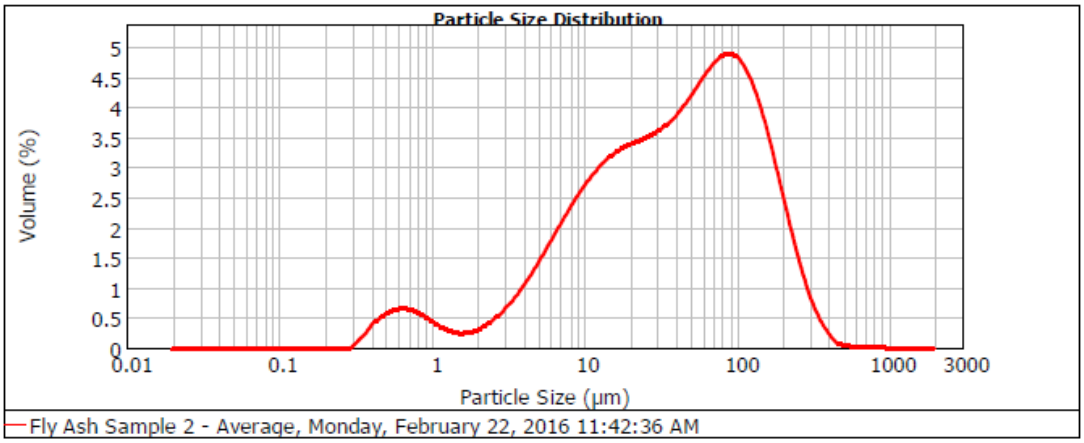

Size (µm)	Volume In %
1.000	1.33
2.000	1.21
3.000	3.39
5.000	3.86
7.000	5.61
10.000	

Size (µm)	Volume In %
10.000	7.89
15.000	6.21
20.000	5.01
25.000	9.92
38.000	8.76
53.000	

Size (µm)	Volume In %
53.000	10.35
75.000	10.98
106.000	9.94
150.000	6.98
212.000	3.51
300.000	

Size (µm)	Volume In %
300.000	1.07
425.000	0.13
600.000	0.05
850.000	0.01
1000.000	0.00
1400.000	

Size (µm)	Volume In %
1400.000	0.00
2000.000	0.00
2800.000	0.00
4000.000	0.00
5600.000	0.00
8000.000	

Size (µm)	Volume In %
8000.000	

MASTERSIZER 2000

Result Analysis Report

Sample Name: Fly Ash Sample 3 - Average
SOP Name: Alab_Fly Ash
Measured: Monday, February 22, 2016 12:00:35 PM
Sample Source & type: Paris
Measured by: Unknown
Analysed: Monday, February 22, 2016 12:00:37 PM
Sample bulk lot ref: 123-ABC
Result Source: Averaged

Particle Name: Fly Ash
Accessory Name: Hydro 2000G (A)
Analysis model: General purpose
Sensitivity: Enhanced
Particle RI: 1.500
Absorption: 0.1
Size range: 0.020 to 2000.000 um
Obscuration: 10.51 %
Dispersant Name: Water
Dispersant RI: 1.330
Weighted Residual: 0.677 %
Result Emulation: Off

Concentration: 0.0166 %Vol
Span : 4.150
Uniformity: 1.44
Result units: Volume
Specific Surface Area: 0.75 m²/g
Surface Weighted Mean D[3,2]: 8.002 um
Vol. Weighted Mean D[4,3]: 74.509 um

d(0.1): 5.106 um **d(0.5):** 40.797 um **d(0.9):** 174.418 um

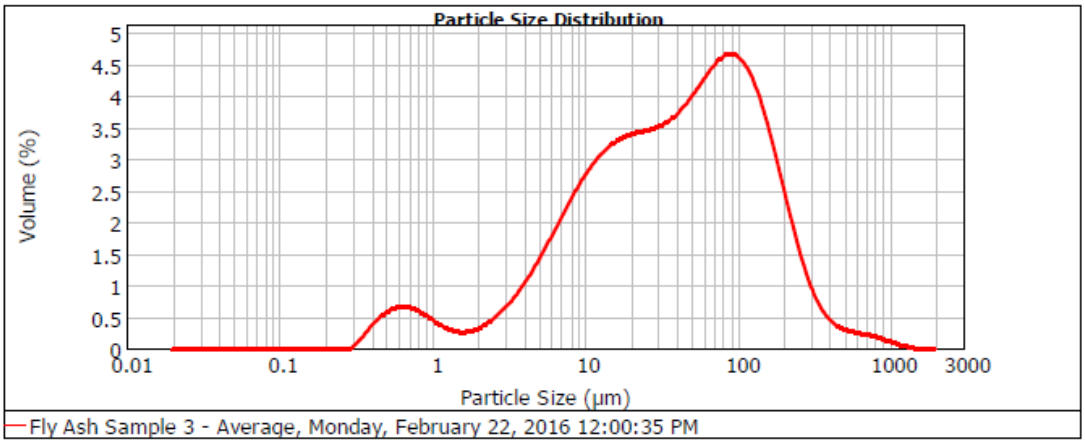

Size (µm)	Volume In %
1.000	1.38
2.000	1.23
3.000	3.36
5.000	3.86
7.000	5.68
10.000	

Size (µm)	Volume In %
10.000	8.03
15.000	6.26
20.000	4.99
25.000	9.67
38.000	8.39
53.000	

Size (µm)	Volume In %
53.000	9.85
75.000	10.49
106.000	9.60
150.000	6.86
212.000	3.64
300.000	

Size (µm)	Volume In %
300.000	1.47
425.000	0.69
600.000	0.48
850.000	0.14
1000.000	0.12
1400.000	

Size (µm)	Volume In %
1400.000	0.00
2000.000	0.00
2800.000	0.00
4000.000	0.00
5600.000	0.00
8000.000	

Size (µm)	Volume In %
8000.000	

MASTERSIZER 2000

Result Analysis Report

Sample Name: Fly Ash Sample 4 - Average
SOP Name: Alab_Fly Ash
Measured: Monday, February 22, 2016 12:12:51 PM
Sample Source & type: Paris
Measured by: Unknown
Analysed: Monday, February 22, 2016 12:12:53 PM
Sample bulk lot ref: 123-ABC
Result Source: Averaged

Particle Name: Fly Ash
Accessory Name: Hydro 2000G (A)
Analysis model: General purpose
Sensitivity: Enhanced
Particle RI: 1.500
Absorption: 0.1
Size range: 0.020 to 2000.000 um
Obscuration: 10.50 %
Dispersant Name: Water
Dispersant RI: 1.330
Weighted Residual: 0.618 %
Result Emulation: Off

Concentration: 0.0182 %Vol
Span : 3.727
Uniformity: 1.19
Result units: Volume
Specific Surface Area: 0.686 m²/g
Surface Weighted Mean D[3,2]: 8.750 um
Vol. Weighted Mean D[4,3]: 69.929 um

d(0.1): 5.851 um **d(0.5):** 44.199 um **d(0.9):** 170.562 um

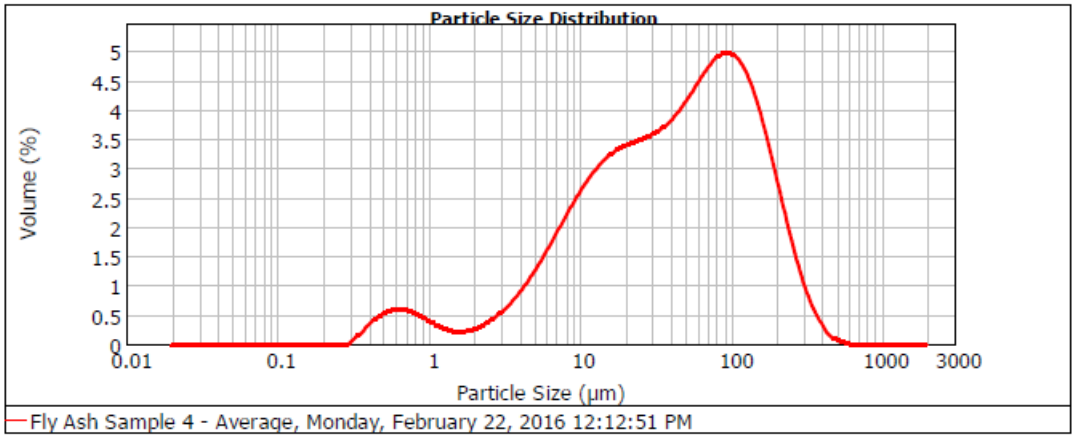

Size (µm)	Volume In %
1.000	1.17
2.000	1.03
3.000	2.91
5.000	3.47
7.000	5.29
10.000	

Size (µm)	Volume In %
10.000	7.76
15.000	6.22
20.000	5.03
25.000	9.87
38.000	8.66
53.000	

Size (µm)	Volume In %
53.000	10.30
75.000	11.17
106.000	10.44
150.000	7.62
212.000	4.05
300.000	

Size (µm)	Volume In %
300.000	1.37
425.000	0.19
600.000	0.00
850.000	0.00
1000.000	0.00
1400.000	

Size (µm)	Volume In %
1400.000	0.00
2000.000	0.00
2800.000	0.00
4000.000	0.00
5600.000	0.00
8000.000	

Size (µm)	Volume In %
8000.000	

MASTERSIZER 2000

Result Analysis Report

Sample Name: Fly Ash Sample 5 - Average
SOP Name: Alab_Fly Ash
Measured: Monday, February 22, 2016 12:23:04 PM
Sample Source & type: Paris
Measured by: Unknown
Analysed: Monday, February 22, 2016 12:23:06 PM
Sample bulk lot ref: 123-ABC
Result Source: Averaged

Particle Name: Fly Ash
Accessory Name: Hydro 2000G (A)
Analysis model: General purpose
Sensitivity: Enhanced
Particle RI: 1.500
Absorption: 0.1
Size range: 0.020 to 2000.000 um
Obscuration: 10.50 %
Dispersant Name: Water
Dispersant RI: 1.330
Weighted Residual: 0.631 %
Result Emulation: Off

Concentration: 0.0177 %Vol
Span : 3.797
Uniformity: 1.21
Result units: Volume
Specific Surface Area: 0.705 m²/g
Surface Weighted Mean D[3,2]: 8.510 um
Vol. Weighted Mean D[4,3]: 68.038 um

d(0.1): 5.623 um **d(0.5):** 42.393 um **d(0.9):** 166.583 um

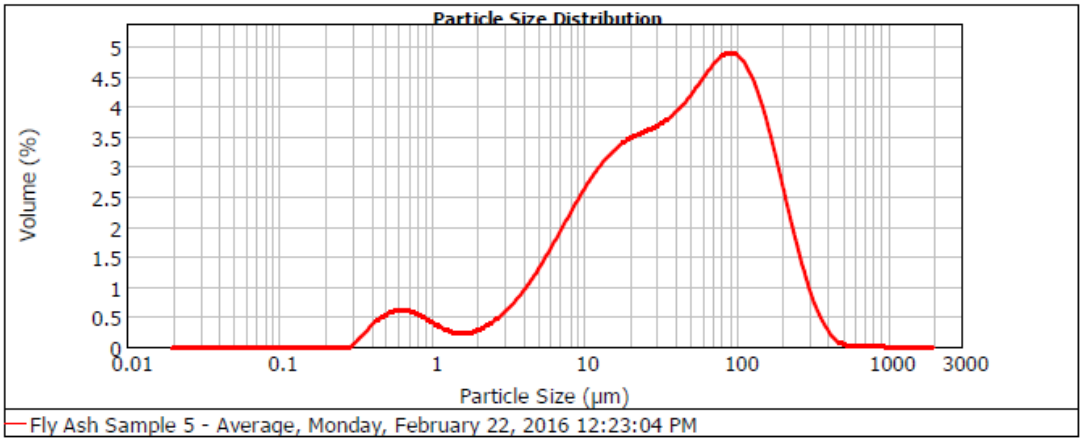

Size (µm)	Volume In %
1.000	1.22
2.000	1.10
3.000	3.04
5.000	3.55
7.000	5.34
10.000	

Size (µm)	Volume In %
10.000	7.83
15.000	6.32
20.000	5.14
25.000	10.12
38.000	8.78
53.000	

Size (µm)	Volume In %
53.000	10.28
75.000	10.98
106.000	10.16
150.000	7.36
212.000	3.85
300.000	

Size (µm)	Volume In %
300.000	1.22
425.000	0.13
600.000	0.03
850.000	0.01
1000.000	0.00
1400.000	

Size (µm)	Volume In %
1400.000	0.00
2000.000	0.00
2800.000	0.00
4000.000	0.00
5600.000	0.00
8000.000	

Size (µm)	Volume In %
8000.000	

RESULTS OF INDEPENDENT PARTICLE SIZE AND DENSITY TESTS

The tables below were extracted from rights protected documents with permission from the owner.

Results of particle density and size tests conducted on PFA from *POWER STATION 2*.

Property Tested	PFA Sample
Solids density (total size fraction)	2 363 kg/m^3
1 000 - 212 micron fraction average solids density	2 685 kg/m^3
212 - 106 micron fraction average solids density	2 603 kg/m^3
106 - 63 micron fraction average solids density	2 422 kg/m^3
< 63 micron fraction average solids density	2 188 kg/m^3
d_{90} particle size	200 µm
d_{50} particle size	57 µm
% +75 microns	40.1
% passing 25 microns	29.5

Results of particle density and size tests conducted on PFA from *POWER STATION 1.*

Property Tested	PFA	BBA
Skeletal solids density	2 200 ± 20 kg/m^3	2 100 ± 50 kg/m^3
d_{90} Particle size envelope	98 µm – 118 µm	869 µm – 10 967 µm
d_{50} Particle size envelope	27 µm – 28 µm	152 µm – 485 µm

Appendix S. Equipment Data Sheets

Technical
Information
TI 291P/00/en

Pressure Transducer
cerabar T PMP 131

Order Code: PMP131-A3B01A2H

Pressure transducer with polysilicon sensor
For absolute and gauge pressures up to 400 bar
Version available for hazardous areas

Application
Cerabar T PMP 131 is designed for measuring absolute and gauge pressure of gases, vapours and liquids.

Features and Benefits
- Finely graduated measuring ranges up to 400 bar or 6000 psi
- Up to 4 times overload resistance
- Extremely stable
- Flush diaphragm process connection or manometer connection for ½ BSP (G ½), ¼ BSP (G ¼) or ½ NPT
- Electronic versions with
  – analogue output 4...20 mA
  – switch output PNP transistor
- Approved for EEx ib IIC T6

Measuring System
- Pressure transducer Cerabar T PMP 131 with 4...20 mA output or switch output.
- Power supply, e.g. RN 221 transmitter power supply unit from Endress+Hauser

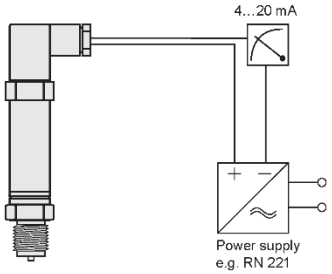

Endress+Hauser
The Power of Know How

TI00436P/00/EN/21.15
No. 71303154

Technical Information
Cerabar M
PMC51, PMP51, PMP55

Process pressure measurement

For Final Test Facility - Order Code: PMC51-IF21JA2KGCGVJA+Z1

Pressure transmitter with ceramic and metallic sensors

Application

The device is used for the following measuring tasks:
- Absolute pressure and gauge pressure measurement in gases, steams or liquids in all areas of process engineering and process measurement technology
- Level, volume or mass measurements in liquids
- High process temperature
  - without diaphragm seals up to 130 °C (266°F), for a maximum of 60 minutes 150 °C (302°F)
  - with diaphragm seals up to 400 °C (752°F)
- High pressure up to 400 bar (6000 psi)
- International usage thanks to a wide range of approvals

Your benefits

- Very good reproducibility and long-term stability
- High reference accuracy: up to ±0.15%, as PLATINUM version: ±0.075%
- Turn down up to 100:1
- Standardized platform for differential pressure, hydrostatics, and pressure (Deltabar S – Deltapilot S – Cerabar S)
- Simple, fast commissioning through a user interface designed for real-world applications
- Used for process pressure monitoring up to SIL2, certified to IEC 61508 Edition 2.0 and IEC 61511 by TÜV NORD
- New TempC diaphragm for diaphragm seals: Minimum temperature effects, maximum diaphragm thickness and short recovery times
- Device versions compliant with ASME-BPE

Endress+Hauser
People for Process Automation

TI00434P/00/EN/18.14
71241482

Products Solutions Services

Technical Information
Deltabar M PMD55
Differential pressure measurement

Order Code: PMD55-I121BA67DGCHA4A1A+PBZ1

Differential pressure transmitter with metal sensor; communication via HART, PROFIBUS PA or FOUNDATION Fieldbus

Application
The Deltabar M differential pressure transmitter is used for the following measuring tasks:

- Flow measurement (volume or mass flow) in conjunction with primary elements in gases, vapours and liquids
- Level, volume or mass measurement in liquids
- Differential pressure monitoring, e.g. of filters and pumps

Your benefits

- Reference accuracy: 0.1%
  as PLATINUM version: up to 0.075%
- Turn down up to 100:1
- Compact transmitter design
- Quick commissioning via DIP switches
- Easy and safe menu-guided operation
  - onsite via display module
  - via 4 to 20 mA with HART
  - via PROFIBUS PA
  - via FOUNDATION Fieldbus
- Continuous modularity for differential pressure, hydrostatic and pressure (Deltabar M, Deltapilot M Cerabar M), e.g.
  - replaceable display
  - universal electronics
- International usage thanks to a wide range of approvals
- Used for process pressure monitoring up to SIL2, certified to IEC 61508 Edition 2.0 and IEC 61511 by TÜV NORD

Endress+Hauser
People for Process Automation

Level Pressure Flow Temperature Liquid Analysis Registration Systems Components Services Solutions

Technical Information

Omnigrad M TR15

Order Code: TR15-E1B8A1FAG7000

Modular RTD assembly
neck tube, barstock thermowell,
available with a flange or as a weld-in unit

Application

- Universal range of application
- Particularly suitable for steam and gas applications with high process pressures and temperatures
- Measuring range: -200...600 °C (-328...1112 °F)
- Pressure range up to 400 bar (5800 psi) for the weld-in units
- Degree of protection: up to IP 68

Head transmitters

All Endress+Hauser transmitters are available with enhanced accuracy and reliability compared to directly wired sensors. Easy customizing by choosing one of the following outputs and communication protocols:

- Analog output 4...20 mA
- HART®
- PROFIBUS® PA
- FOUNDATION Fieldbus™

Your benefits

- High flexibility due to modular assembly with standard terminal heads and customized immersion length
- High compatibility with a design according to DIN 43772
- Neck tube for heat protection of head transmitter
- Fast response time with reduced/tapered tip form
- Types of protection for use in hazardous locations:
  Intrinsic Safety (Ex ia)
  Non-Sparking (Ex nA)

CE Ex

TI260T/02/en
71088514

Endress+Hauser
People for Process Automation

BM11

中航电测 ZEMIC
Measuring Excellence Worldwide

3 X 200kg & 3 X 500kg
Load Cells as Highlighted + Junction Box and Cables

- BM11 load cells are available in the capacities 5kg~500kg.
- Stainless steel construction, welded with bellow, potted by adhesive inside, oil proof, waterproof, anti-corrosive gas and medium making it suitable for all kinds of environments.
- Single point with bellow, easy installation, suitable for crane scales, mechanical conversion scales, hopper scales and other electronic weighing devices.
- Safe and anti-explosive product, can be used in atrocious environment and hazardous areas.

Features

- Capacity 5kg ~500kg
- High accuracy
- Stainless steel construction
- Low profile
- PTB Approval No: D09-06.44
- NTEP Certificates No: CC07-020

Accessories

- BM-11-401 • BM-11-402

Specifications

Capacity	kg	5/10/20/30/50/100/200/250/300/350/500					
Accuracy		C2	C3	A5S	A5M	B10S	B10M
Approvals			OIML R60 C3		III 5000 Multiple		IIIL 10000 Multiple
Maximum number of verification intervals	nmax	2000	3000	5000	5000	10000	10000
Minimum load cell verification interval	Vmin	Emax/5000	Emax/10000	Emax/15000	Emax/15000	Emax/10000	Emax/10000
Combined error	(%FS)	≤±0.030	<±0.020	≤±0.018	≤±0.026	≤±0.035	<±0.050
Creep	(%FS/30min)	≤±0.024	<±0.016	≤±0.012	≤±0.017	≤±0.030	<±0.040
Temperature effect on sensitivity	(%FS/10℃)	≤±0.017	≤±0.011	≤±0.009	≤±0.013	≤±0.030	≤±0.040
Temperature effect on zero	(%FS/10℃)	≤±0.023	≤±0.015	≤±0.010	≤±0.014	≤±0.030	≤±0.020
Output sensitivity	(mv/v)	2.0 0.02					
Input resistance	(Ω)	460 50					
Output resistance	(Ω)	351 2.0					
Insulation resistance	(MΩ)	5000(50VDC)					
Zero balance	(%FS)	1.0					
Temperature, compensated	(℃)	-10 +40					
Temperature, operating	(℃)	-35 ~+65					
Excitation, recommended	(V)	5~12(DC)					
Excitation, max	(V)	18(DC)					
Safe overload	(%FS)	150					
Ultimate overload	(%FS)	300					

Outline Dimension mm(inch)

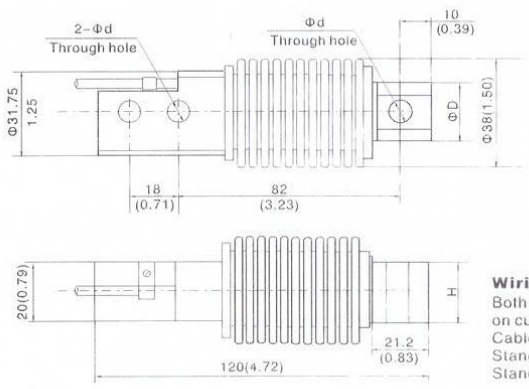

Dimension \ Capacity (kg)	5,10,20,30,50 100,200,300	350,500
d	8.2 (0.32)	10.3 (0.41)
D	23 (0.91)	24 (0.94)
H	20 (0.79)	19 (0.75)

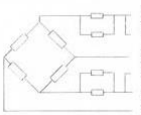

Input (+) Green
Sense (+) Yellow
Output (–) Red
Sense (–) Blue
Input (–) Black
Output (+) White

Wiring:
Both 4 and 6 conductor wires are available on customers' requirements.
Cable diameter: φ5φ0.2mm
Standard length for 4 conductor cable: 3m
Standard length for 6 conductor cable: 6m

Note: Connection of 6 conductor wires are as above. For 4 conductor wires the yellow and blue sense wires are removed

67

HM2D4

中航电测 ZEMIC
Measuring Excellence Worldwide

- HM2D4 load cells are available for manifold accurate measurement in the capacities 0.5t to 20t.
- Alloy steel, hermetically sealed, oil-proof, waterproof and anti-corrosion, suitable for multiform environments.
- Spoke type, suitable for electronic truck scale, hopper scale, automotive testing line and other electronic weighing devices and various force measurement occasions.

Features

- Capacity: 0.5t~20t
- High accuracy
- Alloy steel construction
- Low profile

For Final Test Facility

Specifications					
Capacity	t	0.5/1/2/5/10/20			
Accuracy class		C2	C3	A5S	A5M
Maximum number of verification intervals	nmax	2000	3000	5000	5000
Minimum load cell verification interval	vmin	Emax/5000	Emax/10000	Emax/15000	Emax/15000
Combined error	(%FS)	≤ ±0.030	≤ ±0.020	≤ ±0.018	≤ ±0.026
Creep	(%FS/30min)	≤ ±0.024	≤ ±0.016	≤ ±0.012	≤ ±0.017
Temperature effect on sensitivity	(%FS/10℃)	≤ ±0.017	≤ ±0.011	≤ ±0.009	≤ ±0.013
Temperature effect on zero	(%FS/10℃)	≤ ±0.023	≤ ±0.015	≤ ±0.010	≤ ±0.014
Output sensitivity	(mv/v)	2.0±0.002			
Input resistance	(Ω)	350±3			
Output resistance	(Ω)	351±2			
Insulation resistance	(MΩ)	≥5000(50VDC)			
Zero balance	(%FS)	1.0			
Temperature, compensated	(℃)	-10~+40			
Temperature, allowed	(℃)	-35~+65			
Excitation, Recommended	(V)	5~12(DC)			
Excitation, Max.	(V)	18(DC)			
Safe overload	(%FS)	150			
Ultimate overload	(%FS)	300			

Outline Dimension mm(inch)

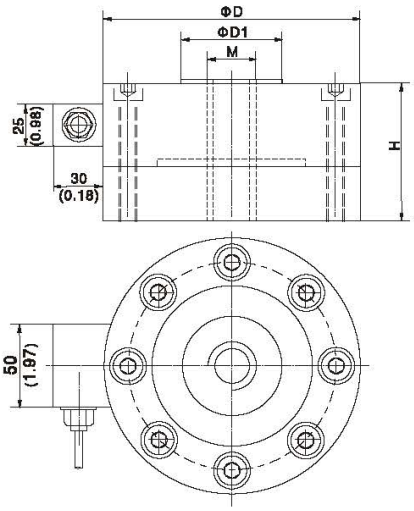

Dimension / Capacity	ΦD	ΦD1	H	M
0.5t~2t	105 (4.13)	28 (1.10)	70 (2.76)	M14×2
5t	120 (4.72)	33 (1.3)	80 (3.15)	M20×1.5
10t, 20t	155 (6.10)	60.5 (2.38)	90 (3.54)	M32×2

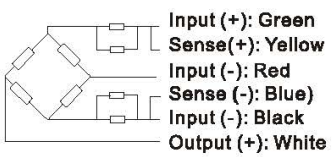

Wiring:
Shielded, 6 conductor cable ϕ5.6mm
Standard cable length:5m

2 X LCA-D

LCA
Load Cell Amplifier

MDK-LCA-R00-060602

USER MANUAL

Ver: 1.0.2

08-20-2002

Technical Sales

(866) 531-6285
orders@ni.com

Requirements and Compatibility | Ordering Information | Detailed Specifications | Pinouts/Front Panel Connections
For user manuals and dimensional drawings, visit the product page resources tab on ni.com.

Last Revised: 2014-11-06 07:14:23.0

NI 9208 + NI9923 Screw terminal block

16-Channel Current Input Module

- 16 current inputs (±21.5 mA)
- High-resolution mode with 50/60 Hz rejection
- 500 S/s sample rate (high-speed mode)
- Voltage supply pins for external power routing (2 A/30 V maximum)
- -40 to 70 °C
- 60 VDC, CAT I bank isolation (1,000 Vrms withstand)
- Optional NI 9933 connectivity kit shown in image on right
- 24-bit resolution

Overview

The NI 9208 current input C Series module has 16 channels of ±21 mA input with built-in 50/60 Hz rejection for noise rejection.

Designed with industrial systems in mind, the NI 9208 has a high-channel density to reduce the number of modules you need. This opens slots for other measurement types and reduces the overall cost per channel of the system.

The NI 9208 has a standard 37-pin D-Sub connection for use with available cables and connector blocks, or the NI 9937 D-Sub connector kit. The NI 9937 contains a D-Sub to screw terminal accessory as well as a protective shell. With this kit, you can create a custom cable that plugs directly into the module, eliminating the need for a separate terminal block.

Back to Top

Requirements and Compatibility

OS Information

- Real-Time OS

Driver Information

- NI-RIO

Software Compatibility

- LabVIEW
- LabVIEW FPGA Module
- LabVIEW Real-Time Module

Back to Top

Comparison Tables

Module	Channels	Sample Rate	Simultaneous	Isolation
NI 9208	16 current	500 S/s	No	Channel-ground
NI 9207	8 current/8 voltage	500 S/s	No	Channel-ground
NI 9219	4 universal	100 S/s/ch	Yes	Channel-channel
NI 9203	8 current	200 kS/s	No	Channel-ground

Back to Top

DATASHEET

NI 9265 Datasheet + NI 9927 Strain Relief Protection

4-Channel, 0 mA to 20 mA, 16-Bit Analog Output Module

- 4 channels, 100 kS/s per channel simultaneously analog output
- 0 mA to 20 mA output range, 16-bit resolution
- Open-loop detection with interrupt, 0.0 mA power-on
- 250 Vrms, CAT II bank isolation
- 10-position screw-terminal or 10-position spring-terminal connectors available
- -40 °C to 70 °C operating range, 5 g vibration, 50 g shock

The NI 9265 is a 4-channel, 0 mA to 20 mA, 100 kS/s simultaneously updating C Series analog output module for any CompactDAQ or CompactRIO chassis. It is ideal for interfacing and controlling industrial current-driven actuators at high rates. The module has built-in open-loop detection, which generates an interrupt in software when an open loop is detected as well as zeroing outputs to ensure safety and avoid driving actuators at system power-on. The NI 9265 requires a 9 V to 36 V external power supply and includes a channel-to-earth ground double isolation barrier for safety and noise immunity.

NI C Series Overview

NI provides more than 100 C Series modules for measurement, control, and communication applications. C Series modules can connect to any sensor or bus and allow for high-accuracy measurements that meet the demands of advanced data acquisition and control applications.

- Measurement-specific signal conditioning that connects to an array of sensors and signals
- Isolation options such as bank-to-bank, channel-to-channel, and channel-to-earth ground

NATIONAL INSTRUMENTS

Technical Sales

(866) 531-6285
orders@ni.com

Ordering Information | Detailed Specifications

For user manuals and dimensional drawings, visit the product page resources tab on ni.com.

Last Revised: 2015-09-14 16:51:17.0

NI CompactDAQ
USB Data Acquisition Systems

+ Screw terminal kit for power supply connection

- Mix sensor measurements with analog and digital I/O in the same instrument
- Run hardware-timed analog I/O, digital I/O, and counter/timer tasks independently
- Simultaneously acquire analog data at up to three different rates
- USB 2.0 or 3.0 communication with NI patented high-speed, parallel streaming
- Measure in minutes with NI-DAQmx software and automatic code generation using the DAQ Assistant
- LabVIEW SignalExpress LE data-logging software included for simple applications
- Four 32-bit general-purpose counters built into chassis (access through digital module or BNC triggers)
- BNC trigger connections on the cDAQ-9178/79 for up to 1 MHz clocks and triggers

Overview

NI CompactDAQ USB chassis provide the plug-and-play simplicity of USB to sensor and electrical measurements on the benchtop, in the field, and on the production line. By combining more than 60 sensor-specific NI C Series I/O modules with patented NI Signal Streaming technology, the NI CompactDAQ platform delivers high-speed data and ease of use in a flexible, mixed-measurement system. Modules are available for a variety of sensor measurements including thermocouples, RTDs, strain gages, load and pressure transducers, torque cells, accelerometers, flow meters, and microphones.

The main advantage of USB over other PC peripheral buses is simplicity of device detection. Connect any NI CompactDAQ USB chassis to a Windows PC with the NI-DAQmx driver installed, and the chassis is automatically detected with no additional configuration needed. The device is ready to run with the included LabVIEW SignalExpress software for simple data-logging applications. In addition, with NI-DAQmx driver software, you can develop a complete test system in LabVIEW, C/C++, Visual Basic .NET, and other programming environments. This ease of setup makes USB a good choice for portable applications that may move from one PC to another.

Back to Top

Comparison Tables

Model	Slots	Counters	Number of Simultaneous Tasks	Number of AI Timing Engines
cDAQ-9179	14	4	12	3
cDAQ-9178	8	4	7	3
cDAQ-9174	4	4	7	3
cDAQ-9171	1	4	6	3

Back to Top

Application and Technology

Mix Analog, Digital, and Sensor Measurements in the Same System

Many devices can measure temperature, voltage, or bridge-based sensors, but NI CompactDAQ can integrate all of these measurements and more into a single device that outputs all of the data via the same bus interface, such as USB. An NI CompactDAQ system can mix multiplexed voltage input signals, simultaneously sampled accelerometers,

Technical Sales

(866) 531-6285
orders@ni.com

For user manuals and dimensional drawings, visit the product page resources tab on ni.com.

Last Revised: 2014-11-06 07:14:59.0

Industrial Power Supplies

NI PS-14, NI PS-15, NI PS-16, NI PS-17

- 24 VDC power supplies for CompactRIO, NI CompactDAQ, NI Single-Board RIO, NI Smart Cameras, and NI touch panel computers
- Full output power between -25 °C and +60 °C
- 115 V/230 V autoselect input
- Efficiencies up to more than 90 percent
- Low input rush current
- 20 or 50 percent power reserves for dynamic loads (NI PS-15 and NI PS-16)
- Toolless spring-clamp terminals for easy field connectivity
- DIN-rail mounting included and panel/side mount accessories available
- -25 °C to 70 °C operating temperature range

Overview

The NI PS-14, PS-15, PS-16, and PS-17 industrial power supplies feature long expected life, generous power reserves, and compact size. The 24 V supplies are ideal for powering any NI CompactRIO, NI Single-Board RIO, NI Smart Camera, NI touch panel computer, NI CompactDAQ, or NI Compact FieldPoint system, as well as heavy accessory loads such as DC motor drives. The DIN-rail system and spring clamp terminals do not require tools and make installation fast and easy. The wide range and autoselect input voltages help you avoid user errors. The wide operating temperature range and extraordinary EMI immunity enables trouble-free operation even under harsh conditions. Depending on the device, NI industrial power supplies guarantee power reserves of 20 to 50 percent. For the PS-15 and PS-16, you can use this extra current continuously for ambient temperatures under 45 °C. With these power reserves, you may not need to oversize for dynamic loads, but you can simply choose a unit that meets the operating requirements. In some cases, you can select a smaller unit to save money and space.

Back to Top

Comparison Tables

Product	Output Voltage (V)	Output Current (A)	Output Power (W)	Input Voltage	Temperature Range (°C)	Size WxHxD (mm)	Weight (g)	Part Number
PS-14	24 to 28	3.3	80	100 to 240 VAC/110 to 375 VDC	-25 to +70	32 x 124 x 102	430	783167-01
PS-15	24 to 28	5	120	90 to 132/180 to 264 VAC	-25 to +70	32 x 124 x 117	500	781093-01
PS-16	24 to 28	10	240	90 to 132/180 to 264 VAC	-25 to +70	60 x 124 x 117	700	781094-01
PS-17	24 to 28	20	480	85 to 276 VAC/110 to 150 VDC	-25 to +70	82 x 124 x 127	1200	781095-01

Back to Top

Application and Technology

Mounting Options

The PS-14/15/16/17 power supplies include clips for DIN-rail mounting. National Instruments provides optional accessories for wall, panel, and side mounting to minimize installation depth. You can couple the included DIN-rail mounting bracket with the side mount kit for a low-profile DIN-rail installation.

Part Number	Product	Installed Width (mm)	Installed Height (mm)	Installed Depth (mm)	Bracket Weight (g)
	Panel Mount Kit for				

Solid State Relays
Industrial, 3-Phase ZS
Type RZ3A -40D40

- 3-phase Solid State Relay
- Zero switching
- Rated operational current: 3 x 25, 40, 55 or 75 A
- Rated operational voltage: Up to 600 VAC
- Control voltage 5 VDC, 4-32 VDC or 24-275 VAC
- Integral snubber networks
- Over-temperature protection option with alarm output
- IP 10 back-of-hand protection
- LED indication of control input and over-temperature alarm status

Product Description

A Solid State Relay family designed to switch various loads such as heating elements, motors and transformers. The relay is capable of switching high voltages up to 600 VACrms.

For higher reliability and load cycle capability three semiconductor power units are soldered directly on to the direct copper bonded (DCB) substrate.
AC- or DC-controlled versions are available. Built-in LED status indication for applied control voltage and over-temperature alarm (optional). A version that can be controlled with 5 VDC @ 15 mA (max) is also available (LD).

The series covers a range of load currents up to 75 AACrms.

Ordering Key

RZ 3 A 60 D 75 P

- Solid State Relay
- Number of poles
- Switching mode
- Rated opertional voltage
- Control voltage
- Rated opertional current
- Options

Type Selection

Switching mode	Rated operational voltage	Rated operational current	Control voltage	Option
A: Zero Switching	40: 400 VACrms 60: 600 VACrms	25: 3 x 25 AACrms 40: 3 x 40 AACrms 55: 3 x 55 AACrms 75: 3 x 75 AACrms	LD: 5 VDC D: 4-32 VDC A: 24-275 VAC/24-50 VDC	P: Over-temperature protection and alarm output (available only for A and D input)

Selection Guide

Rated operational voltage	Control voltage	Rated operational current 3 x 25 A	3 x 40 A	3 x 55 A	3 x 75 A
400 VACrms	5 VDC	RZ3A40LD25	RZ3A40LD40	RZ3A40LD55	RZ3A40LD75
	4-32 VDC	RZ3A40D25	RZ3A40D40	RZ3A40D55	RZ3A40D75
	24-275 VAC/24-50 VDC	RZ3A40A25	RZ3A40A40	RZ3A40A55	RZ3A40A75
600 VACrms	5 VDC	RZ3A60LD25	RZ3A60LD40	RZ3A60LD55	RZ3A60LD75
	4-32 VDC	RZ3A60D25	RZ3A60D40	RZ3A60D55	RZ3A60D75
	24-275 VAC/24-50 VDC	RZ3A60A25	RZ3A60A40	RZ3A60A55	RZ3A60A75

Notes
Over-temperature protection and alarm output: add suffix P to include over-temperature protection and alarm output.
Example: RZ3A60D75P. Not available with "LD" type control.

Insulation

Rated insulation voltage	
Input to output	≥ 4000 VACrms
Output to case	≥ 4000 VACrms

Thermal Specifications

Operating temperature	-30° to +80°C (-22° to +158° F)
Storage temperature	-40° to +100°C (-40° to + 212° F)
Junction temperature	≤ +125°C (+ 257°F)

Specifications are subject to change without notice (01.10.2003) 1

18

Dosing Screws

DS

Bulkmatic Dosing Screws are manufactured to suit customer feed requirements. The units can be supplied as volumetric feeders where a variable speed drive is used to change the dosing rate. Alternatively loadcells can be integrated into the system to provide accurate loss in weight feed of material. For extreme turndown ratios the electric drive motor can be supplied with a cooling fan.

A horizontal paddle above the dosing screw ensures that the material is evenly fed into the dosing screw. This allows accurate feeding of the most difficult materials. Paddle types are selected according to the material fed through the dosing screw.

On the standard version the paddle is driven via the screw shaft with a chain and chain tensioner. Alternatively the paddle shaft and screw shaft can be driven independently by two geared motors.

Dosing screws can be fitted with manual dump hoppers or the inlet hopper sized and designed for automatic refilling – either by using level sensors to control the head of material or by using the integrated loadcells on the loss in weight system.

Both the driven and non-driven ends of the paddle and the driven end of the dosing screw are fitted with stuffing glands to ensure a dust tight sealing arrangement. The outboard bearings are mounted on standoffs to allow easy access to the stuffing gland while the bearings on the driven end are housed under the gear and chain guard.

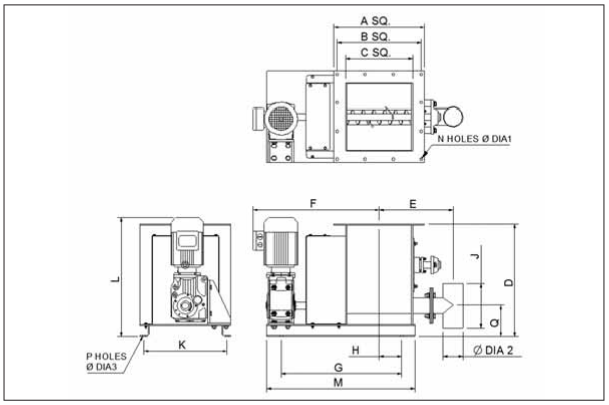

Standard outlet sizes include: 40NB, 65NB, 80NB and 100NB. Other sizes and configurations are available on request.

Dosing Screws

UNIT NO.	A	B	C	D	E	F	G	H	N	DIA1	DIA2	J	K	L	M	P	Q	DIA3	POWER kW	WEIGHT kg
DS-040	405	375	325	503	310	560	537	100	12	14	60,32	100	370	535	657	4	141	12	0,55	120
DS-065	405	375	325	503	330	560	537	100	12	14	88,9	150	370	535	657	4	138	12	0,55	135
DS-080	405	375	325	503	330	560	537	100	12	14	114,3	200	370	535	657	4	130	12	0,55	145
DS-100	405	375	325	503	350	560	537	100	12	14	141,3	200	370	535	657	4	130	12	0,75	170

Bulkmatic

Rotary Vane Feeders - Square BT Type

Bulkmatic Blow Through Rotary Vane Feeders are designed for the pneumatic conveying of products that do not easily vacate the impeller pockets. The inlet and outlet pipe of the blow through rotary feeder are designed to clear out the pocket as the impeller rotates into the air stream.

The design includes outboard bearings, machined stuffing boxes and "oversized" impeller shafts. The inlet ports have "V's" cast into the side wall to create a scissor cutting action between impeller blade and casing. This ensures smooth rotation without the "chopping effect' experienced with other valves. The result is increased bearing and impeller tip life.

The "BT" type valve has an open ended impeller and has adjustable tips fitted as standard. This valve is suitable for applications where the pressure differential is below 100 kPa and is ideal for use in Pneumatic Conveying Systems and heavy duty applications. Various options are available including different materials of construction such as stainless steel, body venting, inlet scrapers, "hard chromed" casings, air purged glands and high temperature construction.

Standard sizes include: 200, 250, 300, 400 and 500. Other sizes manufactured on request.

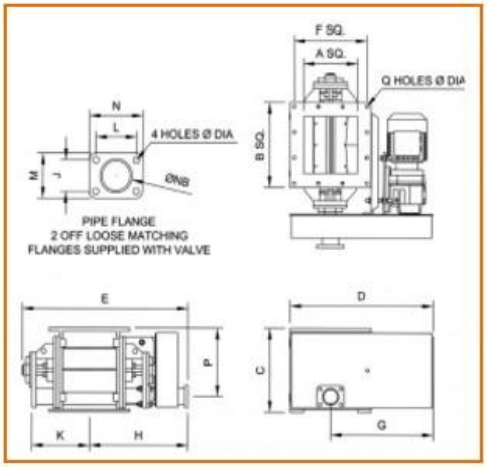

Rotary Vane Feeders - Square BT Type

UNIT NO.	DRIVE kW	NB	A	B	C	D	E	F	G	H	K	J	L	M	N	P	Q	DIA	WEIGHT kg
RVF-0200-BT	0.37	50(2")	200	300	300	530	620	3x90=270	380	366	214	56	76	80	100	244	12	12	120
RVF-0250-BT	0.55	80(3")	250	355	355	600	715	3x105=315	420	420	244	68	94	104	122	286	12	12	200

Cyclone Dimensiones

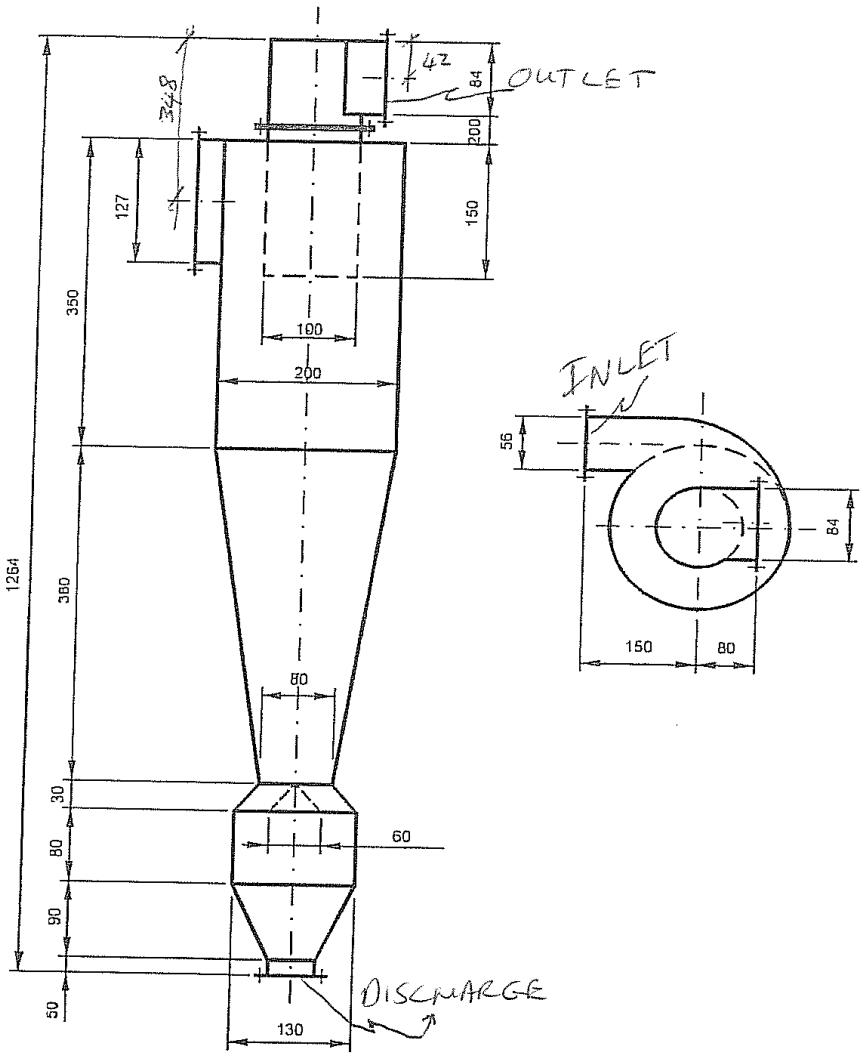

For Filter Pressure Drop

FP-...	305	420	508	610
Dimension H	287	402	490	592
Weight kg (F)	2.7	3.6	4.2	5.0
Weight kg (H)	3.2	4.4	5.2	6.2

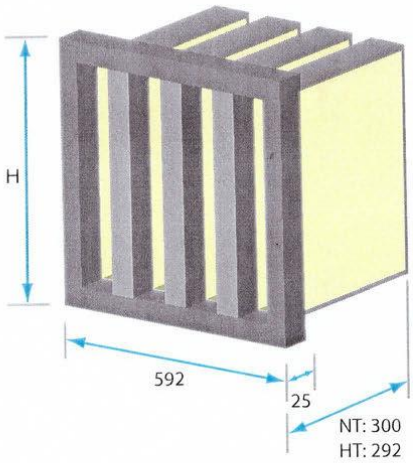

▲ Dimensions (mm)

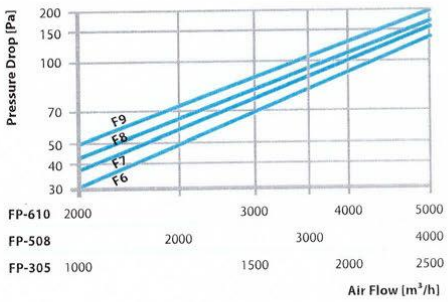

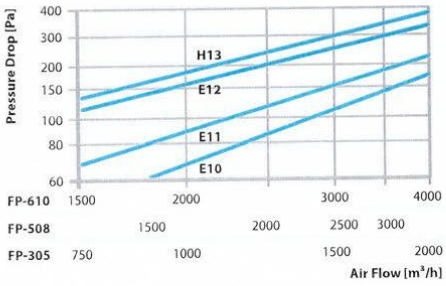

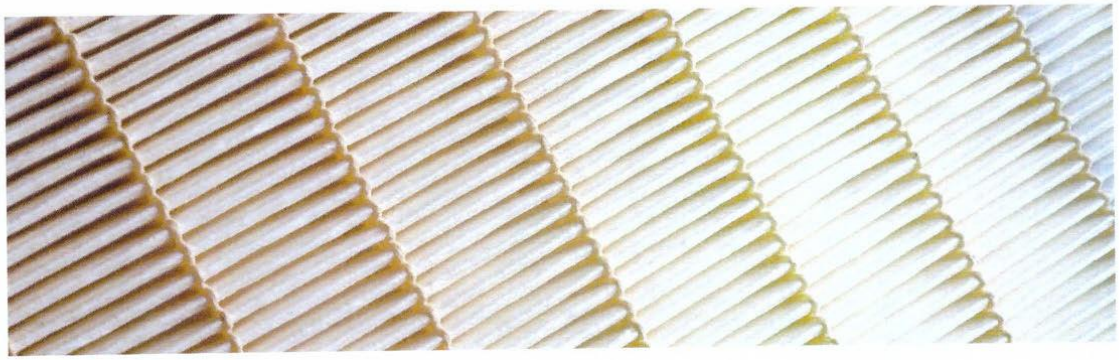

COMPATEX FP

For Final Test Facility

ScandDust SDM 15

ScandDust SDM 15 is the smalles unit in the family. SDM 15 has only one filter cartridge and can be delivered with internal fan alternatively to be connected to an external fan.

In the version with internal fan the collector can also be provided with HEPA filter as final stage to meet extreme demands in connection with recirculation of the air into the room.

The collector is manufactured in a welded, painted design. The circular housing with a tangential air inlet creates a cyclon effect which gives a preseparation of dust before the filter cartridges.

ScanDust SDM 15 can also be delivered in a vacuum design to be used for industrial cleaning etc.

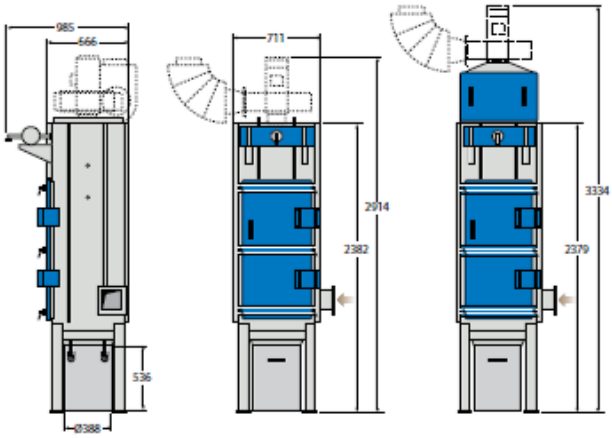

*) With standard dust can

Nom.air flow ..... 900 m³/h
Nom. filter area ..... 15 m²
No. of cartridges 1

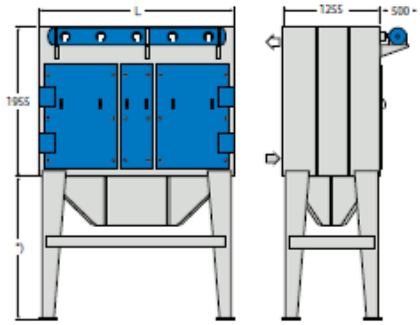

*) depends on selected dust handling system

ScandDust SDM

ScandDust SDM is a modular designed dust collector with rectangular filterhousing. Smallest module has four filter cartridges and largets module has 12 filter cartridges. SDM is always connected to an external fan.

SDM is manufactured as standard out of galvanized sheet metal but can also be delivered in painted or stainless steel design as well as with filterhousing thermally insulated. A: larger airflows multiple modules are connected in parallel.

Size	Nom. air flow m³/h	Nom. filter area m²	No. ef filter cartridges	L
60	3600	60	4	1115
90	5400	90	6	1570
120	7200	120	8	2025
150	9000	150	10	2480
180	10800	180	12	2935

www.vokesair.com

Appendix T. Detailed Electrical Drawings

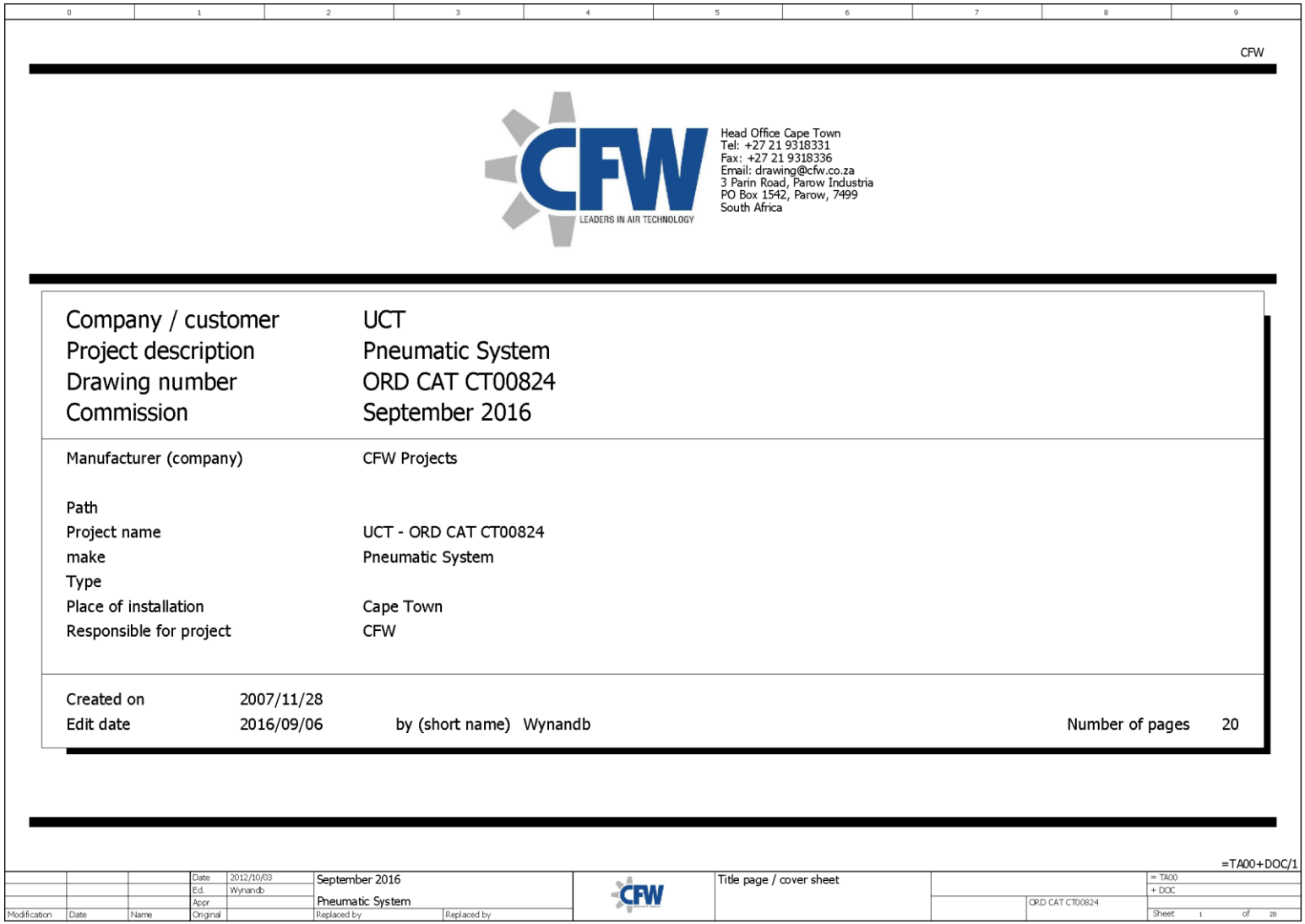

CFW

Head Office Cape Town
Tel: +27 21 9318331
Fax: +27 21 9318336
Email: drawing@cfw.co.za
3 Parin Road, Parow Industria
PO Box 1542, Parow, 7499
South Africa

Company / customer	UCT
Project description	Pneumatic System
Drawing number	ORD CAT CT00824
Commission	September 2016
Manufacturer (company)	CFW Projects
Path	
Project name	UCT - ORD CAT CT00824
make	Pneumatic System
Type	
Place of installation	Cape Town
Responsible for project	CFW

Created on 2007/11/28
Edit date 2016/09/06 by (short name) Wynandb Number of pages 20

=TA00+DOC/1

Date 2012/10/03 | September 2016 | Title page / cover sheet | = TA00
Ed. Wynandb | + DOC
Appr | Pneumatic System | ORD CAT CT00824
Modification | Date | Name | Original | Replaced by | Replaced by | Sheet 1 of 20

Table of contents

Column X: An automatically generated page was edited F06_001

Page	Page description	supplementary page field	Date	Edited by	X
=TA00+DOC/1	Title page / cover sheet	1	2012/10/03	Wynandb	X
=TA00+DOC/2	Table of contents : =TA00+DOC/1 - =TA00+DOC/19.a	2	2016/09/06	Wynandb	
=TA00+DOC/3	Technical data	3	2016/09/05	Wynandb	
=TA00+DOC/4	Panel layout	4	2016/09/06	Wynandb	
=TA00+DOC/5	Terminal layout	5	2016/09/06	Wynandb	
=TA00+DOC/6	Main supply	6	2016/09/05	Wynandb	
=TA00+DOC/7	Control Circuit	7	2016/09/06	Wynandb	
=TA00+DOC/8	Blower fan - 22kW VSD	8	2016/09/06	Wynandb	
=TA00+DOC/9	Auger motor - 0.55kW VSD	9	2016/09/06	Wynandb	
=TA00+DOC/10	Rotary motor - 0.55kW SSR	10	2016/09/06	Wynandb	
=TA00+DOC/11	Analog Inputs	11	2016/09/06	Wynandb	
=TA00+DOC/12	Analog Outputs	12	2016/09/06	Wynandb	
=TA00+DOC/13	Loadcell connections	13	2016/09/06	Wynandb	
=TA00+DOC/14	Field wiring 1	14	2016/09/05	Wynandb	
=TA00+DOC/15	Field wiring 2	15	2016/09/06	Wynandb	
=TA00+DOC/16	Field wiring 3	16	2016/09/06	Wynandb	
=TA00+DOC/17	Field wiring 4	17	2016/09/06	Wynandb	
=TA00+DOC/18	Parts list : - LOV.LPX_LP_B3	18	2016/09/06	Wynandb	
=TA00+DOC/19	Summarized parts list : - LOV.LPC_SL1203	19	2016/09/06	Wynandb	
=TA00+DOC/20	Summarized parts list : LOV.LPX_C10 - LOV.LPX_LP_B3	20	2016/09/06	Wynandb	

1 =TA00+DOC/2

			Date	2016/09/06	September 2016		Table of contents : =TA00+DOC/1 - =TA00+DOC/19.a		= TA00
			Ed.	Wynandb					+ DOC
			Appr		Pneumatic System			ORD CAT CT00824	
Modification	Date	Name	Original		Replaced by	Replaced by			Sheet 2 of 20

Technical Data

Client

UCT

Electrical Panel Design	CFW Projects
Electrical Panel Construct	CFW Projects
Machine Installation	CFW Projects
Site commisioning	CFW Projects

Data

Supply Voltage	3/PEN ~ 50Hz 400V
Control Voltage	24VDC
Controller	National Instruments
Year of construction	2016
Current (Max)	45 Amp

CFW Projects (PTY) LTD
Tel: +27 21 9318331
Fax: +27 21 9318336
1 Parin Road, Parow Industria
PO Box 1542, Parow, 7499
South Africa

Wiring Colours

Phase 1	Red
Phase 2	White
Phase 3	Blue
Neutral	Black
Earth Protection	Green/Yellow
Control Circuit DC 0V	Blue
Control Circuit DC 24V	Violet
Analog signal	White
Analog 0V	Blue
External Voltage	Orange

Main Control Cabinet

Brand	Rittal
Type	1600x800x500
Colour	RAL 7035

2

=TA00+DOC/3

			Date	2016/09/05	September 2016		Technical data		= TA00
			Ed.	Wynand	Pneumatic System				+ DOC
			App					DRD CAT CF00324	
Modification	Date	Name	Original		Replaced by	Replaced by			Sheet 1 of 20

PANEL LAYOUT

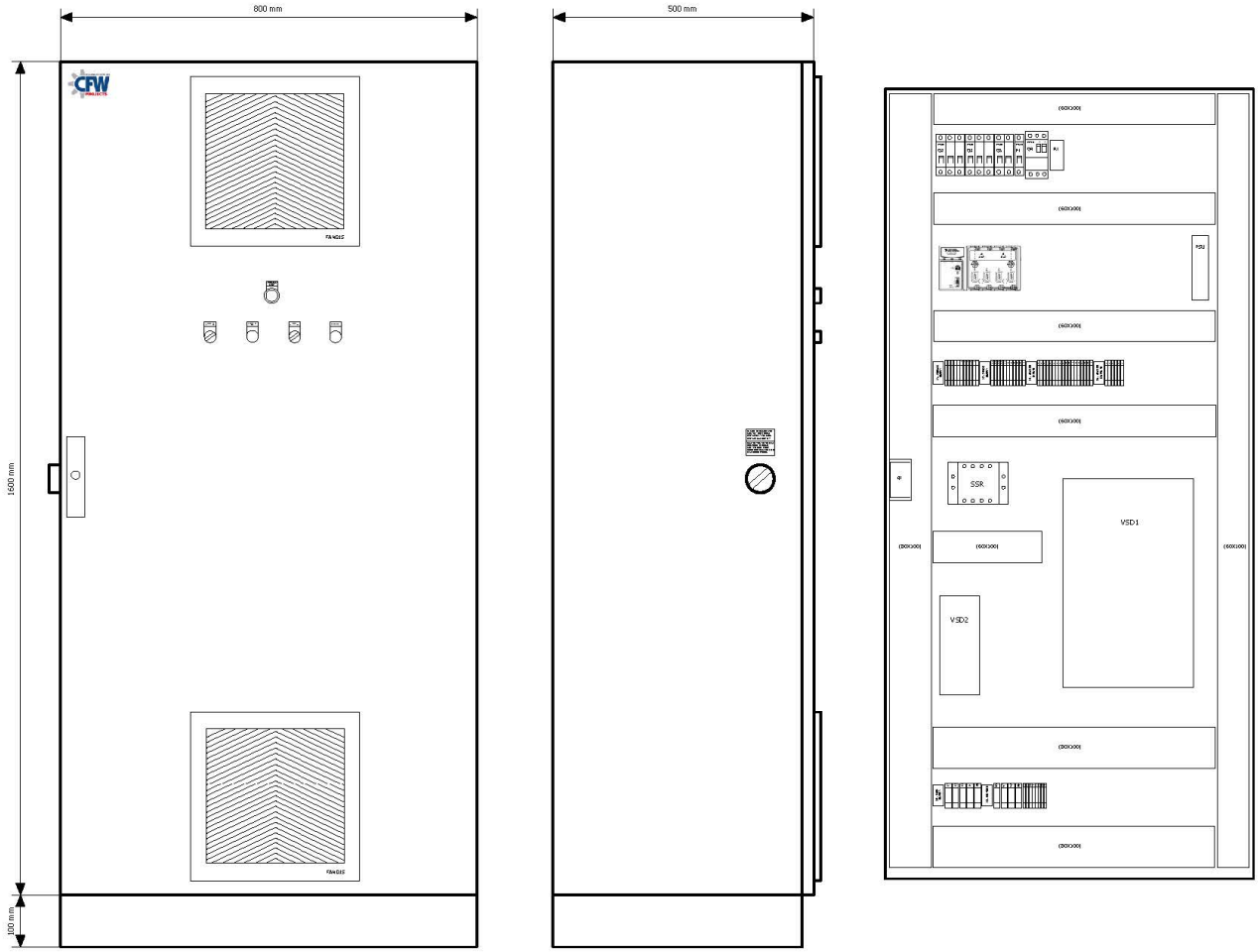

3

=TA00+DOC/4

			Date	2016/09/06	September 2016		Panel layout	= TA00
			Ed.	Wynandb				+ DOC
			Appr		Pneumatic System		ORD CAT CT00824	
Modification	Date	Name	Original		Replaced by	Replaced by		Sheet 4 of 20

TERMINAL LAYOUT

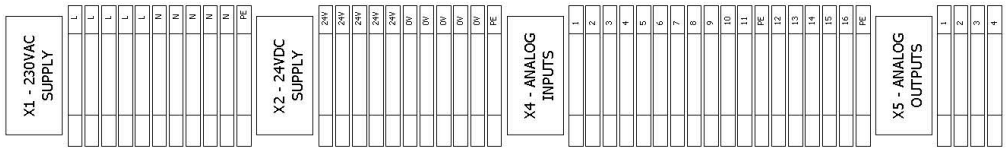

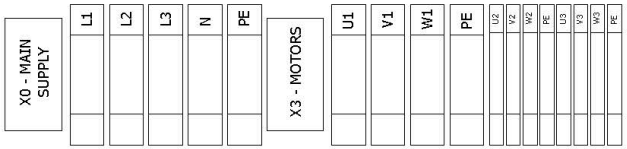

4

=TA00+DOC/5

			Date	2016/09/06	September 2016		Terminal layout		= TA00
			Ed.	Wynandb					+ DOC
			Appr		Pneumatic System			ORD CAT CT00824	
Modification	Date	Name	Original		Replaced by	Replaced by			Sheet 5 of 20

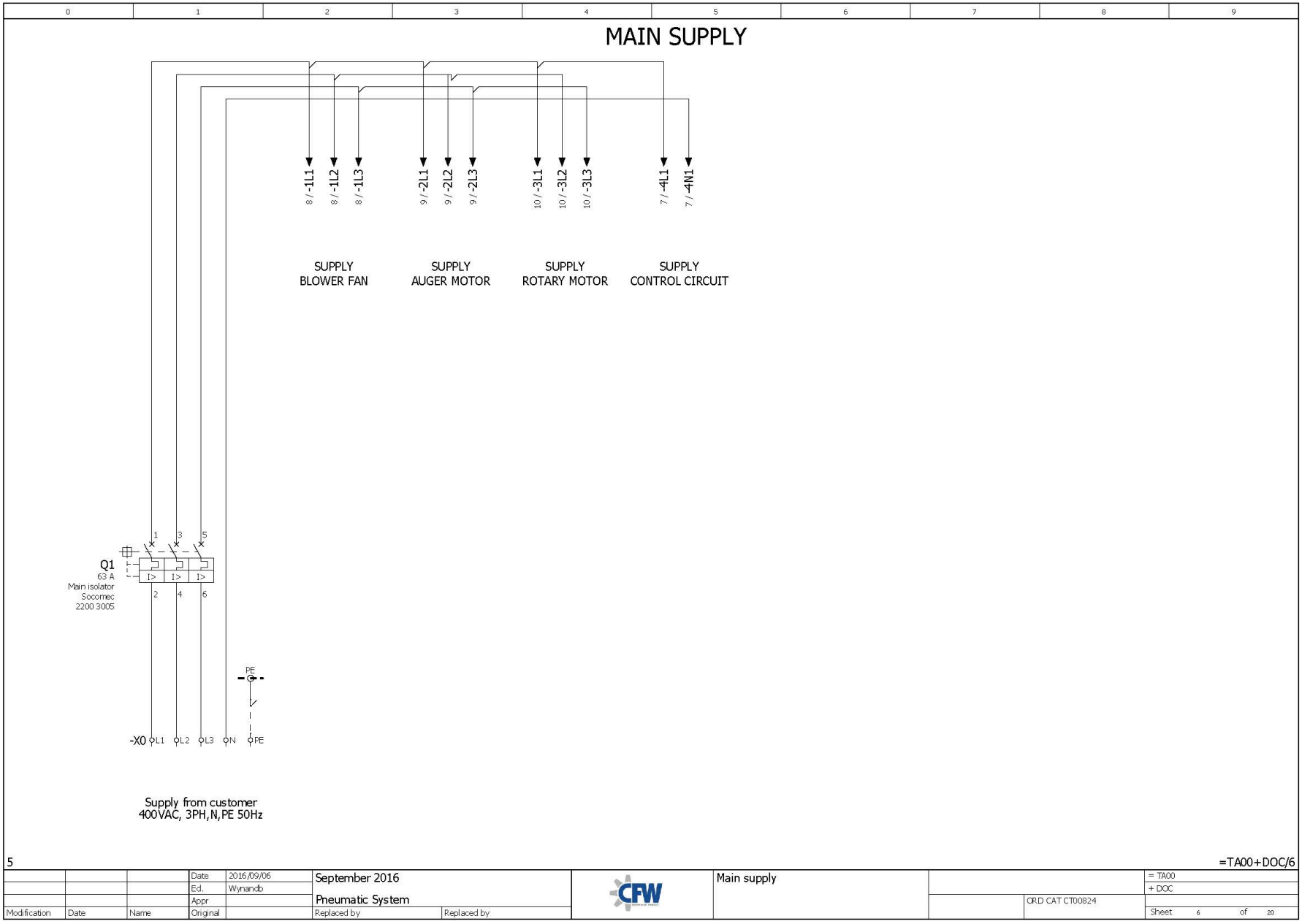
MAIN SUPPLY
8 / -1L1
8 / -1L2
8 / -1L3
9 / -2L1
9 / -2L2
9 / -2L3
10 / -3L1
10 / -3L2
10 / -3L3
7 / -4L1
7 / -4N1
SUPPLY BLOWER FAN
SUPPLY AUGER MOTOR
SUPPLY ROTARY MOTOR
SUPPLY CONTROL CIRCUIT
Q1
63 A
Main isolator
Socomec
2200 3005
1
3
5
2
4
6
I>
PE
-X0
L1
L2
L3
N
PE
Supply from customer
400VAC, 3PH,N,PE 50Hz
5
=TA00+DOC/6
Date 2016/09/06
Ed. Wynandb
Appr
September 2016
Pneumatic System
Main supply
= TA00
+ DOC
ORD CAT CT00824
Sheet 6 of 20
Modification Date Name Original Replaced by Replaced by

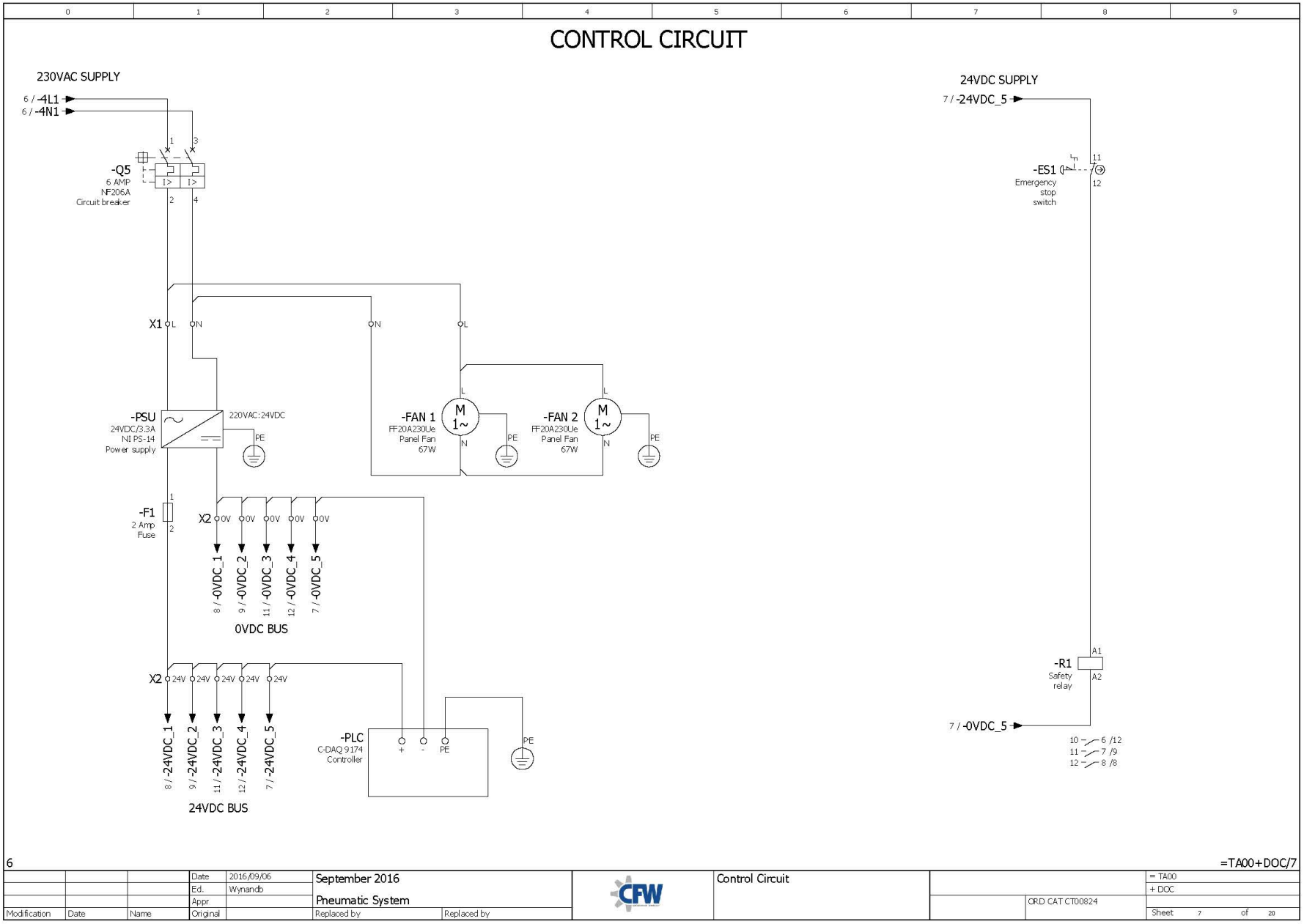
CONTROL CIRCUIT
230VAC SUPPLY
6 / -4L1
6 / -4N1
-Q5
6 AMP
NF206A
Circuit breaker
X1
-PSU
24VDC/3.3A
NI PS-14
Power supply
220VAC:24VDC
-FAN 1
FF20A230Ue
Panel Fan
67W
-FAN 2
FF20A230Ue
Panel Fan
67W
-F1
2 Amp
Fuse
X2
0VDC BUS
8 / -0VDC_1
9 / -0VDC_2
11 / -0VDC_3
12 / -0VDC_4
7 / -0VDC_5
24VDC BUS
8 / -24VDC_1
9 / -24VDC_2
11 / -24VDC_3
12 / -24VDC_4
7 / -24VDC_5
-PLC
C-DAQ 9174
Controller
24VDC SUPPLY
7 / -24VDC_5
-ES1
Emergency
stop
switch
-R1
Safety
relay
7 / -0VDC_5
10 6 /12
11 7 /9
12 8 /8
6
=TA00+DOC/7
Date 2016/09/06
Ed. Wynandb
Appr
September 2016
Pneumatic System
Control Circuit
= TA00
+ DOC
ORD CAT CT00824
Sheet 7 of 20
Modification Date Name Original Replaced by Replaced by

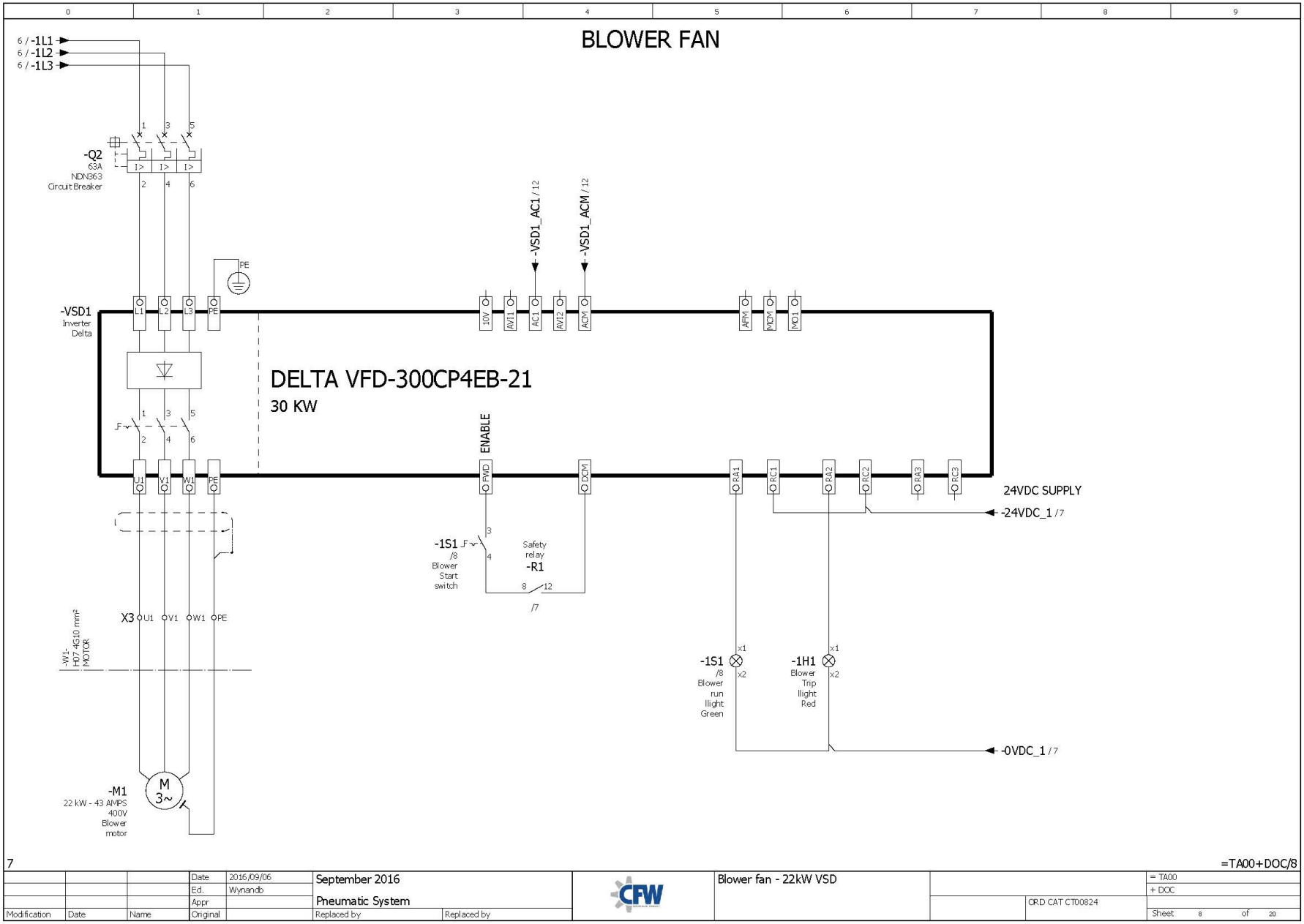
BLOWER FAN
6 / -1L1
6 / -1L2
6 / -1L3
-Q2
63A
NDN363
Circuit Breaker
-VSD1
Inverter
Delta
-VSD1_AC1 / 12
-VSD1_ACM / 12
PE
DELTA VFD-300CP4EB-21
30 KW
ENABLE
24VDC SUPPLY
-24VDC_1 / 7
-0VDC_1 / 7
-1S1
/8
Blower
Start
switch
Safety
relay
-R1
/7
-1S1
/8
Blower
run
light
Green
-1H1
Blower
Trip
light
Red
X3
-W1-
H07 4G10 mm²
MOTOR
-M1
22 kW - 43 AMPS
400V
Blower
motor
7
=TA00+DOC/8
Date 2016/09/06
Ed. Wynandb
Appr
September 2016
Pneumatic System
Blower fan - 22kW VSD
= TA00
+ DOC
ORD CAT CT00824
Sheet 8 of 20
Modification Date Name Original Replaced by Replaced by

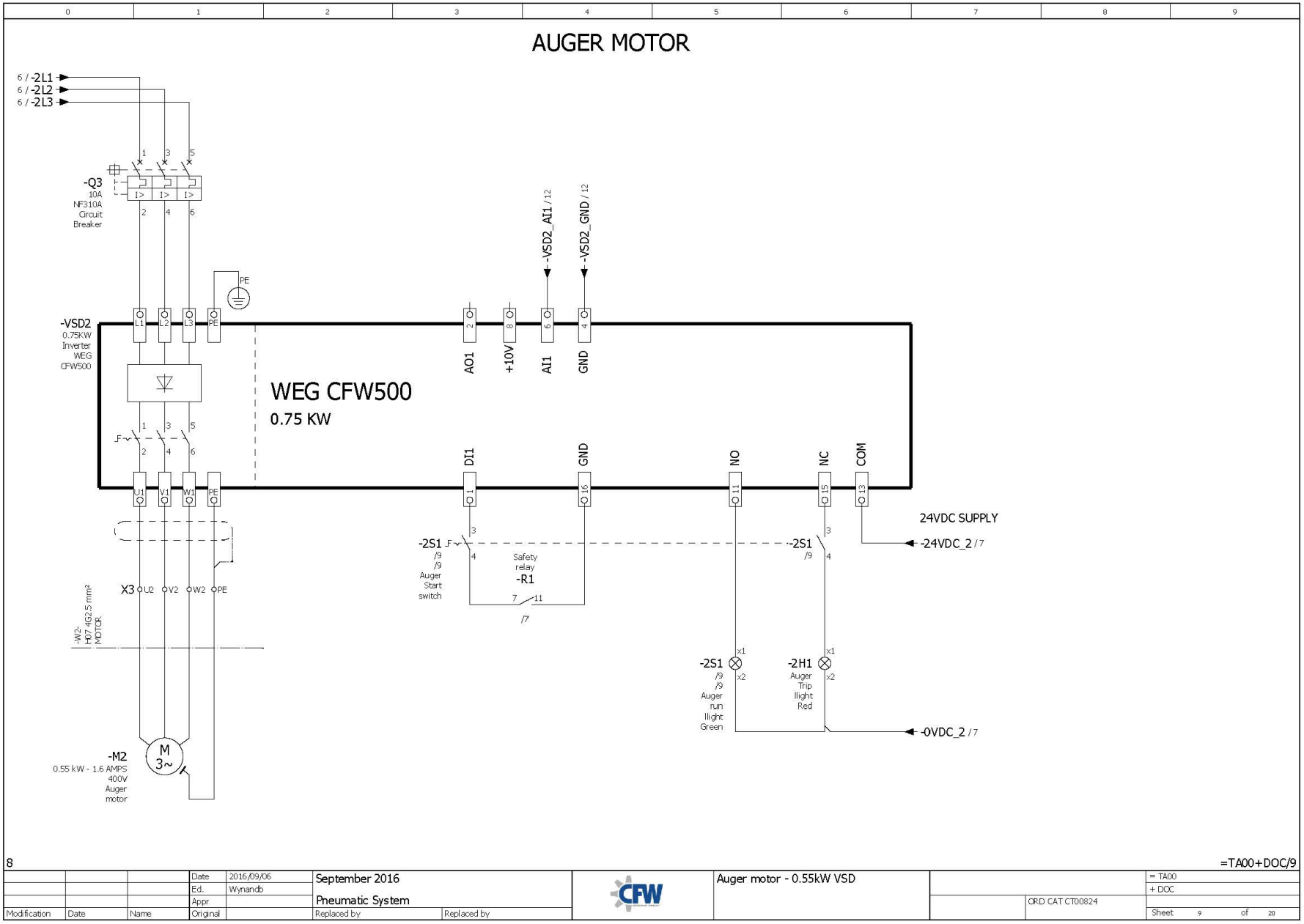
AUGER MOTOR
6 / -2L1
6 / -2L2
6 / -2L3
-Q3
10A
NF310A
Circuit
Breaker
-VSD2
0.75KW
Inverter
WEG
CFW500
WEG CFW500
0.75 KW
-VSD2_AI1 / 12
-VSD2_GND / 12
AO1
+10V
AI1
GND
DI1
GND
NO
NC
COM
24VDC SUPPLY
-24VDC_2 / 7
-2S1 /9 /9 Auger Start switch
Safety relay -R1
-2S1 /9
-2S1 /9 Auger run llight Green
-2H1 Auger Trip llight Red
-0VDC_2 / 7
X3 U2 V2 W2 PE
-W2- H07 4G2.5 mm² MOTOR
-M2
0.55 kW - 1.6 AMPS
400V
Auger
motor
M
3~
8
=TA00+DOC/9
Date 2016/09/06
Ed. Wynandb
Appr
September 2016
Pneumatic System
Auger motor - 0.55kW VSD
= TA00
+ DOC
ORD CAT CT00824
Sheet 9 of 20
Modification Date Name Original Replaced by Replaced by

ROTARY MOTOR

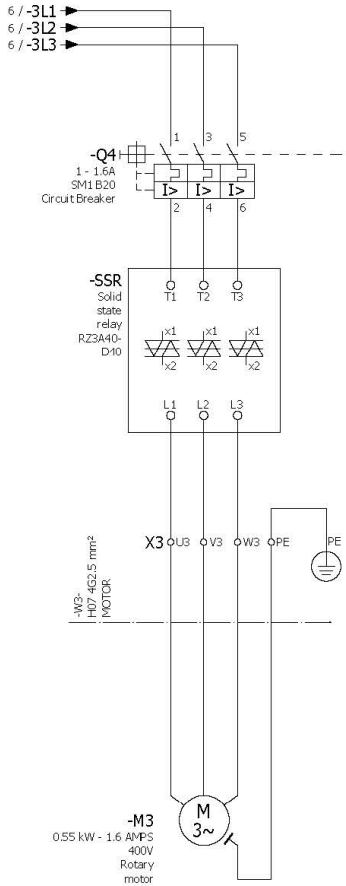

9 =TA00+DOC/10

			Date	2016/09/06	September 2016		Rotary motor - 0.55kW SSR		= TA00
			Ed.	Wynandb					+ DOC
			Appr		Pneumatic System			ORD CAT CT00824	
Modification	Date	Name	Original		Replaced by	Replaced by			Sheet 10 of 20

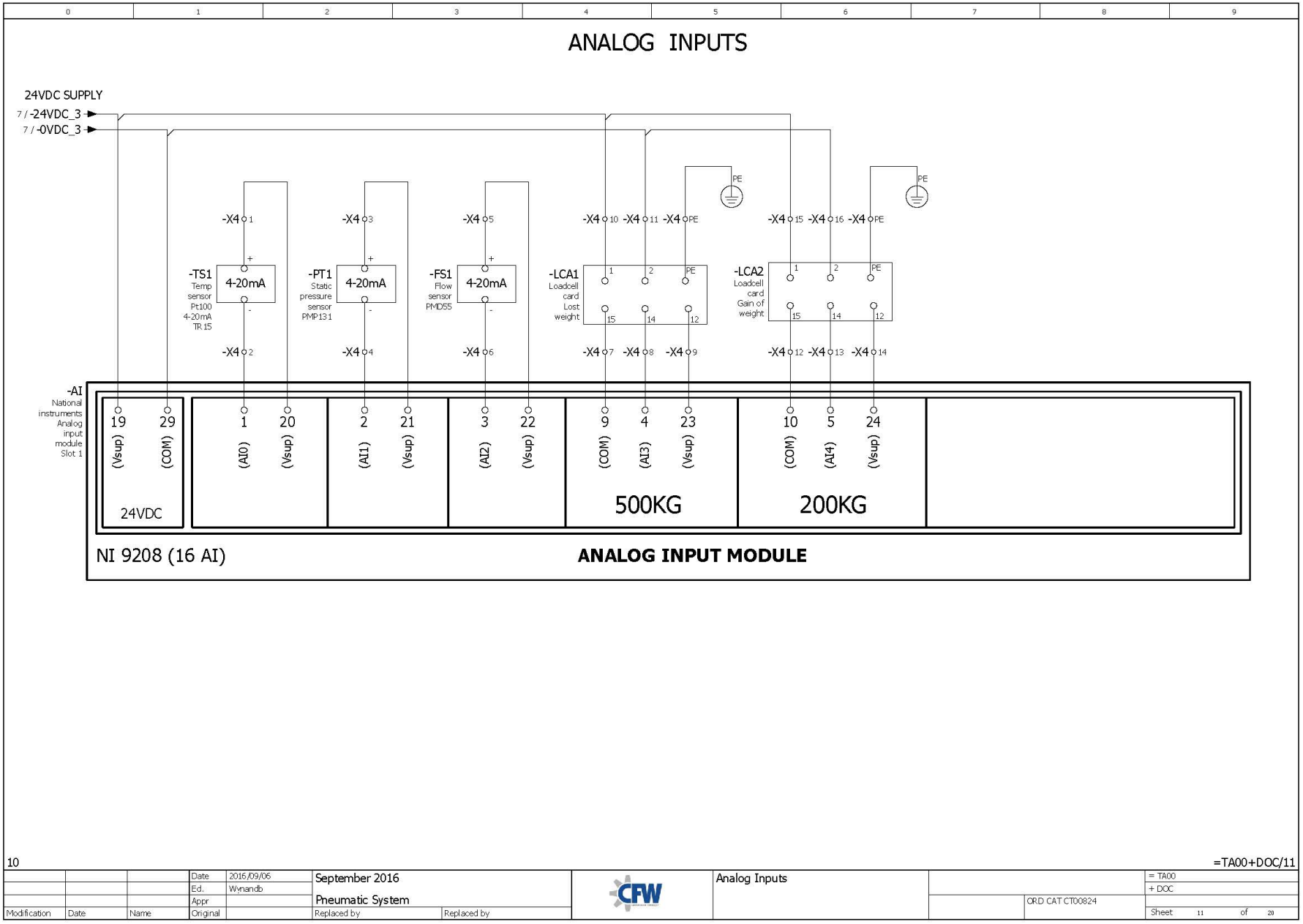
ANALOG INPUTS
24VDC SUPPLY
7 / -24VDC_3
7 / -0VDC_3
-TS1
Temp sensor Pt100 4-20mA TR15
4-20mA
-PT1
Static pressure sensor PMP131
4-20mA
-FS1
Flow sensor PMD55
4-20mA
-LCA1
Loadcell card Lost weight
-LCA2
Loadcell card Gain of weight
PE
-AI
National instruments Analog input module Slot 1
19 (Vsup)
29 (COM)
24VDC
1 (AI0)
20 (Vsup)
2 (AI1)
21 (Vsup)
3 (AI2)
22 (Vsup)
9 (COM)
4 (AI3)
23 (Vsup)
500KG
10 (COM)
5 (AI4)
24 (Vsup)
200KG
NI 9208 (16 AI)
ANALOG INPUT MODULE
10
=TA00+DOC/11
Date 2016/09/06
Ed. Wynandb
Appr
September 2016
Pneumatic System
Analog Inputs
ORD CAT CT00824
= TA00
+ DOC
Sheet 11 of 20
Modification Date Name Original Replaced by Replaced by

ANALOG OUTPUTS

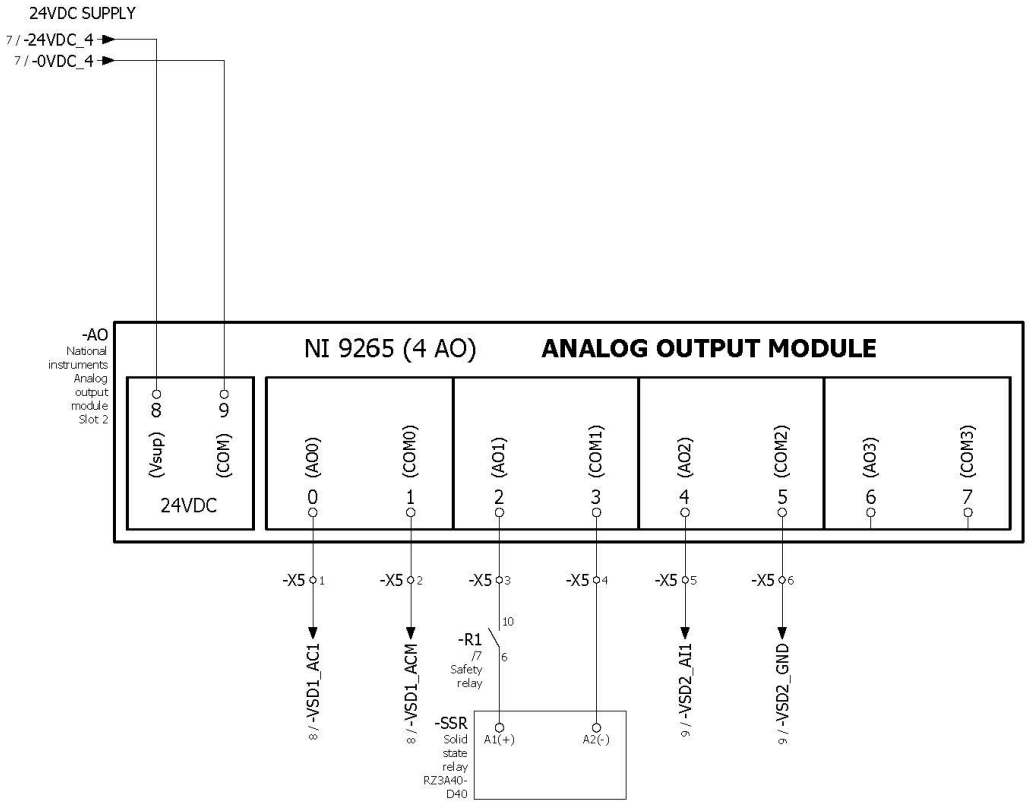

11

=TA00+DOC/12

			Date	2016/09/06	September 2016		Analog Outputs		= TA00
			Ed.	Wynandb					+ DOC
			Appr		Pneumatic System			ORD CAT CT00824	
Modification	Date	Name	Original		Replaced by	Replaced by			Sheet 12 of 20

LOADCELL CONNECTIONS

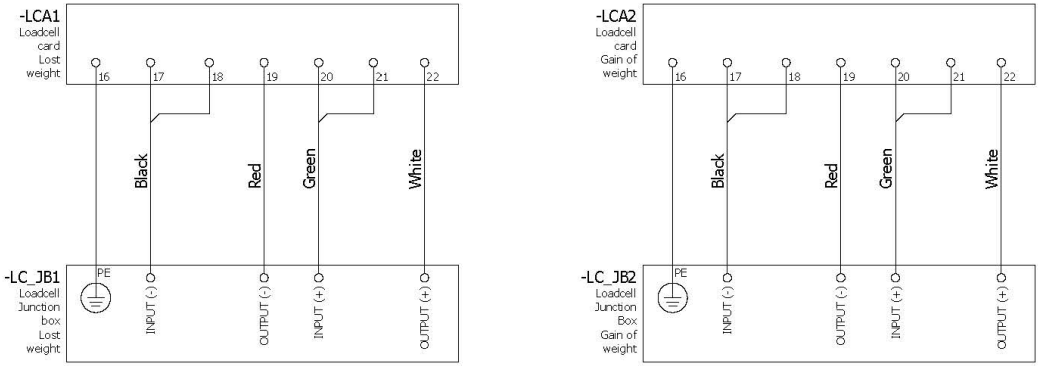

12

=TA00+DOC/13

			Date	2016/09/06	September 2016		Loadcell connections	= TA00
			Ed.	Wynandb				+ DOC
			Appr		Pneumatic System		ORD CAT CT00824	
Modification	Date	Name	Original		Replaced by	Replaced by		Sheet 13 of 20

FIELD WIRING 1

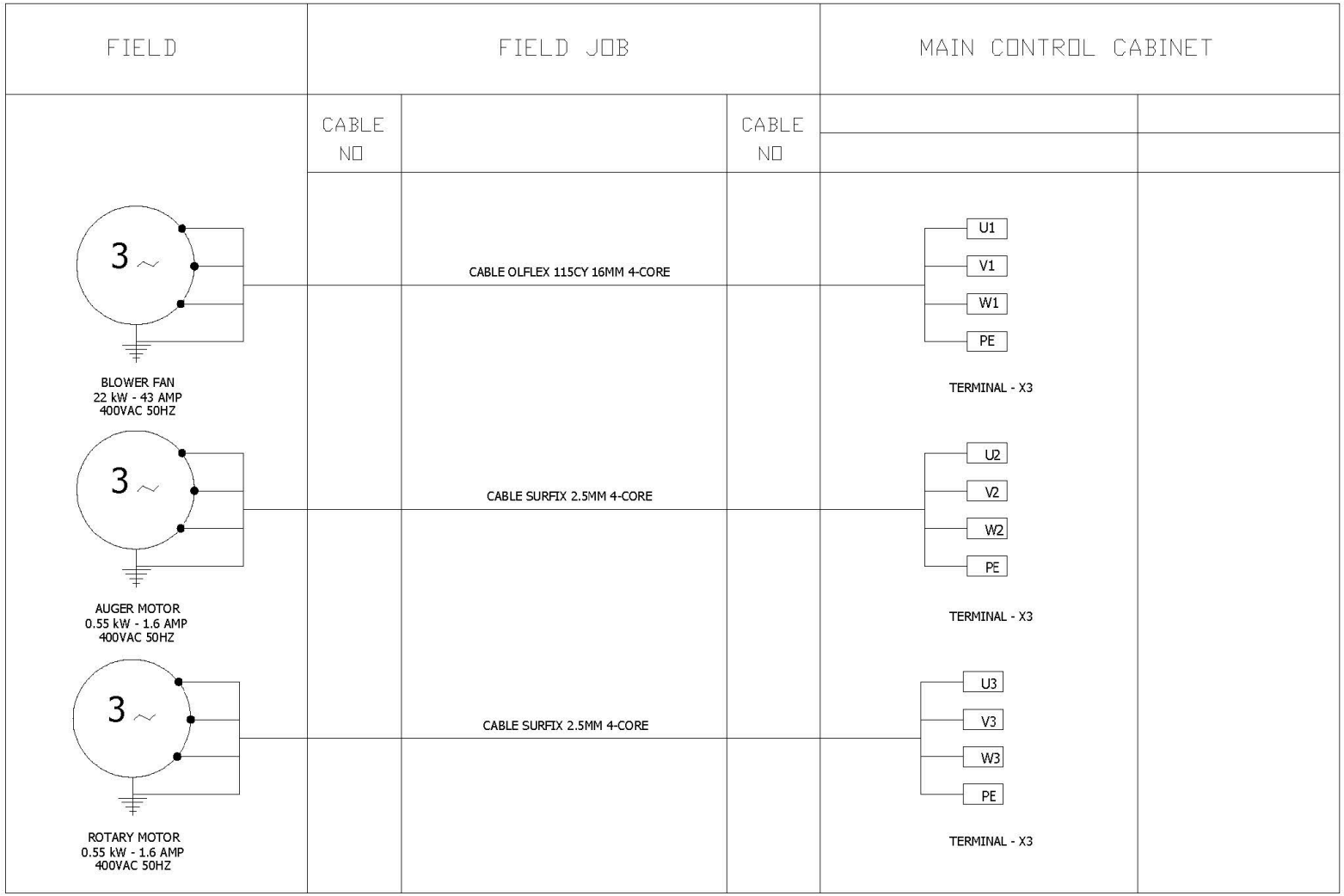

13

=TA00+DOC/14

			Date	2016/09/05	September 2016		Field wiring 1		= TA00
			Ed.	Wynandb					+ DOC
			Appr		Pneumatic System			ORD CAT CT00824	
Modification	Date	Name	Original		Replaced by	Replaced by			Sheet 14 of 20

FIELD WIRING 2

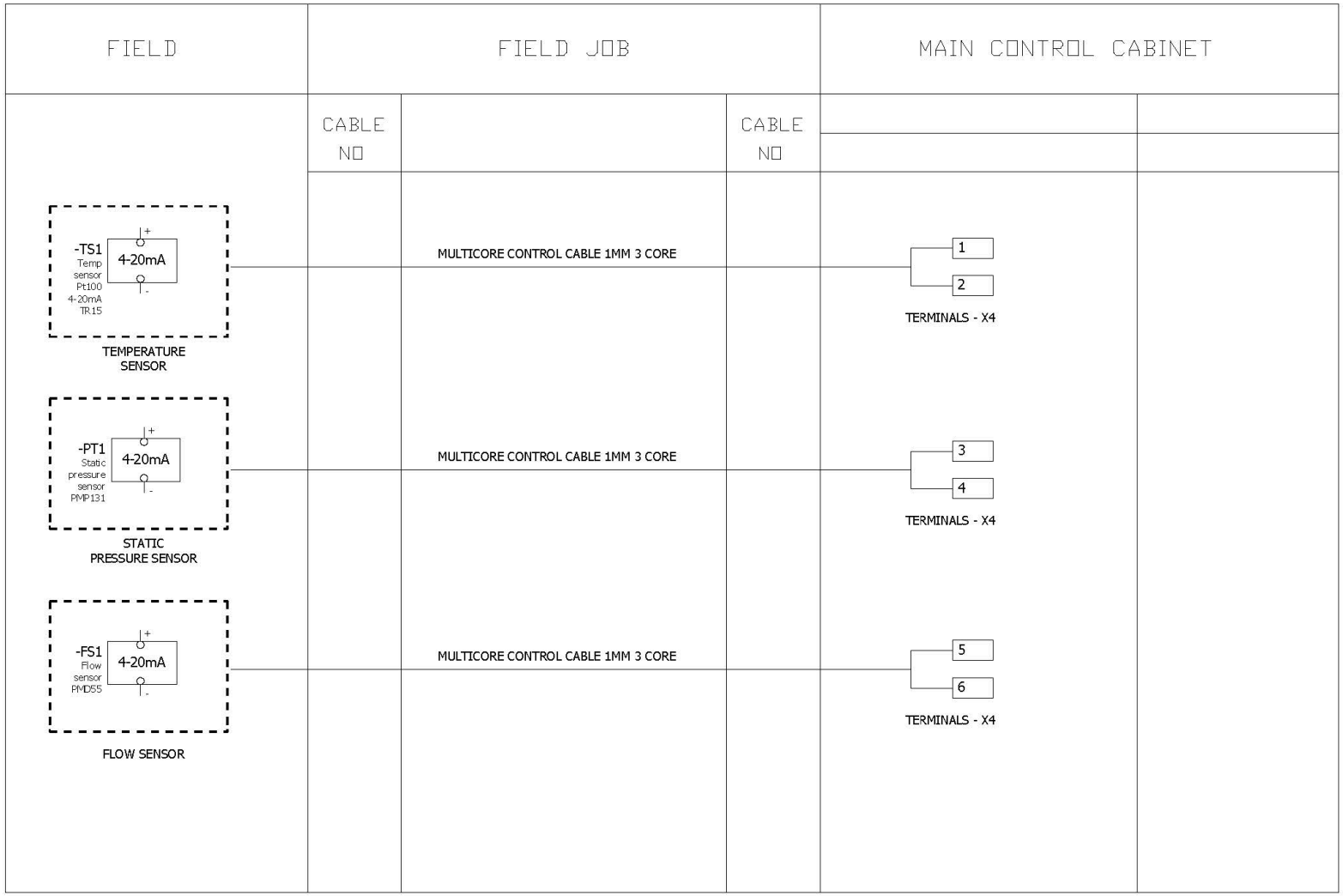

14

=TA00+DOC/15

			Date	2016/09/06	September 2016		Field wiring 2		= TA00
			Ed.	Wynandb					+ DOC
			Appr		Pneumatic System			ORD CAT CT00824	
Modification	Date	Name	Original		Replaced by	Replaced by			Sheet 15 of 20

FIELD WIRING 3

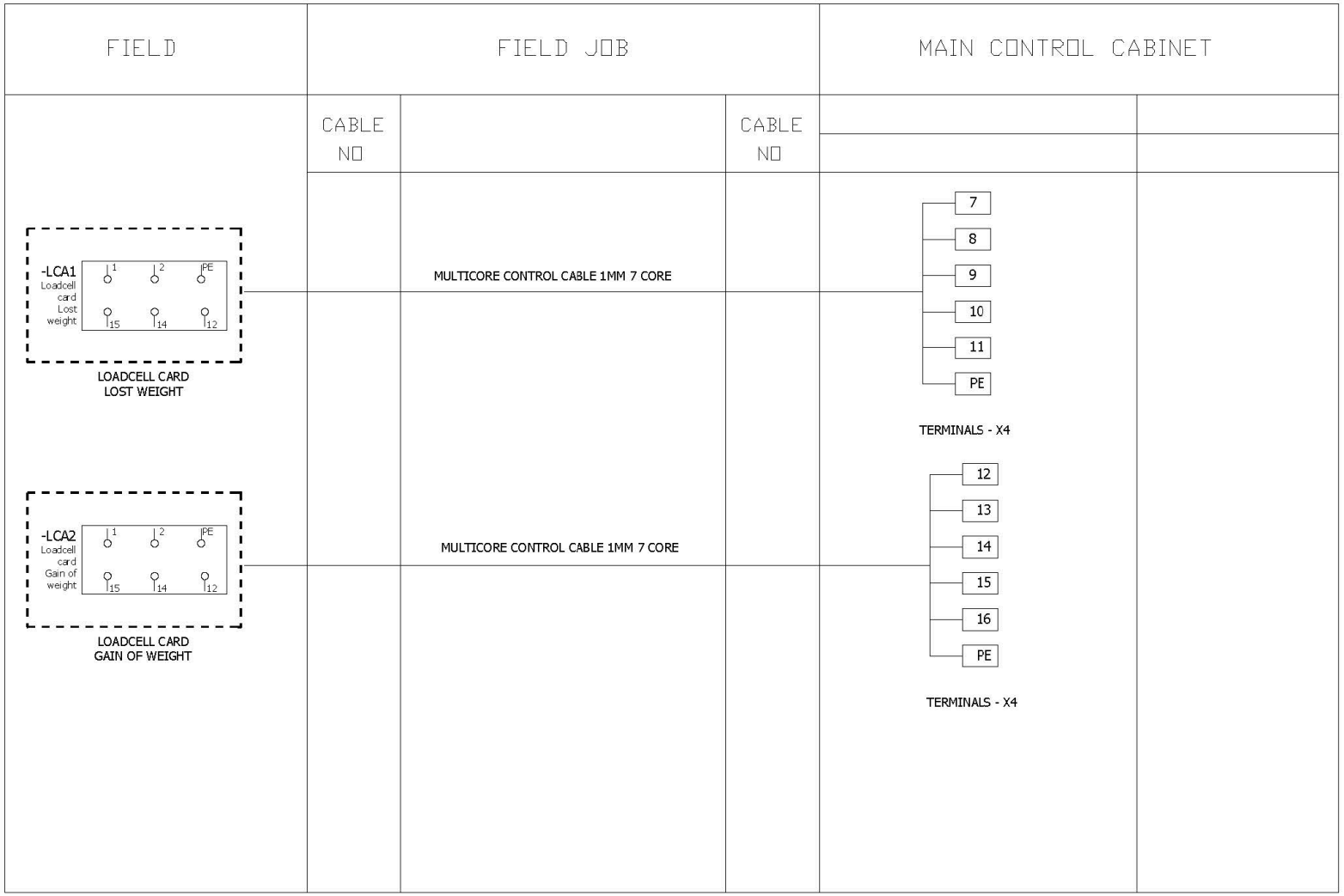

15

=TA00+DOC/16

			Date	2016/09/06	September 2016		Field wiring 3		= TA00
			Ed.	Wynandb					+ DOC
			Appr		Pneumatic System			ORD CAT CT00824	
Modification	Date	Name	Original		Replaced by	Replaced by			Sheet 16 of 20

FIELD WIRING 4

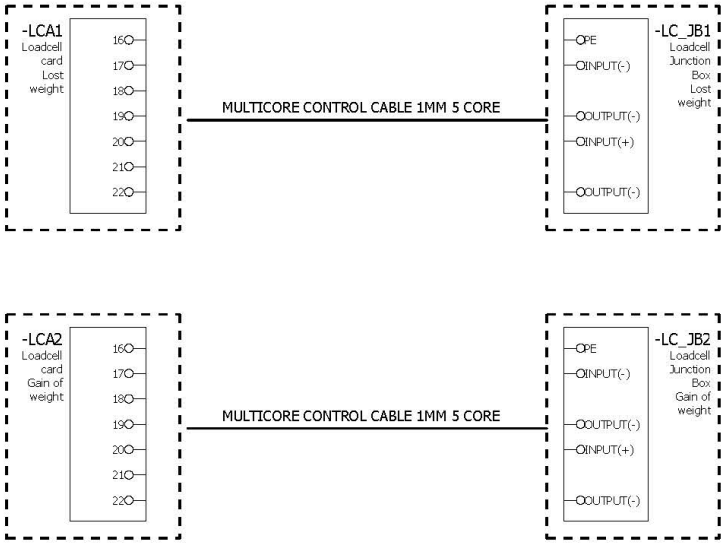

16 =TA00+DOC/17

			Date	2016/09/06	September 2016		Field wiring 4		= TA00
			Ed.	Wynandb					+ DOC
			Appr		Pneumatic System			ORD CAT CT00824	
Modification	Date	Name	Original		Replaced by	Replaced by			Sheet 17 of 20

0 1 2 3 4 5 6 7 8 9

Parts list

F01_001

device tag	Quantity	designation	Type number	supplier	part number
=+-X1	0				
=TA00+DOC-ES1	1	Emergency Stop Button, Twist release	LPC_B6344	ELM	LOV.LPC_B6344
=TA00+DOC-ES1	1	Contact block N/C	LPX_C01	ELM	LOV.LPX_C01
=TA00+DOC-ES1	1	Plastic contact block support	LPX_AU120	ELM	LOV.LPX_AU120
=TA00+DOC-F1	1	Fuse holder 10x38mm 1 pole,32 amp	485101	ELM	DFE_485101
=TA00+DOC-F1	1	Fuse 10x38mm 2 amp	420002	ELM	DFE_420002
=TA00+DOC-FAN1	1	Panel fan, 67W	FF20A230UE	ELM	FAN.FF20A230UE
=TA00+DOC-FAN2	1	Panel fan, 67W	FF20A230UE	ELM	FAN.FF20A230UE
=TA00+DOC-1H1	1	LED pilot light; Red	LP2TILB4P	ELM	LOV.LP2TILB4P
=TA00+DOC-2H1	1	LED pilot light; Red	LP2TILB4P	ELM	LOV.LP2TILB4P
=TA00+DOC-Q1	1	3 pole isolator switch 63 A	2200 3005	ELM	SOC.2200 3005
=TA00+DOC-Q1	1	Handle for Isolator 32 Amp	1472 1111	ELM	SOC.1472 1111
=TA00+DOC-Q1	1	DOOR MOUNTING KIT	2299 3309	ELM	SOC.2299 3309
=TA00+DOC-Q2	1	Circuit Breaker 63A TP D-CURVE	NDN363A	ELM	HAG_NDN363A
=TA00+DOC-Q3	1	Circuit Breaker 10A TP	NF310A	ELM	HAG_NF310A
=TA00+DOC-Q4	1	Motor circuit breaker 1 - 1.6 Amp	SM1 B20	ELM	LOV_SM1 B20
=TA00+DOC-Q4	1	Aux contact for SM1 C/B	SMX11.11	ELM	LOV_SMX11.11
=TA00+DOC-Q5	1	Circuit Breaker 6A DP	NF206A	ELM	HAG_NF206A
=TA00+DOC-R1	1	24VDC Coil	5534902400 40	ELM	FIN.5534902400 40
=TA00+DOC-R1	1	Relay base	9404SPA	ELM	FIN.9404SPA
=TA00+DOC-1S1	1	Illuminated 2 Pos. selector switch (Green)	LPC_SL1203	ELM	LOV.LPC_SL1203
=TA00+DOC-1S1	1	Plastic contact block support	LPX_AU120	ELM	LOV.LPX_AU120
=TA00+DOC-1S1	1	Contact block N/O	LPX_C10	ELM	LOV.LPX_C10
=TA00+DOC-1S1	1	Led Lamp holder green 12-30VAC/DC	LPX_LP_B3	ELM	LOV.LPX_LP_B3
=TA00+DOC-2S1	1	Illuminated 2 Pos. selector switch (Green)	LPC_SL1203	ELM	LOV.LPC_SL1203
=TA00+DOC-2S1	1	Plastic contact block support	LPX_AU120	ELM	LOV.LPX_AU120
=TA00+DOC-2S1	1	Contact block N/O	LPX_C10	ELM	LOV.LPX_C10
=TA00+DOC-2S1	1	Led Lamp holder green 12-30VAC/DC	LPX_LP_B3	ELM	LOV.LPX_LP_B3

17 =TA00+DOC/18

			Date	2016/09/06	September 2016		Parts list : - LOV.LPX_LP_B3		= TA00
			Ed.	Wynandb					+ DOC
			Appr		Pneumatic System			ORD CAT CT00824	
Modification	Date	Name	Original		Replaced by	Replaced by			Sheet 18 of 20

Summarized parts list

F02_001

Order number	Quantity	description designation	Type number part number	manufacturer supplier	unit price	total price	Pos
	0					0.00	
LPC_B6344	1 Stück	Emergency Stop Button, Twist release	LPC_B6344 LOV.LPC_B6344	LOV ELM	0.00	0.00	
LPX_C01	1 Stück	Contact block N/C	LPX_C01 LOV.LPX_C01	LOV ELM	0.00	0.00	
LPX_AU120	3 Stück	Plastic contact block support	LPX_AU120 LOV.LPX_AU120	LOV ELM	0.00	0.00	
485101	1	Fuse holder 10x38mm 1 pole,32 amp	485101 DFE_485101	DFE ELM	0.00	0.00	
420002	1	Fuse 10x38mm 2 amp	420002 DFE_420002	DFE ELM	0.00	0.00	
FF20A230UE	2	Panel fan, 67W	FF20A230UE FAN.FF20A230UE	Fandis ELM	0.00	0.00	
LP2TILB4P	2 pc	LED pilot light; Red	LP2TILB4P LOV.LP2TILB4P	LOV ELM	0.00	0.00	
2200 3005	1 pc	3 pole isolator switch 63 A	2200 3005 SOC.2200 3005	SOC ELM	0.00	0.00	
1472 1111	1 pc	Handle for Isolator 32 Amp	1472 1111 SOC.1472 1111	SOC ELM	0.00	0.00	
2299 3309	1 pc	DOOR MOUNTING KIT	2299 3309 SOC.2299 3309	SOC ELM	0.00	0.00	
NDN363A	1	Circuit Breaker 63A TP D-CURVE	NDN363A HAG_NDN363A	HAG ELM	0.00	0.00	
NF310A	1	Circuit Breaker 10A TP	NF310A HAG_NF310A	HAG ELM	0.00	0.00	
SM1 B20	1	Motor circuit breaker 1 - 1.6 Amp	SM1 B20 LOV_SM1 B20	LOV ELM	0.00	0.00	
SMX11.11	1	Aux contact for SM1 C/B	SMX11.11 LOV_SMX11.11	LOV ELM	0.00	0.00	
NF206A	1	Circuit Breaker 6A DP	NF206A HAG_NF206A	HAG ELM	0.00	0.00	
553490240040	1 pc	24VDC Coil	553490240040 FIN.553490240040	FIN ELM	0.00	0.00	
9404SPA	1 pc	Relay base	9404SPA FIN.9404SPA	FIN ELM	0.00	0.00	
LPC_SL1203	2 Stück	Illuminated 2 Pos. selector switch (Green)	LPC_SL1203 LOV.LPC_SL1203	LOV ELM	0.00	0.00	

18

=TA00+DOC/19

			Date	2016/09/06	September 2016		Summarized parts list : -	= TA00
			Ed.	Wynandb			LOV.LPC_SL1203	+ DOC
			Appr		Pneumatic System			
Modification	Date	Name	Original		Replaced by	Replaced by		ORD CAT CT00824 Sheet 19 of 20

0 1 2 3 4 5 6 7 8 9

Summarized parts list

F02_001

Order number	Quantity	description designation	Type number part number	manufacturer supplier	unit price	total price	Pos
LPX_C10	2 Stück	Contact block N/O	LPX_C10 LOV.LPX_C10	LOV ELM			
LPX_LP_B3	2 Stück	Led Lamp holder green 12-30VAC/DC	LPX_LP_B3 LOV.LPX_LP_B3	LOV ELM			

19

=TA00+DOC/20

			Date	2016/09/06	September 2016		Summarized parts list : LOV.LPX_C10 - LOV.LPX_LP_B3	= TA00
			Ed.	Wynandb				+ DOC
			Appr		Pneumatic System		ORD CAT CT00824	
Modification	Date	Name	Original		Replaced by	Replaced by		Sheet 20 of 20

Appendix U. Photos of Prototype Facility

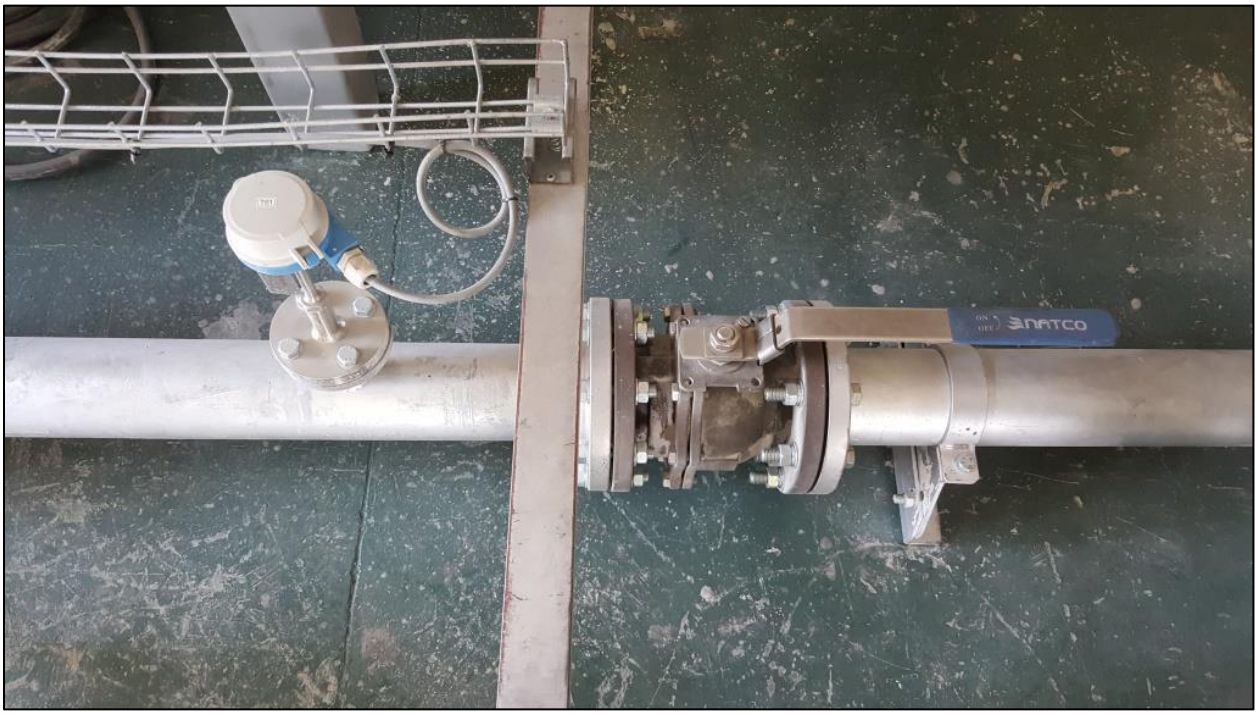
ON
OFF
ΞNATCO

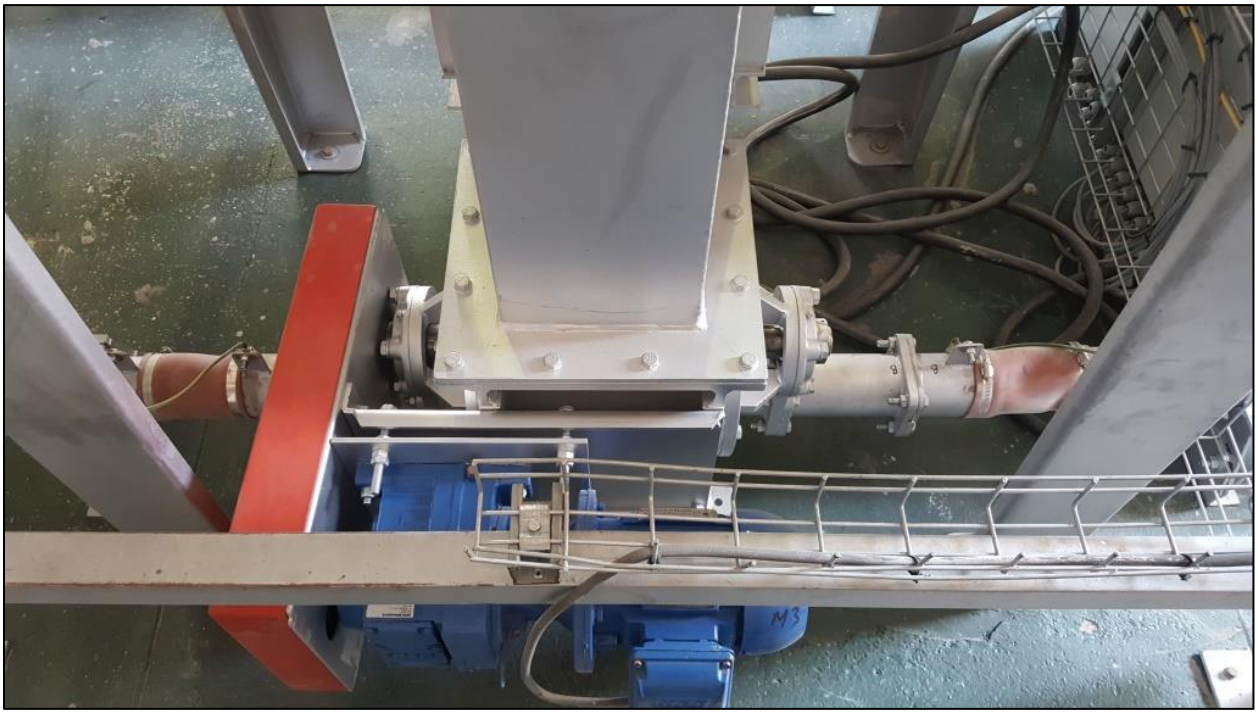

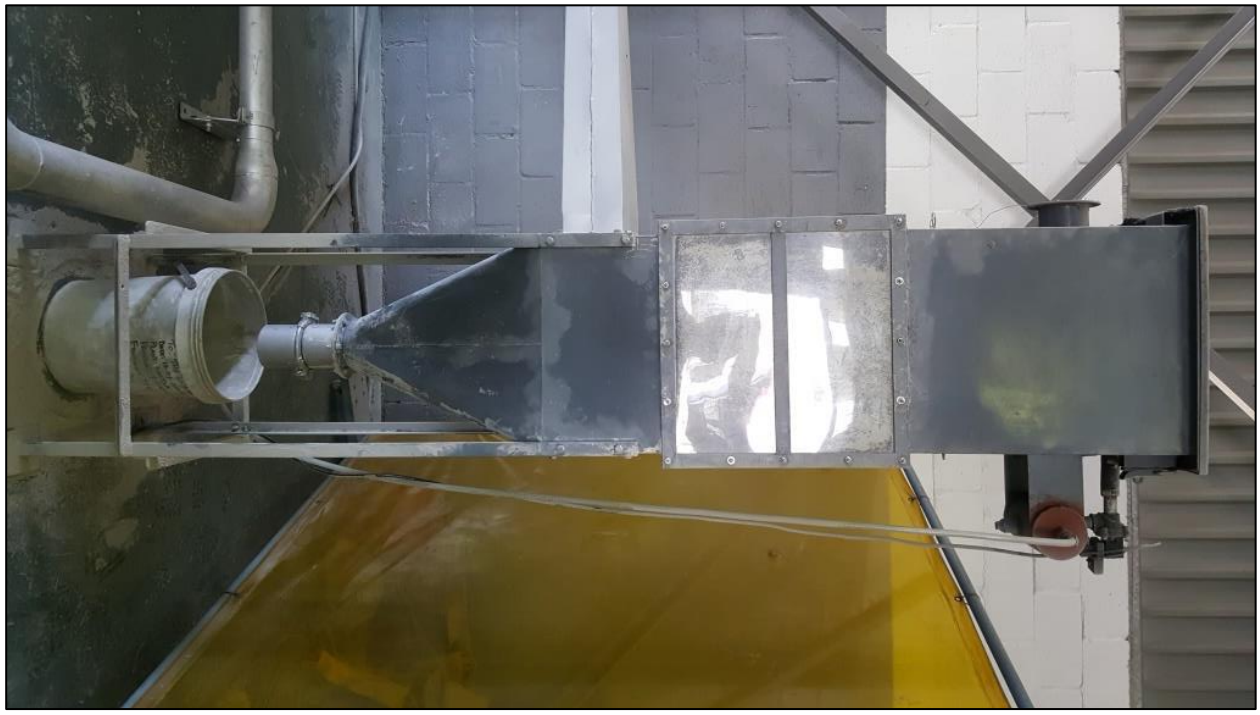

Appendix V. Ethics Clearance

Application for Approval of Ethics in Research (EiR) Projects
Faculty of Engineering and the Built Environment, University of Cape Town

APPLICATION FORM

Please Note:
Any person planning to undertake research in the Faculty of Engineering and the Built Environment (EBE) at the University of Cape Town is required to complete this form before collecting or analysing data.The objective of submitting this application *prior* to embarking on research is to ensure that the highest ethical standards in research, conducted under the auspices of the EBE Faculty, are met. Please ensure that you have read, and understood the **EBE Ethics in Research Handbook**(available from the UCT EBE, Research Ethics website) prior to completing this application form: http://www.ebe.uct.ac.za/usr/ebe/research/ethics.pdf

APPLICANT'S DETAILS		
Name of principal researcher, student or external applicant		Colin Francois du Sart
Department		Mechanical Engineering
Preferred email address of applicant:		dsrcol001@myuct.ac.za
If a Student	Your Degree: e.g., MSc, PhD, etc.,	MSc in Mechanical Engineering
	Name of Supervisor (if supervised):	Pieter Rousseau
If this is a researchcontract, indicate the source of funding/sponsorship		N/A
Project Title		Design and prototyping of a test facility to investigate the transport properties of dilute phase particle flows applicable to coal-fired power plants

I hereby undertake to carry out my research in such a way that:

- there is no apparent legal objection to the nature or the method of research; and
- the research will not compromise staff or students or the other responsibilities of the University;
- the stated objective will be achieved, and the findings will have a high degree of validity;
- limitations and alternative interpretations will be considered
- the findings could be subject to peer review and publicly available, and
- I will comply with the conventions of copyright and avoid any practice that would constitute plagiarism.

SIGNED BY	Full name	Signature	Date
Principal Researcher/ Student/External applicant	Colin Francois du Sart	Signed	28 Nov 2016

APPLICATION APPROVED BY	Full name	Signature	Date
Supervisor (where applicable)	Prof PIETER G. ROUSSEAU	Signed	30/11/2016
HOD (or delegated nominee) Final authority for all applicants who have answered NO to all questions in Section1; and for all Undergraduateresearch (Including Honours).	Tunde Bello -Ochende	Signed	11/1/2017
Chair : Faculty EIR Committee For applicants other than undergraduate students who have answered YES to any of the above questions.			

Page 1 of 1